The Work Function of Titanium and Selected Metals in Vacuum

being a thesis on:

the work function of titanium and noble metal films in vacuum and in hydrogen,

the effects of irradiation and electric field on the work function of stainless steel,

the measurement of contact potentials by the dynamic capacitor method.

by

R.J. D'Arcy, B.Sc.,

and

submitted to the University of Keele, Staffordshire for the degree of Doctor of Philosophy.

Department of Physics,
University of Keele,
1971.

SYNOPSIS

The work functions of titanium films have been measured at room temperature with a scanning probe version of the Kelvin-Zisman dynamic capacitor. The values for the clean surfaces of films deposited onto a gold substrate at 2.10^{-9} torr lay between 4.5 and 6.0 eV. The surface potentials of hydrogen were positive apparently due to penetration of the adsorbed hydrogen atom with a partial negative ionicity below the surface electronic plane. The maximum surface potential increased approximately linearly with the initial work function and varied between 0.26 and 1.30 eV. A surface potential model was proposed which attempted to account for dissociative adsorption of molecular hydrogen and solution of adsorbed atomic hydrogen. The time dependant changes of the surface potential were consistent with the theoretical predictions and the activation energy for solution of atomic hydrogen was derived to be between 0.7 and 1.5 Kcal $gr\text{-}atom^{-1}$. The work function and surface potential of rapidly deposited films at 1.10^{-7} torr onto a silver substrate behaved similarly to those above and mass spectrometric analysis of the residual gas provided evidence for a predominant adsorption of hydrogen. Slowly deposited films at this pressure onto a silver substrate, however, possessed a low work function between 2.5 and 3.8 eV which broadly encompassed the range of values recently published by others for thin titanium films deposited apparently under similar conditions. The low values apparently arise from impurities. The surface potential of the residual gas adsorbate was negative on contaminated films and the time dependant changes were of a similar form to those of purer films. These results are discussed in relation to the hydrogen surface potential model and the adsorption of other gases.

The work function of two polished stainless steel electrodes were 4.65 $\mp$ 0.10 eV at 1.10^{-7} torr and 5.60 $\mp$ 0.10 eV (after baking) at 2.10^{-9} torr. The work function was reversibly decreased by illumination, prolonged exposure to hydrogen and by applied electrostatic fields; it was reversibly increased by an incident electron current. These effects are interpreted as the result of an oxide layer on the steel surface. Theoretical models are proposed which attempt to account for these as due to changes in the density of surface states at a semiconducting oxide surface. The results are generally consistent with the theoretical predictions with the exception of the field effect.

The effect of stray capacitive coupling on contact potential measurements was experimentally investigated. The results were partially consistent with the predictions of a model which is proposed. These effects are shown to be a major source of error if simple precautionary measures are not taken to avoid them.

This thesis is dedicated to my mother and in memory of my late father for their foresight and encouragement.

ACKNOWLEDGEMENTS

The author wishes to express his thanks and appreciation to:

Professor D.J.E. Ingram for the provision of laboratory facilities,

The United Kingdom Atomic Energy Authority, which provided the capital equipment and a maintenance allowance,

Dr. D.E. Davies* for establishing the extra-mural research agreement with the A.W.R.E.,

Dr. N.A. Surplice for his supervision, assistance, advice and interest throughout all of this work,

Mr. F. Rowerth and all his staff for their technical assistance and advice,

The British Ceramic Research Association, Penkhull, Stoke-on-Trent for their kind technical assistance,

My friends and colleagues for their encouragement and interest,

and to Mrs. C. Thomson for her care and cooperation in typing this thesis.

* Now Professor of Physics, University of La Trobe, Melbourne, Australia.

CONTENTS

CHAPTER 1

INTRODUCTION

The surfaces of solids have attracted scientific attention since the early part of the nineteenth century. This has arisen in addition to their fundamental interest because of their important role in many facets of life and from their practical applications in others, among catalysis, adsorption, crystal growth and metallic corrosion. The important practical applications of electron emission and the electric lamp stimulated active research into the fundamental properties of the surfaces of solids in the early part of this century. It was from these studies that Irving Langmuir established the fundamental concepts on which a major portion of present day concepts are formulated in surface physics.

Experimental progress in the past has almost invariably led theoretical advances in the understanding of fundamental surface processes. The effects of crystal orientation, for example, on chemical reactivity was appreciated long before the theory of atomic structure was formulated. Consequently the knowledge of solid surfaces has been far less than that of the bulk counterpart. This is due to a number of reasons. Firstly, the theoretical description of solid surfaces is difficult and complicated due to the distortion of the periodic lattice potential at the surface interface. Secondly, the forces exerted on the surface atomic layer are assymetric. Thirdly,

there is generally a tendency for a reaction to occur with the environment because of the unsaturated nature of the surface forces. The experimental techniques which have been available have not enabled a well defined environment and surface to be prepared and kept free from contamination. Consequently progress has been largely achieved through experimentation and intense efforts to correlate and interpret observations with simple systems.

This research received its impetus from the need for an evaluation of the work function of titanium. Portable neutron generators commonly use titanium hydride cathodes. Field electron emission from the cathode is an important physical gas breakdown mechanism which limits their lifetime. The work function among other factors determines the breakdown voltage at which emission occurs. The objectives of this research were to determine the work function of pure titanium in vacuum, and also in hydrogen at room temperature and to measure any spatial variation. In the course of this work, incidental results were obtained on the work function of gold and silver, on problems associated with the experimental method of work function measurement chosen and also on the effects of surface charge on the work function of stainless steel.

The work function is particularly sensitive to surface contamination and the amount and nature of any adsorbed gaseous molecules. A study of the work function and surface potential of adsorbed gases is a valuable technique in investigating the adsorption of gases on solids. Early research at the beginning of

this century on the work function derived its impetus from several sources. Firstly, there were the practical applications of electron emission. Secondly, there was a fundamental interest in the work function as a intrinsic property of metals predicted by the then new electron band theory of solids. Thirdly, the work function was related to the contact potential difference which had been, and at that time still was, the subject of a warm debate that had remained unresolved for more than a century.

The contact potential method of Kelvin 1898 and Zisman 1932 is used in this work for the measurement of the work function. There had been historical interest in contact potentials long before the formulation of the concept or of any measurement of the work function. The concept of the work function although technically introduced by Richardson and Langmuir is intrinsic in the original theory of Volta in 1797, on the origin of the contact charging of conductors, to whom the discovery of this phenomenon is attributed. Volta proposed that the contact potential difference was an intrinsic property of conductors in contact and that it was wholly located at their junction. The theory was supported in later years by Lord Kelvin, Langmuir and Richardson. There then followed a warm debate between the exponents of the contact theory and those in favour of a chemical theory. The latter proposed that the contact potential was located at the metal-dielectric interface and that it arose from a chemical reaction between them. The discovery of electron emission and also Richardson's theory of thermionic emission (1912) stimulated renewed interest in the contact potential. The thermionic

theory was based on the then new electron theory of metals and postulated that there was a fundamental force across a metal-dielectric interface which was an intrinsic property of conductors. Technological improvements in vacuum science afforded an opportunity to directly test the opposing hypotheses concerning the origin and location of the contact potential. Research which was directed towards establishing Richardson's hypothesis was also directly associated with the theories of the contact potential. He had shown from statistical thermodynamic arguments that the contact potential difference is directly related to the difference in work function of the conductors in contact. At about the same time, 1912, Richardson had demonstrated the equivalence of the work function parameter appearing in the photo-electron emission theory of Einstein with the 'work of extraction' in the thermionic theory. A few years later Millikan and Hennings resolved the conflict on the nature and existence of the contact potential. They experimentally verified the predicted theoretical relationship between the contact potential and the work functions of conductors in contact. It was some years however before the issue was accepted and in 1916 Langmuir wrote "the scepticism regarding electron emission has been largely resolved in the last few years and it is almost accepted that electron emission is an intrinsic property of metals".

An interesting historical account of this period given by Langmuir 1916 and Compton and Langmuir 1930.

Richardson's theory made no assumption regarding the location of the contact potential and the debate concerning it

continued. Helmholtz had shown earlier about 1879 that at any potential discontinuity at a conductor surface there exists a double charge layer. The existence of this layer could be claimed without recourse to any metallic junction and vice-versa. At about this time Schottky was developing the image force theory to account for certain anomalies in thermionic emission phenomena. The image theory was important to the exponents of the contact junction theory since if the work function was solely due to the image force then the concept of double charge layers had no validity. If this was the case, the contact potential could be claimed to be wholly located at the metal junction. The success of the image theory in accounting for the thermionic anomalies lent support to these views. It is now known that the work function is not solely due to the image force however. An account of this period is given by Becker 1935.

The concept of the contact potential was clarified by Chalmers 1942 who supported the view that both electro-static and thermodynamic potentials are involved in its definition. Thermodynamic concepts form the basis of present day views and these are returned to in Chapters 2 and 4.

The quantity of published literature on the work function and adsorption of gases on solids is formidable. No attempt is made to review this broad field in this thesis for this reason, and also because there are a large number of review articles which deal with many aspects of these phenomena. Frequent reference is made

to these where necessary. The work function of solids is reviewed in Chapter 2 together with the adsorption of gases on solids where these are relevant to the study of the work function. The techniques of measuring the work function have been extensively reviewed. These are therefore only briefly discussed in Chapter 2. A detailed discussion of the Kelvin - Zisman method is given later in Chapter 4.

In recent years there has been, in surface science, a development of a variety of physical techniques. These have allowed a new and deeper insight into the structure of surfaces and the elementary atomic processes which occur on them. This has come about with the improvements in the art of ultra high vacuum technology and in the ready commercial availability of hydrocarbon free vacuum pumps, materials of higher purity and residual gas mass spectrometers. These factors have permitted a closer physical definition of the specimen surface, its purity and of the environment in which it is situated. This closer degree of control has allowed important advances to be made in understanding the elementary processes important in the interactions of gases with solids. Research effort has naturally concentrated on simple well defined systems.

The heterogeneity of solid surfaces is well established. Various crystallographic planes of a single element may exhibit as wide a spectrum in their physical properties as among the bulk elements themselves. A variety of different adsorption states may exist on even single crystal planes. The work function, surface potential and relative population of these states may now be

investigated as a function of temperature, crystal orientation and nature of the adsorbed species. The selective adsorption and mobility of different gases upon different crystal planes and their variation among different materials may be examined. There is a body of evidence that partial or complete reconstruction of the uppermost surface layers may occur with particular gas-solid systems to form new ordered structures. These advances in turn have stimulated further theoretical description of the solid-gas interface.

The physical methods used currently for the investigation of the structure and properties of metal surfaces and adsorbed layers are briefly described.

Rare ionised gas atoms approaching a metal may be neutralised by an electron from the surface. Auger neutralisation is accompanied by the ejection of secondary electrons whose yield and energy distributions are sensitive to the presence of adsorbed layers. Auger spectroscopy is becoming important in the study of adsoprtion on solids. The phenomenon is described by Kaminsky 1965 and by Riviere 1969.

The evolution of gas from a heated metal occurs in distinct stages. Flash desorption spectroscopy (FDS) in conjunction with mass spectrometric analysis of the desorbed products allows the nature of the desorbing species, their binding energies, the kinetics of the surface processes and temperature dependance of the desorption to be studied. The techniques and experimental results are reviewed by Ehrlich 1963 and by Hansen and Mineault 1968.

The fundamental experiments of Davisson and Germer in 1927 demonstrated the wave nature of the electron. Low energy electron diffraction (LEED) from the uppermost surface layers of solids has become an important technique for studying the structure and adsorptive properties of metals. LEED has established the similarity between the crystalline structure of the surface layers with that of the bulk metal and also that partial or complete reconstruction of the surface layers during adsoprtion may occur to form new ordered structures. Reviews of LEED are given by Lander 1964 and by Farnsworth 1968.

The nature of the bonding between adsorbed layers has also been investigated by measurements of the electrical resistance of thin metal films and also of the infra-red spectra of adsorbed species. These are little used in comparison to other physical techniques. In the latter there are problems in the interpretation of the spectra and most experiments have been conducted in poor vacuum. The conductivity of thin metallic films is dependant, among other factors, on the free conduction electron density which may be measurably reduced or enhanced on adsorption depending on the nature of the gas-metal bond.

In the case of ferromagnetic substances, a study of the intensity of magnetisation reveals information on the adsorption bond since, the latter affects the surface magnetic dipole. This is not a widely used technique.

The three techniques mentioned are described by Hayward and Drapnell 1964, Hair 1967, Thomson and Webb 1968, Hofer 1968, Blyholder 1968 and by Robertson 1970.

Energetic ions and electrons incident on solid surfaces may desorb ions and neutral adsorbed species. The nature of these is determined by the composition and state of the layer. Electron and ion desorption spectrometry in conjunction with mass spectrometic analysis, enables information relating to the nature of the layer and its composition to be obtained (cf. Rork and Consoliver 1968, Coburn 1968, Simon et al. 1968).

The cold emission of electrons from metals has played a major role in elucidating the kinetics of the formation and mobility of adsorbed layers as a function of temperature on individual single crystal planes. Field emission microscopy (FEM) has afforded a view of the surface on almost an atomic scale since its conception in 1936 by Muller. FEM is reviewed by Good and Muller 1956, Gomer 1961, Ehrlich 1963 and recently by Hansen and Gardner 1968. FEM is also an important technique for the study of the work function of orientated surfaces and the surface potential of adsorbed gases as discussed later in Chapter 2. It has also found application in the study of epitaxy and nucleation phenomena, surface diffusion of metallic adsorbates and in the study of crystal growth.

Field ionisation microscopy (FIM) has not been so successful as its electron counterpart for the study of adsorption because of the onset of field desorption due to the high field strengths employed.

Field desorption, however, has revealed information on the binding energies of adsorbed and parent metal atoms, (cf. Ehrlich and Kirk 1968). FIM has been used for the study of surface structure, defects, deformation and radiation damage, surface diffusion and corrosion reactions among others. This technique and its applications are described in the articles mentioned above.

In addition to the flash filament and field desorption methods described above, the heats of adsorption may be determined by direct calorimetric measurements or by determining the equilibrium adsorption isotherms as a function of temperature. These have been described by Hayward and Trapnell 1964, Kaminsky 1965 and Robertson 1970. Experimental results for similar systems show widespread values implying the adsorption heat is sensitive to the experimental conditions and crystallographic orientation. The heat of adsorption is apparently related to the work function and ionisation potential of the substrate and adsorbate.

The techniques used in this research were largely determined by the objectives of the project. Titanium is no exception to the general rule that clean transition metals are highly reactive to their environment. It has found widespread application as a residual gas "getter" in vacuum tubes for many decades and it has been almost exclusively used as the active elements in evapor-ion and getter-ion pumps since their inception in the late nineteen fifties (cf. Dushman 1962, Roberts and Vanderslice 1964, Hopkins 1968). Titanium is known

to absorb large quantities of gas (cf. Chapter 6) and its hydride may be used as a source of pure hydrogen. It was therefore necessary to prepare the samples under ultra high vacuum conditions if pure surfaces were to be prepared and maintained. The vacuum system and pumping unit chosen were free from hydrocarbon vapours and are described in Chapter 3. The choice of a titanium getter-ion pump afforded the opportunity of preferentially pumping those active gases detrimental to the preparation of clean specimen titanium surfaces.

The specimen surfaces were prepared by collecting metal vapour evaporated from a heated filament of titanium onto a cool substrate. This method had the advantages of low cost and ease of preparation of macroscopic fresh surfaces. The other common techniques of preparing clean surfaces which are reviewed by Menzel 1963, Roberts 1963, Roberts and Vanderslice 1964 were unfavourable because of the high capital outlay for macroscopic single crystals, the ductility of titanium and because of the risk of surface contamination from bulk or gaseous impurities during prolonged cleaning cycles. However, the question of the substrate material on which the film was to grow was important. Titanium reacts strongly with certain glasses (cf. Roberts and Vanderslice 1964). The sublimation of other transition metals on to glass surfaces has been observed to cause an evolution of gas from the glass which may contaminate the growing film (Hickmott and Enrlich 1958). The activation energy for solution of gases in titanium is apparently quite small and the bulk diffusion coefficient at room temperature quite high

(cf. Chapter 6). Adsorbed gas already on the substrate, therefore, may be dissolved by the film and rapidly contaminate the outer surface layers. The complex structure of glasses therefore rendered them unsuitable. However, pure gold or silver appeared to satisfy these demands by providing an inert noble substrate surface free from adsorbed gases in ultra high vacuum. Thick films of these metals were deposited in ultra high vacuum on to clean pyrex glass and these provided the substrates on which the titanium surfaces were formed. The methods of preparing the substrates are described in Chapter 3.

The work functions of gold and silver films in vacuum are well established. The use of these materials as metal substrates provided the reference surface necessary for the evaluation of the specimen work function from contact potential measurements.

There were a number of major practical problems encountered with the form of the contact potential method employed in this work. Firstly, an amplitude instability of the vibrating electrode was caused by a mechanical coupling between the vibrator drive, the vacuum system and the experimental rig. It severely limited the resolution of contact potential measurement on occassions. Secondly, spatial work function measurements necessitated using one of the capacitor electrodes as a small probe. This caused a loss of signal sensitivity. It was partially offset by the use of a differential detector amplifier. However, it demanded a high degree of electrical insulation of the vibrating electrode and considerable difficulty was

experienced in finding an insulator material with suitable properties for this application.

In the course of experimental measurements two further problems arose. Firstly, the use of the differential amplifier allowed contact potential measurements to be sensitive to stray capacitance. The coupling caused significant errors in the values measured. In anticipation of these effects, the material of the vibrating probe was chosen to be the same as the vacuum system walls (stainless steel) since then, the (hopefully) small difference in contact potential would minimise this source of interference. Secondly, the work function of the steel surface, however, was unstable and sensitive to optical irradiation, electro-static fields and also charged particles which were discovered to be emanating from the ion pump. Both of these problems were experimentally investigated since they affected the accuracy and validity of the contact potential measurements.

This introductory chapter is followed by a review of the work function. The third chapter describes the experimental apparatus and techniques. The contact potential method and experimental effects of stray capacitive coupling are described and interpreted in Chapter 4. The work function instability of the stainless steel probe is described in the fifth chapter. An interpretation is given there of the effects of irradiation and electric fields. These chapters provide a background to the measurements of the contact potentials between the noble and titanium metal films and the steel probe. Measurements were also made between titanium and silver covered steel surfaces. These

measurements are introduced by a review of the work function and adsorptive properties of silver, gold and titanium in Chapter 6. The contact potential measurements are described in Chapter 7 together with a discussion and interpretation. A summary of each of the three phases of this work is given in Chapter 8. The appendices contain the mathematical derivations used in the various models and also copies of the papers relating to this thesis published by the writer in co-authorship with Dr. N.A. Surplice.

CHAPTER 2

THE WORK FUNCTION AND SURFACE POTENTIAL

2.1 Definition

The work function ϕ is defined as the change in the thermodynamic potential of a conductor when a virtual charge is transferred from a point within the conductor to a point outside of the conductor where the classical image force is negligible. A distance of about 10^{-4} cm is sufficient. The thermodynamic concept is discussed by Herring and Nichols 1949, Culver and Tompkins 1959 and by Gundry and Tompkins 1968 in terms of the electrochemical potential $\bar{\mu}$ which is equal to the change of Helmholtz free energy per electron.

The electrochemical potential $\bar{\mu}$ of a conductor is dependent on its internal and external state. The chemical potential μ is defined to be dependent on the internal state only so that it is not affected by the external conditions by

$$\mu = \bar{\mu} + e\phi_1 \qquad (2.1)$$

where ϕ_1 is the average internal electrostatic potential over a space small on a macroscopic scale. The work function is defined by

$$\phi = - \phi_2 - (\bar{\mu}/e) \qquad (2.2)$$

(a) METAL SURFACE

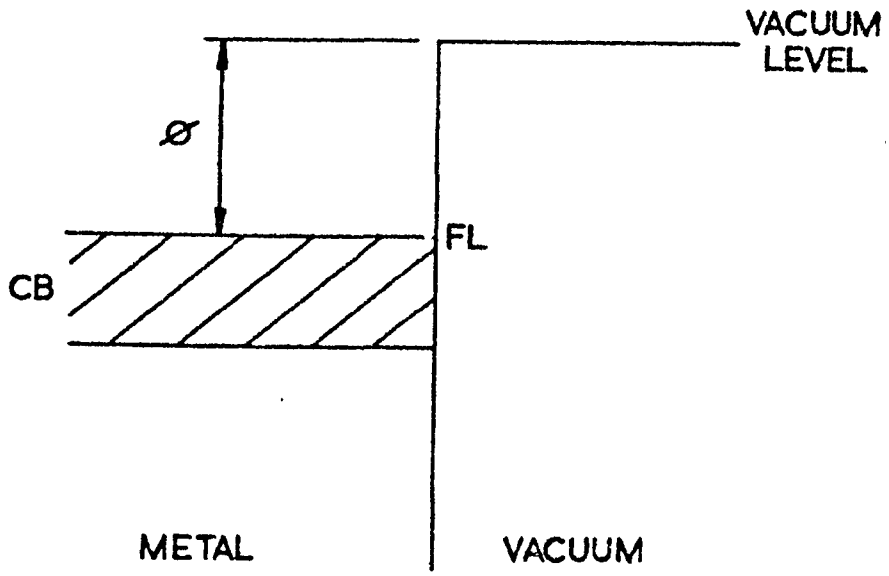

(b) A SEMICONDUCTOR SURFACE (n-TYPE)

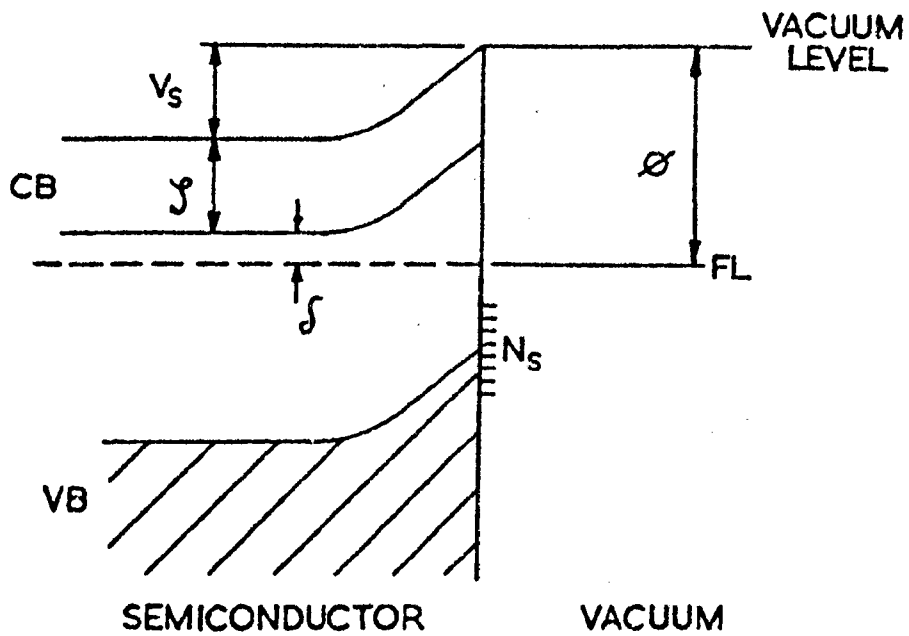

Figure 2.1 The work function ϕ in the electron band theory of solids for a metal and a semiconductor surface. FL, CB and VB are the Fermi level, conduction and valence band respectively.

where Φ_2 is the electrostatic potential at a point outside of the surface. The surface potential χ is defined by

$$\chi = \Phi_2 - \Phi_1 \tag{2.3}$$

and then ϕ is also defined by

$$\phi = -(\mu/e) - \chi \tag{2.4}$$

The work function is considered to consist of two components, the 'inner work function' μ and the surface potential χ*. Since χ may be expected to depend on the crystallographic orientation, equation (2.4) implies a similar dependence for ϕ also. The concept of χ arises from the physical discontinuity of the solid lattice at the surface where there exists an unsymmetrical charge distribution around the surface ions (Figure 2.3 and 2.4). The value of ϕ is dependent on temperature, since μ, $\bar{\mu}$, Φ_1 and Φ_2 may be dependent on temperature.

The thermodynamic definition does not depend on the validity of any theoretical description of the electronic structure of solids. In the electron band theory of metals, electrons are distributed in available electron states according to Fermi - Dirac statistics. The Fermi - level is defined as being the highest occupied energy state at absolute zero temperature. At finite temperatures, the probability of occupancy is a half. In this description, the work function is seen to be the minimum energy required to remove an electron from the Fermi-level to a point outside of the surface. The work function is conveniently shown on the electron energy band diagrams shown in Figure 2.1 (a more accurate description is given in Figure 2.4 discussed later in Section 2.5).

* Calculations by Bardeen show χ may vary from a fraction of a volt (for alkali metals) to as much as a volt for other metals but μ contributes at least 80% of the value of ϕ generally.

In the case of patchy surfaces, Herring and Nichols 1949 define the electrostatic potential Φ_2 outside of the i-th patch by a distance small compared with the scale of the patch

$$\Phi_{2,i} = - \bar{\mu}/e - \phi_i \qquad (2.5)$$

In the absence of any external fields, the potential attains a constant value $\bar{\Phi}_2$ at a distance which is large compared with the patch size. $\bar{\Phi}_2$ is given by

$$\bar{\Phi}_2 = \sum_i f_i \Phi_{2,i} = - \bar{\mu}/e - \bar{\phi} \qquad (2.6)$$

where f_i is the fraction of the surface occupied by the i-th patch. The electrostatic field outside of a patchy conductor falls off exponentially with the perpendicular distance from the surface when the patches are small in comparison with the surface curvature.

The definitions are also valid for semiconductors and insulators. The work function of an n-type semiconductor in the electron band theory is shown in Figure 2.1b. At the surface, localised energy states may exist within the forbidden energy gap. The occupancy of these states leads to a space charge layer, extending into the semiconductor bulk to maintain charge neutrality at the surface. The layer is named after its discoverer, Schottky. The height of the Schottky barrier, V_S is related to the density of occupied surface states, N_S, the depth of the layer, d the density of donors within the semiconductor n_o, and the dielectric constant κ by the equation

$$V_S = 2\pi n_o e d^2/\kappa = 2\pi e N_S d/\kappa = \omega N_S^2 \qquad (2.7)$$

where $\omega = 2\pi\epsilon/n_o\kappa$ and ϵ is the permittivity. The magnitude of N_S may vary from 10^{11} to 10^{14} cm^{-2}. The empirical time constants for the release and the capture of charge in surface states may vary from microseconds to several hours. The value of n_o is typically between 10^{14} and 10^{19} cm^{-3}. The work function of a semiconductor is defined by

$$\phi = V_S + \zeta + \delta \qquad (2.8)$$

where δ is the energy difference between the Fermi level and the bottom of the conduction band, and ζ is the conduction band width. Since V_S is dependent on the electronic state of the surface, ϕ may be sensitive to illumination, adsorption and electrostatic fields. The electronic description of semiconductor surfaces is reviewed by Bardeen and Morrison 1954, Plummer 1962, Wright 1966, Many et al. 1965 and by Frankl 1967.

2.2 Measurement

The techniques of measuring the work function and contact potential have been extensively reviewed. Herrman and Wagner 1951, Herrman 1955, Culver and Tompkins 1959, Eberhagen 1960, Hayward and Trapnell 1964, Jenkins and Trodden 1965, Kaminsky 1965, Gundry and Tompkins 1968 and Riviere 1970 describe and compare most of the methods. Many other review articles refer specifically to one or more of the different methods and these are cited below.

The methods naturally fall into two broad classes. The first includes the direct methods which involve the measurement and transport of charged particles into or from the surface. This class includes all the electron emission methods. The second is concerned with the indirect methods, some of which also involve charge transport in the vacuum space.

Direct measurements of the work function are made by photo-electric, thermionic or field excitation and emission of electrons. They are of special significance in the technical application of emission phenomena. Direct methods may only be used at low gas pressures if electron scattering or gaseous breakdown is to be avoided, and they also run the risk that the surface may be disturbed by photon or charged particle irradiation.

Thermionic emission (TE) and photo-electric emission (PE) methods have been reviewed by Dushman 1930, Hughes and DuBridge 1932, Becker 1935, DeBoer 1935, Reiman 1935, Herring and Nichols 1949, Wright 1953 and also by Nottingham 1956 in addition to the general reviews cited above. The thermionic method is unsuitable for low temperature studies and also for those substances which give no appreciable emission below their melting points. Technical problems may arise in the preparation of clean surfaces since thermal treatment alone is often insufficient. Photo-electric methods may require vacuum ultra violet techniques and the emission currents may be very small. Spurious photo-currents from other surfaces within an experimental system may be troublesome.

Field electron emission (FEE) methods have been reviewed by Good and Muller 1956, Gomer 1961, Ehrlich 1963, Hansen and Gardner 1968 and other discussions are given in the book edited by Uren 1970. The high electrostatic field strengths needed for measurable field electron currents from cold metals have technically limited the general application of FEE to sharp tips of the refractory metals.

Other direct techniques, which are less frequently used include the calorimetric method and the surface ionisation method. These are described in the general reviews above.

The direct class of contact potential methods is composed of two subclasses depending whether charge flows in the vacuum gap between the free surfaces of the metals in contact, or through their common electrical interface only.

One of the principal disadvantages of indirect methods is that an auxilary surface of known work function is needed for absolute work function measurements. A value of the reference surface is commonly inferred from the published literature. It is never certain, however, that the reference surface has the same work function as that measured in another experiment. These problems are further discussed in Chapter 4.

The indirect methods are discussed in the general reviews above and also by Patai and Pomerantz 1951 and by Gundry and Tompkins 1968. The emission contact potential methods are based on the

principle of the thermionic diode. The retarding potential or space charge limited regions of the diode characteristic may be explored to measure any change in the anode work function. Holscher 1966 and Haas and Thomas 1966 have refined the method allowing a detailed investigation of the work function distribution across a patchy surface. Other techniques in this group include the magnetron method due to Oatley and the electron reflection microscope method. The emission type of contact potential methods share the disadvantages of the direct techniques.

The second class of indirect methods include the static and dynamic capacitor methods. The static method allows only changes in the contact potential to be measured. The dynamic method enables both the change and the absolute magnitude to be determined. This method has the disadvantage, however, that mechanical vibration must be introduced into the vacuum system. The principal of both methods is similar and described in more detail in Chapter 4. These methods possess a general simplicity of operation and interpretation. They lend themselves to the study of a far wider range of metal-gas systems and throughout a wider range of temperatures and pressures than the emission methods. The dynamic capacitor method was the most suitable for the present application. The particular experimental form used is described in the third and fourth chapters.

2.3 Interpretation of Measurements

The surfaces of most solids experimentally prepared are not uniform. In general they are composed of an unknown number of crystal orientations, each of an unknown area and work function. The various methods of measurement may yield different numerical values of the measured work function. This is due to the fundamental differences between each in the excitation or transport of charge. Riviere 1970 has reviewed these problems.

In thermionic and photo-electric measurements, patch fields tend to suppress electron emission from the high work function areas. Consequently, the measured value is weighted towards the low work function patches. In the thermionic case, Herring and Nichols 1949 define two limiting cases, where the applied field is (a) much stronger or (b) much weaker than the patch field. If ϕ^* is the apparent work function of the ith patch, and w_i is the fraction of the total zero field current carried by the patch, then theory shows for case (a) that the composite work function ϕ^{**} is given by

$$\phi^{**} = \Sigma \; w_i \quad \phi_i^* \qquad (2.9)$$

ϕ^{**} is usually the quantity derived from the Richardson thermionic plot. Riviere 1970 discusses case (b) which yields a composite work function $\overline{\phi}^{**}$ some what larger than the arithmetic mean value, $\overline{\phi}$. The difference between ϕ^{**} and $\overline{\phi}^{**}$ is roughly equal to the maximum difference between the individual patch work functions. The thermionic

work function is also dependent on the applied field due to the Schottky effect. An extrapolation is needed to obtain the field free value.

Similar considerations as these apply to photo-electric and field emission measurements. Experimental considerations suggest the value of the work function derived from the total field current in the FEE method is close to the mean value $\bar{\phi}$ (Riviere 1970). The indirect methods also yield a composite value. The value derived in the case of the capacitor techniques is the true arithmetic mean value $\bar{\phi}$ defined by

$$\bar{\phi} = \Sigma f_i \phi_i \qquad (2.10)$$

where f_i is the fraction of the surface occupied by the ith patch of work function ϕ_i. The retarding potential and space charge limited indirect methods yield a value weighted towards the low work function patches which, for the latter, is almost the mean value. Experimental work, described below, suggests Anderson retarding potential method gives the mean value $\bar{\phi}$.

Riviere 1970 concludes that many of the emission measurements bear no simple relationship to the patch work function distribution or arithmetic average.

Only a few direct comparisons have been made between different methods with the same surface. An agreement within 20 mV or

less has been reported between measurements by the dynamic capacitor method and the photo-electric method (Glasoe 1931, Dillon and Farnsworth 1957). A similar agreement was found with the retarding potential method (Anderson 1952, Hopkins and Ross 1964) and also with the space charge limited diode (Mignolet 1950 and 1952). The retarding potential and photo-electric methods were also found to be in close agreement by Anderson 1938. These measurements refer to randomly orientated metal films. A close agreement may not occur for polycrystalline surfaces which possess a large patch work function distribution. Farnsworth and Winch 1940 have found a close agreement between the dynamic capacitor and the photo-electric methods for orientated metal surfaces. Hopkins and Smith 1968 have compared the dynamic capacitor and the retarding potential methods with differently orientated turgsten surfaces which were subsequently coated with films of barium. There was a clear disagreement between the values measured by each method for both pairs of surfaces. They showed that the differences could be accounted for by either a change in the electron reflection coefficient from zero to 0.6 for the coated surface, or if there had been a patch work function variation of 1.0 eV (in a two patch model).

The disagreement between Anderson and Hopkins and Smith may have been due to a different form of structures investigated by them. In one case these were randomly orientated thin films and in the other they were orientated surfaces. Lea and Mee 1968 have found the photo-electric and the dynamic capacitor to yield values of the work function of uranium films which were in close agreement. The electron

beam contact potential method, however, gave values higher than either of these for the surface investigated. This was probably due to a change in the electron reflection coefficient as uranium was adsorbed on tungsten.

2.4 Work Function of Pure Surfaces

2.4.1 Introduction

Numerous surveys of a review or bibliographic nature deal with the results obtained with specific methods. Thermionic emission measurements have been reviewed by Dushman 1930, Reimann 1934, DeBoer 1935, Herring and Nichols 1949, Wright 1953, Nottingham 1956 and Weissler 1956. Photo-electric measurements have been reviewed by Hughes and DuBridge 1932, DeBoer 1935 and Weissler 1956. Field emission measurements have been discussed by Gomer 1955, Good and Muller 1956 and by Gomer 1961. Hopkins and Riviere 1964 have reviewed reliable contact potential data. Wider surveys of the results of all measuring methods have been made by Michaelson 1950, Culver and Tompkins 1959 and Eberhagen 1960.

Many early measurements may not be representative of pure surfaces because of the difficulties of vacuum and experimental techniques. Riviere 1970 has reviewed and discussed the reliable measurements of the work function of the elements, alloys and compounds.

2.4.2 Polycrystalline Surfaces

Measurements of the work function have mainly been carried out with polycrystalline surfaces. Comparison of the data is complicated by the anisotropy and temperature dependance of ϕ, its sensitivity to contamination and also by the natural differences in the composite values measured with different techniques. The published values for any particular element may vary by up to a volt or more (cf. Michaelson 1950).

The work functions of the elements lie within the range from less than two to about six electron-volts. The alkali and rare earth metals form a group having the lowest values, of which the lowest is possessed by caesium. The other elements have a work function generally larger than three volts and platinum has the highest value of all.

The work function of oxides, nitrides and carbides and also the elemental semiconductors lie typically within the range for metallic elements (cf. Wright 1953, Riviere 1970). The work function of various glassy insulators has been measured to lie within the range from 4.5 to about 5.0 eV (Rohatgi 1957, Nelson 1963).

2.4.3 Effects of Structure

Real surfaces are generally far from uniform and they possess numerous defects of various types and differently orientated

crystallites (Menzel 1963). The structure of polycrystalline surfaces has an important effect on the work function measured by any of the methods as described in Section 2.3. The surfaces prepared at low temperatures are usually unstable and require annealing. At elevated temperatures, atomic diffusion may occur and the surface may recrystallise thus reducing the defect density and promoting the growth of larger grains. The relative contribution of non close-packed crystal faces decreases with the increase in grain size which accompanies recrystallisation.

Thin films formed by vapour deposition are often in a state of strain and possess a large defect density and small grain size. Sintering normally causes ϕ to increase by as much as a few tenths of a volt. The work function of gold and silver films may be less than that of bulk polycrystalline substrates of the same elements. The values become the same after annealing (cf. Chung and Farnsworth 1952).

The crystallinity and orientation of thin films may be influenced by the degree of preferred orientation and nature of the substrate. It may, therefore, directly influence the work function of a film overlay. The work function of silver films, for example, deposited onto single crystal faces of the same element have a lower work function than that of the substrate, even when they have the same structural properties as revealed by electron diffraction. The values become the same after annealing (cf. Clarke and Farnsworth 1952). Indirect measurements of thin metal films on glassy and different metallic substrates have also indicated a dependance of ϕ

on the degree of preferred orientation of the substrate (Hopkins and Riviere 1964).

The work function of thin films has, on occassion, been observed to be dependant on their thickness in the case of the elements Ag, Al, Au and Ur (Rauh and Thorn 1959, Garron 1962). A study by Fryla and Feldman 1962, however, failed to find any dependence with Ag, Au or Pt. These variations may be due to the effects of structure or contamination, among others.

Surface structural damage may be induced by energetic charged particles. The production of defects and occluded gaseous impurities in the target has been observed to cause changes in ϕ of several tenths of a volt (cf. Dillon and Oman 1963, Lawson and Carter 1968). The original surface is normally restored by annealing.

There have been few direct studies of the effects of bulk structural changes. Cardwell 1949 and Fry and Cardwell 1962 have observed unusual variations in the photo-electron emission of iron, nickel and uranium as the temperature was cycled through their transformation points. Paddock has investigated titanium and his results are discussed later in Chapter 6.

The inducement of strain in thin metal strips or films may also promote changes in the work function. Such effects are normally smaller than those of recrystallisation (cf. Wallis and Farnsworth

1951, Craig 1969). The cause of these effects is not certain but may involve changes in the defect density.

Linder 1927, Johnson and Shockley 1936 and Martin 1939 among others performed the first investigations of the anisotropy of thermionic and photo-electron emission from one point to another across bulk metal surfaces. The early work in this area has been reviewed by Herring and Nichols 1949.

The patch work function distribution of bulk samples of graphite and gold after various treatments was as large as 0.7V in the experiments performed by Parker and Warren 1962. The electron beam scanning retarding potential method has also detected spatial variations similar to those above (Haas and Thomas 1966). The work function distribution of a flashed tungsten ribbon was only 0.2V in comparison to variations as large as a volt for nickel, stainless steel and for various oxides. Hampson 1966 detected only a small spatial variation in the work function of Ni films on glass of less than 15 mV. The spatial resolution of his measurements however was poorer than that in either of the two experiments above.

2.4.4 Work Function of Alloys

The work on alloys is reviewed by Riviere 1970. The work function generally reflects the relative composition of the component elements and the phase diagram. Important differences may exist if intermetallic compounds are formed. In such cases, the composite

Face/ Method	110	111	112	113	116	100	01	013	122	123	233
FE	± 5.84 ± 0.15	± 4.40 ± 0.01	4.65 - 4.88	4.50	± 4.27 ± 0.05	4.71 - 5.00	4.34	± 4.34 ± 0.02	4.35	4.52	4.46
TE	± 5.30 ± 0.12	± 4.40 ± 0.03	4.80 - 5.24		± 4.30 ± 0.03	± 4.58 ± 0.08					
CPD	5.05 - 5.15			4.66 - 4.71		4.67					
SI	4.60 - 5.43	4.49	5.25								
FE		4.32		4.54							

TABLE 2.1 The work function (eV) of single crystal faces of tungsten (adapted from Riviere 1970). Mean values from several individual measurements are shown with an error limit. In other cases where insufficient values exist to determine a mean, the spread of values or individual determination is given. (S.I = surface ionization)

work function may lie outside of the range encompassed by the values of the individual elements themselves. Sachtler and Dorgelo 1965 in a study of the work function of copper-nickel film alloys, have found that stratified metallic layers may readily interdiffuse at room temperature. The work function of tungsten single crystal surfaces is only slightly disturbed by small concentrations of rhenium in solution (Abey 1968).

2.4.5 Work Function of Orientated Surfaces

Some of the earliest investigations on specific orientated metal surfaces were performed by Rose 1933 and Martin 1939. Experiments by Muller 1937 and by Mendenhall and deVoe 1937 with the field emission also supported the earlier evidence for the dependance of the work function on crystal structure. The early evidence is reviewed by Herring and Nichols 1949 among others.

Field emission microscopy has been widely used for the study of orientated surfaces. These measurements have been supported by others using alternative techniques which also provide a useful check on the validity of the theoretical models on which FE is founded.

Riviere 1970 has reviewed many of the measurements on single crystal faces. A summary of his results for tungsten is shown in table 2.1. The work function of the lowest work function planes is known most accurately. There is some disagreement between the FE results for the (110) face and for those by other methods. There is a comparative close agreement between these other methods. This

has led to the suggestion that one of the assumptions in the FE theory may not be valid for this plane.

Measurements have been made for individual faces of Ag, Cu, Fe, Ni, Mo and Ta. In the case of Mo, the work function of the (100), (110) and (111) faces encompassed the range from 4.10 to 4.85 eV.

Thermal imperfections in the surface of orientated surfaces may have a similar effect on the work function as discussed previously for polycrystalline surfaces (cf. Muller 1955).

There have not been many studies of the effects of structure on the work function of semiconductors. Indirect measurements have shown that the contact potential between the (100), (111) and (110) faces of Si is less than 0.2V. Similar measurements on the same faces of Ge yielded a contact potential of less than 0.1V. There is a wide variation in the values of the work function of about 0.6V for the (111) face of Si between different techniques.

2.4.6 Dependence on Temperature

Early measurements of the temperature coefficient are possibly unreliable because of the likely presence of temperature dependant contamination. These are reviewed by Becker 1935 and Herring and Nichols 1949. The temperature coefficient of metals is negative and of the order of 10^{-4} to 10^{-5} eV $^{o}K^{-1}$ (cf. Wilson 1966).

Measurements of the coefficient of low melting point elements is difficult because of their high vapour pressure. Field emission measurements on single crystal planes of tungsten indicate the temperature coefficient may be dependant on the surface structure (Van Oostrom 1963).

2.5 Surface Potential and Adsorption

2.5.1. Introduction

The change in the work function $\delta\phi$ of a clean metal surface when gas becomes adsorbed is loosely called the surface potential, SP. The adsorbate SP is really the change in the value of χ the surface potential of the metal substrate as defined in equation (2.4). The SP is negative when $\delta\phi$ is positive and positive if $\delta\phi$ is negative. The measurements of the SP of physically and chemically adsorbed gases on metals have been reviewed and discussed by Culver and Tompkins 1959, Eberhagen 1960 and by Gundry and Tompkins 1968. The differences between chemical and physical adsorption have been discussed by Young and Crowell 1962 and Haynard and Trapnell 1964.

The adsorption of gases in general displays a pronounced structural dependance and preference for specific crystal planes for any particular metal substrate (c.f. Hansen and Mimcault 1968). Many of the SP measurements have been made with polycrystalline surfaces and the results often vary widely for any particular gas-metal system. This may be due partly to the effects of impurities or to differences in the atomic structure of the metal surfaces. In the case of thin films the SP of gases has been observed to be dependent on the sintering temperature due to surface structural changes with the temperature (c f. Crossland

and Pritchard 1964, Delchar and Tompkins 1968).

2.5.2 Chemical Adsorption of Gases

The condensation of a chemically interacting gas normally proceeds via a weakly bound precursor state. Evidence for this has come from measurements of the sticking coefficient in which it has been found (for atomic states) to be almost independent of coverage over a wide range (c.f. H_2 on W, Tamm and Schmidt 1970). Chemisorption of oxygen, nitrogen and hydrogen on clean metals is normally dissociative and increases the metal work function. The work function typically increases linearly with coverage θ at first and then assymptotes to an equilibrium value near $\theta \simeq 1.0$ The SP shows a pronounced structural dependence, it may even change sign for some systems and also be temperature dependent. The SP of hydrogen for example at room temperature varies from -0.54 on the (100) plane to -0.30 eV on the (111) plane of tungsten, for the (110) plane the overall SP reached +0.14 eV (Hopkins and Pender 1966 and figure 7.16). Consequently it is difficult to assign typical values. However, for the primary adatom layer on transition metals at normal temperatures the SP may be typically between zero and -0.5 eV and -0.5 and -5.0 eV respectively for hydrogen and oxygen. For nitrogen the values lie between these ranges. Exceptions to these ranges may be frequent however.

When a non-metallic molecule or atom is adsorbed on a clean metal surface it forms chemical bonds with the metal atoms in the neighbourhood of the adsorption site characterised by a binding energy. A number of different states may exist even for a given gas adatom and metal crystal plane each characterised by a particular binding energy.

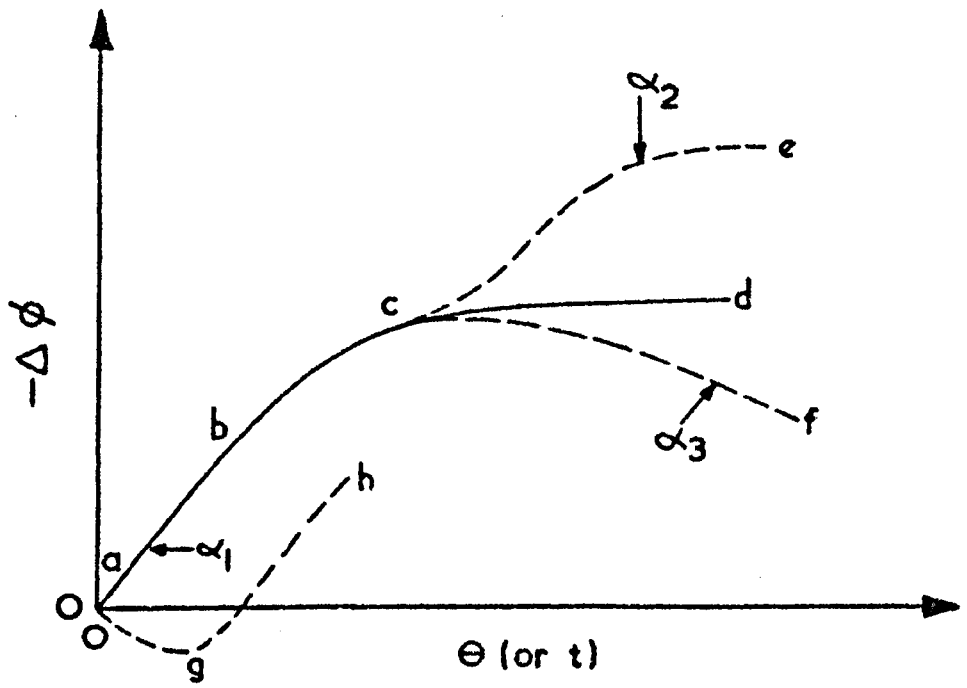

Figure 2.2 Diagramatic illustration of the various forms that the SP ($-\Delta\phi$) isotherm may take as a function of coverage θ or exposure time t to an adsorbing gas such as O_2, N_2, H_2 or CO on a clean metal surface. Typically SP α θ at low coverage (a-b) and assymptotes to a stable value (c-d) resulting from adatoms in a single state α_1. If other states exist (α_2, α_3) the SP isotherm may change curvature, the direction being dependent on whether the state is electronegative (α_2) or electropositive (α_3).

Similar or different states may exist for other crystal faces of the metal. The adatom population of each state is temperature dependent among other factors. Generally the magnitude and sign of the SP is dependent on the adatom population and may vary from one state to another. Evidence for the existence of multiple binding states for hydrogen on tungsten single crystal planes and on other transition metals has been given by Delchar and Tompkins 1968, Adams et al 1970 (among others). Multiples state of nitrogen on tungsten are discussed below.

The general characteristics of the SP isotherm are shown in figure 2.2. In the case of hydrogen the SP has been observed to vary linearly with coverage θ (or exposure time) over a wide range of θ on the single crystal planes of tungsten and other metals (c f. Boudart 1952, Estrup and Anderson 1966, Hopkins and Usami 1970). For oxygen and nitrogen an initial linear variation has also been observed but typically over a smaller fractional range of coverage than for hydrogen (Boudart 1952, and Kisluick 1961 and Hopkins et al 1971 report examples for O_2 on Pt and W(110) and for N_2 on W(310)). Becker 1955 has given several examples of changes in the curvature of the SP versus coverage plots for O_2, N_2 and H_2 on the crystal planes of W (curve ace in figure 2.2). Similar results have recently been reported for hydrogen (Adams et al 1970) and oxygen (Hopkins et al 1971) on the single crystal faces of W. These results have been interpreted as due to adsorption in multiple binding states (α_1 and α_2 in the diagram) on the surface having different dipole moments and adatom (or admole) population. Adams et al above combined flash desorption and LEED to investigate the kinetics of the states. Dissociative adsorption may also occur at very low temperatures and also results in a negative SP (c f. Hopkins et al 1967, Delchar and Tompkins 1967 and 1968).

The adsorption of nitrogen on tungsten has been extensively studied (c.f. Delchar and Ehrlich 1965, Clavenna and Schmidt 1970, Adams and Germer 1971 among others) and illustrates the diversity of adsorption phenomena on single crystal faces. At room temperature nitrogen is not adsorbed on the smooth (110) face. At lower temperatures a weak γ state is populated. The SP of γ-nitrogen was small and positive. On the (100) face two weak γ states existed but the SP of adatoms in these states had an opposite polarity. N_2 was also adsorbed on this face in a strongly bound β state which resulted in a positive SP of +0.4 eV. On the rougher (111) face N_2 was adsorbed into two strongly bound states (α and β) each resulting in a negative SP. A weak γ state also existed for the (111) associated with a small positive SP. The dipole polarity of the β state is apparently dependent on the roughness of the substrate plane. A similar complexity has been found for other systems which have been studied in detail (c.f. N_2 - M_o, Abon and Teichner 1967, Hayek et al 1968).

There have been frequent reports of a positive surface potential for oxygen, nitrogen and hydrogen adsorbates on many clean metals. These have generally taken two forms: in the first the normal negative SP changes slope and increases with further exposure i.e. the work function of the composite surface decreases (curve acf in the diagram) second (and less frequently reported) the work function of the clean metal surface initially decreases on exposure and subsequently increases normally as expected (curve agh in the diagram). Positive excursions of the SP have been suggested to be due to:

(a) weakly bound electropositive states
(b) penetration of an electronegative adatom below the surface electronic plane so that the direction of the dipole moment is such as to reduce the work function

(c) rearrangement processes between the metal surface atoms and the adatoms.

Weakly bound electropositive states have been reported for nitrogen on tungsten as discussed above. They have not been reported apparently for oxygen except recently for the W(110) plane (Hopkins et al 1971). In the latter system at room temperature two electronegative states (α,β) were sequentially populated causing a change in the curvature of the plot of SP versus exposure (curve ace). The β state was temperature dependent and required an activation energy. At low temperatures it was not observed and instead the α state and a weakly bound γ electropositive state were observed (curve acf). The γ state was interpreted as physisorbed molecular oxygen. For hydrogen, electropositive states have been reported on Mo (Abon and Teichner 1967), W (Hopkins et al 1967 , Adams et al 1970), Pt (Rootsaert et al 1962, Lewis and Gomer 1969) and also for N_i (c.f. Lichtman et al 1968). In particular Crossland and Pritchard 1964 and Delchar and Tompkins 1968 have measured the SP of hydrogen on nickel films. At 90 and 300^{o}K molecular hydrogen was dissociatively adsorbed on the clean metal into a primary electronegative state giving rise to a negative SP (c.f. curve abc in figure 2.2). When further gas is adsorbed the SP changes positively (c.f. curve cf in figure 2.2) due to the population of a weakly bound molecular and electropositive state on top of the primary adatom layer. The magnitude of the positive excursion increased with the pressure and inversely with the temperature. The reduction in ϕ became so large in some cases that the value of the clean metal surface was obtained. When the supply of gas was reduced, the positive increment decayed and this was interpreted as due to migration of the weakly bound adsorbate to the inner pores of the film. This led Delchar and Tompkins to suggest that the

main cause of the concavity of the curve of the SP versus coverage was due to the distribution of adsorbate between the outer and inner surfaces of the film and not apparently to depolarisation effects in the outer adlayers.

Positive surface potentials arising from causes (b) and (c) above have not been reported for hydrogen since in the latter case there is little evidence for surface rearrangement in adsorption (c.f. Delchar and Ehrlich 1968 using SP measurements and others discussed below). In the case of oxygen, however, several cases are known where the initial exposure of the clean metal to the adsorbate reduced the work function at low coverage and afterwards increased (c.f. curve agh in figure 2.2) with further exposure c.f. O_2 on T_a (110) (Fehrsand Stickney 1967), on Ur films (Riviere 1964) and on Aℓ films (Roberts and Wells 1969) at room temperature. Similar effects have been reported for I_2, Cℓ, Br and F on transition metals (Burshstein and Shurmovskaya 1964, Duell et al 1966, Fehrs and Stickney 1969 and cited works). Jowett et al 1969 and Jowett and Hopkins 1970 have reported similar results for the halogens on the single crystal faces of W where both the magnitude and sign of the SP was dependent on the surface structure. The common explanation of these positive SP effects at low coverage has been penetration of some of the electronegative adsorbate below the surface (case (b) above). In the case of the halogens, however, it has been pointed out (Sargood et al 1970) that this explanation is not consistent with the SP results for single crystal plane substrates . Polarisation has also been suggested (Sargood et al 1970) but estimates of this effect have shown (Jowett and Hopkins 1970) that it cannot account for the structure anisotropy. The latter authors have shown that the appreciable anisotropy of the dipole moments with surface structure is not easily explained by dipole lengths or differences in the

dipole density. They suggest that charge transfer processes and changes in the degree of smoothing of the electron distribution in the surface plane (the Smolochowski effect discussed later) due to the adsorbate should be considered. In the case of O_2 on Ta above Fehrs and Stickney also discussed the evidence for reconstructional processes (case (c)) at low coverage.

Transient positive excursions of the negative SP of chemisorbed oxygen have been frequently reported at higher coverages due to reconstructional processes (case (c) above). Quinn and Roberts 1964 reported transient positive decays in the negative SP when doses of oxygen were introduced to several metal film surfaces. For any particular metal the magnitude and rate of decay of the positive transient typically increased with the temperature and also with the magnitude of the negative SP (i.e. the adsorbate density or coverage). The coverage at which the positive decay first became apparent typically reduced with increasing temperature. These effects occurred at 300°K for Ni and Cu and even at very low temperatures for Fe and Cr. The transient was not generally observed with Mo however. The ease of incorporation for an oxygen adatom was found to be Fe > Cr > Ni > Cu > Mo. Similar results have been observed for Ni by Delchar and Tompkins 1967 between 77 and 273°K who also give a detailed analysis if the incorporation of O by Ni and also for Aℓ and Pb (Roberts and Wells 1967, 1969). These results have been generally interpreted as due to time dependent place exchange or substitutional diffusion surface processes between oxygen electronegative adatoms on the outer metal surface and metal atoms in the surface. For Aℓ and Ni the activation energy for this process was apparently very small < 3 and ∿ 7 Kcal mole $^{-1}$ respectively. In most of the above cases it occurred for a coverage $\theta < 1.0$.

This interpretation is supported by the fact that positive transients were also induced by heating the surfaces covered with electronegative oxygen which also regenerated fresh electronegative sites on the surface, indicating that the surface oxygen had become incorporated into the metal. Recently Delchar 1971 has reported similar effects for the (110) and (100) faces (but not the (111) face) of Cu which were consistent with the known features of reconstruction from other LEED experiments. Huber and Kirk 1967 (and cited work) have also studied the oxidation of Aℓ with SP measurements but concluded that incorporation did not occur until $\theta > 1.0$ in disagreement with Roberts and Wells. They contended that an impurity was responsible for the positive transients observed by the latter authors. However this suggestion may not easily account for the regenerative effects observed. Positive surface potentials of oxygen have been reported for other metals, viz.W(Duell et al 1966, Zingermann and Ischuk 1967) Fe (Burshstein and Shurmovskaya 1964, Kobayashi and Kato 1969), Ti (Klemperer 1962) and Ur (Riviere 1964). In most of these the amount of gas adsorbed corresponds to many monolayers and hence the reduced work function may be simply that of the oxide.

Roberts 1970 has recently reviewed the experimental evidence from LEED and other methods for the incorporation of adsorbed gases (mainly for oxygen) into metals and Horgan and King 1970 present further evidence for O_2 on Fe, Ni, M_o and W surfaces. For oxygen and nitrogen experimental evidence exists for these processes even at very low temperatures (c.f. May 1965, Germer 1966, Haas 1968 and Roberts 1970). Because of the low scattering power of electrons, hydrogen has not been so widely studied with LEED and interpretation of the patterns is difficult. However, it appears that reconstruction is not so frequent with H_2 as far O_2 and N_2 although on some surfaces it is known to occur (i.e. Ni (110), May 1965,

Estrup and McRae 1971). May and Germer 1968 have investigated with LEED the formation of oxide layers on Ni (110). Oxygen initially diffused directly into the lattice interior leaving the surface sites vacant until the bulk concentration had become sufficiently high when a surface oxide phase was precipitated. Direct diffusion into the bulk occurred at less than 500°K and under certain conditions reconstruction occurred on initial adsorption of oxygen even at 300°K. There have been few combined LEED and SP measurements of the adsorption of gases. Farnsworth and Hayek 1967 and Hayek et al 1963 for example have used both LEED and SP measurements to study the adsorption of oxygen on M_o at 300°K. On the (110) face the initial adsorption of oxygen resulted in an ordered structure with zero SP, further adsorption beyond a coverage $\theta = 0.25$ produced another structure which resulted in a negative SP. The adsorbate layer was disordered at full coverage $\theta = 1.0$ and for $\theta > 1.0$ the SP was constant. Adsorption at high temperatures under certain conditions produced ordered structures and zero SP. These effects have been interpreted as due to place-exchange processes in which only the outer adsorbed layer (and not apparently the subsurface layer of oxygen) produced any change in the work function. At low coverage the oxygen adatoms diffused directly into the subsurface region leaving the metal work function undisturbed. Similar phenomena have been observed in surface potential measurements of oxygen on transition metals at higher temperatures (c.f. Zingerman and Ischuk 1967, Bassett 1968).

Only a few measurements of the SP of water vapour have been reported. For tungsten and platinum surfaces the SP is negative and approximately the same magnitude as for oxygen (Jowett et al 1969, Sargood et al 1970). The adsorption of water on clean tungsten surfaces is

is dissociative and is commonly viewed as the formation of atomic hydrogen and OH radicals bound by the oxygen atom at low coverage. At higher coverages, the adsorbed hydrogen adatoms are apparently replaced by further OH radicals and molecular hydrogen is desorbed. The surface potential of carbon monoxide is typically negative on transition metals. Multiple binding states have been reported for CO as for other gases with a variation of the SP of the adsorbate in each state (c.f. Klein 1970, Mathews 1970) on many metals but adsorption of CO is not accompagnied by reconstructional processes apparently.

In summary, the variation of the SP with coverage of a gas on a clean metal surface may arise from complex processes even at normal and constant temperatures. In the case of O_2 and N_2 the concavity of the SP isotherm (c.f. curve ad in figure 2.2) may be due to the competing processes of simple adsorption on the metal surface, diffusion into the metal and structural rearrangements between the adatoms and the metal surface atoms (as recently suggested for O_2 on Ni, Delchar and Tompkins 1967). In the case of H_2 and CO the SP isotherm may be the result of simple adsorption into several states on the outer metal surface and the depleting process of diffusion (for thin films) from the outer to the inner surfaces of porous metals. In addition, direct interstitial diffusion may also occur for hydrogen adatoms into metals such as Zr, Ti and Pa which have a large solubility for hydrogen. The SP variation with coverage may therefore show a complex behaviour with temperature and surface structure.

2.5.3. Physical Adsorption of Gases

The SP resulting from physical adsorption of gases on metals is positive. Although the adsorbate-metal bond may be weak the SP may be very large and vary significantly with the surface structure. The SP of Xe for example varies from +0.9 to +2.4 eV among different single crystal planes of tungsten (Engel and Gomer 1970(b)). Similarly Palmberg 1971 reported a value of +0.9 eV for the SP of Xe on Pd. For a given crystal plane the SP may vary widely for different adsorbates. Engel and Gomer reported values of +0.46, +0.83 and +1.13 eV for the SP of Ar, Kr and Xe respectively on the W(100) plane. Similar variations were observed for the other planes of W studied. Rootsaert et al 1962 have also given evidence for a structural dependence of the SP on the planes of tungsten. Culver and Tompkins 1959 review the early results for a number of adsorbates and metals by Mignolet and others.

Molecular physisorption (or weak chemisorption) may also occur on metal surfaces and result in a positive surface potential. Some examples of these were given in the preceding section. In addition carbon monoxide is physically adsorbed on clean copper, silver and gold surfaces resulting in a positive surface potential (Culver et al 1957). Recently Delchar 1971 has reported negative values of the SP of CO on various single crystal faces of Cu at room temperature and below.

2.5.4. Adsorption of Metals

The SP of the alkali metals has been extensively studied on transition metals. The SP is positive and increases with increasing coverage θ. It typically reaches a maximum value before decreasing

slightly and subsequently becomes almost independent of the quantity adsorbed. The plateau value is attained near the point where $\theta = 1.0$. The SP of alkali metals on W may be as large as +3.0 eV. FEE experiments with single crystal faces of metals have shown a pronounced sensitivity of the SP on the work function of the adsorbing crystal plane (Ovchinnikov 1967 and 1968, Ovchinnikov and Tsarev 1968, Voronin 1968). In the K-W system for example the maximum and plateau values of the composite work function ϕ for a particular crystal plane are linearly dependent on the value of ϕ for $\theta = 0$. Similar results are found for Cs, Na and Sc on Rh and W. These results infer that the SP for a given system is directly proportional to the adsorbent plane work function (for $\theta = 0$) and that the constant of proportionality varies from one system to another.

Many of the important features of the structural arrangement of alkali adatoms on metal surfaces and their relationship to the surface potential have been unknown. Macrae et al 1969, Chen and Papageorgopoulos 1970, Fedorus and Naumovets 1970 and Gerlach and Rhodin 1970 (among others) have recently investigated with LEED and SP measurements the structure of alkali metals on tungsten and nickel. For Cs on W it appears that the minimum in the work function curve with coverage is associated with the formation of a definite two dimensional structure of the ionic adsorbate while successive layers have a metallic hexagonal close packed structure. Structural rearrangement between the surface atoms and the adsorbate apparently does not occur (at least for Ba on W, Frank and Schmidt 1968). The SP variation with coverage for other metals has not been extensively investigated. Recently Anderson and Thompson 1971 have measured the variation of the work function of tungsten and rhenium with the coverage of titanium. The form of the SP versus coverage curve was similar to that

of the alkali metals. Adsorption of metals other than the alkali metals may be complex and involve alloying or structural rearrangement with the substrate (c.f. May 1965, Taylor 1966, Collins and Blott 1968).

2.5.5. Adsorption on Non-Metals

The surfaces of semi-conductors and insulators and adsorption of non-metallic atoms and molecules has been reviewed and discussed by Plummer 1962, Volkenstein 1963, 1967, May et al 1965 and Frankl 1967. According to popular views (c.f. Kisselev 1967) a neutral gas molecule (or atom) becomes initially physically adsorbed according to the laws of physical adsorption. Physical adsorption may apparently cause a significant change in the work function ϕ of the substrate. The work function and surface potential are related to the Schottky barrier height V given in equations (2.7) and (2.8). On semiconductors, physisorbed adatoms (or molecules) may have dipole moments several orders of magnitude larger than expected from those on metal substrates. The surface barrier height V (and subsequently ϕ) may also be changed due to the adspecies disturbing the recombination rate parameters of electrons and holes at the surface. Some of the neutral adsorbate may become "electronically adsorbed" by charge capture from the conduction and valence bands of the substrate thus changing the density of surface states at the vacuum - substrate surface and subsequently also V and ϕ. The localised and trapped charge on the adspecies may also affect the recombination rate parameters. Adsorption of an electronegative gas such as oxygen is depletive since as the concentration of O^- ions (or O_2^-) increases so V increases thus reducing the supply of electrons and the rate of conversion of $O \rightarrow O^-$ (and similarly for O_2). The concentration

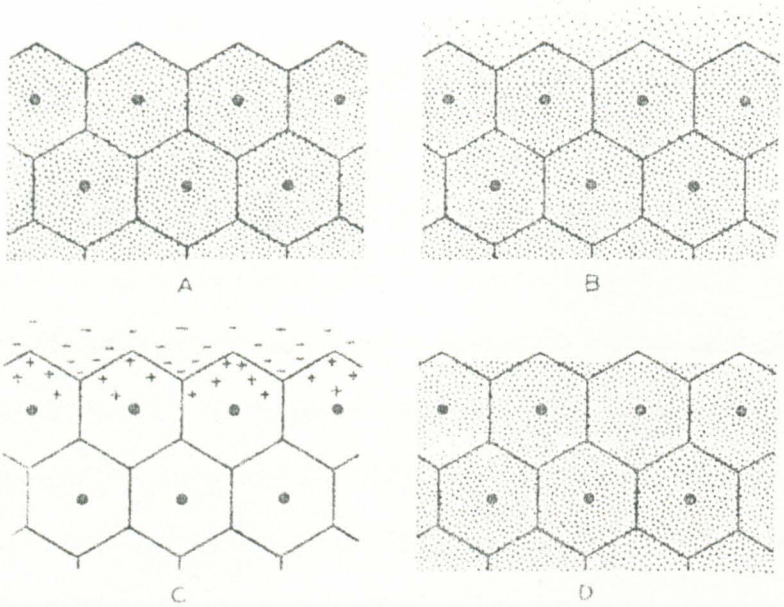

Figure 2.3 Formation of a double layer at a metal surface by spreading out of the electron distribution. The density of the stipling represents the time average of the electron density, the dots represent the centres of the atoms and the hexagons represent the unit cells. A: electron distribution as it would be if the charge distribution about the surface atoms were the same as that about the interior atoms, no spreading or smoothing of the distribution. B: actual distribution, complete spreading and partial smoothing. C: charge density for B minus A, equivalent to a double layer. D: illustration of complete smoothing and no spreading of the distribution. (Herring 1952).

of electronically adsorbed gas is consequently small and typically a fraction of a monolayer although very large changes of ϕ ($\sim$ volts) may occur during adsorption. Hydrogen and water vapour are normally found to be donor adspecies and lead to a reduction of V and ϕ. The quantity of "electronically adsorbed" gas and the changes in ϕ are partly determined by the kinetics of charge transfer from the bulk to the surface of the substrate. Volkenstein 1963 and 1967 has developed an electronic theory of adsorption on semiconductors. The SP in this type of adsorption is often sensitive to illumination due to photo-induced changes in the density of states at the surface. Adsorption or desorption may be induced with corresponding changes in the SP.

In the case of insulators the thermal equilibrium concentration of free electrons is much less than that of semi-conductors and electronic chemisorption may not spontaneously occur except in the presence of external irradiation.

2.6 Theoretical Description

2.6.1 The Work Function

The work function ϕ of a metal surface is normally viewed as being formed by two parts: the inner work function and the surface potential (c.f. equation 2.4, section 2.1). The former is a volume contribution determined by bulk metal properties and it is unaffected by the surface conditions. X arises from the surface double charge layer which is a consequence of the extension of the free electron charge distribution beyond the surface atomic plane. The spreading out occurs because it lowers the electron energy. The formation of the double layer is shown in figure 2.3. In this figure A shows the electron distribution as it would be if the

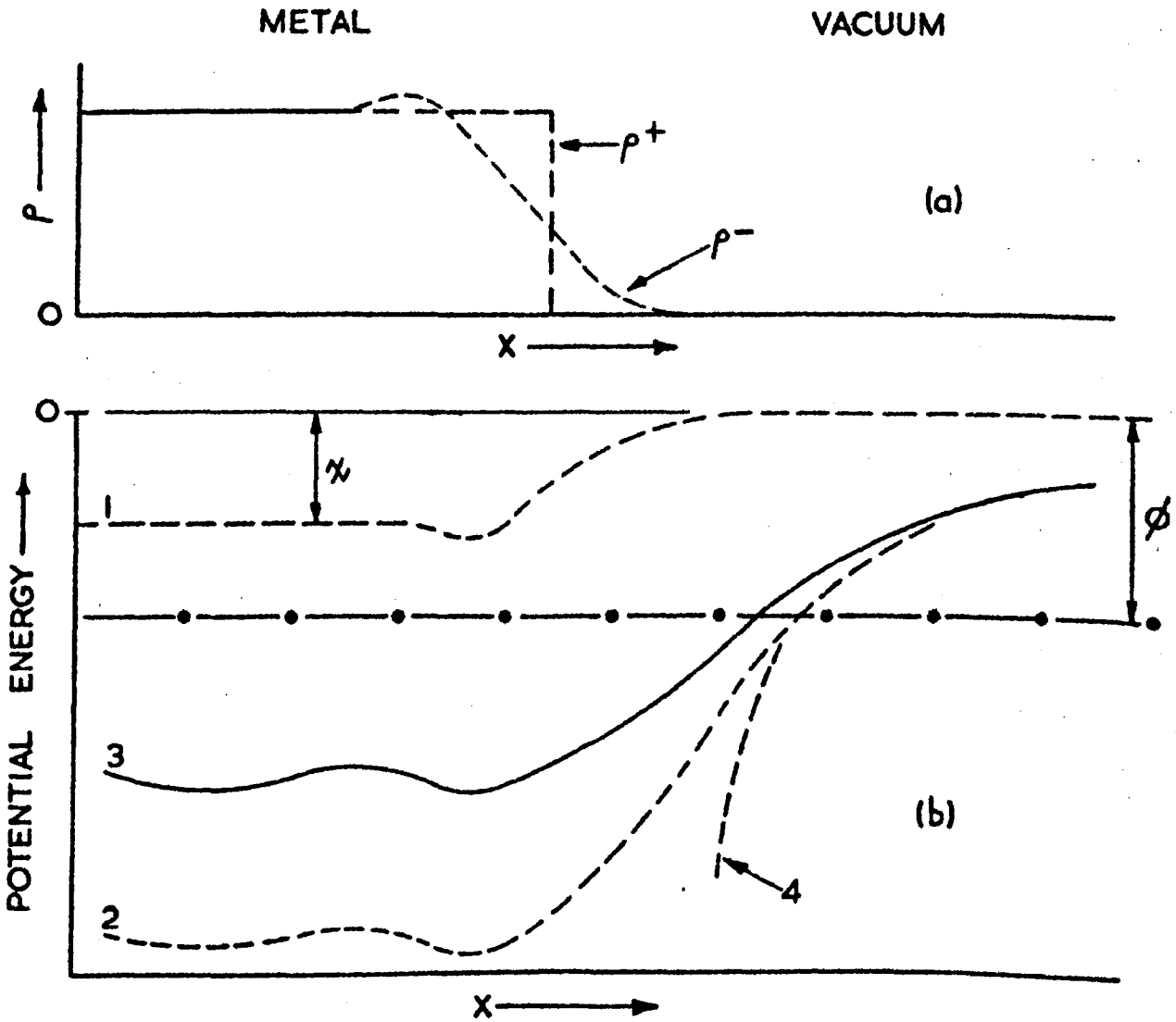

Figure 2.4 Schemmatic potential energy diagram for a simple one dimensional metal surface of (a) densities of electronic and positive charge density (b) the various contributions to the effective potential energy of an electron for (curve 1) the electrostatic double layer, (curve 2) potential energy of a classical point charge, (curve 3) potential energy of a moving electron and (curve 4) the image potential. The oscillatory structure predicted by Juretschke is shown in curves 2 and 3.

charge distribution about the surface atoms were the same as in the metal bulk, B shows the actual distribution and the difference between A and B is shown in C. The variation of the charge density across the surface and the potential variation due to the double layer is shown in figure 2.4.

There have been several attempts to find a correlation between the empirical work functions of the elements and their atomic and chemical properties (c.f. Michaelson 1950, Gordy and Thomas 1956 and cited references). Varley 1960 has deduced a semi-empirical relationship between the experimental work functions and a theoretical value of the Fermi energy for a simplified model in which surface structural effects (and electron-electron interactions for monovalent metals) were assumed negligible. The empirical data on which many of these have been based is generally unsound and they have a reduced importance due to the development of other theories (c.f. Herring and Nichols 1949).

The theoretical concepts and models have been reviewed by Herring and Nichols 1949 and Herring 1952. The theoretical description of the work function dates back to Bardeen in 1930's (among others). The surface barrier to an electron moving within the metal and across the surface into the vacuum is schematically shown in figure 2.4. The barrier for a uniform metal surface is composed of three parts (a fourth due to the Smolochowski effect is discussed later). The first is the classical electrostatic potential barrier due to the positive charge density and the time average of the density of negative electron charge as shown in figure 2.4. Within and close to the metal surface short range exchange and correlation quantum interaction potentials make an important contribution but rapidly diminish in importance as the distance from the surface plane increases.

Thirdly, at larger distances from the surface the potential barrier is almost entirely due to the classical image potential arising from the electrostatic interaction between a classical test charge and its induced image in the surface plane of the metal. The classical image potential $V(x) = -e^2/4x$ breaks down at short distances from the surface where quantum interactions become significant, as shown by Bardeen (but appreciated long before this by Langmuir and others). The internal potential is assymptotic to the image potential outside of the surface as shown in figure 2.4.

Estimates of the surface potential were made by Bardeen who showed that χ may only constitute a small fraction of the total work function and for a complete calculation of ϕ the other factors must be considered. These calculations are quantum mechanical in nature and consequently have been based largely on one dimensional simplified models of uniform metal sufaces largely neglecting the effects of anisotropy of the crystalline structure of metal surfaces. The exchange potential essentially accounts for a spin dependent repulsion between electrons of like spin due to the exclusion principle. The correlation potential arises from the polarisation of the electron distribution due to a lack of statistical independence of the positions of the electrons (even for anti-parallel spins). Both of these effects result in a screen of the field of any one electron (tending to keep other electrons away). This causes a local charge deficiency about an electron (often termed an exchange hole) which accompanies the electron in its motion through the lattice. Consequently the potential of the electron is reduced from the value of the classical electrostatic potential within and close to the metal surface (curve 2 in figure 2.4) for a

classical (static) test charge. The motion of free electrons produces a further reduction in the potential (which is dependent on their energy) since the polarisation charge around a moving electron does not have time to adjust itself (unlike a classical charge). When this is taken into account curve 3 in figure 2.4. results which also assymptotes to the image potential.

Bardeen, in his model, considered a fixed distribution of uniform positive charge and a system of neutralising negative charge. Using an estimation for the correlation interaction potential he arrived at a theoretical value of the work function of sodium in close agreement with the experimental value. He showed that the surface potential was largely due to exchange and correlation forces rather than ordinary electrostatic forces. This conclusion has often been stated to be true for all metals by others. Smith 1969, however, as discussed later below has shown that for many metals this may not be the case although it may be true for Na. The shape of the potential barrier at the surface has an important consequence on theoretical models of internal electron reflection and field emision. The distance from the surface x_o at which the classical image law breaks down is typically a few angstroms (for Na). Bardeen and Sachs and Dexter 1950 have made estimates of x_o. Juretschke 1953 extended Bardeen's model for Na by including the effects of the (average) exchange potential. The SP exhibited a distinct oscillatory structure as a function of the distance from the surface (c.f. figure 2.4). Similar results using more refined calculations and including the effects of correlation were obtained for Na by Loucks and Cutler 1964. The calculations for Na above excluded the surface dipole potential which did not contribute to the work function significantly (for Na). Similarly Davies 1968 and Gadzuk 1968 have also investigated the effects of

correlation on the surface barrier of N_A. These authors used different analytical methods but also arrived at similar conclusions to Juretschke apart from differences in the degree of damping of the oscillatory structure.

Smith 1969 has recently calculated the surface potential of twenty six elements using the free-electron model of a plane uniform metal surface. For some metals, including sodium, the surface potential was largely composed of the exchange and correlation potentials substantiating Bardeen's earlier conclusions. For most metals, however, the ordinary coulomb potential barrier was a significant fraction of the surface potential in contrast to the case for sodium. There was a reasonable agreement between the theoretical and experimental values of the work functions. The deviation of the latter from the former was within the range conceived for the effects of crystallographic orientation on the experimental values.

Smolochowski 1941 has made the only attempt apparently to calculate the effects of surface atomic structure on the work function. He considered a simplified model which included only the coulomb potential and ignored the exchange and correlation potentials. The spreading of the charge distribution perpendicular to the surface plane did not vary very much with the anisotropy of the structure. Negative charge tended to accumulate in the troughs between atoms in the surface plane thus smoothing out the contours of constant electron density. The degree of smoothing varied appreciably with the atomic structure and effectively produced a negative contribution to the surface potential thus reducing the work function. The degree of smoothing typically increased with the atomic roughness of the surface and as the atomic packing density decreased. Some extreme cases of smoothing are shown in figure 2.3. There is no smoothing in case A and

partial and complete smoothing in cases B and D respectively. Smolochowski's theory (although for an idealised surface) predicted a tendency for the surface atoms on a dense plane to have a higher work function than those on an open plane. Measurements of the work functions of the single crystal planes of copper and tungsten are consistent with these predictions (c.f. Delchar 1971).

The potential barrier for non-uniform surfaces includes an additional factor to account for the non-uniform distribution of the image charge which modifies the classical image force at large distances x from the surface. Periodic irregularities of atomic dimensions may disturb the ideal classical image potential at small distances. The correction factor is typically a few per cent and becomes vanishingly small for $x >> 2A^{o}$ (Modinos 1967). For larger macroscopic irregularities the image potential may be reduced by a significant fraction (Lewis 1954) but the patch electrostatic field associated with the irregularity compensates for the disturbance leaving the barrier shape unaffected (Morant and House 1956).

The theory of the temperature dependence of the work function of clean metal surfaces has been reviewed by Herring and Nichols 1949. Jain and Krishnan 1954 have further discussed the theoretical problem for monovalent metals. The major factors are the thermal expansion of the lattice and the thermal agitation of the atoms in the lattice which cause a temperature dependence of the inner work function and the surface double layer moment. The various effects predicted from simplified models cancel one another resulting in a very small temperature coefficient of the work function in agreement with the experimental evidence. Recently Hopkins et al 1969 have determined the values for a foil and the (110) and (100) faces of W. The variation of the coefficients with surface structure was

consistent with the expectation of a major contribution from the temperature dependence of the smoothing of the electron distribution in the surface due to the Smolochowski effect.

A theoretical explanation has been given by Tinder 1968 of the change in work function due to stress in which the Fermi level was shown to be dependent on elastic strain. Experimental results on the positive-ion and thermionic emission from heated Fe filaments are apparently in qualitative agreement with the theory (Antypas and Tinder 1968). Craig 1969 has given a discussion of the theories and experimental work on stress induced changes in the work function of metals.

2.6.2 Surface Potential

A non-metallic molecule such as O_2, N_2 or H_2 is normally spontaneously and dissociatively adsorbed on clean transition metal surfaces. Recently Avoird 1969 has treated the problem with a quantum mechanical perturbation theory for hydrogen on transition metals in a simplified model in which the activation energy for dissociation was shown to be very small. A non-metallic atom chemisorbed on a clean metal surface makes chemical bonds with neighbouring metal atoms surrounding the adsorption site. Qualitatively, the number of bonds depends on the size of the adatom and the lattice spacing. The chemical bonds between oxygen or nitrogen and a metallic surface are normally covalent. For hydrogen the field of the proton core is screened by the metallic conduction electrons and the bond is essentially metallic in character or of the resonating covalent type of Pauling. Culver and Tompkins 1959 and Gundry and Tompkins 1968 discuss the experimental evidence and the characteristics of the bonding between metals and non-metallic adsorbates. These bonds have a certain degree of ionicity and possess a

dipole moment. The component M_o perpendicular to the surface may be negative or positive if interstitial adsorption occurs. The latter may be the first stage of solution.

The classical surface potential model assumes that the image force is valid and that the electrical image of the charged adatom on the metallic conducting surface constitutes a dipole. The polarity of the dipole depends on the direction of charge transfer between the adatom and the surface and the position of the adatom in respect to the surface plane. For alkali metal adsorption negative charge is transferred to the metal, the dipole moment is positive and since the adion is adsorbed on the outer metal surface the work function is reduced. In a simple model of an electronegative adatom of oxygen or nitrogen adsorbed on the outer metal surface the dipole moment is negative since negative charge is transferred effectively to the adatom and the work function increases. Clearly in either case a dipole of opposite polarity results when the adatom penetrates below the electronic plane and the direction of change of work function is then reversed. If the outer metal surface becomes covered with $\sigma = \sigma^o\theta$ atoms cm^{-2}, θ being the fraction of the total number σ^o of sites available per cm^2 then a surface double charge layer is formed. If the dipoles are non-interacting then $M_o = qd$ where q is the charge on the adatom and d is the effective length of the dipole. According to classical electrostatics an electron experiences a force $F = 4\pi\sigma qe$ inside the double layer and since $Fd = 4\pi\sigma qed = 4\pi\sigma^o e M_o\theta$ then the change in work function $\Delta\phi$ is:

$$\Delta\phi = 4\pi e\sigma^o M_o\theta \qquad (2.11)$$

The correctness of this equation depends on the assumption that the dipoles are non-interacting. This depends on the values of M_o and the adatom polarizability α . At low coverage the prediction that $\Delta\phi \propto \theta$ is often observed experimentally (c.f. figure 2.2). For hydrogen, for example, on tungsten Boudart 1952 cites a case where $\Delta\phi \propto \theta$ for $\theta < 0.7$. Similar results have been found for H_2 and other gases on other metals (c.f. section 2.5.2). Oxygen atoms have a larger value of α than hydrogen and lateral interactions should become apparent for smaller values of θ as typically found to be the case (c.f. section 2.5.2). Equation (2.11) is also only valid for adsorption into a single state. Multiple binding states are known to exist and the dipole moments may vary from one state to another. In the case of a two state (1 and 2) system the equation becomes of the form:

$$\Delta\phi = 4\pi e \left(\sigma_1^o M_{1,o} \theta_1 \pm \sigma_2^o M_{2,o} \theta_2\right) \qquad (2.12)$$

where the + or - sign is used to denote that the second state may be electronegative or electropositive and this includes the assumptions previously and also that the two states are not mutually interacting. An equation of this form may qualitatively describe the changes in curvature of the SP variation with coverage (c.f. figure 2.2) which have been reported and interpreted as due to multiple states (c.f. section 2.5.2).

In a single state system the surface potential normally varies non-linearly with adatom coverage and assymptotes to a final value (c.f. figure 2.2). The non-linearity is probably partly the result of direct dipole-dipole repulsion between the surface bonds which result from the sharing of electrons between the metal and adsorbate. The

polarizability of metallic adsorbates is much larger than that of simple diatomic gases and depolarisation effects are expected to play a more important role. Attempts have been made with classical models to calculate the mutual depolarisation as a function of coverage θ from which the variation of ϕ with θ may be predicted. Boundart 1952 discusses some of the early models based on an assumed dipole distribution. These classical models are generally consistent with the experimental results for alkali adsorption on metals for small fractional ranges of coverage only (i.e. $\theta < 0.4$). Recent theories have yielded agreement over a much wider range of coverage. Gyftopoulos and Levine 1962 proposed a model which was based on an extension of the concept of electronegativity for composite surfaces using a semi-empirical depolarisation function for a fixed array of surface dipoles. Rasor and Warner 1964 treated the problem differently but also included a semi-empirical polarisation function. Schmidt and Gomer 1966 have also proposed a model based on a simple depolarisation field from a point dipole array. MacDonald and Barlow 1966 (and in their cited previous work) have presented a sophisticated model also. The simple classical model breaks down even at low coverages and does not account for the gross differences in the dipole moments from one crystal face to another. The more sophisticated treatments above can be fitted to experimental results over a much wider range of coverage. Blott et al 1965 and Lea and Mee 1968, for example, have found a reasonable agreement between the Gyftopoulos and Levine model and experimental results for Cs and Ur on tungsten. The former authors did not find such good agreement with the Rasor and Warner theory. Schmidt and Gomer found that their model was consistent with the results for K on tungsten. Others have not found a good agreement for Cs on W with either of the G-L or R-W theories (c.f.

Coggins and Stickney 1968). The above models are generally based on an assumed distribution of point dipoles among other simplifying assumptions. Their detailed interpretation and justification requires knowledge of the surface structure of the adsorbate. It is only recently that such investigations with LEED have been made (c.f. section 2.5.4).

In recent years there has been an increasing interest in the quantum mechanical description of the surface potential and adsorption for hydrogenic and alkali metal adsorbates. Toya has given one of the few quantum models from first principles and recently reviewed these for hydrogen (Horiuti and Toya 1970). For metals two states (r and s) were predicted. Hydrogen atoms in r states are located above the metal surface atom outside of the electron cloud of the surface and increase the work function. The theory implied that the negative polarisation of the r-adatom became reduced as the work function of the metal increased because of a mutual repulsive interaction between adatoms. This arose because of the competition between adatoms for metal electrons which tended to weaken each other's bonds. Hydrogen adatoms in s states were located in interstitial sites in the surface embedded in the electron cloud of the surface and resulted in a reduction of the work function. Bennett 1968 (and cited works) has given a quantum mechanical treatment of alkali-substrate interaction and the effective charge on the adion with coverage. The adsorbate-mutual interaction due to a direct overlap of localised orbitals had a strong effect on the adion charge but this was compensated for by other effects. The change in the surface potential with coverage in a simplified model was shown to be due at low coverages to mainly long range coulomb adion interactions.

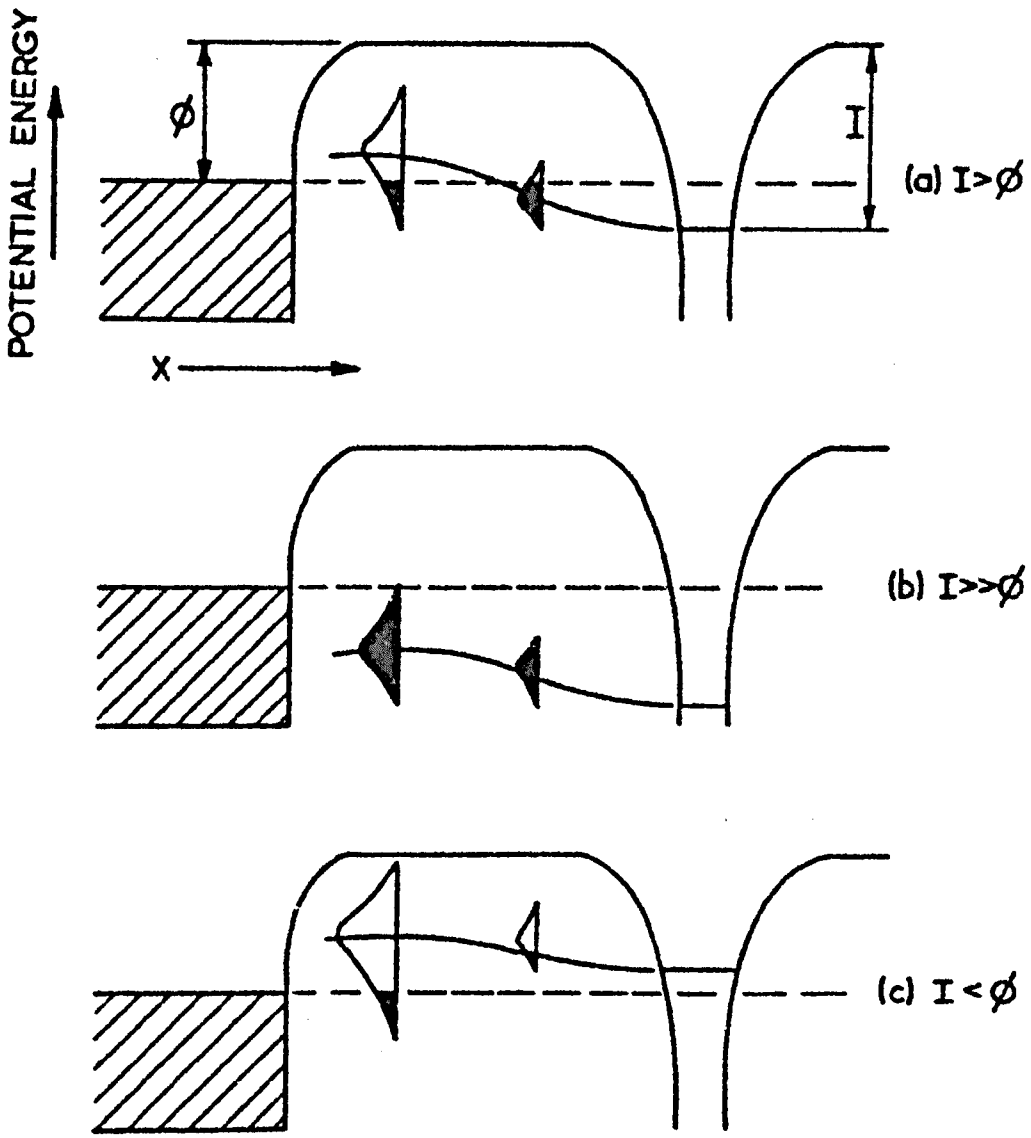

Figure 2.5 Schematic energy level diagram of electropositive adsorbate - metal interaction showing the raising and broadening of the ionisation level (I) as a function of adatom distance and the adatom charge q for (a) $I > \phi$, partial positive q and polar-metallic bond, (b) $I >> \phi$ metallic bond, q negative, (c) $I < \phi$, large positive q and polar-ionic bond (Schmidt and Gomer 1965, 1966).

Gurney had shown in the 1930's that the valence level of the adsorbate electron was raised and broadened when an atom became adsorbed (c.f. Gadzuk 1967, Gerlach and Rhodin 1970). The broadening is regarded as the formation of an adsorbate band and that the band is filled to the level of the Fermi level. Consequently the effective charge q on the adatom depends upon the position of the raised level with respect to the Fermi level and subsequently on the work function and on the distance between the adatom and the metal surface. The situation for electropositive adatoms is shown in figure 2.5. Ionic adsorption ($q > 0$) requires that the entire raised band lies entirely above the Fermi level. Consequently for electropositive adsorbates a high degree of ionicity is favoured by a high work function. The metal-adsorbate bond in this scheme will be ionic, polar-metallic or metallic if the raised and broadened level lies above, at or below the Fermi level respectively (Schmidt and Gomer 1965,1966). Gadzuk 1967 (a) has applied a first order perturbation theory to alkali - substrate interactions and calculated the shift and broadening of the atomic level as a function of the adatom distance from the metal surface. This enabled the average charge of the adion to be calculated and consequently the dipole moment. Gadzuk (and also Bennett) used the classical image law as describing the potential between the ion cores and the metal. Polar-metallic bonds did not appear to produce a sufficient dipole moment to account for the experimental results and a net transfer of an electron to the metal was required. The transferred charge became essentially localised inside the metal near the adion to form a polar-ionic bond with the alkali ion core. This was equivalent to forming a dipole moment $M_o = q\xi(s)$ where $\xi(s)$ was the effective distance of the location of the polarisation charge from the ion core. In another paper Gadzuk 1967 (b) treated the adsorption of a

hydrogenic atom on the surface of a dense electron gas neutralised by a distribution of positive ions. In this theory the wave functions of the impurity ion extended into free space but were prevented from penetrating into the substrate due to repulsion. Extending the model to real conduction band electron densities, he showed that hydrogen atoms increased the work function (similar to Toya's r-states above) due to the effects of a screening polarisation charge in the metal surface. Gadzuk extended the Rasor and Warner theory (which was known to be inconsistent with experimental results for small adatoms i.e. Li) to show that the latter and also his own were consistent with experimental results for Li on W. Recently Gadzuk 1969 (a) has improved his theory by including a more exact treatment of the polarisation screening. In it he showed that the classical image charge approach was not generally applicable since the induced screening charge of the adion was within the bulk and not on the metal surface. Consequently volume polarisation led to a larger dipole length (for small distances of the adion from the surface) than classically expected. Gadzuk concluded that the agreement in his previous theory which involved the classical assumption was fortuitous. Both theories predicted a variation of the dipole moment with the substrate crystallinity. In his more recent theory the dipole moment $M_o = q\,\xi(s)$ depended on the effective charge q and the distance $\xi(s)$ between the adion core and the location of the polarisation charge . Both of these factors depended on the free electron density of the substrate. As the density became reduced so $\xi(s)$ became increased since the volume polarisation charge extended further into the bulk (i.e. the screening became less effective) and q became reduced since the reduction in the electron density effectively reduced the ionicity of the adion-metal bond. The dipole moment will increase or

decrease depending on which of these parameters is dominant as the free electron density varies. Newnes 1969 has also given a quantum mechanical treatment of the interaction of hydrogen with transition metals in which he ignored surface structure and assumed only the d band interaction with the adatom was important. The theoretical charge densities on the adatom varied from 1.4e for Ti to 1.2e for Ni. These were too large (though of the correct sign for charge transfer) to account for the negative experimental dipole moments since they predicted dipole lengths much smaller than experimentally expected. Gadzuk 1970 has compared Newnes' theory with his own and concludes that apart from some numerical differences they both give the same results. A recent discussion and short review of the classical and quantum developments in the theory of adsorption has been given by Gerlach and Rhodin 1970.

Gerlach and Rhodin 1969,1970 have investigated the SP of Na, K and Cs on Ni single crystals using absolute measurements of the adatom coverage. Good agreement was not found with the Gyftopolous and Levine theory. The previous reported agreement by others between experimental results and this latter theory may have been due they suggest to the use of relative coverage measurements. Gerlach and Rhodin found much better agreement with the Gadzuk model and discuss some of the problems of its application to surface potential measurements. Fehrs and Stickney 1971 however conclude from meausrements of the dipole moments of Cs, K and Na on W and Ni single crystal planes that the classical model predicts values in much closer agreement with experiment than Gadzuk's model although other (cited) studies have not found this.

It has been appreciated qualitatively for some time that the magnitude of the surface potential is related to the nature of the metal -adsorbate bond and consequently to the electronic structure and surface properties of the metal (c.f. Ehrlich 1966.Madey amd Yates 1967, Gundry and Tompkins 1968). Attempts have been made to find an empirical relationship between the surface potential and the properties of the metal substrate and these are reviewed by Culver and Tompkins 1959. For simple gases the sign of the SP has been suggested to be related to the difference between the electronegativities χ of the metal taking $\chi = \emptyset$ and the adsorbate $\chi_a = (I + A)/2$ where I is the ionization potential and A is the electron affinity of the atom. The dipole moment $M = c(\emptyset - \chi_a)$ where c is an empirical conversion factor. On this basis the sign of the surface potential is negative for gases and positive for metallic adsorbates. Mignolet has found that the surface potential V is related to $\emptyset$ and χ_a by the empirical equation:

$$V = 0.29\ (\emptyset - 3.15\ \chi_a) \qquad (2.13)$$

which described the SP of O_2, I_2 and H_2 on several transition metals reasonably well. This rule is violated however, by the observations of an initial positive SP of nitrogen on W(100) and of oxygen on T_a(110) as described in section 2.5.2. Delchar and Ehrlich 1965 found an empirical correlation between the sign of the SP of N_2 on W with the roughness of the crystal plane substrate but this has not been substantiated by other studies however (Madey and Yates 1967). These empirical correlations have used ill-defined experimental results. Recently Sargood et al 1970 have attempted a fresh correlation between recent values of the SP of Cs, Ba,

Ur, I_2. Br, Cℓ , O_2 and H_2O on four single crystal faces of tungsten with the electronegativity. Although many simplifying assumptions were made in the analysis, they found a high degree of correlation in which each metal surface i was characterised by an effective electronegativity χ_i which was linearly related to the work function of the crystal plane ϕ_i :

$$\chi_i = 2.3\ \phi_i - 2.5 \qquad (2.14)$$

instead of the earlier assumption that for a metal $\chi_i = \phi_i$ above. Empirically the SP of each adsorbate V was described by:

$$V = - a\ r_i(\chi_a - \chi_i) \qquad (2.15)$$

where r_i is the ionic radius. The slope of the curve a was an empirical constant varying inversely with ϕ_i between 0.26 and 0.27. The SP of hydrogen and nitrogen did not fit into the above scheme and this may have been due they suggest to the small size that H and N adatoms may take enabling them to penetrate into the metal surface. For hydrogen, $r_i = 2.06\ A^o$ and $\chi_a = 6.6$eV from which the correlation predicts that a reversal of sign of the SP occurs for $\chi_w < \chi_a$ i.e. for $\phi \lesssim 4.0$ eV. Sargood et al did not include in their analysis the Russian results for alkali metals on the single crystal faces of transition metals (section 2.5.4). These results are also described by an equation of the form $V = a + b\phi_w$ for $a > 0$ and $b > 0$ where the constants a and b depend on the adsorbate and substrate. This is of the same form as equation (2.15) for alkali metals and it is in qualitative agreement with Sargood et al's conclusions.

Recently Engel and Gomer 1970(a) have measured the SP of oxygen on single crystal faces of tungsten. The negative SP became more positive (i.e. the magnitude of the SP decreased) and the magnitude of the negative dipole moment decreased as the clean substrate work function ϕ_o increased. The results for the SP of hydrogen on tungsten (reported by Hopkins and Pender 1966) are plotted in figure 7.16 as a function of ϕ_c. A similar effect to that above also occurs for hydrogen. Engel and Gomer suggested that for electronegative adatoms (with a large ionisation potential) such as oxygen the variation of the dipole moment with ϕ_o may be qualitatively accounted for by a similar model to that proposed by Schmidt and Gomer earlier for alkali-substrate interaction (figure 2.5). In this case, for oxygen, the empty affinity level is lowered by the interaction with the substrate, and it would be maximally broadened and maximally filled by the lowest value of ϕ_o. Thus the magnitude of the negative charge on the adatom (and therefore the SP) increases as ϕ_o decreases. For oxygen, the affinity level is too high but a similar effect occurs if it had a resonance level at $R \sim \phi$. A similar scheme may also apply to hydrogen involving an affinity resonance level at $R \sim -6.5$ eV.

There is no generally accepted explanation of the positive surface potential which arises in physical adsorption. Engel and Gomer 1970(b) discuss some of the proposals that have been made. The interaction of rare gases with metals has been assumed to be of the Vander Waals type resulting from dispersion forces which arise from the interaction between fluctuating dipoles in the adsorbate and the image in the metal. The large dipole moments which arise in physisorption have been suggested to be due to polarization of the adsorbate in the electric field of the metal

surface. The degree of polarization may be expected to be greatest on the highest work function planes of a metal and the variation of the SP of several rare gases on the crystal planes of W is consistent with this possibility (Engel and Gomer 1970). Gomer points out however that polarization may be insufficient since the metal field dies off at a short distance from the surface. Alternatively Mulliken has proposed a charge transfer between the adsorbate A and the metal M without the formation of a bond in which the electron transfer $A + M \rightarrow A^+ + M^-$ was stabilised by a resonance between the core A^+ and M. In this model Engel and Gomer showed that maximum charge transfer was also favoured by a maximum substrate work function. In a similar picture to that of the broadening and raising of the valence level of an alkali atom in adsorption, a net positive charge on the adsorbate may result if the adsorbate has an excited state near the metal Fermi level. The magnitude of the SP in this scheme then depends on structural parameters as in the case of the alkali model. Recently Palmberg 1971 has found the variation of the SP of Xe on Pd (100) face to be well described by the depolarisation model of Schmidt and Gomer 1966 over a wide range of coverage. Polarization has also been suggested to be the cause of the positive surface potential which arises in molecular physisorption.

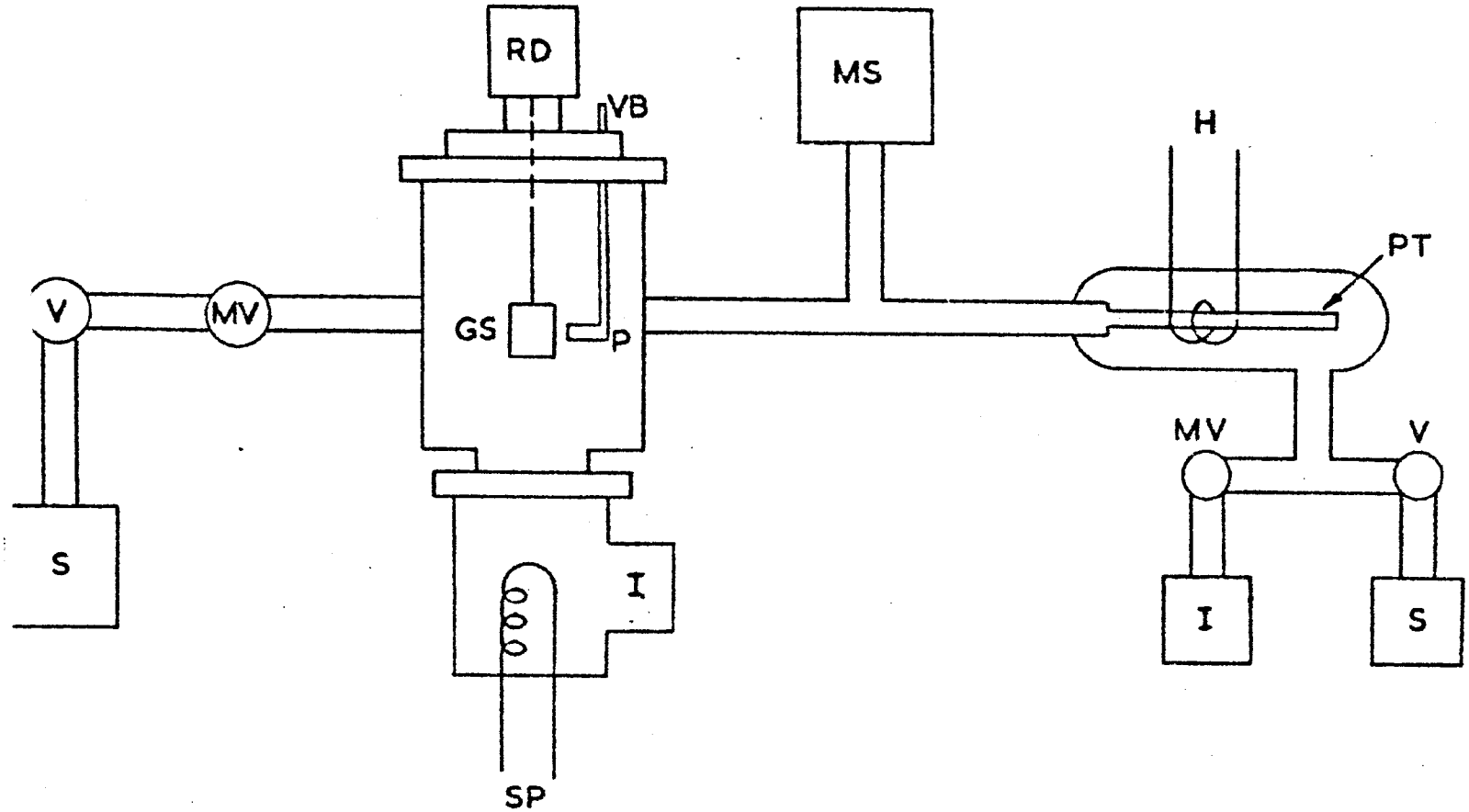

Figure 3.1 Diagram of the vacuum system and experimental tube (not to scale): V viton valve, MV metal valve, S sorption pump, I getter ion pump, SP sublimator pump, MS mass spectrometer, RD rotary drive, VB vibrator bar, GS glass substrate, P probe electrode, H heater coil, PT palladium thimble.

CHAPTER 3

EXPERIMENTAL DETAILS AND METHOD

3.1 The Vacuum System

The system was exhausted by a titanium getter ion pump in preference to a diffusion pump for the reasons given in the introduction. It was not necessary to provide an auxiliary pressure measuring device since the pressure could be measured from the ion pump current using the manufacturer's calibration for air. The particular pump used was the Ultek "Boostivac" which had a pumping speed of 25 ℓ sec^{-1}. It also incorporated a water cooled titanium sublimation pump, which had a maximum speed of 500 ℓ sec^{-1}, and two internal bake-out heaters. The sublimator was not finally used in the experiments. The system was initially pumped from atmospheric pressure to a pressure of about 10^{-3} torr with a chilled zeolite sorption pump.

In the last experimental run two more ion pumps were added which increased the total pumping speed by about 140 ℓ sec^{-1}.

The experimental tube is shown in Figures 3.1 to 3.4. It was manufactured from a low carbon grade 304 stainless steel (type EN58E) which provided some advantages in preference to glass. The tube was designed to allow vibrational motion to be introduced into the vacuum and relative translational motion between the pair

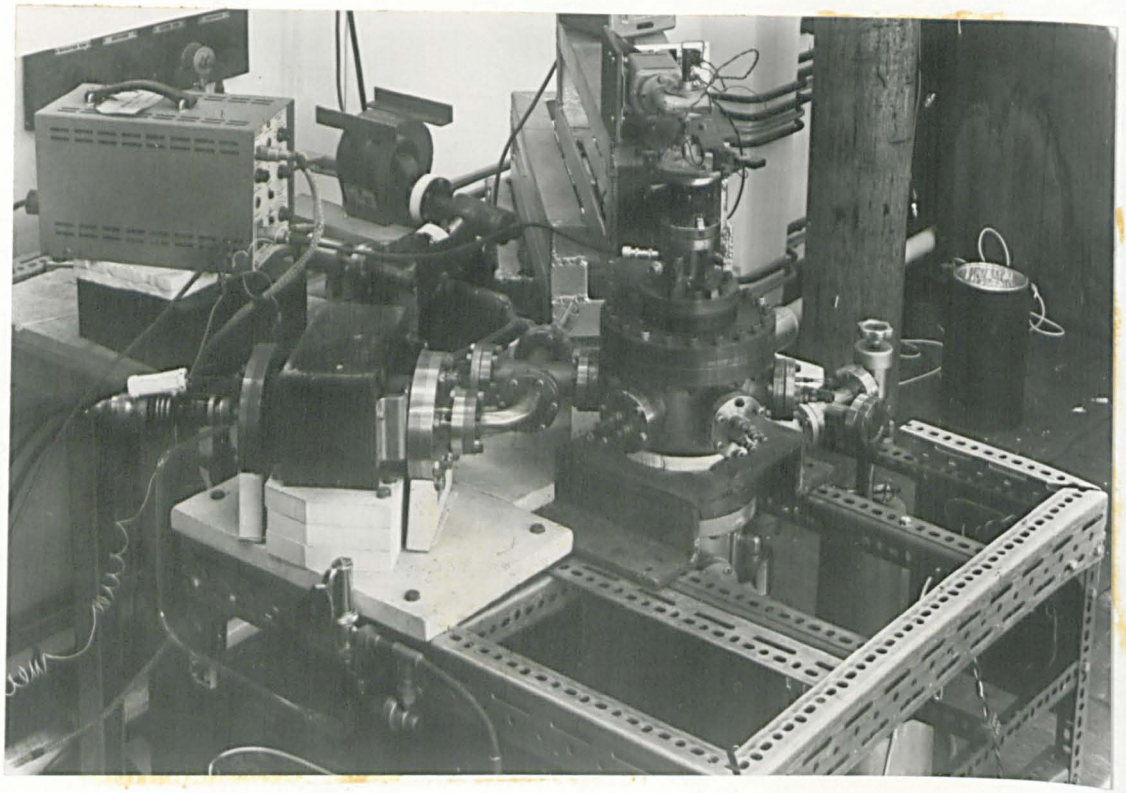

Figure 3.2 Photograph of the experimental equipment, vacuum system and the light weight handy-angle frame (used in experiments A and B).

of metals forming the dynamic capacitor. Electrical leads were brought into the vacuum by means of insulated current feed-throughs mounted into ports set about the tube body.

The dynamic capacitor and its associated electrical wiring was mounted on a single metal flange, the capacitor flange. This arrangement allowed it to be independantly and easily removed from the system. It is shown in Figures 3.5 and 3.6. The body was made from 6.0 inch internal diameter tubing, about which six mating ports were symmetrically located. The bottom was welded to a reducing flange of the same size as that of the Boostivac pump which was bolted directly onto the end. The top of the tube was welded to a 6.0 I.D. flange, onto which was bolted a solid blanking plate. A hole was cut in the plate to accommodate the capacitor flange, with its assembly protruding downwards through the hole into the tube.

Small flanges of 1.5 inches I.D. were welded to the ports about the body of the tube to mate with the standard size of conflat flange used on components commercially obtainable. These accommodated a pyrex glass window, connections to a gas supply and the backing pump line and several electrical instrumentation feed throughs. A vacuum connection to auxiliary ion pumps and a mass spectrometer was added in later experiments. The electrical instrumentation flanges were of a heavy current duty type which carried three 30A copper leads; a universal type having only two 30A and also three 5A leads and lastly an instrumentation type which carried eight light current leads. The insulation breakdown voltage

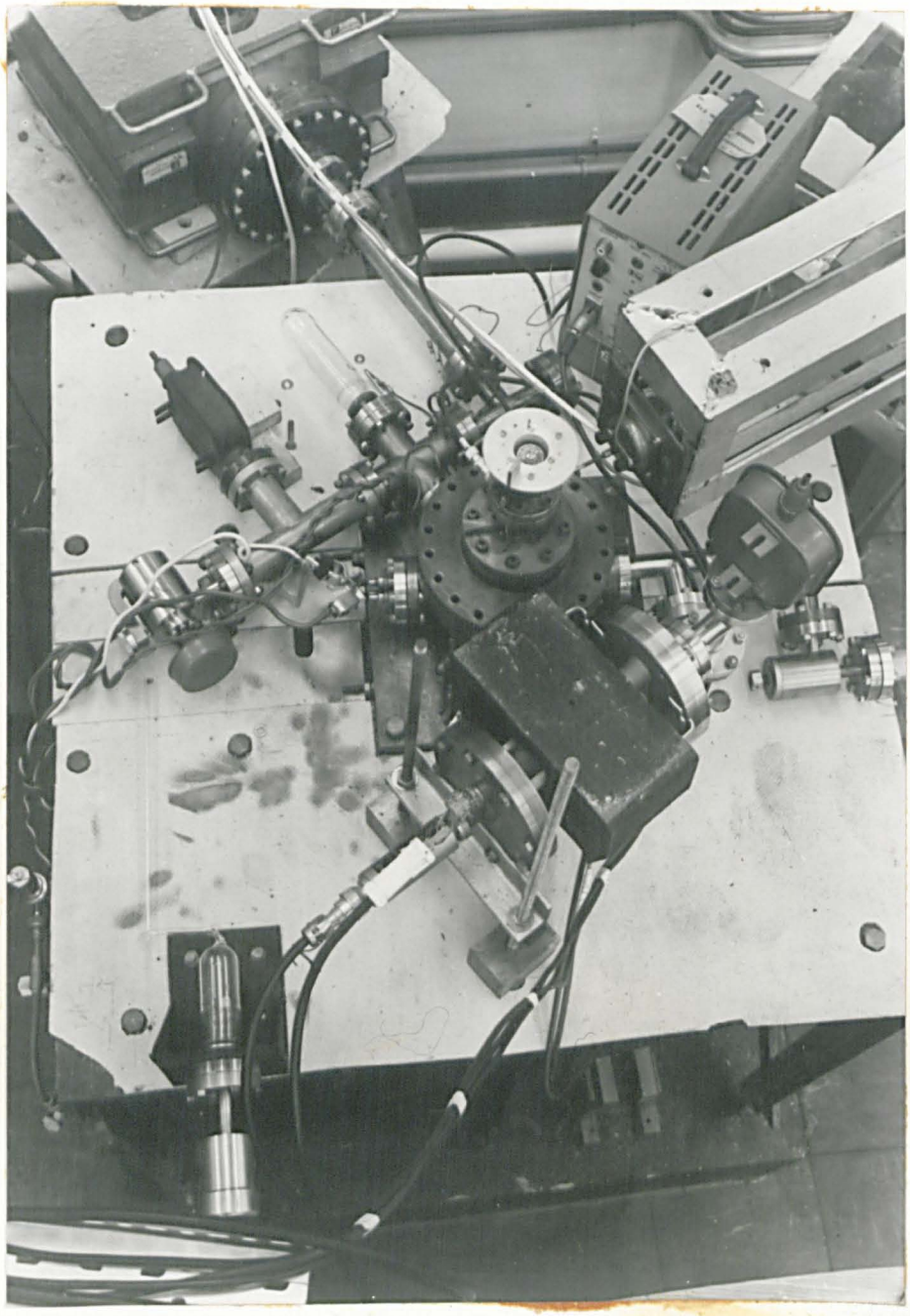

Figure 3.3 Photograph of the vacuum system and layout on the rigid steel frame (used in experiment C).

of each lead was stated by the manufacturer to be 1KeV or greater (Ferranti Limited). A detailed view of the tube is given in Figures 3.2 and 3.3.

Vacuum line connections were made between the tube and auxiliary equipment with stainless steel tubing. Glass to Kovar metal seals were used in providing a connection between pyrex glass vacuum lines and the metal system. The foreline was sealed off from the high vacuum side by a bakeable metal ultra high vacuum valve.

Argon arc welding techniques were used throughout in the metal welds. The mating flange connections conformed to the standard conflat design commonly used in ultra high vacuum hardware. Commercially available oxygen-free high conductivity copper gaskets were used on all the flanges to provide a vacuum seal. The internal surfaces of the steel system and auxiliary apparatus were either electrolytically polished or cleaned after manufacture by sand shot-blasting.

The auxiliary vacuum equipment and soft-ware were purchased from Ferranti Limited and Vacuum Generators Limited. The former company also manufactured the basic experimental tube and capacitor flange to customer specifications. A number of the blanking flanges, vacuum line connections and extension pieces were made by the workshop staff in this department.

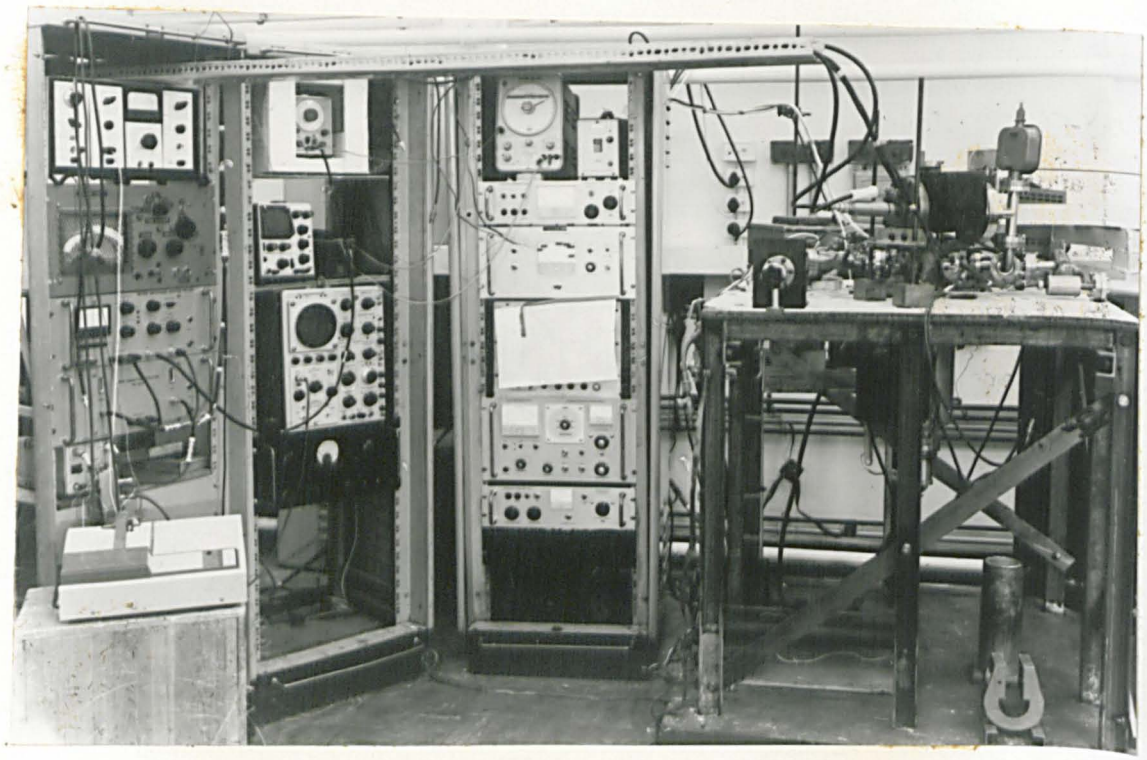

Figure 3.4 Photograph of the equipment, vacuum system and steel frame.

The experimental tube and ion pump were supported vertically by a split iron collar about the reducing tube connecting the pump and the chamber. The original experimental system is shown in the photograph in Figure 3.2. The collar was bolted to a rigid 'handy angle' frame. This arrangement was mechanically unstable and affected the precision of measurements (cf. Section 3.4 and Chapter 4). Various modifications failed to improve the situation and another supporting structure was built for the later experimental runs. The second system is shown in Figure 3.3 and 3.4. It was made of two inch steel U-channel sections, whose legs were embedded in a concrete block approximately a foot deep. The frame was braced by cross member sections of steel. A three foot square plate, half an inch thick, was bolted to the top of the frame. It was isolated from the frame by thick and anti-vibration machine mounting material. The top surface of the plate was covered with an asbestos board. The vacuum system was secured through the centre of the top plate by a heavy split iron collar, a foot square by one inch thick. The experimental tube and the ion pump extended above and below the plate respectively as before. The instability was reduced.

In later experimental runs, an aluminium baffle was inserted into the throat of the Boostivac pump. Its function was to prevent a direct line of sight from the discharge elements of the ion pump to metal surfaces within the experimental tube (cf. Chapter 5).

In the last two experimental runs, a fine mesh stainless steel screen was mounted around the internal vertical walls of the tube. It

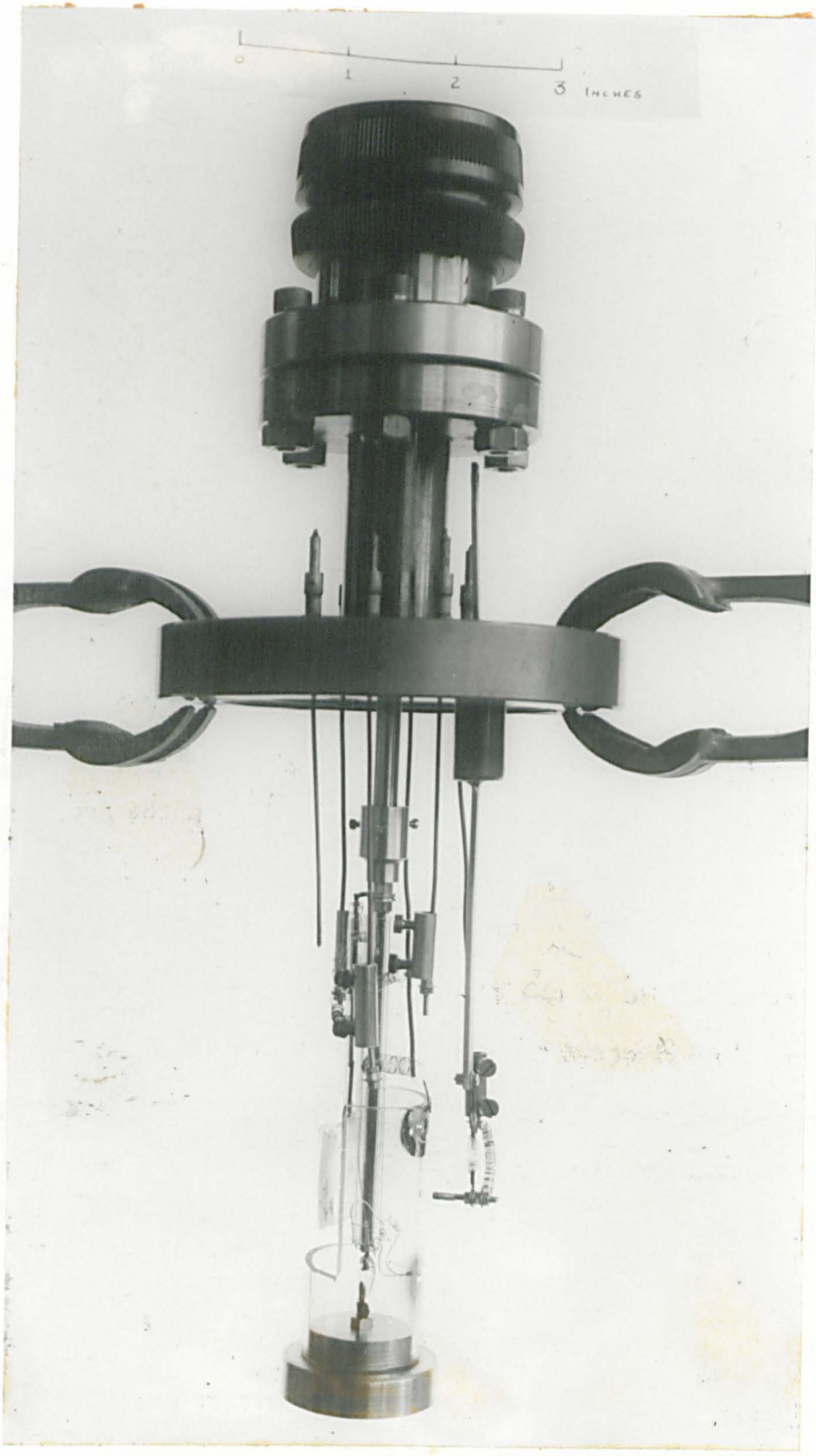

Figure 3.5 Photograph of the capacitor steel flange with one of the early capacitor designs (used in experiment A).

was insulated from the tube by ceramic fish beads. Holes were cut in the screen where necessary to allow the intrusion of electrical leads and evaporation filaments into the tube. Its function is described in Chapter 4.

3.2 The Capacitor Flange

A photograph of the complete capacitor flange is shown in Figures 3.5 and 3.6. A silver steel metal bar was gold brazed at its centre through a stainless steel well. The well was argon-arc welded into the flange as shown. Vibrational motion was introduced into the vacuum by transversely driving the free end of the bar in the air.

The principle of the dynamic capacitor is described in Chapter 4. The electrodes of the capacitor were composed of a stainless steel probe mounted on the vibrator bar and a metallic film on a substrate which was mounted opposite the probe. The probe was made from a circular rod and had an area of about one tenth of a square centimetre. The end of the probe was threaded and it was secured in a hole in the bar by stainless steel nuts and washers. The area of the metal film on the pyrex substrate was about 5 to 10 cm^2. The substrate was cut from circular pyrex tubing.

A detailed view of the substrate arrangement is shown in the photograph in Figure 3.7. The substrate was supported on a stainless steel cylindrical block. The block was mounted onto a drive rod

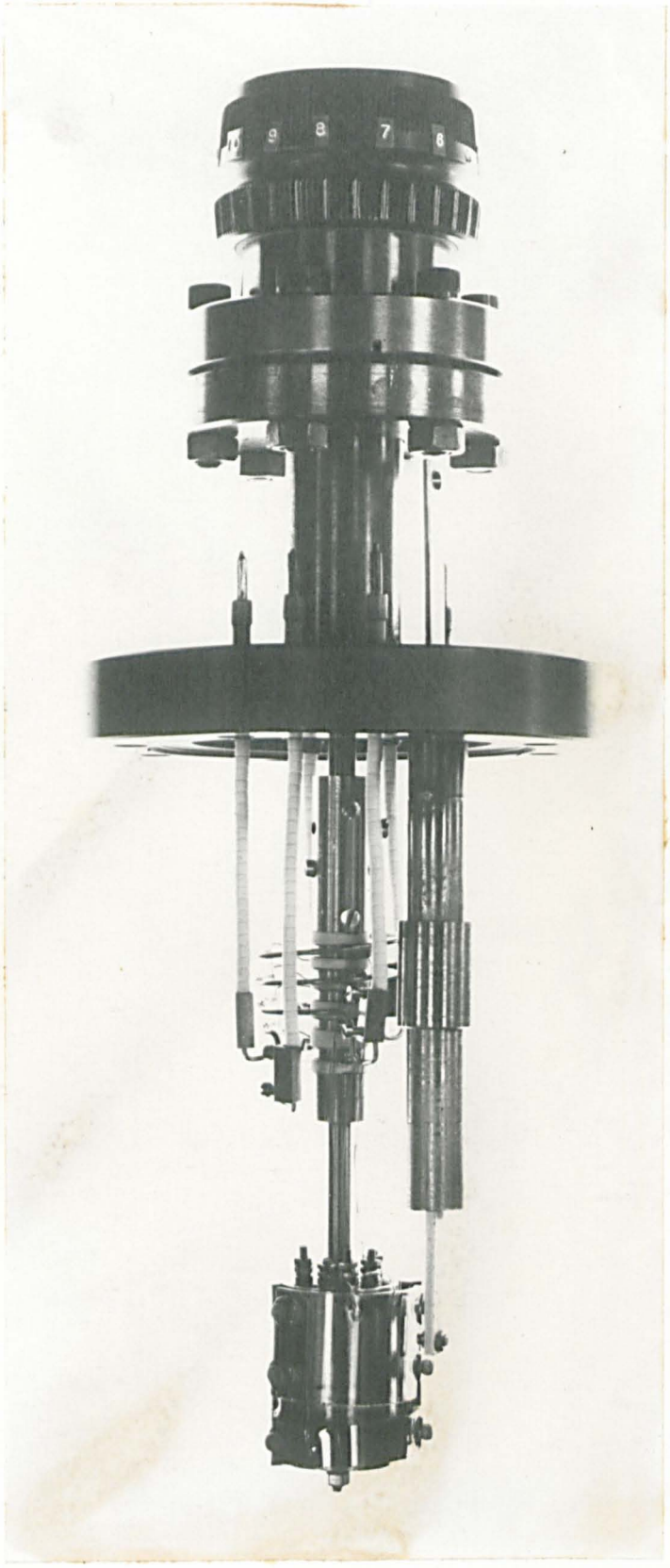

Figure 3.6 Photograph of the final form of the capacitor design and the rotary connector assembly (used in experiments B and C).

passing through its axis. The rod in turn was axially aligned to the drive shaft of a rotary magnetic drive, using an online steel connector. In this way, different portions of the film and substrate could be brought opposite the steel probe for the purpose of spatial contact potential measurements.

The sides of the substrate were screened from stray evaporant flux with tantalum foil screwed into the support. The substrate was directly supported by several small stainless steel bolts screwed into the block. In order to prevent shorting of the metal film to earth potential by the bolts, their heads were coated with a liquid solution of ceramic paste. The paste was vitrified at a temperature of about 500°C.

The first five experimental runs were conducted with the substrate design in Figure 3.5. In these experiments, a simple steel disc was attached to the drive extension rod, onto which a glass substrate was mounted. Insulation of the metal film was attempted in two ways. In the first, the support was insulated from the drive rod by an online tungsten to pyrex glass seal connector. In the second, a portion of the area of the substrate exposed to the metal evaporant was protected by metal screens which prevented the film from making contact with the disc. Neither of these methods was entirely satisfactory, due either to fracture of the online connector or to stray metal evaporant which destroyed the insulation. The first experimental results were obtained with the second of these preliminary designs. They were dispensed with,

Figure 3.7 Detail photograph of the substrate assembly in Figure 3.6.

however, for the remaining experiments in favour of that shown in Figures 3.6 and 3.7.

The method of making electrical connection to the film is described in section 3.5. The electrical leads from the substrate were taken to stand-off electrical connectors mounted on top of the substrate support as shown in Figure 3.7. These were made from threaded steel rod set into machined ceramic supports which were screwed into the support block. The connectors were located in a well in the top of the block thereby screening them from metal evaporant.

A five way stainless steel slip ring and brush assembly was built to provide an electrical interface between the fixed vacuum electrical feed throughs in the flange and the movable substrate assembly, Figures 3.6 and 3.7. The rings were electrically isolated from each other by ceramic bushes. These and the steel rings were mounted onto a ceramic tube which provided a means of insulation between them and the metal drive rod onto which the assembly was mounted. The drive rod and the ceramic sleeve were machined to accept a ceramic key running the length of the assembly, which caused it to rotate with the drive shaft. Each ring was fixed to the sleeve by a fine steel bolt, which also functioned as an electrical connector. Electrical connection was made with fine tungsten wire between the slip rings and the stand off terminals on the substrate support block. The electrical potentials from the substrates were picked up from the rings by

tungsten ribbon brushes. These were spot welded onto a glass - tungsten five-way electrical connector. The connector and brushes were rigidly held in their correct positions by heavy nickel leads, circumscribing the assembly, which also electrically connected them to the instrumentation feed throughs in the flange. The feed throughs were centrally placed about the port in which the rotary drive was mounted.

The stainless steel probe was insulated from the vibrator rod with an alumina ceramic plate (Figure 3.6). The plate was initially made from machinable 'ceramtec', but this was an unsatisfactory material since it frequently fractured during vibration. A similar plate was cut from alumina with diamond machine tools and this material was found to be satisfactory. The plate was kindly prepared by the B.C.R.A* Electrical connection was made between the probe and the slip ring assembly with a very fine tungsten wire which did not impede the probe vibration.

The slip ring assembly was screened from stray evaporant flux by a large glass sleeve securely held in the throat of the upper flange. It completely enclosed the assembly, except for a small portion cut away to avoid the vibrator drive bar. The external surface of the glass was coated in situ with gold to prevent any charge accumulation which might have disturbed the measurements.

* British Ceramic Research Association

The substrate could be rotated 330° about the drive axis and thereby positioned in front or away from any of the ports in the system walls. The electrical insulation resistance of the films was better than that of the electrical feed throughs in the capacitor flange which were $\sim 10^{10}$ Ω.

Preliminary experiments demonstrated the need for electrostatic screening of the vibrator bar from the capacitor film electrode. This was achieved by the (de-mountable) on-line steel connector shown in Figure 3.6. The female acceptor was welded onto the base of the vibrator well.

3.3 Production of Hydrogen

Hydrogen was introduced into the system through a heated palladium-silver thimble. The thimble was sealed via a graded glass joint to a pyrex vacuum line as shown in Figures 3.2 and 3.3. In some experiments the thimble was isolated from the high vacuum system by a bakeable metal valve. The heater coil surrounded the thimble but it was placed several inches away from the graded seal to avoid heating the glass. The high pressure side of the thimble was enclosed in a pyrex jacket. A pyrex vacuum line led to a glass to metal seal and conflat steel flanges. The vacuum line was exhausted with a chilled zeolite pump and a small getter ion pump. The auxiliary pumping system was necessary since at atmospheric pressure hydrogen continued to be evolved from the thimble after operating in a normal fashion. Consequently it

prevented ultra high vacuum from being quickly established again in the experimental tube. The thimble, however, appeared to become poisoned in a residual vacuum of 10^{-3} torr. These problems were avoided if the residual pressure was reduced to about 10^{-6} torr or less on the high pressure side of the thimble before introducing hydrogen.

It was possible to vary the pressure of hydrogen in the tube from the base value of 2×10^{-9} torr to a maximum value of 10^{-5} torr. The pressure of hydrogen required on the high pressure side of the thimble to achieve this range varied from 10^{-6} to 10^{-3} torr with the thimble at a typical temperature of a few hundred degrees centigrade at most.

3.4 Instability of the Dynamic Capacitor

The stainless steel probe was vibrated at about 115 Hz, which was the natural resonant frequency of the vibrator bar. The free end of the bar was rigidly coupled to a moving coil transducer (Pye-Ling Limited). The coil was driven with a high stability oscillator (type TF 2100, Marconi Limited). The transducer unfortunately presented a variable load to the oscillator. Consequently, they were mutually isolated with a high stability buffer power amplifier (Dawe Limited, type 440B). The experimental set-up is shown in Figures 3.2 and 3.3 and the driving circuit in Figure 3.8.

A Q-factor of the mechanical bar resonator was determined experimentally to be approximately 750. A frequency drift of less than 0.1 Hz from resonance caused the vibrational amplitude to fall by about a factor of e. The frequency instability of the oscillator originally used, the Dawe 440B, limited the precision of contact potential measurements to about $\mp$ 0.1 V. It was impractical to operate at a frequency other than at resonance since the signal sensitivity became so low. The TF 2100 had a frequency and output amplitude stability of 0.001% per hour and 0.3% per hour respectively. It was more sensitive to temperature than desirable however, having a frequency and amplitude drift of 0.01% per ^{o}C and 0.4% per ^{o}C respectively. The oscillator was generally satisfactory. It was mounted in a thermal enclosure to reduce the effects of short term temperature fluctuations as shown in Figure 3.4.

At resonance, the whole of the system and rig were driven at the frequency of vibration. The mechanical coupling was sufficient to disturb the stability of amplitude of the vibrating probe, with similar consequences to that of the frequency instability described above. The problem was reduced by rigidly mounting the transducer onto a steel girder frame set into a massive concrete block, Figures 3.2 and 3.3. The data from the experimental runs 5 and 6 were obtained with this system and the original (but heavily damped) handy angle rig. The problem was only partially resolved, however, and consequently another rig was constructed (cf. section 3.1) as shown in the photograph in Figure 3.3. With this rig and the transducer

mounted as shown, a power dissipation of less than 0.25W was sufficient to drive the whole of the vacuum system and the steel rig (weighing over 5 cwt) at the resonant frequency of the capacitor. The stability of the vibrational amplitude of the capacitor electrode was, however, considerably improved allowing a high degree of sensitivity to be attained.

The frequency and mechanical amplitude stability of the capacitor was a severe problem with the rigid form of drive coupling between the vibrator electrode and the vacuum system. It would have been a major undertaking to redesign and rebuild the system in order to accommodate a flexible bellows coupling.

3.5 Preparation of Clean Surfaces

3.5.1 Vacuum Components

The following cleaning procedure was followed for all the vacuum components.

The component was washed in commercial detergent and finally rinsed in water to remove dust and gross contamination. It was then washed in successive fresh solutions of de-ionised water, trichlorethylene and (or) acetone. It was finally rinsed in de-ionized water and dried naturally in dust-free air. The clean components were handled only with dry clean cotton gloves.

3.5.2 Thin Film Substrates

Substrates were cut from scratch free stock pyrex glass tubing of about 1.0 inch diameter. (They were approximately one inch in length). They were lightly flame polished in air. A fine platinum lead was flame fused into the surface. A small portion of the glass enclosing the lead was coated with liquid bright platinum, Figure 3.5. The platinum film was slowly dried with a torch flame. Substrates were initially cleaned with successive solutions of commercial detergent and water. They were then rinsed in successive fresh solutions of reageant and analar acetone, nitric and chromic acid and ammonium hydroxide. In between each of these rinsings the substrates were washed in fresh solutions of de-ionized water. The clean items were stored to dry in a dust free atmosphere. Immediately before mounting in the system, they were again rinsed in solutions of analar acetone and de-ionized water. Extreme care was taken with them and they were handled only with clean metallic hand tools or with clean dry cotton gloves.

In the case of the thin film resistance monitors, the whole of the substrate was painted with platinum save for a narrow strip at the centre as shown in Figure 3.6.

In the last experimental run an erbium-molybdenum alloy substrate was used instead. It was covered, on one half, with a gold film. It was provided by the A.W.R.E. and maintained as

supplied under vacuum ($\sim 10^{-4}$ torr) until it was used. The substrate was exposured for less than a day to the dry laboratory atmosphere before the system was pumped down.

3.5.3 The Steel Electrode

The stainless steel electrode forming one plate of the dynamic capacitor, Figure 3.4, was cleaned after manufacture, in the same way as the vacuum components above. It was then polished with successively finer grades of wet carborundum powder and lastly with a commercial metal polishing solution. It showed a uniform and bright surface finish after polishing. Electrolytic polishing solutions were found to be unsuccessful. The polished surface was thoroughly washed in detergent and water again. It was then rinsed thoroughly in alternate solutions of de-ionised water and analar acetone before a final water rinse. The probe was subsequently treated in the same way as the clean substrates.

The steel probe and the substrates received in vacuuo only the normal bake out treatment. Attempts to outgass a test probe by electron bombardment in vacuuo were unsuccessful.

3.5.4 Thin Metal Films

Thin films of the metals Ag, Au and Ti were deposited onto pyrex substrates at room temperature from a charge of the

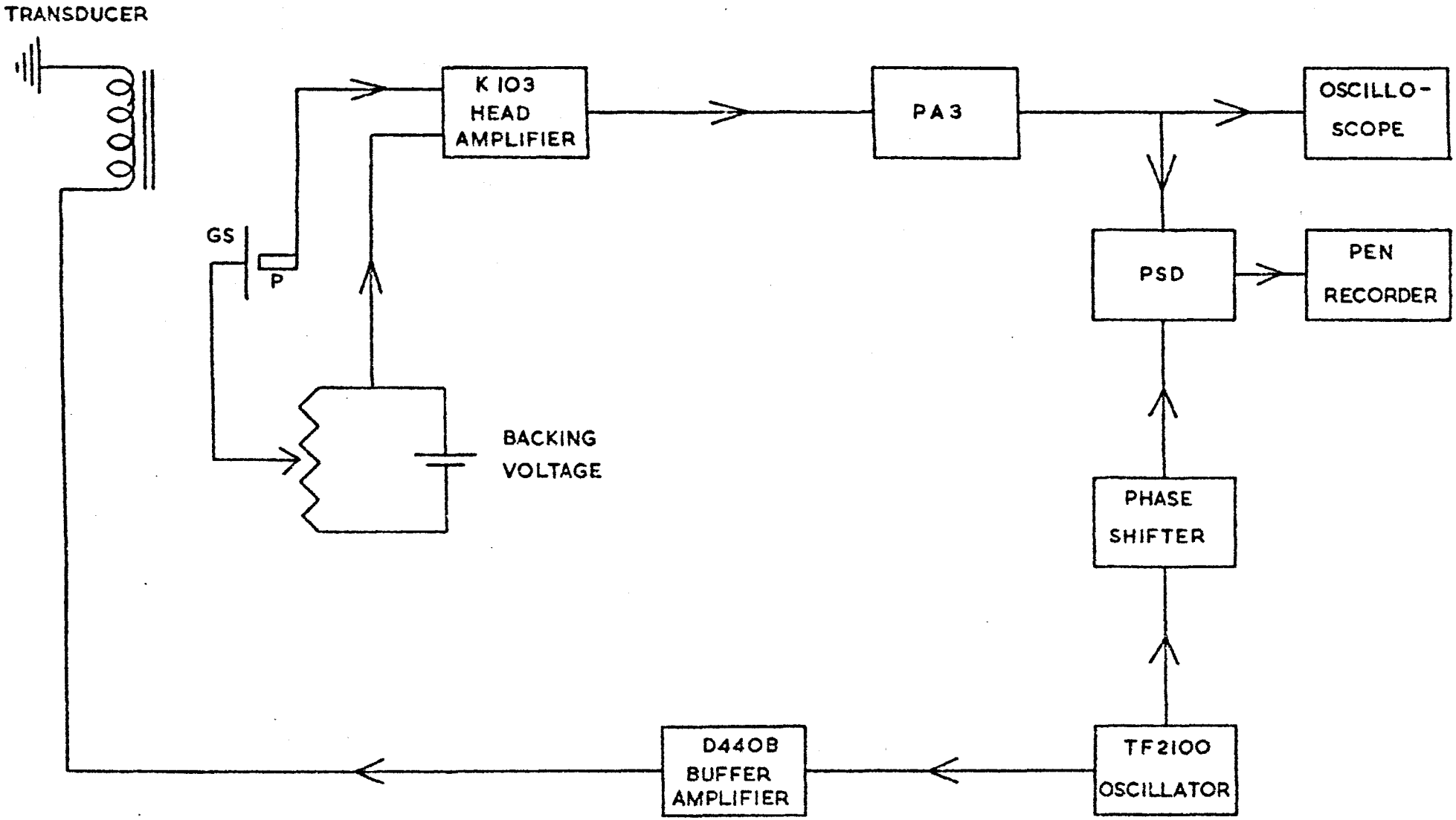

Figure 3.8 Circuit diagram of the Kelvin-Zisman dynamic capacitor and the electronic detection and recording system.

respective element at its sublimation temperature. The charges were supported on pure tungsten multi strand coils which were heated by a direct current. Fine wires of the noble metals and tungsten were obtained from Johnson Mathey Limited. They were stated to be 99.99% pure. The titanium was obtained in wire form and it was stated to be 99.6% pure (Koch Light Laboratories).

Multi stranded tungsten wire was formed into hairpin filaments. The filaments were mounted with stainless steel connectors onto the heavy current duty electrical feed throughs and reduced in hydrogen. Two filaments were mounted on each flange. The copper leads were sheathed in pyrex tubing to protect their insulators. The evaporant wire was wound onto the reduced filament and fused in the hydrogen atmosphere. The evaporator flanges were bolted onto the radial ports of the experimental tube. The same care was taken with the prepared evaporators as with the other cleaned components.

3.6 Electronic Detection

The electronic detection system is shown in Figure 3.8. The alternating current flowing between the electrodes of the dynamic capacitor was detected across the input impedance of a differential head amplifier (Keithly 103). It had an input impedance of 5×10^7 Ω and its bandwidth was restricted to 100 - 300 Hz. Its peak to peak noise referred to the input was 20 μV.

The output signal was further amplified (Telequipment PA3). The overall gain of the system was variable over the range from 10^3 to 10^5. The amplified signal was monitored with an oscilloscope and detected with a (Brookdeal PSD 629) phase sensitive detector. A reference voltage was taken from the driving oscillator. Its phase was adjusted with a (Brookdeal MS 320) phase shifter to give a maximum rectified output dc signal. The detector bandwidth was reduced to a value allowing a response time of one second and reasonable signal to noise ratio.

The Keithley head amplifier was supported on anti-vibration mounting on top of a separate support rig (Figures 3.2 and 3.3). This arrangement reduced microphonic pickup. The connecting electrical lead between the vacuum system and the head amplifier was doubly screened to reduce pickup. Coaxial brass elbow connectors were designed to screen the output electrical leads on the capacitor flange. The connectors were held in position by a common brass base sitting on the flange (cf. Figure 3.4).

The principle of measurement is described in Chapter 4. The backing voltage was supplied from a floating screened dc battery supply. The output potential was continuously variable in millivolt increments from -10 to + 10V. The dc potential was applied in series with the static electrode and the head amplifier input. The potential was measured with a calibrated Crompton voltmeter.

The measurement of the contact potential was performed in one of two modes. In the first mode, the backing voltage was adjusted to give a null dc output from the phase sensitive detector. The balance point was checked by sweeping the voltage firstly from one side, and then from the other. In this mode, about thirty seconds were required for each measurement. Under favourable conditions the null point could have been determined with an accuracy of two millivolts or less. In the second mode, the low impedance dc output from the detector was fed directly into a floating input high impedance and free running (Beckman) potentiometric pen recorder. The recorder had an input impedance of several megohms and a time constant of one second. The recorder deflection was calibrated with a series of known increments in the backing off voltage which simulated changes in contact potential. The contact potential was checked regularly using the first mode whenever the recorder method was used. Mode 2 was used in measurements on the work function of steel and on titanium where $d\phi/dt$ was often too fast to be accurately followed in Mode 1. (cf. Chapters 5 and 7). The sensitivity of Mode 2 was similar to that of Mode 1. For practical reasons measurements were only made to an accuracy of 5 or 10 mV.

3.7 General Experimental Procedure

The general experimental procedure was as follows. Fresh substrates and evaporation flanges were prepared and mounted in

the system. The rotary drive was radially calibrated for the particular experimental arrangement within the tube. It was not possible to accurately locate the substrate position with respect to the evaporation sources or the condenser probe visually through the window port. In some of the later experiments thin film resistance monitors were placed near the evaporators to monitor the deposition. These were screened with tantalum foil to prevent contamination from other evaporators. An electrical continuity check was made before finally assembling the system.

The system was pumped out to about 1×10^{-3} torr with the foreline pump. The foreline valves were closed and the pressure reduced to about 10^{-7} torr with the ion pump. The high pressure side of the palladium diffusion unit was also pumped out to about 10^{-7} torr in the same way. The complete system was baked at $250^{\circ}C$ for several days with the internal pump heaters and also with a removable oven (on loan). The bake out temperature was adjusted to maintain the system pressure at all times at less than 10^{-6} torr. After cooling the system and pumping for a further two days or so, the base pressure of the system was equal to or less than 2×10^{-9} torr.

The diffusion thimble and evaporation filaments were successively outgassed over a period of about three days or or more until there was no increase in the base pressure when they were raised to their normal operating temperatures. During

this period the substrate was rotated out of sight of the evaporator being outgassed.

Stray electrical charges on the glass substrate disturbed measurements. Consequently film evaporation was continued onto the substrate, rotated into line of sight of the evaporator, until sensible results were obtained. Additional films were successively deposited for the purpose of measurements. After each deposition the substrate was rotated in front of the probe. The calibration of the magnetic rotary drive allowed the same portion of the substrate to be measured on each film. Spatial contact potential variations were investigated by rotating the substrate, bringing a different area of its surface opposite the probe. The amplitude of vibration of the probe was reduced each time the substrate was moved for the purpose of deposition. Successive films were deposited until the evaporator filament fused or the charge became exhausted. Deposition was monitored by measuring the resistance of the thin film on the monitor substrate mounted beneath the primary film substrate (cf. Figure 3.6). An 'avometer' or laboratory R-C bridge was used for this purpose.

Hydrogen was diffused into the system by adjusting the partial pressure of hydrogen on the high pressure side of the thimble and its temperature. Preliminary experiments allowed a crude temperature-pressure calibration of the diffuser to be made.

At the end of each experiment the system was let up to atmospheric pressure with cylinder purity nitrogen gas.

CHAPTER 4

THE DYNAMIC CAPACITOR METHOD AND THE EFFECTS OF STRAY CAPACITANCE

4.1 The Contact Potential

When two conductors, i and j, are brought into electrical contact, free electrons may flow from one to the other. If the value of the electrochemical potential $\bar{\mu}$ in each is different originally, the change transfer continues until the value of $\bar{\mu}$ in each is the same. This condition implies a difference of potential V_{ij} between two points just outside of the surfaces of the conductors which is given from equation (2.2) if the subscripts are omitted by:

$$V_{ij} = \Phi_i - \Phi_j = \phi_j - \phi_i \tag{4.1}$$

Equation (4.1) was originally derived by Richardson and its experimental verification was described in Chapter 1. The electrostatic potential outside of a patchy surface is given by equation (2.6) and it follows that the difference in potential between two points outside of patchy conductors is given by:

$$V_{ij} = \bar{\Phi}_i - \bar{\Phi}_j = \bar{\phi}_j - \bar{\phi}_i \tag{4.2}$$

where $\bar{\phi}$ is the arithmetic average work function defined by equation (2.10).

(a) BEFORE CONTACT

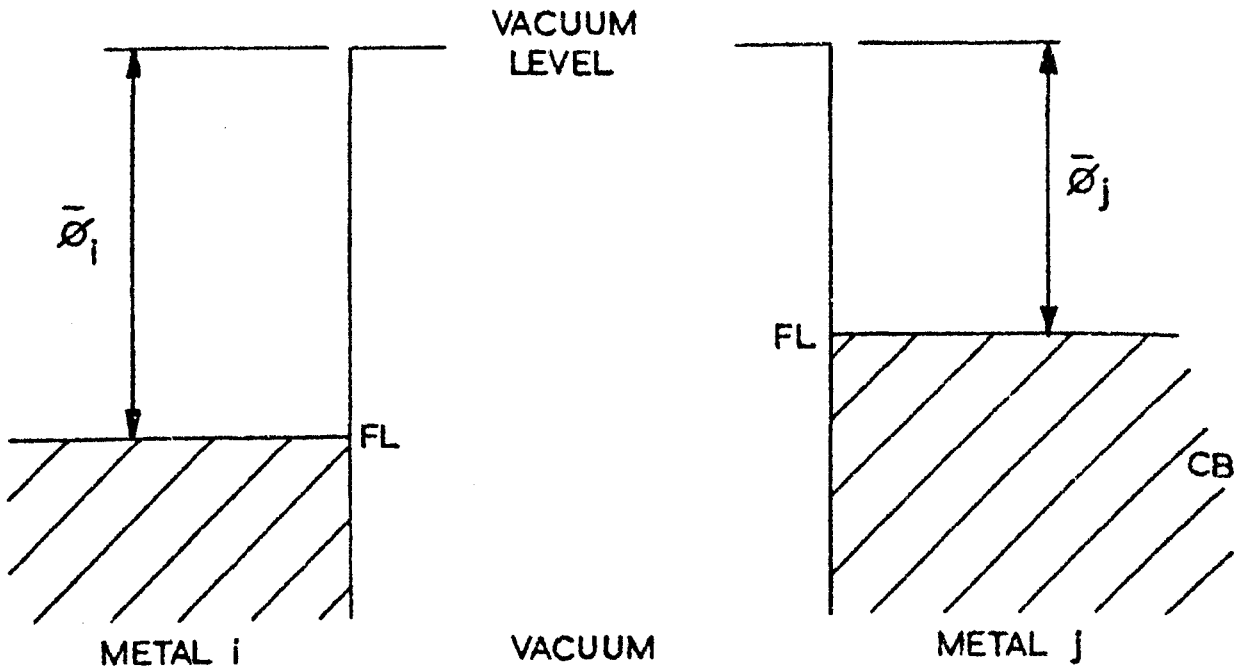

(b) AFTER CONTACT

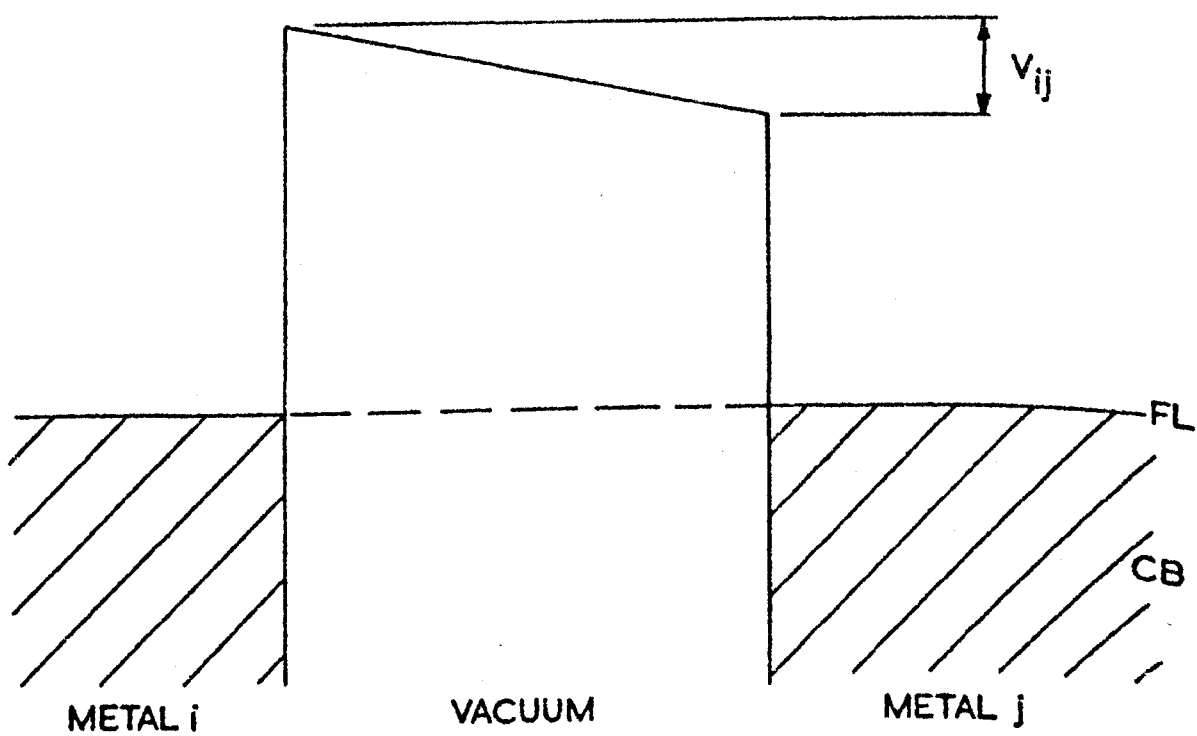

Figure 4.1 The energy band diagram of two patchy conductors i and j before and after electrical contact. V_{ij} is the contact potential difference.

A contact potential also must exist between points along the surface of a patchy conductor when the distance from the surface is small compared to the patch size. Equation (4.2) is valid for distances sufficiently large from the surface that the patch electrostatic field is small. The work function appearing in this equation is that of the free metal surface and the contact potential V_{ij} is therefore associated with the potential discontinuity at the free surfaces. Intermediate conductors do not affect the contact potential between the free metal surfaces.

The situation before and after electrical contact is shown in the energy band diagram in Figure 4.1. The metal having the largest work function, i say, is charged negatively by the electron transfer leaving the other positively charged.

4.2 Dynamic Capacitor Method

The capacitor method was originally proposed by Kelvin in 1898 and is currently used in the form due to Zisman 1932. The two metal surfaces, whose contact potential is to be measured, are arranged to form a capacitor C, and they are electrically connected through a resistor R, cf. Figure 3.8. The charge on each is given by $Q = CV_{ij}$. A displacement of either electrode causes a charge flow ΔQ between the free surfaces. ΔQ is detected by the voltage developed across R. If an external dc backing voltage V_b is included in series in the circuit and adjusted until any displacement of either electrode produces no voltage drop across R, then V_b and V_{ij} are related by:

$$V_b = - V_{ij} \qquad (4.3)$$

The theory of this method is discussed by Chalmers 1942, Domenicalli 1954 and Gundry and Tompkins 1968.

In the Zisman method, one of the electrodes is vibrated continuously so that an alternating voltage is developed across R. This development lead to easier amplification of the signal and its detection by cathode ray oscilloscopes or phase sensitive detectors. The principle of the static capacitor method is similar to that above. In this technique, the electrodes are stationary and the change in contact potential ΔV_{ij} causes a current ΔQ to flow in the external circuit which is detected across R (Delchar et al 1963).

Various refinements have been made to the methods for electronic detection and vibrating the electrode for improved stability and for automatic recording of the contact potential. These are reviewed by Gundry and Tompkins 1968.

The use of a small vibrating electrode to study patch effects on the other stationary electrode has been described by Parker and Warren 1962 and by Wolff et al 1969. The design of the scanning vibrating electrode capacitor used in this work and described in Chapter 3 was based on that of Parker and Warren.

4.3 Reference Surfaces

The dynamic capacitor method is indirect and a reference work function is needed to deduce the work function of the other electrode from the contact potential measurement. It is never certain that the work function of the reference surface has the

same value that has been measured in another experiment, nor that the changes in contact potential are solely due to the other active surface. The work function of six clean gold films, for example, measured in four different laboratories ranged from 5.22eV to 5.45eV (Huber 1966, Riviere 1966, Holscher 1966, Satchtler et al 1966). Therefore to infer that the mean value of 5.34eV applies to any other gold film in similar conditions leaves the result of any contact potential measurement subject to an uncertainty of about 0.1eV. A similar conclusion can be arrived at for aged tungsten foils (cf. Haas and Thomas 1969, Hopkins and Riviere 1963). The latter authors recommended aged tungsten to be used as a standard reference surface in contact potential work. The evidence favouring the use of noble metal films as reference surfaces in SP work is discussed in Chapter 6. Reference surfaces of fresh gold and silver films were used in the present research.

4.4 Technical Factors

The alternating voltage v developed across the resistor R by a sinusoidal modulation of the capacitance C was derived by Myers 1953. If the capacitance modulation is described by:

$$C = C_o \ (1 + (a/d) \ \sin \omega t)^{-1} \qquad (4.4)$$

where C_o is the mean capacitance and a, d and ω are the amplitude of vibration, the mean distance between the electrodes and the pulsatance respectively, then v is given by:

$$v = - a \ \omega \ A \ R \ Y \ V_{ij}/4\pi \ d^2 \qquad (4.5)$$

where $Y = \cos \omega t/(1 + (a/d) \sin \omega t)^2$ and V_{ij} is the contact potential. Equation (4.5) is valid for a plane parallel plate capacitor of area A.

Equations for the true wave form of the generated signal have been derived by Anderson and Alexander 1952 and by Macdonald and Edmondson 1961 since in a real capacitor the modulation of C is not strictly sinusoidal. They also discussed the harmonic content and sensitivity of the method under various conditions. Briefly, the harmonic content increases with the amplitude of the modulation of the capacitor, with the reciprocal time constant and with non-parallelism of the electrodes.

The conversion efficiency ξ may be defined as the ratio of the ac voltage to the overall dc voltage in the circuit by:

$$\xi = v/(V_{ij} + V_b) \tag{4.6}$$

ξ is approximately proportional to the fractional change of capacitance $\Delta C/C$ and to the modulation factor $m = a/d$. If a phase sensitive detector is used then v is rectified to give a proportionate dc output v' and ξ is proportional to $v'/(V_{ij} + V_b)$. ξ may be experimentally determined by measuring the change in dc output for a series of known impressed dc voltages and is given by:

$$\xi = v/(V_{ij} + V_b) \propto v'/(V_{ij} + V_b) \propto \Delta C/C \leq a/d \tag{4.7}$$

where v, ΔC and m are peak values. In the first two expressions for ξ the numerators are not independent of the denominators, consequently $\xi \to o$ as $V_b \to - V_{ij}$.

A high conversion efficiency is needed to obtain a good signal to noise ratio Sn which may be defined by:

$$Sn = \xi(V_{ij} + V_g)/\Pi \qquad (4.8)$$

where Π is the peak noise. It is advantageous to use a large capacitor and a high conversion efficiency. Ideally Π is composed only of the input noise to the head amplifier.

4.5 Noise Problems

The following sources of noise are superimposed on the desired signal: amplifier noise, electromagnetic pickup and microphonic noise. Amplifier noise has been discussed in detail by Parker and Warren 1952. They deduced the theoretical optimum value of Sn for an equivalent circuit of the capacitor and head amplifier. The theoretical values were in good agreement with those measured experimentally. Briefly, the optimum value of ξ was approached if A, R, ω and m were allowed to take their maximum practical values. The theory suggested that a value of Sn could be attained which would allow a resolution in the measurement of V_{ij} of a few tens of microvolts if ω was sufficiently high. Unfortunately these parameters are technically limited by the mechanical response of the system designed.

The head amplifier must have a high input impedance and low input noise. Its input resistor is usually between 10^7 and $10^{10}\Omega$. The parallel input impedance of the cable between

the capacitor and the amplifier, $1/\omega C$, must be kept sufficiently high not to bypass R. The product $1/\omega CR$ should be kept small, but as ω increases the resistor noise becomes less important than valve or transistor noise.

Electromagnetic pickup is reduced by the standard precautions. Microphonic noise can be a far greater source than the others combined. The rigid mechanical coupling between the moving-coil type of transducer and the vacuum system used in the present work was troublesome in this respect and it was found essential to mount the transducer and head amplifier on a separate block as described in Chapter 3.

Mignolet 1950 drew attention to the emf induced by the vibration of an electrode in a stray magnetic field. Calculation showed the mean emf to be much smaller than other sources of noise in the present experiments.

In this work, the following values were typical for $R = 5 \times 10^7 \Omega$ $m \simeq 0.5$, $\omega \simeq 115$ Hz and $A \simeq 0.1$ cm^2 which resulted under favourable conditions in a conversion efficiency of $\xi \sim 0.1$ due primarily to the small area of the probe electrode. The input peak noise to the head amplifier was typically 20 μV. The narrow band amplifier and phase sensitive detector reduced the noise level and under favourable conditions the contact potential could be measured to an accuracy of a few millivolts.

4.6 Effect of Stray Capacitance

The dynamic capacitor is capactively coupled to the walls of the vacuum chamber and to other surfaces inside it. The detected signal may include a component due to this stray capacitance which has the same frequency but not necessarily phase as the true signal given by Equation (4.5). A manifestation of this is the very large effect of static charge on glass surfaces (Mignolet 1950). To reduce this undesired signal, Anderson 1952 recommended, firstly, that the screen should be made of the same metal as the vibrating electrode, secondly, that the support for each electrode should be coated with a film of the same metal as the electrode surface, and have the same degree of cleanliness. Other such criteria are: using a large capacitor and a large amplitude of vibration, keeping the electrodes a large distance from the vacuum chamber walls and ensuring the inner surfaces are conducting (Mignolet 1950, Anderson 1952).

Potter 1940 found that changing the potential V_s of a metallic electro-static screen around his apparatus altered the measured value of the contact potential between dissimilar metals V_{12} by about one tenth of V_s and in the same direction. He concluded that V_s would affect all values of V_{12} by the same amount and that for measuring changes of V_{12} the value of V_s was unimportant. He also concluded that when measuring the absolute value of V_{12}, the potential difference between the shield and the electrode that was connected to the detector should be equal and opposite to their

contact potential. If this was not the case, there could be a systemmatic error caused by the stray capacitance. He adjusted V_g until there was "zero contact potential" between two "identically contaminated" tungsten filaments.

Hackerman and Lee 1955 observed an approximately linear change of as much as 80mV in the measured value of the contact potential when the mean electrode spacing or amplitude of vibration was altered. It also changed if one electrode was rotated with respect to the other and these effects may be explained as the results of stray capacitance.

Simon 1959 investigated the effect of stray capacitance by measuring the apparent contact potential V_{app} as a function of the interelectrode spacing d for a series of amplitudes of vibration a. For a constant value of a, V_{app} increased to a limiting value as the conversion efficiency ξ increased, i.e. as d was decreased. The limiting value itself decreased as a was decreased. For the range of values of a and d investigated by Simon, V_{app} varied by more than 0.14V. He qualitatively explained these effects by considering the relative changes in the true capacitance and the stray capacitance. A small change in d has a large effect on the former, but has little effect on the latter because its other electrode, e.g. the vacuum chamber wall, is relatively far away from the vibrating electrode. Simon concluded that with a suitable choice of a and d, the error in the measured value of V_{ij} was only a few mV, although it is not clear how he

arrived at this figure. Recently Weissmann et al 1968 also observed V_{app} to increase by a few mV when the inter-electrode spacing d was decreased.

It is apparent that although several simple technical criteria help in reducing the effects of stray capacitance, they are insufficient alone to justify an assumption that these effects are negligible.

4.7 Theory of Stray Capacitance

If the vibrating electrode is called number 1, the stationary electrode number 2 and the stray electrodes numbers 3, 4 ...., n, then the total charge Q on electrode 1 is given by:

$$Q = \sum_{j\geq 2} C_{1j}\ V_{1j} = C_{12}\ V_{12} + \sum_{j\geq 3} C_{1j},\ V_{1j} \qquad (4.9)$$

where C_{1j} and V_{1j} are respectively the capacitance and potential difference between electrode number 1 and the jth stray surface. The signal across the input resistor of the detector is the sum of the oscillatory currents I due to the amplitude modulations of the capacitances C_{12} and $\sum C_{1j}$ assuming all the currents are in phase. If the electrode spacing is modulated so that its instantaneous value is given by $\{d + a.\ f(\omega t)\}$, where d is the mean spacing between electrodes of area A, a is the amplitude of modulation and ω is the angular frequency, then the instantaneous value of the capacitance is :

$$C_t = (\varepsilon_o A)/d \{1 + mf(\omega t)\} \qquad (4.10)$$

where $m = a/d$ and the oscillatory current is:

$$dQ/dt = - V_{1j} C_{1j} m \{1 + mf(\omega t)\}^{-2} f'(\omega t) \qquad (4.11)$$

For simplicity (4.11) may be written:

$$I_{1j} = V_{1j} \Delta C_{1j}$$

where $\Delta C_{1j} = m C_{1j} \{1 + mf(\omega t)^{-2} f'(\omega t)$.

If V_{app} is the apparent contact potential in the presence of stray capacitances, then the null point is given by $I = 0$ when the backing voltage $V_b = - V_{app}$ is in series with V_{12} and V_{1j}. Using this condition gives:

$$0 = \Delta C_{12} (V_{12} - V_{app}) + \sum_{j \geq 3} \Delta C_{1j} (V_{1j} + V_b) \qquad (4.12)$$

$$V_{app} = V_{12} + \left(\frac{\sum_{j \geq 3} \Delta C_{1j} (V_{1j} + V_b)}{\Delta C_{12}} \right)$$

and since $V_{1j} + V_b$ is the potential difference between the vibrating electrode and the stray capacitance in the presence of a backing voltage, this equation is equivalent to the one given by Simon 1959.

It is not easy to predict the variation of V_{app}. The simplest case is to assume that all the capacitances are of the parallel plate type, of area A, with instantaneous electrode spacings $d \{1 + mf(\omega t)\}$, to obtain an approximation for the ratio of the capacitances in Equation (4.12) by using a binomial expansion to the first power of m. This however leads to:

$$dC_t/dt = \Delta C_{1j} = (\varepsilon_o A_{1j}) \{m_{1j} f(\omega t)\}/d_{1j}$$

In Equation (4.12) the fraction $\Sigma\Delta C_{1j}/\Delta C_{12}$ reduces to $(\Sigma C_{1j}/C_{12})(d_{12}/d_{1j})$ and it follows that:

$$\sum_{j\geq 3} \Delta C_{1j}/\ C_{12} = \sum_{j\geq 3} (C_{1j}/d_{1j}\ \varepsilon_o\ A_{12})(d_{12})^2 \qquad (4.13)$$

for $m << 1$.

Equation (4.12) predicts therefore that V_{app} varies with $(d_{12})^2$ which disagrees with the experimental results presented in Section 4.9. The reasons for this failure may be firstly, that although $m << 1$ for the stray capacitances, it is quite large (e.g. 0.3) for the dynamic capacitor and, secondly, the stray capacitances are not all of the parallel plate type. The stray capacitive signal was observed to be in antiphase with the true one. The expression for ΔC_{12} should either be expanded to a higher power of m or else the full expression for dC/dt given in Equation (4.11) should be used, but neither of these lead to a simplification of Equation (4.13).

4.8 Experimental Method

The effect of stray capacitance was first detected when, in one of the preliminary experimental runs, the substrate support collapsed and dropped off the rotary drive. The design of this particular assembly was of the preliminary type described in Chapter 3. In the absence of the substrate which formed the stationary electrode of the capacitor, a stray capacitive signal was clearly observable.

These experiments were conducted in the unbaked system at a pressure of 10^{-7} torr. As described in Chapter 3 the vibrating electrode was insulated from the drive bar. The bar itself was screened by an earthed cylinder, Figure 3.6. There was no detectable capacitive coupling (i.e. < 0.1 pF) between the bar and the stationary electrode. In order to evaluate the effect of stray capacitance a stainless-steel screen of fine mesh was mounted just inside of the wall of the vacuum system and electrically insulated from it, as described in Chapter 3. The potential difference between the vibrating electrode and the screen was varied by an external circuit in order to simulate changes in contact potential between the electrode surface and the walls. The amplitude of vibration was adjusted by varying the driving voltage to the transducer, although its response was non-linear. The mean spacing between the Kelvin capacitor electrodes was varied by using an almost semi-circular substrate electrode so that the spacing was changed when it was rotated to a new position relative to the vibrating electrode. The conversion efficiency ξ was determined by measuring the change in dc output for a known impressed dc voltage (as given in Equation (4.7)). Finally by moving the stationary electrode completely away from the vibrating one it was possible to observe the signal due to the modulation of the stray capacitance alone. The stray capacitive signal alone could alternatively be observed by detecting the signal from the screen across the input resistor of an auxiliary head amplifier. In this arrangement the apparent and stray capacitive signal could be monitored on a double beam oscilloscope.

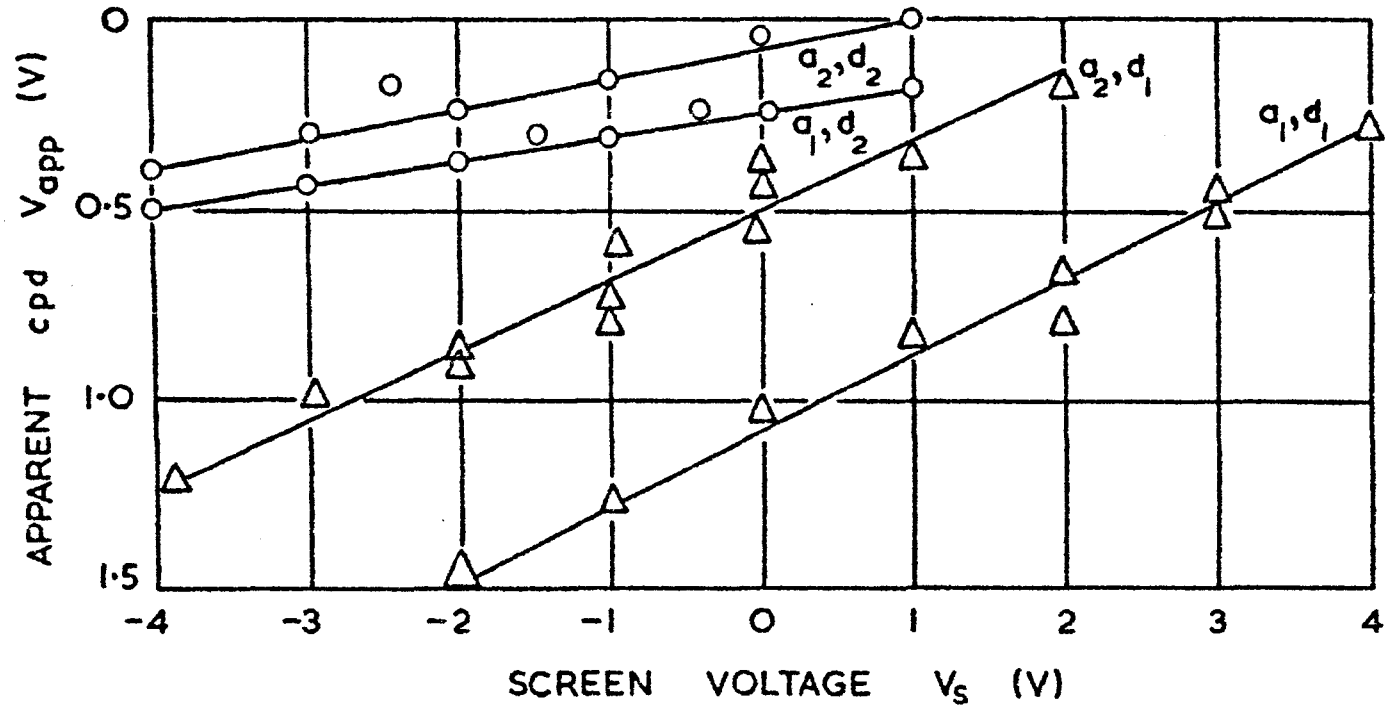

Figure 4.2 The apparent cpd as a function of screen voltage, at two electrode spacings ($d_1 > d_2$) and two amplitudes of vibration ($a_1 > a_2$).

During these series of experiments the pairs of the surfaces of the electrodes of the Kelvin capacitor were films of silver and erbium oxide (previously exposed to air), silver and gold, silver and silver, silver and titanium films.

4.9 Results

The apparent contact potential V_{app} was measured as a function of the screen potential V_s for different values of the spacing d and two amplitudes of vibration a. The results are shown in Figure 4.2. They show the linear dependance of V_{app} on V_s and therefore on V_{1j} and also that it varies with d and a. The magnitude of the change in V_{app} for two different values of d was 0.16V and 0.4V respectively for a change of 2V in V_s. Such large changes in V_{1j} may be realised by the accumulation of static charge on insulating surfaces, by gross contamination or by oxidation. A change in work function of the vibrating electrode will affect V_{1j} and subsequently V_{app} in a similar way.

This experimental evidence supports Anderson's suggestion described in Section 4.6 and disputes Potter's claim that the error in the measured contact potential was independant of the magnitude of the potential difference across the stray capacitance.

The stationary electrode was moved completely away from the vibrating electrode, so the signal due to the stray capacitance alone could be observed. Before it was moved away the contact

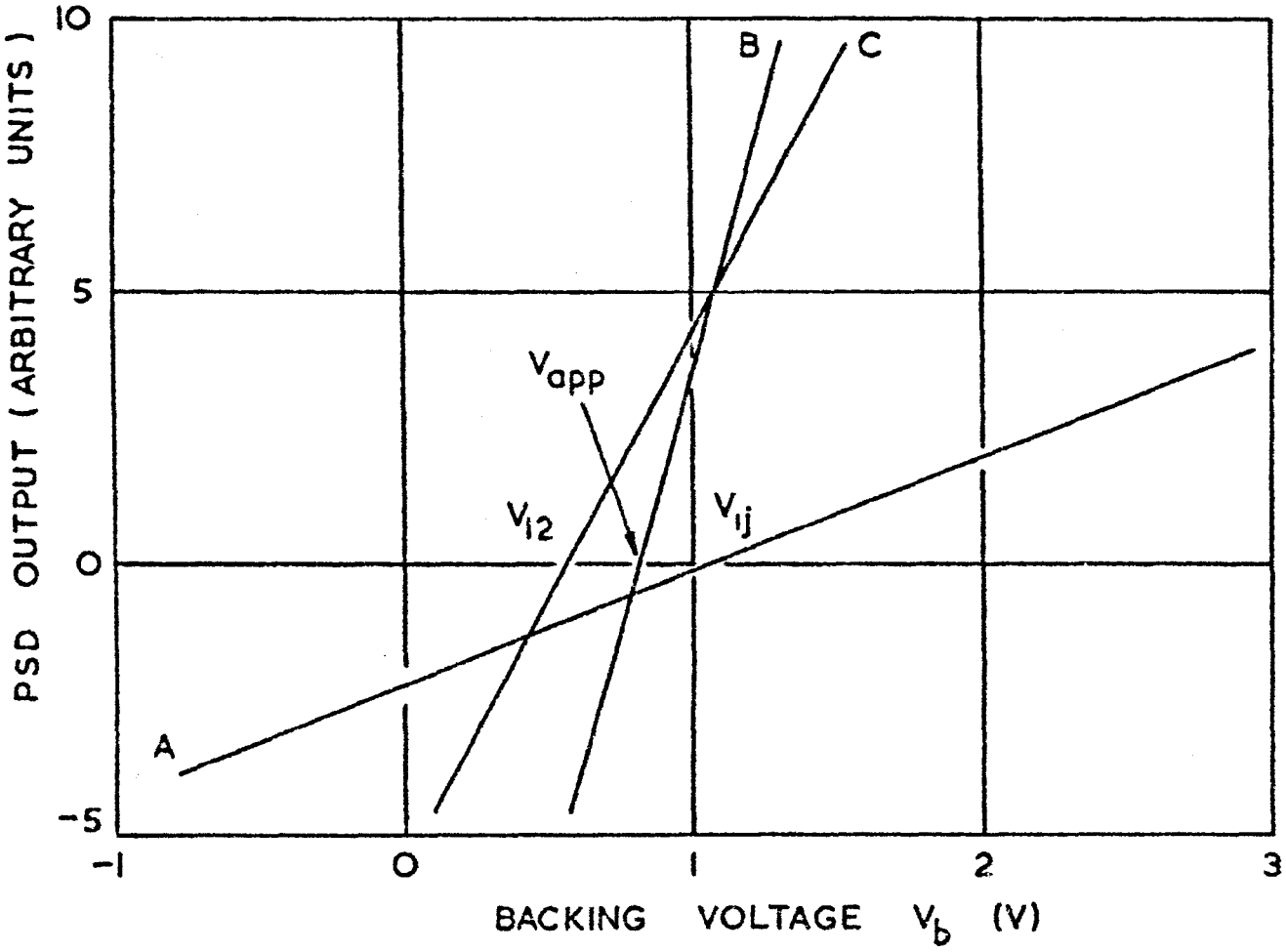

Figure 4.3 Response of: A stray capacitance, B, C Kelvin capacitor to backing voltage. Line B is for $V_s = 0$, line C for $V_s = -V_{1j}$.

potential between the Kelvin electrodes could be measured with a sensitivity of a few mV in the backing voltage. After it had been moved away not even a change of 5V in V_b could be detected, thus showing that all the signal in this arrangement would be from the stray capacitance. The vibrating electrode and the screen were then used in the manner of the Kelvin capacitor in order to find their contact potential. A backing voltage V_b was put in series with them and the signal they produced detected in the normal way. Figure 4.3, Curve A shows how the output from the phase sensitive detector varied with V_b. Its intersection with the abscissa is V_{lj}.

The stationary electrode was returned to its normal position and the signal from the Kelvin capacitor was measured as a function V_b, firstly with $V_s = 0$ which is shown in Curve B of Figure 4.3, and secondly with $V_s = - V_{lj}$, which is shown by Curve C. These two curves have a much sharper response than A because the conversion efficiency was much greater for the Kelvin capacitor than for the stray one. As intuitively expected, the response curve for the normal substrate position with the screen earthed, Curve B, was approximately the sum of the individual curves from both capacitors Curves A and C. An exact agreement would not be expected since the real and stray capacitive currents were out of phase. The difference between the intercepts of curves B and C with the abscissa shows that, in this instance, the difference between the apparent and true contact potential was 0.2eV. If the true contact potential changed this would correspond to Curve C being displaced along the axis and the error

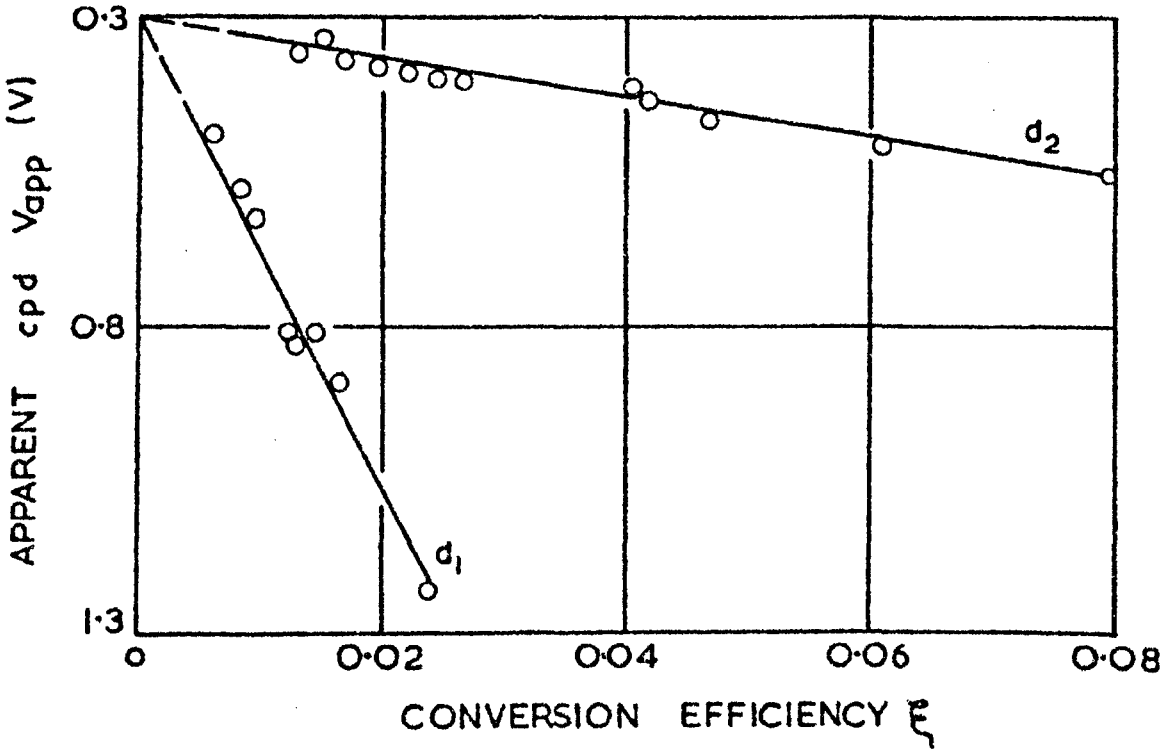

Figure 4.4 Variation of the apparent cpd with the conversion efficiency ξ as the amplitude of vibration a was increased (for two electrode spacings $d_1 > d_2$).

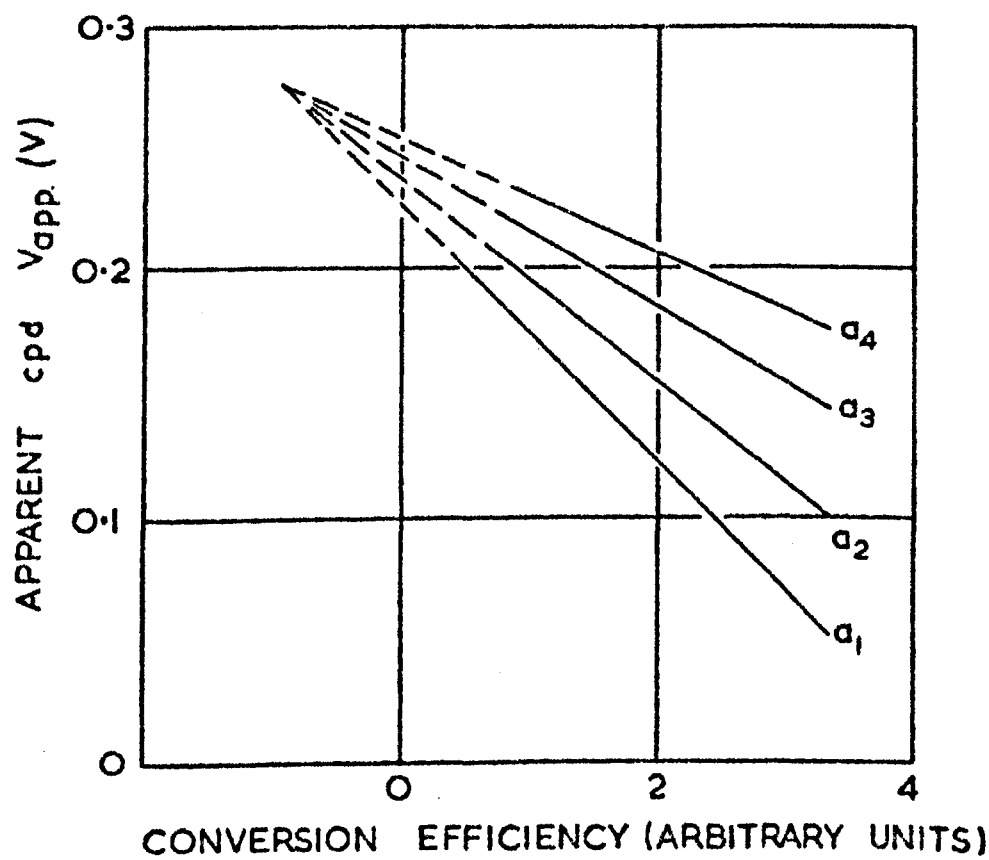

Figure 4.5 Simon's (1959) results redrawn to show variation of apparent cpd with conversion efficiency at a constant electrode spacing d (for four amplitudes of vibration $a_1 > a_2 > a_3 > a_4$).

would therefore also change with it. If the results shown in Figures 4.2 and 4.3 are combined then they are described by the empirical equation:

$$V_{app} = V_{12} + f_1 (V_{1j} + V_b) \qquad (4.14)$$

where f_1 is a constant.

The variation of V_{app} was measured as a function of the conversion efficiency ξ (which is approximately proportional to a/d) for two fixed values of the spacing d. For convenience the screen was maintained at earth potential. The results are given in Figure 4.4 which show that V_{app} varies linearly with ξ when d was constant. The extrapolated curves each cut the ordinate at the same value of V_{app}, seemingly the true contact potential. From Equation (4.7) $\xi \simeq a/d$ and the results are described by the empirical equation:

$$V_{app} = V_{12}\ f_2\ (a/d) \text{ for constant d} \qquad (4.15)$$

Simon 1959 also studied the variation of V_{app} with ξ, but for constant values of a rather than d. For technical reasons it was not possible in the present work to repeat his measurements. However, Figure 4.5 shows that when his results for V_{app} were replotted as a function of $1/\xi$ they gave a straight line for each value of a. Three of these lines could be extrapolated to intersect a common point which was probably the true value of V_{app}. Since his values for ξ were in arbitrary units, this may account for their intersection point lying on the negative side of the

axis at V_{app} = 0.23V, although Simon considered the true value to be 0.21V. It follows that:

$$V_{app} = V_{12} f_3 (d/a) \text{ for constant } a \qquad (4.16)$$

Some effects of stray capacitance on the variation of the work function across a film on a substrate are described in Chapter 7.

4.10 Conclusions

The empirical equations (4.15) and (4.16) show that the model used in deriving the theoretical value of V_{app} given in Equations (4.12) and (4.13) was over simplified. Combining the experimental evidence summarised in Equations (4.14), (4.15) and (4.16) gives the equation:

$$V_{app} = V_{12} + K \, ad \, (V_{1j} + V_b) \qquad (4.17)$$

where K is a constant whose magnitude and sign depends on the experimental apparatus and conditions. This equation may be compared with the theoretically expected one given in Equation (4.12).

A simple and effective way to avoid the effects of stray capacitance is to connect the vibrating electrode to the earth line and the stationary one to the input terminal of the detector. In these conditions, the current oscillating between the vibrating electrode and the walls of the vacuum chamber (which contribute most to the stray capacitance) does not flow through the input

detector in series with the Kelvin electrodes. This corresponds effectively to the condition that $V_{1j} + V_b = 0$ in Equations (4.12) and (4.17). Its effectiveness can be tested by showing the value of V_{app} is independant of one or more of the parameters a, d and $(V_{1j} + V_b)$. If a detector is used with a differential input (as in the present work) this precaution cannot be taken and the increase in signal to noise ratio does not compensate for the serious effects of stray capacitance.

In conclusion, the effects of stray capacitance have been discussed in detail and results have been presented which show the general relationship between the apparent contact potential and the stray capacitance. It has been shown that their effects may lead to substantial errors in contact potential measurements. Simon's analysis of the dependance of the apparent contact potential on the potential between the oscillating electrode and the surface forming the stray capacitance is shown to be correct. The change of this potential may lead to further errors of measurement. The variation of the apparent contact potential with the modulation factor has been studied and analysis of Simon's data supports the empirical results summarised in Equation (4.17).

CHAPTER 5

THE EFFECT OF IRRADIATION AND ELECTRIC FIELD ON THE WORK FUNCTION OF STEEL

5.1 Introduction

The work function of the stainless steel vibrating electrode was changed by optical and charged particle irradiation, exposure to H_2 at high pressures ($\sim 10^{-6}$ torr) and by externally applied dc electric fields. In the absence of these its work function was constant. These effects were observed for two steel electrodes although only results from one of these are presented. They are interpreted as the result of changes in the distribution of charge within or on an oxide layer. The electrode received only the normal bake-out treatment in vacuum after polishing in air (cf. Chapter 3). The experiments were conducted in the baked vacuum system at a pressure of 10^{-9} torr. The reference surface was a gold film deposited at 10^{-9} torr on the glass substrate. A current of charged particles emanating from the ion pump was incident on the electrodes since the experimental construction unfortunately allowed a direct line of sight between them and the pump discharge elements. A baffle was placed in the throat of the Boostivac pump after these experiments to prevent their access into the experimental chamber as described in Chapter 3. The charge effects were completely eliminated in a later experimental run by depositing in-situ a film of Ag on the electrode (cf Chapter 7).

The effects of electrical charges on the work function of metal surfaces have been frequently observed in oil-diffusion pumped systems. In such instances they have been attributed to the presence of a dielectric contaminant on the metal surface (Stewart 1934, Lindholm 1960, Petit-Clerc and Carette 1968 (a) and (b)) and from adsorbed gases (Marmet and Morrison 1962). Similar effects were recently reported by Dobrozemsky and Haltau 1970 in an unbaked system using viton gaskets and exhausted with a getter-ion pump and chilled sorption pump. In their experiments at $\sim 10^{-6}$ torr, an incident electron current $<10^{-8}$ A mm^{-2} on metal surfaces produced changes in ϕ of up to a volt. The clean surfaces of graphite and gold however changed less than 0.1 eV. The decay constants of the surface charge varied from 30 minutes to several hours.

Similar phenomena have been reported for metal surfaces immersed in a low pressure gas discharge (cf. Hopkins and Vick 1960 and Davies et al 1961 and cited references). ϕ changed by as much as 10 eV even for small discharge currents when various oils were deliberately introduced into the system (Davies et al).

The thermionic work function of aged stainless steel ribbon has been measured by Wilson 1966. The work function in ultra high vacuum varied from 4.34 eV at 1080°K to 4.22 eV at 1395°K. Morozova et al 1962 have measured the contact potential between gold films and stainless steel subjected to various oxidising treatments in vacuuo in an oil-diffusion pumped system

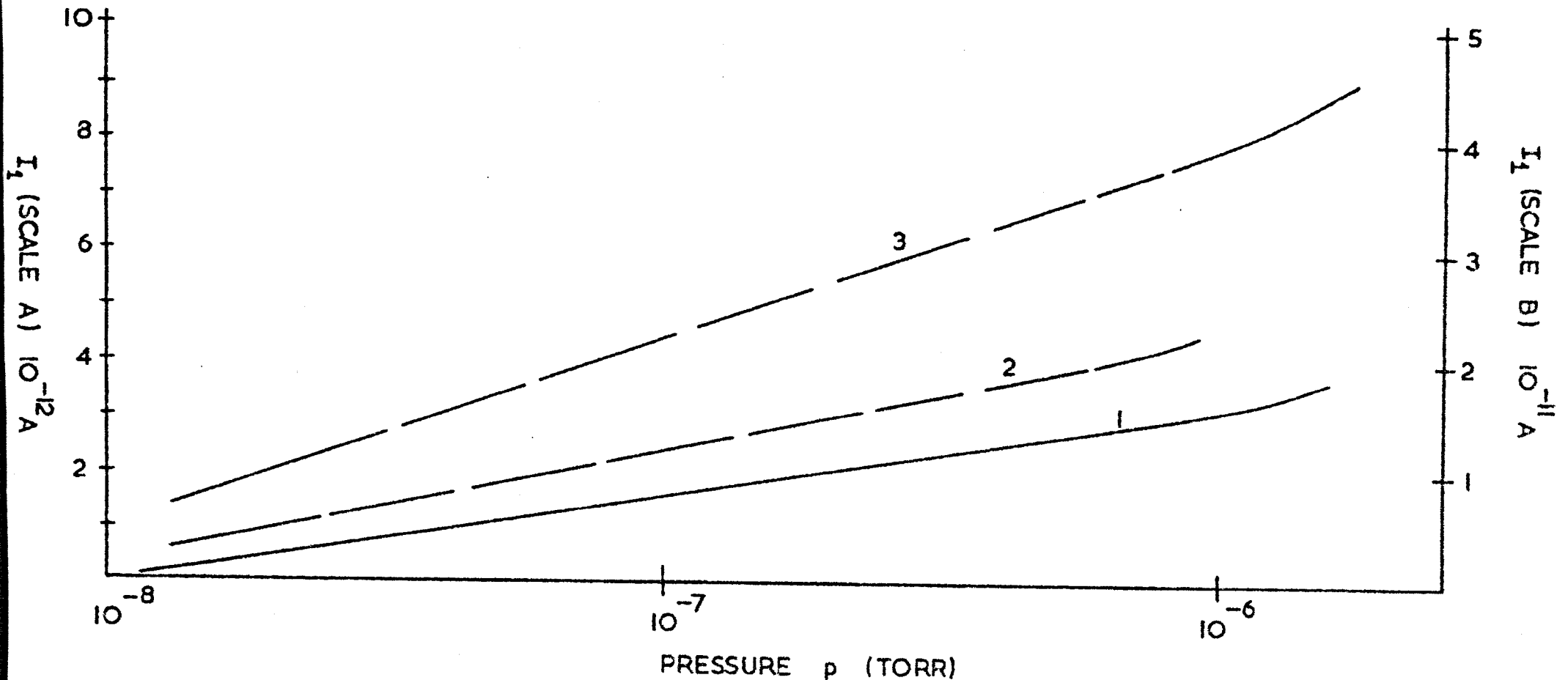

Figure 5.1 Variation of the electron current I_1 to the substrate with the pressure of hydrogen for a floating bias (1), - 25V bias (2) and a + 25V bias (3). Scale A is for curves 1 and 2, scale B for curve 3.

at 10^{-6} torr. If the work function of their gold samples lies within the range from 4.2 to 4.9 eV (cf. Chapter 6) then the work function of the steel oxides lay within the range from 4.5 to 5.1 eV.

5.2 Experimental Method and Results

5.2.1 Effect of Neutral and Charged Particles

The current collected by the steel electrode was dependant on the partial pressure of H_2 as shown in Figure 5.1 and also on the potential of the electrode. The electron current collected varied from $\sim 10^{-13}$A at 10^{-9} torr (H_2) to $\sim 10^{-11}$A at 10^{-6} torr (H_2). Insulated (floating) electrodes and positively biased ones collected negative current carriers and negatively biased ones collected positive carriers. The negative current was typically 10 to 30 times the positive current for equal but opposite biasing potentials at constant pressure. When the ion pump was switched off this current decayed to zero, and under these conditions hydrogen was introduced through the palladium thimble to a maximum pressure of 10^{-6} torr. After a few minutes the gas pressure was reduced to avoid overheating the pump. During this cycle there was no change in the work function of the steel specimen within the experimental resolution of $\overline{+}$ 10 mV.

The effect of an electron current was investigated by gradually increasing the partial pressure of hydrogen with the ion

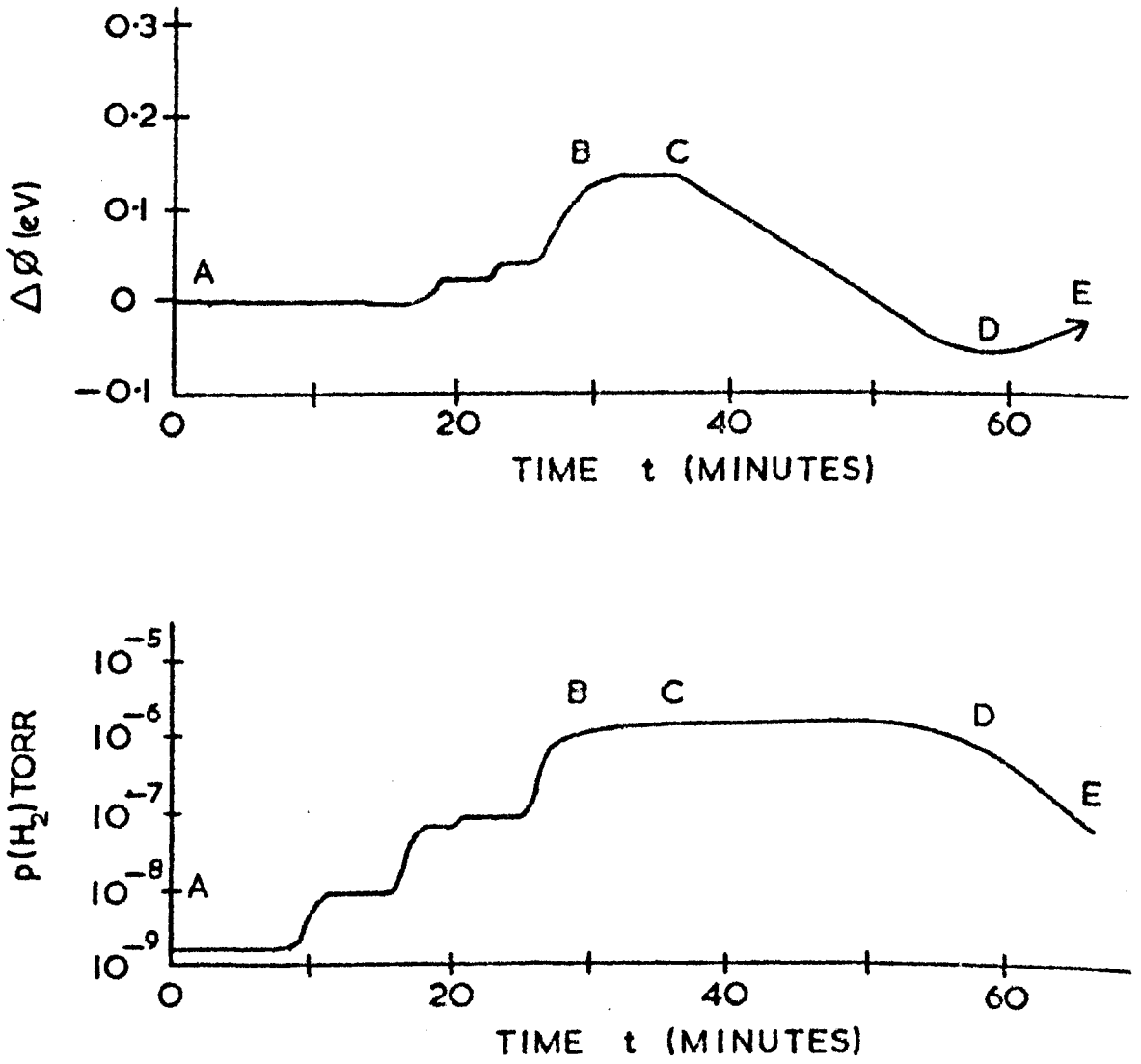

Figure 5.2 Typical change of the work function $\Delta\phi$ of stainless steel with the pressure of hydrogen $p(H_2)$ as a function of time. Curve A-B is due to the pressure dependent electron current incident on the surface (cf. Figure 5.1) and curve CD is due to adsorption of hydrogen.

pump switched on. The typical variation of the steel work function ϕ is shown in Figure 5.2. The initial introduction of H_2 to a pressure of 10^{-6} torr, with the ion pump operating, increased ϕ. Both the magnitude of the change and the rate of change depended on the incremental increase of gas pressure and the rate of pressure rise. The change in ϕ at each constant pressure and incident current is shown in Table 5.1. If the pressure was maintained at 10^{-6} torr (cf. point B in Figure 5.2) then ϕ reached an equilibrium value and after a few minutes decreased linearly at a rate of $\sim$ 10 mV min^{-1} (Curve CD in the diagram) and eventually became smaller than the original work function. Although this reduction showed no evidence of stopping the gas pressure was reduced at point D. When the H_2 was pumped away these curves were retraced in the reverse direction although with a longer time scale until the original value of ϕ was obtained in ultra high vacuum.

5.2.2 Effect of Illumination

The work function decreased when the electrode was illuminated and this occurred whenever internal filaments inside the system were heated above yellow heat. Quantitative measurements were obtained with a mercury high pressure discharge lamp (Wotan 250W) shining through a clean pyrex window in one of the vacuum chamber ports. The lamp generated a continuous spectrum of approximately constant intensity throughout the ultra-violet, visible and infra-red regions on which were superimposed several intense lines. The

Pressure (H_2) Torr	I_1 $10^{-12}Acm^{-2}$	t mins	$\phi_\infty - \phi_0$ mV
3.10^{-9}	< 0.1	5	0
1.10^{-8}	0.1	11	- 10
8.10^{-8}	1.4	15	+ 20
1.10^{-7}	1.6	20	+ 40
2.10^{-6}	3.5	25	+130

TABLE 5.1 The variation of the equilibrium change in the work function ($\phi_\infty - \phi_0$) of stainless steel with the incident electron current I_1 as the pressure p of hydrogen was incrementally increased from figures 5.1 and 5.2. The error in $\phi_\infty - \phi_0$ is $\pm$ 10mV and t is the time for equilibrium to be established for each increment of p.

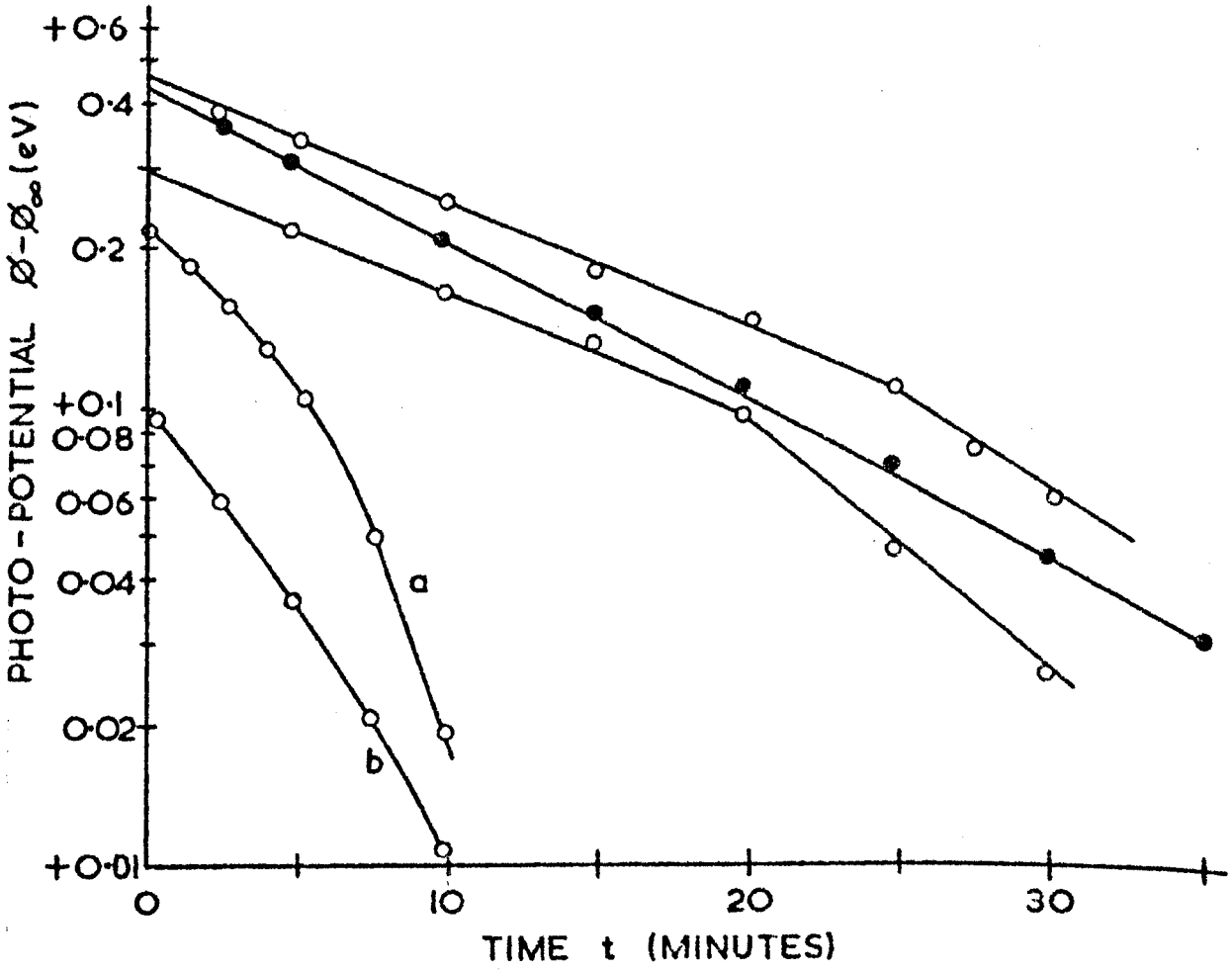

Figure 5.3 Typical reduction in the work function ϕ of the steel probe when illuminated at constant intensity with white (mercury) light at 2.10^{-9} torr. Curves a and b were obtained with a low illumination intensity.

most important of these were at 3650, 5461 and 4358 A^{o} (Vaidya and Daudawate 1966). The transmission coefficient of pyrex is almost constant at approximately 0.9 throughout the visible region but falls off sharply at ∿3500 and ∿ 2500 A^{o} to ∿ 0.5 or less (Shand 1958). Attempts to identify the optical frequency responsible were unsuccessful. No vacuum photo-electron current from the steel specimen could be detected above the sensitivity limit of an electrometer detector (∿ 10^{-13} A dc). The photo-potential (i.e. change in ϕ) was independent of the neutral gas pressure at a maximum pressure investigated ∿ 8. 10^{-7} torr (H_2). It was independent of the flux of charged particles when the ion pump was operating provided the pressure was less than ∿ 3. 10^{-8} torr (H_2). Above this value, the magnitude of the photo-potential was reduced by the opposing effects of incident electrons on the steel work function.

When mercury light was incident on the steel surface (by reflection from the internal walls of the system) the photo-voltage $\phi_o - \phi$ exponentially increased and assymptoted to an equilibrium value with a time constant of about 30 minutes, Figure 5.3. The curves appeared to be distorted in the presence of the ion pump current but these may have been unreliable because of unstable or low intensities of illumination. Other experiments showed that the electron current retarded the development of the photo-potential in time and also reduced the magnitude of the equilibrium change in ϕ. At low pressures the time development was not affected and the data shown in Figure 5.3 is free from

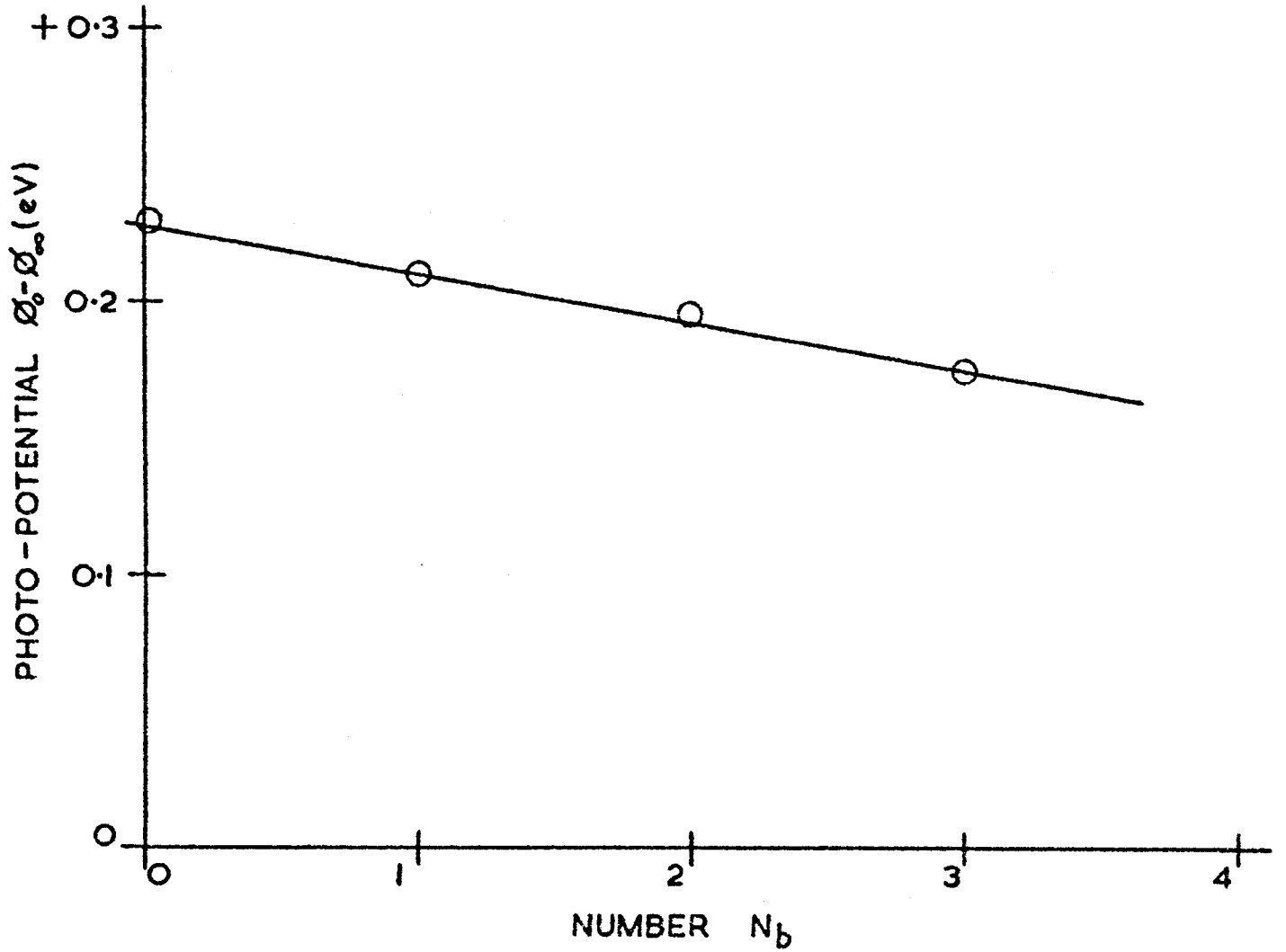

Figure 5.4 Variation of the equilibrium photo-potential ($\phi_o - \phi_\infty$) of the steel probe with the intensity of illumination (white mercury light). N_b is the number of similar optical filters in the light path.

these effects. Technical difficulties prevented a quantitative investigation of the effect of the current on the photo-potential. The equilibrium value of the photo-potential increased with the intensity of illumination as shown in Figure 5.4 as a function of the number of clean identical quartz spectrosil filters inserted into the optical path. These results were obtained by illuminating the steel with the mercury light through the filters and removing them one at a time allowing equilibrium to be established each time. The maximum photo-potential observed was - 0.5eV.

In the absence of the ion pump current the photo-voltage maintained its equilibrium value for fifteen minutes or more after the illumination was removed. The photo-voltage could be quenched by increasing the pressure of H_2 with the ion pump on and the time constant of the decay depended on the current. The original value of the work function was eventually regained.

5.2.3 Effect of Electric Field

The mean separation between the capacitor electrodes was approximately 0.5 cm. When a dc potential difference V_e was applied between the steel surface and the reference electrode, so that the negative pole of the battery was connected to the steel electrode, the work function ϕ decreased exponentially in time until the change in ϕ was equal to $|V_e|$. The effect was repeated if V_e was further increased and in this way ϕ was reduced by 1.6eV on

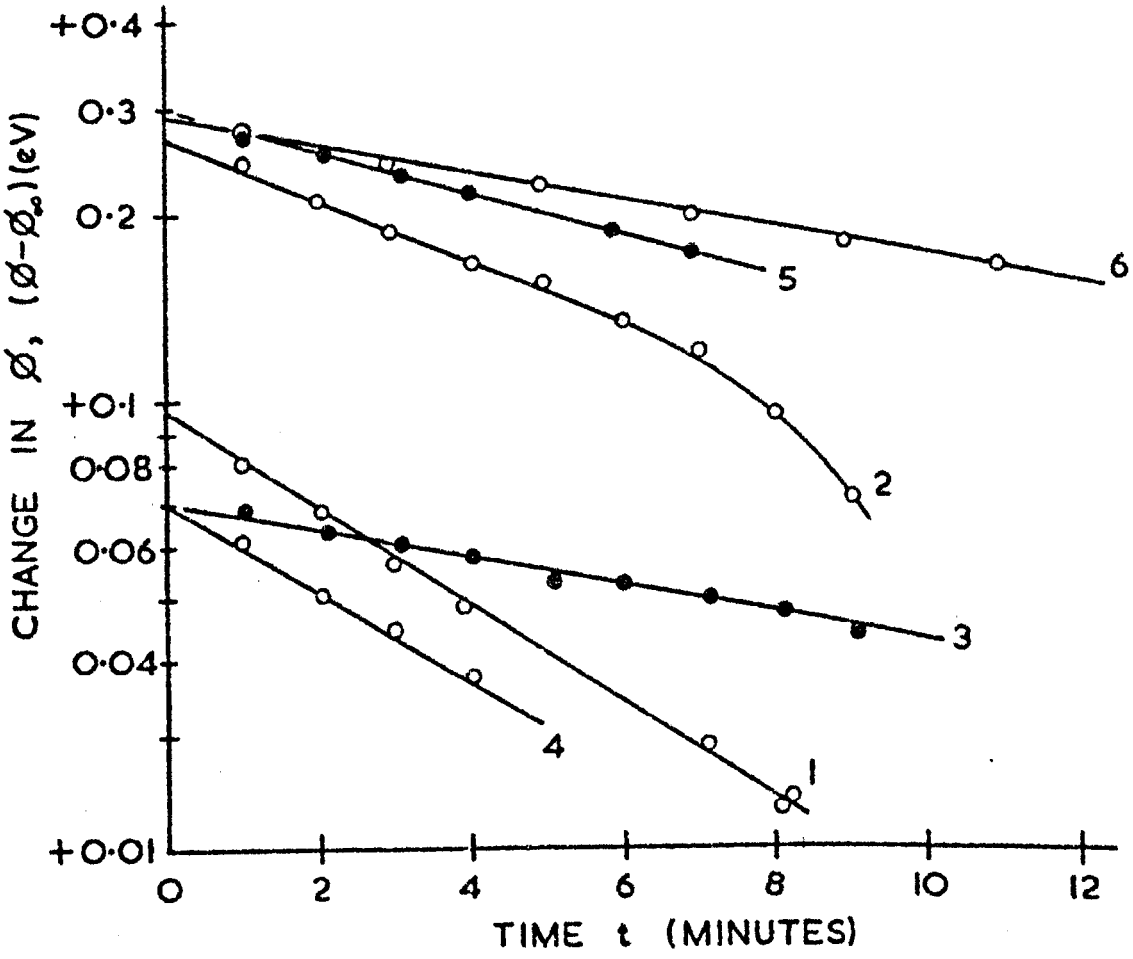

Figure 5.5 Typical examples of the reduction in the work function ϕ of the steel probe at 2.10^{-9} torr in the Field Effect when a negative bias potential $|V_e| = \phi_o - \phi_\infty$ was applied. The results are summarised in Table 5.2.

one occassion. The original work function was regained on reducing V_e to zero. A potential difference of opposite polarity however caused no change in ϕ below the maximum value of V_e = 1.0eV inves gated in this case. This field effect occurred whether or not the ion pump was operating and the ion pump current did not influence it until the gas pressure was greater than 4×10^{-7} torr (H_2). Above this pressure an incident electron current opposed the field effect. Some typical examples of the change in ϕ when a potential V_e was impressed are shown in Figure 5.5. The exponential time constant generally increased with the magnitude of V_e as shown in Table 5.2.

When equilibrium was established for the initial value of V_e, ϕ could be decreased still further by increasing the applied potential difference to a larger value. The data accuracy was poor for these additional changes and consequently the results could not clearly distinguish whether the exponential time constant for each incremental pulse was independent or not of the magnitude of the incremental increase in V_e.

On reducing V_e to zero, ϕ increased quickly and then assymptoted to its former value. The recovery period was also exponentially time dependant and behaved similarly to the initial reduction in work function.

TABLE 5.2

Curve	$\lvert V_e \rvert$ Volts	τ mins	% Error in τ $\pm$
1	0.10	13	8
2	0.26	20	15
3	0.07	41	25
4	0.07	12	8
5	0.30	43	33
6	0.30	27	12

The exponential time constants from the field effect data shown in Figure 5.5 as a function of the impressed dc potential V_e.

5.3 Discussion

The main constituents of EN58E stainless steel are iron (72.3%), chromium (19.1%) and nickel (8.1%). When an iron film is grown in vacuum at $\sim 300^{\circ}K$ and exposed to the atmosphere, an oxide film of thickness $\sim 30\ A^{\circ}$ is formed (Kruger and Yolken 1964). The mechanical polishing of the steel electrode undoubtedly caused local heating and severe surface damage on a microscopic scale. Consequently the electrode probably possessed a surface oxide whose thickness was likely to be significantly greater than $30\ A^{\circ}$. Commercial irons and steels contain appreciable quantities of H_2 since its solubility at $300^{\circ}K$ is high. At higher temperatures ($\sim 500^{\circ}K$) the diffusion coefficient of H_2 in F_e is large and its reliberation occurs easily (Dayton 1960, Calder and Lewin 1967). The oxides of iron, however, are not reduced by H_2 below $800^{\circ}K$. Iron oxides are n-type semiconductors and at 10^{-9} torr the electrode surface was likely to be covered with a mixture of oxygen, hydroxyl groups and possibly some water vapour which may have been readsorbed after bake-out. With the exception of H_2O, these molecules are electron acceptors. Other likely surface contaminants may have been carbon and sulphur which have diffused from the bulk of the steel to its surface (Harris 1968).

It is unlikely for such small incident electron currents ($\lesssim 10^{-11}$A) that electronic and photon desorption of adspecies from the surface or irradiation damage were of primary importance. The incident mean primary particle energy was unlikely to be

greater than 25eV since a negative retarding potential of this value was sufficient to establish a net positive current. At such low primary energies secondary electron emission is unlikely to be important. Adsorbed molecular gases on stainless steel are known to be desorbed by energetic primary electron impact (McCracken et al 1967) or dissociated. Either process may result in a reversible work function change of the correct direction to account for the results in Figure 5.2. The electron desorption efficiencies of electronegative gases from stainless steel are known to be highly sensitive to their thermal history and to vary from 5×10^{1} to 10^{-7} molecules per incident electron at an energy of a few hundred electron-volts (McCracken et al 1967). However, even if the cross-section for either process is unity, the rate of change of surface coverage would be too small by several orders of magnitude to account for the changes in ϕ observed if the surface was metallic.

Structural damage or sputtering is improbable at low primary energies. If the effect of particle bombardment on W is considered, for example, a dose of $\sim 10^{15}$ cm^{-2} of He^{+} (or Ar^{+} ions) at $\sim$ 200eV is required to change the work function by typically a few tenths of a volt (Lawson and Carter 1968). In the present case, a total electron dose of $\sim 10^{11}$ cm^{-2} resulted in a change in ϕ of $\sim$ 0.1eV which is much larger than expected from the results for W. Similar conclusions apply to photo-desorption in the case of illumination.

The conclusion is drawn therefore that none of the above physical processes is likely to be primarily responsible for the effects of irradiation on the work function. The steel electrode was apparently behaving in a non-metallic way.

The surfaces of real insulators, semiconductors and metal oxides are characterised by numerous imperfections and adsorbed impurities. These constitute surface states which act as traps for electrical charge. The charge in the surface states is accompanied by an extended space charge layer, the Schottky barrier, at the surface causing the potential at the vacuum interface to be different than in bulk. It satisfies the need for electrical neutrality of the surface and is sustained by the high dielectric constant and low conductivity of the semiconductor. The height of the barrier is related to the surface state density by Equation (2.7) and to the work function by Equation (2.8) as described in Chapter 2. Processes which disturb the equilibrium surface state density (i.e. illumination, adsorption, incident charged particles or electric fields) may be expected to disturb the work function. Such affects are well known and are reviewed by Bardeen and Morrison 1954, Plummer 1962, Volkenstein 1963, Many et al 1965, Kisselev 1967, Frankl 1967 and in the articles in the book edited by Frumkin 1964. Similar effects have also been observed for oxidised or catalytic surfaces of Pt, Ag, Au and Co (cf. Minc and Siejka 1973 and their earlier cited work) when irradiated with gamma rays or ultra-violet light.

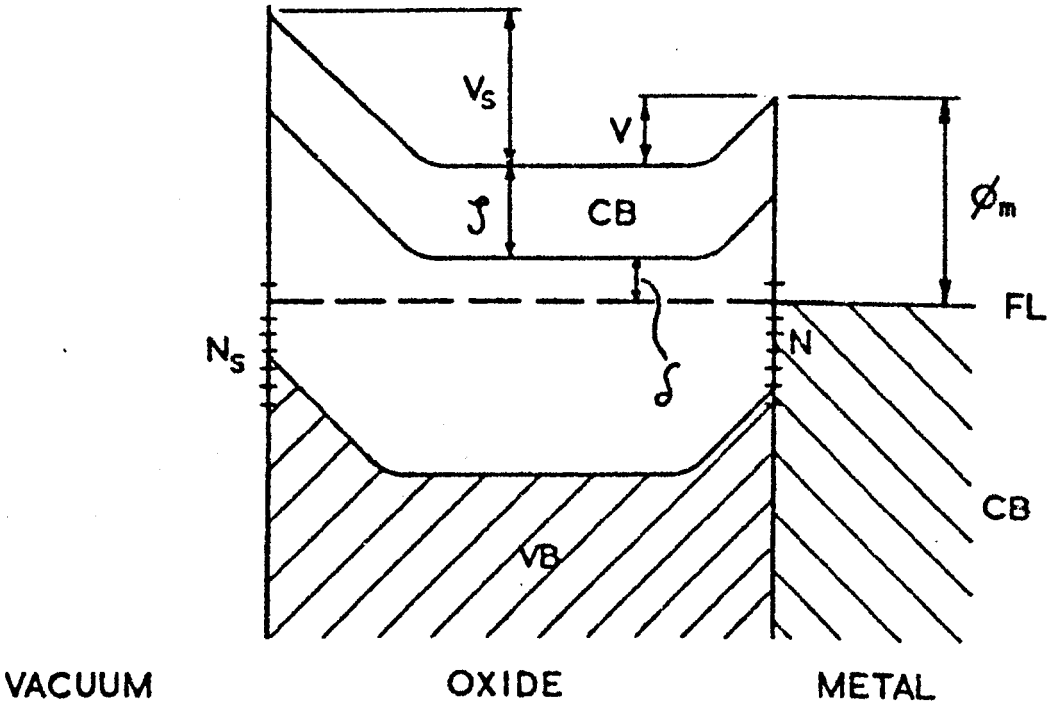

Figure 5.6 A model energy band diagram of an n-type oxide layer on a metal surface.

The results are ascribed to charge redistribution processes on an oxide surface of the steel electrode. The assumption that the surface was oxidised is empirically supported by the low sensitivity of its work function to neutral hydrogen. Hydrogen is only weakly adsorbed on iron oxides at 300°K (Hayward and Trapnell 1964, p86, Pearce et al 1969). It tends to reduce the work function of lightly oxidised metal films by a few tenths of a volt for iron and chromium although by $\sim$ 1.2eV for nickel (Quinn and Roberts 1964). However these measurements probably do not apply to a true oxide.

5.4 Theoretical Models

The oxide is assumed to be n-type and sufficiently thick to support a Schottky barrier at both the vacuum and metal-oxide interfaces. The energy band diagram is shown in Figure 5.6. The surface charge densities at the vacuum and metal-oxide interfaces are denoted by N_s and N respectively and V_s and V are the corresponding heights of the Schottky barriers. The apparent (or effective) work function of the steel electrode ϕ is related to the work function ϕ_m of the metal surface by:

$$\phi = \phi_m + V_s - V = \delta + \zeta + V_s \qquad (5.1)$$

Consequently ϕ may be altered by changing δ, V_s or V and their effects are considered separately below. The temperature T and the capture cross-sections η and γ for holes and electrons are assumed constant.

Model A

If a fraction f of the incident primary electron current I_1 or photo-generated electrons within the oxide come into thermal equilibrium with the oxide lattice and stay in the conduction band CB then the potential energy of all of the oxide is raised relative to that of the metal. A steady state is reached between the arrival rate of electrons and their loss rate I_2 over the barrier V into the metal. This process reduces V but not V_s by δV and therefore increases ϕ by δV. Any subsequent changes in I_1 or I_2 are assumed small in Model A and are considered in the other models. The solution of the continuity equation for the electron density n in the CB is:

$$dn/dt = f\ I_1 + P - A\exp - eV/kT + I_m \qquad (5.2)$$

where A is a thermionic constant, P is the rate of photo-generation of electrons in the CB and I_m is the current from the metal to the oxide. The solution of this equation is given in the Appendix A for the assumption that the changes in n and V are small and linearly related to each other:

$$\phi_\infty - \phi = (\phi_\infty - \phi_o)\exp - e(f\ I_1 + P)t/CkT \qquad (5.3)$$

where the equilibrium change $\phi_\infty - \phi_o$ is:

$$\phi_\infty - \phi_o = (kT/e)\ \log\ (f\ I_1 + P)$$

This model may account for the effects of the incident electron current in the absence of illumination (P = o) and electric fields as shown later.

Model B

The work function ϕ and V_s may be changed by the effects of trapping incident or photo-electrons and gas molecules in the surface states N_s at the vacuum-oxide boundary. In this model the fraction of incident primary and photo-electrons thermalised in the CB is assumed to be negligible and similarly any changes in N or V (which are considered in model C). The rate of change of N_s depends on the following factors: the rate of arrival G of electronically active gas molecules on the oxide-vacuum surface, the electron current I_1 incident on the surface, the electron current flowing to the surface states from the oxide CB, the hole current J to the surface states from the oxide VB, the total density of surface states N_s^o which can be occupied and the electron and hole capture cross-sections γ and η at the surface. The continuity equation for the vacuum-oxide surface is given by:

$$dN_s/dt = G + \{I_1 + P + A \exp(- eV_s/kT)\}\{N_s^o - N_s\}\gamma - N_s(J + P)\eta \qquad (5.4)$$

where the hole current J = Mev, M is the hole concentration and v is their average velocity. It is assumed that J is independant of V_s and that the rate of thermal generation of electrons and holes near the oxide surface and the rate of thermal escape of electrons from occupied surface states are both negligible. It is also

assumed that there is a negligible probability of photons releasing electrons from the states N_s. The barrier height V_s is related to N_s from equation (2.7) by:

$$V_s = \omega N_s^2 \tag{5.5}$$

where ω is a constant defined in Chapter 2. The solution of Equation (5.4) is given in the appendix B. In the absence of adsorption effects (G = o) and for the assumption that the changes in V_s and N_s are small the general solution is:

$$\phi_\infty - \phi = (\phi_\infty - \phi_o)\exp -\{(I_1 + P)\gamma + A\gamma \exp - eV_s/kT + (P+J)\eta\}t \tag{5.6}$$

where

$$\phi_\infty - \phi_o = (kT/e)\{\log a - \log(N_{s_\infty}(J+P)\eta - (I_1+P)(N_s^o - N_{s_\infty})\gamma)\}$$

and a is a constant defined in the model.

It is shown later that this general solution may be simplified and that changes in surface state density in this model may account for the effects of H_2 (at high pressure), incident electrons and photons observed.

Model C

In this model changes in the surface state density N_s at the vacuum surface assumed negligible and that only the density N at the metal-oxide interface is changed. If N^o is the total density of states which may be occupied then the continuity equation is:

$$dN/dt = I_4 (N^o - N)\gamma - N(P+J)\eta \tag{5.7}$$

where the electron current I_4 passes from the oxide CB to the surface states and it includes a term for the photo-generation rate of electrons in the oxide. If the photo-electron energies are large and they are not thermalised in the CB then I_4 may be written:

$$I_4 = P + A \exp - eV/kT \qquad (5.8)$$

but if they are thermalised then:

$$I_4 = (P+A) \exp - eV/kT \qquad (5.9)$$

It is implicitly assumed in Equation (5.7) that the electron current I_m from the metal to the oxide does not populate the surface states. If this is not the case then this term must be added to (5.8) and (5.9). In (5.8) the form of the equation is unchanged if the photo-electrons are excited from the metal to the surface states (instead of from the oxide) and it applies to both cases therefore. The general solution of the continuity equation which is derived in Appendix C for small changes in N and V and when the photo-term P in equation (5.8) is dominant is:

$$\phi - \phi_\infty = (\phi_0 - \phi_\infty) \exp - (I_4\gamma + (P+J)\eta)t \qquad (5.10)$$

This equation is valid for the non-thermalised photo-electron current defined by I_4 in Equation (5.8). A solution is not derived for the more complex case of I_4 given by (5.9).

The general value for $\phi_0 - \phi_\infty$ is dependant on the term for I_4 and for non-thermalised photo-electrons (or photo-electrons from the metal) according to (5.8) then $\phi_0 - \phi_\infty$ is:

$$\phi_o - \phi_\infty = (kT/e) \{\log a - \log (b - P((N^o - N_\infty)\gamma - N_\infty n))\} \quad (5.11)$$

where a and b are constants in the model.

It is shown later that these general solutions may be simplified and that this model may account for the effects of photon irradiation.

5.5 Application of the Models

5.5.1 Incident Electrons

Models A and B predict that ϕ increases exponentially with time at a constant incident electron current I_1 as given by Equations (5.3) and (5.6) for the photo-term P = o and providing that I_1 is dominant over the thermal electron current reaching the states. The time constants of the change in ϕ are predicted differently by the models. They also both predict that ϕ is reversible when I_1 ceases. The data shown in Figure 5.2 for any constant value of I_1 is not sufficiently accurate to distinguish between an exponential rise of ϕ and some other law.

The maximum change $\phi_\infty - \phi_o$ at a constant value of I_1 is predicted by model A to be proportional to log I_1 and by model B to be proportional to $\{b - \log (c - d\ I_1)\}$. The experimental results shown in Table 5.1 were obtained over a small range of ϕ and they fit equally well the empirical laws where $\phi_\infty - \phi_o$ is proportional to I_1 or log I_1 and log $(\phi_\infty - \phi_o)$ proportional to

to log I_1. The prediction from model A agrees qualitatively with the data of Petit-Clerc and Carette 1968 (a). The results of Dobrozemsky and Haltau 1970 were obtained over a range of nearly two orders of magnitude in ϕ and their results approximated more closely to a log $(\phi_\infty - \phi_0) \propto \log I_1$ law which disagrees with the predictions from both models A and B.

5.5.2 Effect of Hydrogen

The absence of any significant SP of neutral hydrogen on the steel surface to a pressure of 10^{-6} torr (H_2) is consistent with previous work on iron oxides discussed in Section 5.3. It is implicitly assumed that H_2 was not adsorbed on the gold reference surface and the evidence for this assumption is discussed in Chapter 6. The positive SP observed beyond point C in Figure 5.2 occurred when both electrons and hydrogen molecules were incident on the electrode surface after a few minutes exposure at 10^{-6} torr (H_2). The initial negative SP with increasing pressure from 10^{-9} torr to 10^{-6} torr curve AB in the diagram was ascribed (Section 5.5.1) to the incident electron current. It is apparent that at high exposures a second and opposing physical effect becomes significant with the effect of electrons and at even higher exposures this effects dominates causing ϕ to decrease at a linear rate. The positive SP is attributed to molecular hydrogen being adsorbed on the oxide surface. This does not contradict the empirical result described above in Section 2.5.1 that the SP was negligible for an adsorbate pressure of 10^{-6} torr or less since in this case the exposure period was much less than that which accompanied the

positive SP in Figure 5.2. Hydrogen is an electron donor adsorbate on semiconductors cf. Many et al 1965, Kisselev 1967 and may form a layer of hydrogen ions which effectively reduce the surface state density at the oxide-vacuum interface and consequently V_s and also ϕ.

The adsorption of simple gases on semiconductors was discussed in Chapter 2. A diatomic gas molecule may be adsorbed on a semiconductor in two ways (Hayward and Trapnell 1964, Volkenstein 1963, Frumkin 1964, Kisselev 1967, Many et al 1965, Minc and Sieka 1968). It may be initially adsorbed into a neutral α state which is physically bound and in direct equilibrium with the gas phase according to the kinetics of physical adsorption. In the case of a donor gas such as hydrogen, $\alpha(H_2)$ may lose electrons to the (n-type) oxide becoming ionised to form a second β state $\beta(H_2^+)$ as observed for example in the $H - Z_nO$ system (cf. Kisselev 1967) or $\beta(H^+)$. The β states form extrinsic surface states on the oxide-vacuum surface which are in direct and proportional equilibrium with the α state. The continuous creation of β - states results in a reduction of the barrier height V_s and therefore ϕ until equilibrium is established with the rate at which they are neutralised by the increasing thermal electron current from the oxide CB over the barrier V_s. The sticking coefficient s of H_2 on iron oxide is small at room temperature. The general continuity equation for the vacuum-oxide surface is given by model B in Equation (5.4) and in the absence photons and charged particles reduces to:

$$dN_s/dt = G + A \exp(- eV_s/kT)(N_s^o - N_s)\gamma - N_s J\eta \qquad (5.12)$$

The term G and the solution of the continuity equation are derived in the appendix E where it is shown that if the gas term G is dominant then at low coverage ($n(\beta) << N_{s_o}$) the change in ϕ is described by:

$$\phi_o - \phi \simeq 2\omega\, a\, b\, s\, N_{s_o}\, t \qquad (5.13)$$

where the constants ω, a and b are defined in the model. This model predicts that $d\phi/dt$ at constant pressure increases with the gas pressure (which is included in the parameter a), with the sticking coefficient s and with the fraction (b) of α - states which may become β - states as intuitively expected. It predicts a linear reduction of ϕ with time which is compatible with the experimental observations at high exposures to H_2 shown in the later part of Figure 5.2. At these pressures the effects of H_2 on ϕ were evidently much greater than those of the electron current from the ion pump which tended to increase ϕ and which were dominant at pressures < 10^{-6} torr. The model suggests that at low pressures (< 10^{-6} torr) the population of the α state was small and consequently the change in ϕ with the pressure of H_2 (in the absence of the ion pump current) from $\sim 10^{-9}$ torr to $\sim 10^{-6}$ torr was very small also. At longer exposures of H_2 at 10^{-6} torr the population of α and β - H_2 became such as to cause a measurable change in ϕ which is compatable with the model. When the gas pressure was reduced the model suggests that the population of the α state decreased and consequently also that of the β - state

and so the barrier height rose to its original value where the effects of the incident electron current were dominant once again.

5.5.3 Illumination

Model A accounted for photo-electrons which became thermalised in the oxide conduction band thereby increasing the density of electrons. It predicted that ϕ would increase on illumination which is contrary to the experimental observations. Illumination could reduce ϕ in both models B and C provided in the former case a photo-hole current to the vacuum surface states was dominant over the electron current, and in the latter case providing an electron current was dominant at the metal-oxide surface states.

The solution of the continuity equation in model B for photo-effects only is given by Equation (5.6) for $I_1 = o$ and if the photo-hole current is dominant then:

$$\phi_\infty - \phi = (\phi_\infty - \phi_o) \exp - (P+J)\eta t \qquad (5.14)$$

and from (5.6) the equilibrium change becomes

$$\phi_\infty - \phi_o = (kT/e) \{\log a - \log N_{s_\infty} (J+P)\eta\}$$

It is shown in appendix B that $N_{s_\infty} J\eta \sim a$ and if P is dominant then this equation becomes

$$\phi_o - \phi_\infty = (kT/e) \{\log P + \log N_{s_\infty} \eta\} \qquad (5.15)$$

Thus model B predicts an exponential reduction of ϕ with time and $\phi_o - \phi_\infty$ is dependant on log P when P >> J the thermal hole current. Model B did not assume that the photo-electrons were thermalised or not in the oxide CB since an assumption was unnecessary if the photo-hole current was the dominant factor.

Model C took account of changes in the surface state density at the metal-oxide interface due to a photo-electron and hole current. The solution of the continuity equation is given in Equations (5.10) and (5.11). It predicted that ϕ would decrease exponentially with time providing the photo-electron current dominated the effects of the photo-hole current and under these conditions the solution reduces to:

$$\phi - \phi_\infty = (\phi_o - \phi_\infty) \exp - P\gamma t \qquad (5.16)$$

where

$$\phi_o - \phi_\infty = (kT/e)\{\log a - \log(JN_\infty\eta - P(N^o - N_\infty)\gamma)\} \qquad (5.17)$$

and $\phi_o - \phi_\infty > o$ since $a \sim JN_\infty\eta$ as shown in the model. This model also predicts an exponential reduction in ϕ with time and that the equilibrium change $\phi_o - \phi_\infty$ is dependant on a logarithmic function of P. This model however only took account of photo-electrons which were not thermalised in the oxide conduction band. In the other case the expression for the current passing to the surface states given in Equation (5.9) resulted in a complex continuity equation the solution of which was not given in the appendix. It seems reasonable to suppose that some of the photo-generated electrons have sufficient energy to escape across the

metal-oxide barrier V although the band gap of the oxide and V are unknown. Photo-potentials were observed when an internal filament was raised to yellow heat giving approximately a black body distribution of photon energies and also with the mercury light whose spectrum was cut-off by the transmission limit of the pyrex window at $\sim$ 3eV.

Both models B and C predict a logarithmic increase of the equilibrium photo-potential $\phi_o - \phi_\infty$ with the photo-generation rate P. It is shown in appendix E that P is related to the intensity of illumination T by the equation:

$$P = q\, T_o \exp - a_b\, N_b \qquad (5.18)$$

where a_b is the absorption coefficient, N_b is the number of optical absorbers in the optical path and q is a constant in the model. The equilibrium photo-potential in model B is dependant on the intensity of illumination and if P is substituted in Equation (5.15) then:

$$\phi_o - \phi_\infty = C - a_b (kT/e) N_b \qquad (5.19)$$

where $C = (kT/e)\{\log qT_o + \log N_{s_\infty} \eta\}$

which describes the change in $\phi_o - \phi_\infty$ as a function of the number of optical absorbers placed in the optical path. The equivalent equation for model C is obtained by substituting for P in Equation (5.17) which gives an equation of the form:

$$\phi_o - \phi_\infty = (kT/e)\{\log a - \log(b - d \exp - a_b N_b)\} \qquad (5.20)$$

where $b = JN_\infty \eta$, $C = qT_o(N^o - N_\infty)\gamma$ and a is defined in the model.

Model B predicts a linear reduction of the equilibrium photo-potential as given by Equation (5.19) which is compatible with the experimental result shown in Figure 5.4 described by the empirical equation:

$$\phi_o - \phi_\infty = m - n N_b \qquad (5.20)$$

where the constants take the empirical values m ≃ 0.02eV and b ≃ 0.2eV. Model C however predicts a functional dependance of $\phi_o - \phi_\infty$ on N_b which is more complex and less easily compared with the experimental data.

Consequently it is difficult to distinguish whether the photo-voltage is the result of a photo-hole current to the oxide-vacuum surface states as in model B or of a photo-electron current to the oxide-metal surface states as described by model C.

Both models correctly predict the reduction of ϕ and an exponential dependance with time. Model B predicted also the relationship between the equilibrium photo-voltage and the intensity of illumination as experimentally observed while model C predicted a more complex relationship.

5.5.4 [illegible]

The external electric field effect was unidirectional and occurred only when the negative pole of the battery was connected to the steel surface i.e. when the potential of the steel and its oxide layer was raised relative to the reference electrode and negative charge was induced on the surface. If the oxide layer did not screen the metal from the electric field then after the field was applied there would be a potential gradient within the oxide. Before applying the field the current I_2 from the oxide to the metal exactly compensates that from the metal I_3 to the oxide. When the field is applied the direction of the potential gradient is such as to reduce I_2 (leaving I_3 undisturbed) and consequently a net flow of electrons would occur into the oxide conduction band. This corresponds to model A and leads to an increase in ϕ contrary to the experimental results.

The reduction in ϕ may be caused by a decrease in N_s at the oxide-vacuum interface or by an increase in N at the oxide-metal surface corresponding to models B and C respectively. If the oxide screens the metal then the induced negative charge associated with the impressed field potential will reside in the oxide-vacuum surface. If this is not the case then the charge resides in the metal surface near the metal-oxide interface. If the induced charge in either case became trapped in the respective surface states model B would imply an increase in ϕ and in the case of model C, ϕ would be reduced. A similar case to model C might

be envisaged if a double charge layer is formed across the metal-oxide interface composed of the induced negative charge on the metal surface and an additional induced positive space charge on the oxide surface established by a hole current. Such a double layer might lead to a reduction in ϕ due to the potential difference across it. It is difficult, however, in all of these models to qualitatively account for the unidirectional property of the field effect.

5.6 Conclusions

The work function of stainless steel was stable in time in ultra high vacuum and for short exposures to H_2 at a pressure of $\sim 10^{-5}$ torr. It was disturbed, however, by prolonged exposure to H_2, illumination and incident charged particles and electric fields. Several physical processes were discussed for metallic surfaces which were unable to readily account for these effects. The behaviour was consistent with a hypothesis that the metal surface was an oxide. Three oxide models were considered which took account of changes in the density of electrons in the conduction band, model A, changes in the density of occupied surface states at the vacuum- oxide surface and at the metal-oxide interface, models B and C respectively.

Models A and B predicted a reversible and exponential increase in ϕ with time due to incident electrons in agreement with the experimental results although the latter might fit equally

well another time-dependant law. Both models predicted that the equilibrium change increased with a log function of the current in agreement with the experimental results although the latter also fitted other functions since the range of change in ϕ investigated was small. The results predicted by the models were in agreement with the qualitative experimental results obtained by Petit-Clerc and Carette although neither accounted for those observed by Dobrozemsky and Haltaf who investigated a much wider range of charge in ϕ.

Short exposures to H_2 at $\lesssim 10^{-6}$ torr resulted in no change in ϕ which was consistent with the previous work on iron oxides. Longer exposures at $\sim 10^{-6}$ torr caused ϕ to decrease slowly and approximately linearly with time. This was interpreted as the result of adsorption and conversion of weakly adsorbed gas to a charged form of hydrogen $\beta(H_2^+)$. A simple model based on model B predicted a linear and reversible of ϕ in time as experimentally observed.

Photo-illumination reduced the work function. Both models B and C predicted an exponential reduction of ϕ with time as experimentally observed. Both also predicted that the equilibrium change should increase with a logarithmic function of the photo-generation rate. Model B predicted that the equilibrium change should linearly decrease with the number of optical absorbers in the optical path in agreement with the experimental observation.

The prediction from model C was more complex however. Consequently it is difficult to distinguish whether the dominant factor causing the photo-potentials was a photo-hole current to the vacuum-surface or a photo-electron current to the metal-oxide surface. Model C also incidentally described the changes if the electrons were emitted from the metal into the oxide surface but this is perhaps unlikely since the photon-energies were typically less than 3eV and the work function of the metal was probably $\sim$ 4.5eV. The Dember effect was not considered since the potential changes associated with it are very small.

Several mechanisms were discussed in relation to the cause of the electric field effect. It was not possible to even qualitatively account for the unidirectional property although one of them might account for the correct change of ϕ experimentally observed.

CHAPTER 6

REVIEW OF PREVIOUS WORK ON GOLD, SILVER AND TITANIUM

6.1 Measurements on Gold

6.1.1 Work Function of Gold

Sachtler et al. 1966 have tabulated the published measurements prior to 1966. The results for both bulk and metal film surfaces vary widely from about 4.0 to more than 5.0eV. All of these experiments were conducted in systems exhausted with diffusion pumps and Huber 1966 has shown that Au is sensitive to small traces of Hg vapour. The measurements in diffusion pumped systems are therefore unreliable. Huber found that in a getter-ion pump system the work function ϕ_{Au} of pure Au films deposited at 300°K on polished stainless steel was 5.22 $\pm$ 0.05 eV and independant of their thickness. He used a dynamic capacitor method with several different metals as reference surfaces. These results were independantly confirmed by Riviere 1966 who arrived at a value of 5.28eV for gold films deposited at room temperature onto aged rhuthenium in an ion pumped system.

Sachtler et al. 1966 measured the photo-electric work function of gold films deposited on glass in a system exhausted with a getter-ion pump. At a substrate temperature of $\sim$ 330°K

during deposition ϕ_{Au} was 5.30eV and increased by 80mV when the film was annealed at 400 - 500°K. Holscher 1966 arrived at a value of 5.45 eV for a gold film deposited on glass at about 450°K using the field emission retarding potential method. Hampson 1966 deduced a value of 5.18eV for Au films deposited onto W films (on polished Pt) by the dynamic capacitor method in an ion pump system assuming a value of 4.54eV for the work function of a W reference surface. All of the above experiments employed ultra high vacuum techniques.

The value of ϕ_{Au} is sensitive to the surface structure and increases during sintering. Ying and Farnsworth 1958 have reported a gradual reduction in ϕ_{Au} of about 0.1eV with increasing film thickness on a bulk substrate of the same element. After reaching a particular thickness ϕ_{Au} varied apparently randomly from one deposition to the next. Bryla and Feldman 1962 have observed a small change in ϕ_{Au} with increasing thickness h of Au films on glass when the resistivity was $\geq 10^8$ Ω Sq^{-1} after which ϕ became independant of h. Ying and Farnsworth concluded that the value of ϕ_{Au} for films was less than that of bulk polycrystalline gold substrates but increased to their value after annealing. These structural effects may only be valid for contaminated surfaces in view of Huber's experiments described earlier.

6.1.2 Adsorption on Gold

Bulk gold is difficult to purify in vacuum and varies with the state of outgassing (cf. Morris 1931, Parker and Warren 1962). Many of the common residual gases are adsorbed on outgassed bulk gold and this is probably related to adsorbed impurities (Hughes and DuBridge 1932, Dillon and Farnsworth 1957).

Trapnell 1953 investigated the adsorption on evaporated films of Au in a system having a base pressure of less than 10^{-6} torr. He adopted the criterion that if less than 2% of the geometric surface was covered in thirty minutes at an equilibrium adsorbate gas pressure between 10^{-3} and 10^{-2} torr then adsorption did not occur. On this basis H_2, N_2 and O_2 were not adsorbed at room temperature. C_2H_2 and C_2H_4 were reversibly adsorbed at room temperature and also CO at - 78°C.

Culver et al. 1957, Pritchard and Tompkins 1960 and Pritchard 1962 have measured the SP of H_2, X_e and CO on Au films. X_e and CO resulted in a positive SP of + 0.5 and + 0.93 eV respectively. These gases were adsorbed at less than or $\sim$ 190°K except for molecular H_2. H_2 was only adsorbed if previously dissociated and it was completely desorbed at $\sim$ 200°K. Adsorption of molecular or atomic H did not occur at 300°K. SP measurements by Riviere and colleagues (Hopkins et al. 1964, Riviere 1964 and cited works) have also shown that ϕ_{Au} is not affected by N_2 or H_2. Some adsorption of H_2 may occur at high

Year	Substrate	Pressure Torr	Surface	ϕ eV	Method	Notes	Author
1936	Glass	10^{-8}	Film	4.33	CP	b	Anderson
1940	-	$\lesssim 3\ 10^{-8}$	(111)	4.75	PE		Farnsworth and Winch
	-	$\lesssim 3\ 10^{-8}$	(100)	4.81	PE		
1941	Glass	10^{-8}	Film	4.47	CP	a	Anderson
	Rocksalt	10^{-8}	(100)	4.79	CP	d	
1950	-	$< 5\ 10^{-8}$	bulk	(4.60 - 4.76)	PE		Blackmer and Farnsworth
	-	$< 5\ 10^{-8}$	(100)	4.81	PE		
	-	$< 5\ 10^{-8}$	(111)	4.75	PE		
	Mo	$< 5\ 10^{-8}$	Film	4.41	PE	e	
	Glass	$< 5\ 10^{-8}$	Film	4.41	PE	e	
	Bulk Ag	$< 5\ 10^{-8}$	Film	(4.4 - 4.6)	PE		
1952	Ta	10^{-8}	Film	4.31	CP		Anderson
1952	W	$< 5\ 10^{-8}$	Film	4.33	CP		Mitchell and Mitchell
1953	C	$< 10^{-7}$	Film	4.31	TE	c	Jain and Krischnan
1957	Fused Pt on Glass	$< 10^{-8}$	Film	4.31	CP		Riviere
1964	Glass	$\lesssim 10^{-9}$	Film	4.30	CP		Hopkins and Riviere
(1964)	-	(?)	bulk	4.29	CP		Hopkins

TABLE 6.1 Measurements of the work function of Ag. All of the experiments were conducted in diffusion pump systems and at room temperature unless otherwise indicates. Notes: a ϕ = 4.56eV for T = 500°K, b T = 90°K, c T = $\sim$ 1300°K, d T = 500°K, e sintered value.

temperatures however (Holden and Rossington 1964).

Hopkins et al. 1964, Riviere 1964 and Sachtler et al. 1966 have shown that O_2 is not adsorbed on Au films at 300°K. In these experiments there was no change in ϕ within 10mV or so for evaporated (or sputtered) films whether sintered or otherwise in systems exhausted with diffusion or getter-ion pumps on exposure to O_2 at a pressure of a few torr. An earlier report cited by Riviere of a positive SP of O_2 on Au was suggested to be caused by an impurity. At elevated temperatures O_2 has been observed to be adsorbed and result in a SP of - 0.7eV (cf. Sachtler et al. 1966).

Most of these gold surfaces have probably been contaminated with mercury or oil vapour. However, the close agreement between the experiments performed in both getter-ion and diffusion pumped systems for the SP of O_2 gives some confidence in the measurements and also their general application to pure gold surfaces.

6.2 Measurements on Silver

6.2.1 Work Function of Silver

The measurements of ϕ_{Ag} since 1936 are summarised in Table 6.1. Prior to this time the results for bulk specimens varied widely from 3.56 to 4.7 eV and probably reflect the effects of contamination (cf. Reiman 1934, Anderson 1952). The values shown in the table also lie within this range.

Anderson measured the value for an orientated film in the (100) plane grown on a cleaned rocksalt substrate at 500°K. The value was in good agreement with that of a bulk crystal in the (100) orientation measured by Farnsworth's group. There is a close agreement between the measurements on an aged wire and on the (111) face of Ag. Anderson has suggested this may have been the result of thermal facetting of the wire leaving the surface recrystallised in the (111) plane.

The measurements on thin films show a good consistency between different laboratories and among different methods. The values lie within the range from 4.31 to 4.47 eV for films on glass, Mo, Ta and W substrates at 90 and 300°K. A single value on an aged Ag bulk substrate is higher than these.

The work function of Ag films shows some structural dependance on the orientation and degree of crystallinity of the substrate (cf. Anderson 1952 and Farnsworth 1958 and their earlier cited works). Hopkins and Riviere 1964 have inferred a small but significant increase in ϕ_{Ag} in the substrate sequence glass, W and Ta due to an apparent increasing degree of crystallinity in the substrate. The value of ϕ_{Ag} for unsintered films has been reported to vary with thickness and with sintering in a similar way to that of Au films described above (Blackmer and Farnsworth 1950, Bryla and Feldman 1962). When bulk or orientated substrates of the same element are used the annealed value of the film becomes equal to that of the substrate (cf. Farnsworth 1958 and cited works).

Studies of the nucleation and growth of Ag films have shown that the nature, structure and preferred orientation of the substrate may affect the growth, structure and defect density of the film overlay (cf. Duell and Ross 1964, Jaeger et al. 1969). Clarke and Farnsworth 1952 have concluded from electron diffraction experiments that Ag films which are deposited onto orientated bulk Ag substrates adopt their structure and orientation as proposed earlier by Anderson for mica substrates. The effects of structure on the value of ϕ_{Ag} is generally consistent with the known features of the growth and structure of Ag films. Wallis and Farnsworth 1956 have observed that induced strain in polycrystalline Ag strips may result in a change in ϕ_{Ag} by as much as 30 mV although the cause of this was not clear.

The results given in Table 6.1 imply that ϕ_{Ag} varies by $\sim$ 0.5eV or more among its individual crystal planes and the smaller differences between the values for thin films may reflect structural differences in the films as discussed above. Substrate contamination may also affect the film growth and defect density although the evidence is inconclusive (cf. Bachmann and Shin 1966, Jaeger et al. 1969).

6.2.2 Adsorption on Silver

As discussed for the case of bulk gold, outgassed bulk Ag may adsorb many of the common gases and this is also likely to be due to adsorbed impurities (cf. Hughes and DuBridge 1932). In similar

experiments to those described earlier for Au, Trapnell 1953 has shown that Ag films do not chemisorb H_2, N_2, CO, C_2H_2 or C_2H_4 from temperatures near their boiling points to room temperature. O_2 however was slowly adsorbed at room temperature and more rapidly at lower temperatures. It reached an equilibrium coverage of ~ 0.1 at a pressure of $\sim 10^{-3}$ torr at $300^{\circ}K$. Steiger et al. 1969 have studied adsorption on orientated surfaces of Ag by LEED and ellipsometry techniques. At room temperature and below O_2, C_2H_2, C_2H_4, Kr and Xe were physically adsorbed on the (100) and (110) faces with heats of adsorption of $\lesssim 6$ Kcal $mole^{-1}$. There was a rapid adsorption at low temperatures of apparently residual H_2O but at $\sim 300^{\circ}K$ the rate of adsorption was much slower. Weissler and Wilson 1953 also reported that ϕ_{Ag} decreased by as much as 0.2eV on exposure to H_2O at ~ 20 torr but the purity of the surface is unknown.

Mercury vapour does not apparently adsorb on Ag films at room temperature (Huber 1966). Surface potential measurements have shown that N_2 and molecular H_2 are not adsorbed on Ag films at room temperature (Culver et al. 1957, Pritchard and Tompkins 1960, cited unpublished works of Riviere 1964 and Hopkins and Riviere 1964) although atomic hydrogen was adsorbed below $200^{\circ}K$, however. Culver and Tompkins 1959 cite the previous work of Ogawa on the SP of H_2 but point out that his results probably refer to a contaminated surface. They also cite the work of Suhrmann et al. who arrived at value of - 0.49eV for the SP of H_2 on Ag.

Emikeev et al 1960 have reported that CO_2 is not adsorbed on Ag films at 300 ^{o}K unless the surface is oxygenated previously. CO is adsorbed on Ag films at $\sim$ 200^{o}K or less resulting in a SP of + 0.4eV (Culver et al. 1957).

There have been several reports that O_2 is adsorbed with a negative SP on Ag at room temperature. Pritchard and Tompkins 1960 measured a SP of - 0.42eV for O_2 on Ag films probably at 90^{o}K and similarly Ogawa (cited by Culver and Tompkins 1959) arrived at a value of $\sim$ - 0.4eV (at 90^{o}K). Emikeev et al. 1960 and also Rentschler and Henry (cited by Riviere 1964) have observed a negative SP for the adsorption of O_2 on bulk and sputtered film surfaces of Ag at $\sim$ 300^{o}K. Degeilh 1969 has studied orientated surfaces at $\sim$ 300^{o}K. Adsorption of O_2 occurred in a single irreversible state on the (111) plane and resulted in a SP of - 0.95eV at 10^{-6} torr (O_2). A similar state existed for the (100) plane which resulted in a SP of - 0.85eV. The (100) also possessed another but slow and partially reversible state which was due to impurities and when these were desorbed by outgassing only the former normal state was present. May and Linnett 1967 have reported that clean surfaces of Ag adsorb atomic oxygen at 300^{o}K to form a thin surface oxide layer and Muller 1966 has studied adsorption of O_2 on the (111) face of Ag at room temperature by LEED. Oxygenated Ag surfaces are known to adsorb other gases (cf. Enikeev et al. 1960, Hayward and Trapnell 1964, Degeilh 1969). Conversely O_2 adosrption may be completely absent on some faces of Ag at $\sim$ 300^{o}K unless outgassed to desorb impurities (Degeilh 1969).

6.3 Measurements on Titanium

6.3.1 Work Function of Titanium

Evaluation of the published work is difficult because of the general lack of detailed experimental information given by the authors with one or two exceptions. The results are summarised in Table 6.2. Prior to 1960 ϕ_{Ti} was apparently reasonably established to be $\sim$ 4.0eV. Since then, however, recent measurements have varied widely between $\sim$ 3.5 and 5.8eV which is surprising in view of the higher purity metals available and the improvements in vacuum technology.

The earliest measurements are apparently those of Schulze 1934 and Klein and Lange 1938 in systems of poor base pressure who arrived at values in close agreement with each other. Rentschler and Henry 1945 measured a value for Ti films deposited from a powder which was also in close agreement with the previous measurements but did not mention any variation of ϕ_{Ti} after deposition or details of the gas pressure. Uhlig 1951 has also measured the cpd between Pt. and bulk Ti in air. Jain and Krischnan 1952 measured the thermionic value of ϕ for a film deposited and aged on graphite which was apparently prepared in an auxiliary vacuum system and transferred in air to the measurement tube. No details were given of the gas pressure, outgassing conditions or changes of ϕ. Malamud and Krumbein 1954 performed their experiments in poor vacuum $\sim 10^{-4}$ torr and these are unlikely to refer to clean surfaces. None of the above results are likely therefore to be representative of pure Ti surfaces.

Suhrmann et al 1962 have made measurements on very thin films of Ti deposited onto a glass substrate at $90^{\circ}K$ in a system having a base pressure between 10^{-9} and 10^{-10} torr. The deposition took 30 to 50 minutes after which the film thickness was between 45 and 70 A°. The work function of the 'clean' unsintered film was 3.52eV. Although they did not state how long after deposition the measurement was made it is likely that the results refer to a freshly deposited film. Impurities on the glass substrate or gettering during the long evaporation time may have contaminated the film. The film was annealed for about two hours at $\sim 400^{\circ}K$ and ϕ became 3.81eV. This result may also be unrepresentative because of the possibility of contamination during the annealing period. Wilson 1966 has made the first measurements in an ion-pump system. He found the effective TE value of two Ti ribbons varied from 3.5 to 4.4eV. The temperature coefficients of ϕ varied from $-1.0\ 10^{-3}$ to $-8.8\ 10^{-4}$ eV $^{\circ}K^{-1}$. The base pressure was $\lesssim 10^{-9}$ torr and one of the ribbons was outgassed for several hours at $\sim 1400^{\circ}K$ and the other at $1500 - 1630^{\circ}K$ for a few minutes. The measurements were made between 1100 and $1585^{\circ}K$ and therefore the results refer to the high temperature β - phase of Ti. Wilson concluded that ϕ_{Ti} decreased with increasing outgassing times or temperature which may have been the effects of impurity. Few details were given of the outgassing cycles or change of ϕ with time or temperature during these or with the gas pressure.

Paddock and Magee 1966 have measured the TE work function by the diode method of a wire in a system with a base pressure between 5.10^{-8} and 5.10^{-7} torr. ϕ_{Ti} for three different wires lay between 5.21 and 5.79eV between 1170 and 1400°K. The value for a fourth sample which was heated to only 900°K was 3.77eV which subsequently increased to 5.22eV when the wire was heated for several hours above 1170°K the allotropic transformation temperature. They suggested this was the result of the change in structure from the α to the β phase but the higher value may have been caused by impurities diffusing to the surface at the higher temperature or due to adsorption from the residual gas. Few details were given of any outgassing cycles or variation of ϕ. The wires had apparently become distorted by the heating which may cast doubts on the validity of applying the diode theory since this implies cylindrical symmetry and consequently also on the numerical results. Magee 1967 has briefly reported a PE work function of Ti films deposited on aged Ni. He gave very few experimental details and did not state the pressure. The purity of the substrate is questionable. ϕ_{Ti} for two different films was 3.52 and 3.60eV but these are unreliable since the time which elapsed between the end of deposition and the time of measurement was not stated. This is supported by the fact that ϕ_{Ti} increased by only 80 mV afterwards over a period of six days which is uncharacteristic of a clean transition metal.

Vladimirov 1968 has measured a field emission average work function of titanium films deposited onto W emittor tips. ϕ decreased with increasing coverage and attained a value of 3.6eV. The system pressure, outgassing conditions of the Ti (on Ta) source and the cleanliness (or cleaning cycles) of the substrate were not stated. The evaporation rate was very slow (~ 250 seconds to attain a coverage $\theta \sim 1$) and the deposit was heated between 1000 and 1100°K. The reliability of this measurement is questionable due to the possibility of contamination. Anderson and

Thompson 1971 have recently performed similar measurements of the FE average work function at ~ 10^{-10} torr and at 293°K in an oil diffusion-pumped vacuum system. The work function of Ti FE tips lay between 2.2 and 2.6 eV due apparently to bulk impurities near the surface which could not be removed. They cited a measurement by Elinson and Kudintseva (1962) of the work function of TiC (ϕ = 2.72eV) suggesting the impurity may have been carbon. Consequently thin films of Ti were deposited at 293°K onto W (ϕ = 4.5eV) and Re (ϕ = 5.0eV) outgassed FE tips. In both cases ϕ decreased with increasing θ to a value (for $\theta \gtrsim 2$) independent of thickness. In some experiments an initial increase of ϕ occurred at very small values of θ of about 0.2eV. The FE pattern for Re was characteristic of an hcp deposit suggested to be α - Ti(hcp) epitaxed to Re(hcp) for which $\phi = 4.00 \mp 0.05$eV. When the Ti on W deposit was heated briefly above the transformation temperature a pattern characteristic of a bcc deposit was obtained apparently β - Ti (bcc) epitaxed to W(bcc) for which $\phi = 3.65 \mp 0.05$. This value for β- Ti is close to that of Valdimirov above but less than that of Zhubenko (1963) who obtained ϕ = 3.7 - 3.8eV (after a small correction by Anderson and Thompson) for a heated deposit on W. All of these values for β - Ti are much less than those of Wilson 1966 and Paddock and Magee 1967 (Table 6.2) by a volt or more when account is taken of the temperature dependence of ϕ. Anderson and Thompson did not state their evaporation rate but the reproducibility of their results (in four experiments for W and in two for Re) apparently excludes the possibility of contamination from the vacuum system.

The work function of TiC has been reported to be 3.35eV (Goldwater and Haddard 1951), 2.27eV (Elinson and Kudintseva (1962) cited by Anderson and Thompson 1971) and 4.09eV (Ingold 1967) for samples which received extensive outgassing between 1600 and 2300°K at pressures less than 10^{-7} torr (G and H) and ~ 10^{-9} torr (I). The conditions of the other measure-

Year	Gas	Base Pressure Torr	Surface	Temp. °K	ϕ_o eV	SP eV	Notes	Method	Author
1954	Cl	$\sim 10^{-4}$	Ribbon	300	4.45	- 0.31	a,e	PE	Malamud and
						- 0.8 to - 1.1	b		Krumbein
1953	Xe	j	j	j	j	+ 0.84	e	CP	Mignolet
1962	Cl	?	Film	300	j	+ 0.4	c	CP	Anderson and
						- 2.1	e		Gani
1962	O_2	j	Film	300	j	< 0	d	PE	Klemperer
1962	H_2	$\lesssim 10^{-9}$	Film	90	3.81	- 0.35	a,e,f,g	PE	Suhrmann et al.
1967	H_2	?	Film	300 (?)	3.60	+ 0.12 to + 0.22	g	PE	Magee
1967	N_2	$\sim 10^{-9}$	Film	300	j	- 0.22	e	CP	Czarycki
1968	O_2	10^{-9}	Film	296	j	-1.4 ∓ 0.2	e	CP	Muller

TABLE 6.3 Surface potential of gases on titanium. The adsorbate pressures were (torr); 10 Malamud and Krumbein, $\lesssim 10^{-5}$(?) Anderson and Gani, $10^{-5} - 10^{-2}$ Suhrmann et al., $\sim 10^{-8}$ Czarycki, and the others are unknown. ϕ_o is the value of the clean surface and all the experiments employed diffusion pumps. Notes: a after several hours, b after heating and cooling in the gas, c at a coverage $\theta \lesssim 0.1$, d after annealing at 300°K, e Maximum value, g after annealing at $\sim$ 400°K for 1 hour, g dependant on the atomic Ti/H ratio, j not measured or stated.

ment (E and K) are unknown. Wright 1953 and Herman and Wagener 1951 (p.217) have cited values of 3.7 and 4.7eV for the work function of titanium oxide. The work functions of the oxides and carbides are in close agreement with those for supposedly pure surfaces of Ti (except in two cases in Table 6.2).

6.3.2 Surface Potential Measurements

The measurements of the SP are summarised in Table 6.3. Mignolet 1953 briefly reported the SP of Xe on Ti which was large and positive but the experimental details were not given. Malamud and Krumbein and also Anderson and Gani have measured the SP of Cl at $\sim 300^{\circ}K$ which was negative on Ti and its magnitude increased when the sample was heated and cooled in the vapour. Anderson and Gani found that Cl initially reduced ϕ_{Ti} of their thin films by 0.4eV until the coverage exceeded ~ 0.1 when ϕ_{Ti} increased. At saturation the SP was - 2.1eV.

Klemperer 1962 has investigated the effect of O_2 on the PEE from Ti films but few experimental details were given. The films were annealed at $300^{\circ}K$ and cooled to $90^{\circ}K$. When oxygen was introduced the photo-current was initially reduced but after several days the emission recovered again. When further O_2 was introduced the effect was repeated. When the film was heated to $\sim 400^{\circ}K$ in O_2 the emission often increased above the value for the 'clean' surface. The regenerative effects were interpreted as being due to solution of oxygen into the metal. Muller 1968 has reported a

large negative SP of O_2 on clean titanium films at $\sim 275^{\circ}K$ prepared in ultra high vacuum and measured by a CPD method (Table 6.8).

Suhrmann et al. 1962 and Magee 1967 have investigated the SP of H_2 on Ti films. It was concluded in the discussion preceding this section that the values of ϕ_{Ti} arrived at by these workers were possibly unreliable and unlikely to refer to clean surfaces of Ti. The SP results therefore may refer to adsorption of H_2 on contaminated films. In Suhrmann's experiments, H_2 was introduced from the base pressure $\sim 10^{-5}$ torr (H_2) above a film at $90^{\circ}K$ which had been annealed for an hour or so at $\sim 400^{\circ}K$ after deposition at $90^{\circ}K$ in vacuum. ϕ_{Ti} increased by only 40 mV. The resistivity of the film also increased. At higher pressures $\sim 10^{-5}$ to 10^{-2} torr (H_2) ϕ_{Ti} increased further and attained a maximum SP of - 0.25eV at $90^{\circ}K$ and - 0.35eV at $273^{\circ}K$. The relative film composition was estimated to be $TiH_{0.6}$ and $TiH_{1.2}$ at these temperatures respectively. These concentrations were attained after $\sim$ 13 hours exposure to H_2 and the possibility of contamination of the film during this period casts doubts on the validity of the results. The resistivity measurements enabled the conclusion to be drawn that atomic hydrogen was dissolved and had diffused into the film although no simple relationship was found between the resisitivity or pressure and the SP results. Magee however disagrees with these results and found that ϕ_{Ti} was reduced by 0.12eV and 0.22eV for two different films when the concentration of H in solution had reached an estimated value of $TiH_{0.016}$ and $TiH_{1.6}$ respectively.

Gas	Year	Base Pressure Torr	Substrate	s_o	Notes	Author
O_2	1960	$<10^{-7}$	?	$\sim$ 1.0	f	Brennan et al.
	1961	2.10^{-8}	Ta	$\sim$ 0.85		Clausing
	1969	$\sim 10^{-9}$	?	0.85		Ehrhard and Cassuto
CO, CO_2	1961	2.10^{-8}	Ta	$\sim$ 0.4 - 0.9	e	Clausing
N_2	1957			0.25		Wagener
	1961	2.10^{-8}	Ta	0.08 - 0.17	e	Clausing
	1965	2.10^{-9}	Cu	0.1 - 0.13	b,h	Elsworth et al.
	1967	$\lesssim 10^{-9}$ (?)	g	0.18 - 0.37	b,c	Harra
	1967			0.18 - 0.76	b,c,d	Harra and Hayward
	1967	$\sim 10^{-10}$	Pt (?)	0.35		Czarycki
	1968	$\sim 5.10^{-10}$	Glass	0.5		King and Hayward
H_2	1961	3.10^{-8}	Ta	0.05 - 0.19	e	Clausing
	1965	2.10^{-9}	Cu	0.01	b,h	Elsworth et al.

TABLE 6.4 The initial sticking coefficients s_o of gases on titanium (films) at $\sim 300^{\circ}K$. All of the experiments were performed in diffusion pump systems unless otherwise noted. Notes: b dependant on thickness, c ion pump system, d dependant on thickness of underlying film, e dependant on structure, f sintered at $40^{\circ}C$, g not stated, h pressure rose to $\sim 10^{-8}$ torr during deposition.

Czarycki 1967 measured the SP and sticking probability of N_2 at 300°K on Ti films deposited on stainless steel at a base pressure of $\lesssim 10^{-9}$ torr. The major residual gases were CO and N_2, CH_4 and H_2 in that order. When N_2 was introduced to $\sim 10^{-8}$ torr ϕ_{Ti} increased by a maximum value of 0.22eV at a coverage of $\sim 13.10^{14}$ mols cm^{-2}. The clean value of ϕ was not measured but the results appear reliable.

6.3.3 Sticking Coefficient

Measurements of the sticking coefficients of gases on clean Ti surfaces at 300°K are summarised in Table 6.4. The initial values s_o for O_2 are very high. For H_2 however s_o is apparently small but this may reflect the difficulties of producing pure films since contamination is known to affect the values for H_2 (Stout and Gibbons 1955, Clausing 1961). There is disagreement as to whether the initial getter rate of films for O_2 is dependant on the thickness (cf. Zdanuk and Wolsky 1961, Wagener 1957). In the case of N_2 and H_2 the initial values or getter rates vary widely with the film thickness and also in the case of N_2 with that of the underlying film for successive depositions (Elsworth et al. 1965, Harra 1967, Harra and Hayward 1967). Such effects may also reflect the presence of contamination however. The initial values generally increase with a reduction in the film deposition temperature although it is not clearly established whether this is solely due to a structural effect or not. The values for H_2 vary from 0.16 to 0.85 around 100°K (Clausing 1961 Elsworth et al. 1965, Prevot and Sledziewski 1968). Larger coefficients also result when the film is continuously deposited

in the presence of the gas when the concentration dissolved may allow the compounds TiH_2 and $TiN_{1.5}$ to be formed (Clausing 1961, Harra 1967).

The sticking coefficient of H_2 is apparently independant of the number N_{ad} of adsorbed molecules at room temperature over a range of N_{ad} varying between a factor of 10 to 10^3 depending on the film structure (Clausing 1961). Elsworth et al. 1965 also reported that the sticking coefficient remained at a high value for long periods at 5.10^{-8} torr (H_2) above a 250 A^o thick film. The value decreased only after several hours exposure. At low temperature, however, $s(H_2)$ may not be independant of N_{ad}. In the case of N_2, s is dependant at room temperature on $N_{ad}(N_2)$ (Elsworth et al. 1965 and previous cited work, Czarycki 1967, Harra 1967, Harra and Hayward 1967, King and Tompkins 1968). Harra and Hayward found that s was approximately described by:

$$s/s_o = \exp(- N_{ad}/N_o) \qquad (6.1)$$

Elsworth et al. found that the getter rate was related to the exposure time at constant pressure (between 10^{-8} and 3.10^{-7} torr (N_2)) by a logarithmic law. The sticking coefficient of O_2 linearly decreases with the quantity of gas adsorbed over a fractional range of coverage from $N_{ad}/N_{ad\infty} = 0$ to $N_{ad}/N_{ad\infty} \approx 0.35$ at room temperature (Erhardt and Cassuto 1969).

At room temperature O_2, H_2 and N_2 may be absorbed by Ti films. Elsworth et al. above observed that five monolayers of H_2 were absorbed at 5.10^{-8} torr (H_2) although saturation was not complete. The capacitance c of the film for H_2 increased with the film thickness and inversely with the temperature in agreement other studies described later. Although contamination affects the sticking coefficients for H_2 it did not appear to affect the value of c. Oxygen is absorbed after the formation of a chemisorbed monolayer and results in the growth of an oxide at room temperature (Erhardt and Cassuto 1969). These authors employing measurements of the sticking coefficient and N_{ad} have studied the growth kinetics at 300°K and below and at $\sim 10^{-7}$ torr (O_2). There is some disagreement on whether the capacity of Ti films for O_2 (at 300°K) is dependant on the film thickness (cf. Wagener 1957, Zdanuk and Wolsky 1961). Nitrogen is also dissolved by Ti films. Elsworth et al. found the initial sticking coefficient was related to the pressure p by:

$$s_o = k\, p(N_2)^{\frac{1}{2}} \qquad (6.2)$$

where the constant k depended on the film area. At constant pressure and after an induction period of $\sim$ 30 minutes the quantity of adsorbed gas became proportional to $t^{\frac{1}{2}}$ indicating the diffusion of atomic N . The adsorption satisfied a theoretical diffusion equation from which they deduced a value between 4.10^{-7} and 10^{-18} cm^2 sec^{-1} for the diffusion coefficient of N in Ti. They applied a simplified diffusion equation for a semi-infinite solid and deduced that the surface concentration c of N_2 at a

constant pressure p was proportional to $p^{\frac{1}{2}}$. The equilibrium coverage of N experimentally fitted a Langmuir adsorption isotherm and using this they showed that the equilibrium coverage, the sticking coefficient s and the sorptive capacity c of the film were expected to be proportional to $p^{\frac{1}{2}}$ as experimentally observed.

The inert gases are not adsorbed at room temperature on Ti and their sticking coefficients are very small (Causing 1961).

6.3.4 Adsorption on Titanium

The common residual gases H_2, N_2, O_2, CO, CO_2 and H_2O are apparently dissociatively adsorbed on clean Ti from $\sim 80^{\circ}K$ to temperatures $\sim 1500^{\circ}K$. Adsorption is accompanied by the formation of stable oxides, nitrides and carbides of Ti and at a rate which may increase by orders of magnitude with temperature throughout the above range (Gulbransen and Andrews 1949, Stout and Gibbons 1955, McCracken et al. 1968).

Brennan et al. 1960 have derived a value of ~ 236 Kcal $mole^{-1}$ for the heat of adsorption of O_2 on Ti films in close agreement with the heat of oxidation. The value of the heat and the sticking coefficient were almost independant of coverage θ until $\theta \sim 0.6 - 0.7$ after which they both decreased. Fehlner 1966 and Erhardt and Cassuto 1969 have studied the oxidation of Ti films at $300^{\circ}K$ or less at low pressures ($10^{-8} - 10^{-6}$ torr (O_2)) by resistivity and direct adsorption measurements respectively.

two of these were weak and reversible and populated at low temperatures. At room temperature only the third state (βN_2) was populated which was irreversible. Ellsworth et al. found that less than 0.03% of adsorbed N_2 at 300°K was released by heating to 500°K for several hours in vacuum.

At 300°K and below CO is irreversibly adsorbed on clean Ti with a heat of adsorption of $\sim$ 153 Kcal mole^{-1} and a large sticking coefficient (Table 6.4). CO_2 is dissociatively adsorbed between 78 and 1500°K with a heat of adsorption and sticking coefficient similar to that of CO (Trapnell 1953, Stout and Gibbons 1955, Clausing 1961, Hayward and Trapnell 1964 p205 and 244). In the dissociative adsorption of CO_2, CO is desorbed apparently. There is some disagreement whether CH_4 is adsorbed on Ti films at normal temperatures (Trapnell 1956, Clausing 1961, Frances and Jepsen 1963). At higher temperatures up to at least 1500°K CH_4 is dissociatively adsorbed with the production of TiC and the liberation or solution of H_2 (Stout and Gibbons 1955). Other hydrocarbons, C_2H_2, C_2H_4 and C_2H_6 are irreversibly adsorbed at 300°K with no desorbtion products and a high degree of coverage (Trapnell 1953, Roberts 1963).

Stout and Gibbons 1955 reported that H_g vapour did not affect the adsorptive properties of Ti at high temperatures and pressures. Stow 1959 however has stated that the getter rate of thin films of Ti at normal pressures and temperatures is affected by oil vapour from diffusion pumps.

6.3.5 Desorption from Titanium

The above experimental results show that Ti reacts with common residual gases to former compounds over a wide range of temperature and pressure. The oxides are not reduced by H_2 and their decomposition temperature is typically greater than 2000°K. N_2 and C react to form the nitride and carbide of Ti which are stable compounds to at least 1200°K and possibly 3000°K (for TiN) and ∿ 3400°K (for TiC) (Gulbransen and Andrews 1949, Rutherford et al. 1961). H_2 is soluble in Ti and its concentration decreases with temperature (cf. Section 6.3.6). When Ti is heated in vacuum it getters residual active gases at a rate which increases with temperature as described in Section 6.3.4 but H_2 is desorbed. Levine and Lichtman 1960 have studied the outgassing properties of bulk Ti at high temperatures and found that the principal desorbed gases were H_2 (∿ 97%) and H_2O (∿ 1%). At temperatures near the sublimation point (∿ 1600°K) gaseous oxygen and hydrogen (or dissolved impurities) may react with adsorbed C to produce CO, CO_2 and CH_4 (Holland et al. 1961, Elsworth et al. 1965). At the sublimation temperature the relative concentration of C impurity in Ti wires is known to increase as Ti atoms are sublimated. It has been suggested that some C may also evaporate with Ti atoms (Rutherford et al. 1961).

6.3.6 Adsorption of Hydrogen

Hydrogen is soluble in Ti and the reaction has been studied mainly at high temperatures and pressures. The properties of

absorption by Ti have been reviewed by Libowitz 1960, Mikheeva 1960, Mackay 1966 and Kolachev 1968 among others. The phase diagram of the H_2-T_i system is complex (cf. McQuillan 1951 and cited work). H_2 is initially absorbed to form a solid solution, the α - phase. Adsorption at constant $p(H_2)$ and T obeys an atomic diffusion law:

$$dN_{ad}/dt = k_1 t^{\frac{1}{2}} \tag{6.3}$$

where t is the exposure time and k is a constant (Mikheeva 1960). The concentration c in solution obeys Sievert's law over a wide range of temperatures and pressures:

$$c = k_2 p^{\frac{1}{2}} \exp (Q/RT) \tag{6.4}$$

where R is the gas constant. The heat of solution Q of molecular H_2 is $\sim$ 11 Kcal gr - mole^{-1} and $k_2 \sim 10^{-2}$ (cf. the above review articles and McQuillan 1951, Mikheeva 1960). The solubility of H_2 in α - Ti at 300°K is small ($\sim$ 0.1 atomic %). When c exceeds this value Sievert's law is no longer applicable and a Ti hydride compound is precipitated. The hydride may be one of several phases depending on the concentration and temperature. The atomic structure varies from one phase to another and with c and T within any one phase. Hydridic phases may be precipitated even at very low temperatures and pressures because of the low solubility.

Hydrogen is very mobile in α - Ti (and also in the hydridic phases). The diffusion rate is apparently $\sim 10^8$ times higher than any other impurity interstitial (Kolachev 1968). The

diffusion coefficient D is normally measured at high temperature and related to the activation energy for diffusion Q_d by:

$$D = D_o \exp - Q_d/RT \qquad (6.5)$$

For α-Ti Kolachev cited a value of $D_o \sim 10^4$ cm^2 sec^{-1} and $Q_d \sim 5 - 12$ Kcal grm - atom^{-1} (Mackay 1966, McCracken et al. 1968, Kolachev 1968).

There have been few studies at low pressure and temperature. Suhrman et al. 1962 investigated the resistivity of Ti films $\sim 70A^o$ thick at 90 and 273°K in an ultra high vacuum system as a function of $p(H_2)$ up to 10^{-2} torr. These experiments were described previously in Sections 6.3.1 and 6.3.2 where it was concluded that the films were probably contaminated. However, R increased when H_2 was introduced until the concentration of H in the film reached a value H/Ti ≃ 0.12. As the ratio H/Ti increased further (as p was increased) R increased further at 90°K but decreased at 273°K. The resistivity measurements fitted an atomic diffusion law but there was no simple explanation for the effect of T. They concluded that solution of H, was preceded by the formation of a monolayer of adsorbed H . These results are not inconsistent with the suggestion that the surfaces were contaminated before adsorption of H_2 since from other studies it is known that H can diffuse through a contaminated surface layer on Ti and co-exist with other gases in solution also (cf. Gulbransen and Andrews 1949, Stout and Gibbons 1955). Iwanoski and Schirjaev 1965 have studied the adsorption of H_2 by pure Ti films deposited

in ultra high vacuum at low temperatures (78 - 178°K) and pressures (10^{-10} - 10^{-7} torr). Within this range H was in solution and the equilibrium concentration at constant p decreased rapidly with increasing temperature and their results empirically fitted an electrolytic solution law. Small quantities of H_2 were rapidly absorbed but several hours were needed to reach a concentration of H/Ti = 0.75. At 77°K the equilibrium pressures of $\sim 1.10^{-8}$, 1.10^{-9} and 1.10^{-10} torr (H_2) resulted in the equilibrium concentrations of H/Ti $\sim$ 1.0, 0.4 and 0.09 respectively. The adsorption times needed were $\sim$ 3 - 4, 0.5 - 1.0 and 0.2 - 0.5 hours respectively. Giorgi and Ricca 1967 studied the absorption of H_2 on Ti powders extensively outgassed in ultra high vacuum which obeyed Sievert's law over a wide range of temperature (600 - 1200°K) and pressure (10^{-7} - 10^{-3} torr (H_2)).

There is no generally accepted theory of H in Ti. Two theories are used each of which accounts for various experimental results and the residual metallic properties of hydrides. They are discussed in the review articles mentioned above and also by Gibb 1962. In the metallic theory absorbed hydrogen has a positive charge and a shift of electrons occur to the metal conduction band. Wesolowski et al. 1963 have presented evidence suggesting the atom is almost completely ionised in $TiH_{2.0}$. In the ionic theory the H atom has a net negative charge and the residual metallic properties are accounted for by metallic bonding by valence electrons. Gibb 1962 has suggested that the positive form of H may be really a resonating bond form of H^-. In this

case both forms may exist in sufficient amounts to account for the high mobility of H and also the overall structural and thermodynamics of the system which are more easily accounted for by the ionic theory. Suhrman et al. 1962 concluded from their surface potential measurements that adsorbed hydrogen on Ti at 90 and 273°K was negatively charged. Magee 1967 however observed a positive SP on Ti. In both of these experiments the surfaces were probably contaminated and structural changes may also have occurred since the concentrations of hydrogen probably exceeded the solubility limit. These factors complicate the interpretation of the resistivity and SP data. Suhrmann et al. observed a change in the direction of change of R with increasing concentration of H at 90 and 273°K. Although this maybe due to one of the above effects it suggested that H may exist in two electronic forms in Ti (or strictly in the hydride).

6.4 Conclusions

A suitable reference value for the work function of unsintered gold films deposited onto glass in ultra high vacuum at 300°K is 5.20eV in an ion pump vacuum system. The work function of pure gold surfaces is not affected by O_2, N_2, H_2, CO within 10mV or so at room temperature and at pressures below a few torr. C_2H_2 and C_2H_4 are reversibly adsorbed at room temperature but no SP data for these or for H_2O appear to have been published.

The work function of Ag for thin unsintered films on glass and various polycrystalline metallic substrates is reasonably well established to be 4.30eV at 300°K. Higher values occur for orientated surfaces and for films on substrates of the same element. The value of ϕ_{Ag} may be affected by structure and thickness. Pure films do not chemisorb H_2, N_2, CO, CO_2, C_2H_2 or C_2H_4 at room temperature and ϕ_{Ag} is known to be stable on exposure to H_2, CO and N_2 at room temperature. O_2 is adsorbed (sometimes irreversibly) at room temperature on orientated surfaces and thin films with a negative SP up to - 0.9eV. The results of Steiger et al. and Degeilh on the adsorption of O_2 on the (100) face are in disagreement.

The published values of the work function of titanium vary from 3.5 to 5.8eV. Many of these are close to those of the oxides and carbides of titanium. In many cases the measurements probably refer to contaminated surfaces and in others they are perhaps unreliable because insufficient information was given to evaluate their measurements. Titanium adsorbs with the formation of oxides, hydrides, nitrides and carbides many of the residual vacuum gases from low temperatures to temperatures close to its sublimation point at a rate which increases with temperature*. Outgassed bulk samples in vacuum therefore may be free of H but are likely to be contaminated. Auger spectroscopy of out-gassed T_i foils in ultra high vacuum upto at least 1300°K have revealed the presence of sulphur, carbon and oxygen impurities which were not altogether removed by heating alone (Bishop et al. 1970). With the exception of Wilson's measurements all the experiments were apparently

---

* with the exception of hydrogen.

performed in diffusion pump vacuum systems and there has been one report that oil vapour is detrimental to the production of clean Ti surfaces. The activation energy for solution of H_2 , N_2 and O_2 in Ti is small and their diffusion rates are large. The presence of these gases adsorbed on the substrates onto which Ti films are deposited may lead therefore to contamination of the growing film. Rentschler and Henry 1945 have in fact observed that thin films of Ti may react with adsorbed oxygen on the substrate and result in a value of ϕ which is lower than for thicker supposedly pure films. The sticking coefficients of O_2 are large at room temperature but the values for H_2 and N_2 are lower and more diverse which may reflect the difficulties of producing clean surfaces. The values also vary with the film structure and only in the case of H_2 apparently is the coefficient independant of the quantity adsorbed at room temperature. Few reliable SP measurements have been reported. The SP of N_2 and O_2 is apparently negative and may attain large values. In many cases the adsorbent was contaminated probably before introducing the adsorbate gas or during the adsorption period and in others insufficient details were given for a reliable evaluation to be made. Suhrman et al. and Magee disagree on the sign of the SP of H_2 on Ti films (which were of doubtful cleanliness) and in the former case the films were very thin ($\sim$ 40 - 70A^o) and may have reacted with H_2O on the glass substrate at 90^{o}K. Steiger et al. as discussed above in Section 6.2.2 have found evidence for thick layers of H_2O on very cold substrates at low pressures.

CHAPTER 7

CONTACT POTENTIAL RESULTS WITH GOLD, SILVER, STEEL AND TITANIUM

7.1 Introduction

The preliminary contact potential (cpd) experiments were unsuccessful owing to various faults in the apparatus. The first results were obtained with the fifth run, experiment A, although a leak in the gold brazing of the vibrating bar in the capacitor flange limited the base pressure to ~ 2.10^{-6} torr. The sixth run experiment B was made in ultra high vacuum and the seventh experiment C in high vacuum (~ 1.10^{-7} torr). The effects of stray capacitance on the cpd and surface charge on the work function of steel (described in Chapter 4 and 5) were investigated in experiment B. All of the results except for some in experiment C are subject to a systemmatic stray capacitance error estimated to be about 0.3 ∓ 0.1 eV (cf. Chapter 4). The results from experiments A and B are also affected by the surface charge on the steel probe. In the last experiment C the probe was coated in-situ with Ag and they are free from these effects.

The results from runs A and B were obtained with the first experimental rig shown in Figure 3.2 and the last results in run C with the sturdier rig shown in Figure 3.4 (cf. Chapter 3). In experiment C a metal baffle was placed between the Boostivac pump and the experimental chamber. This prevented stray currents from the pump from reaching the film surfaces and the reduction in pumping speed was offset by the addition of two other ion pumps

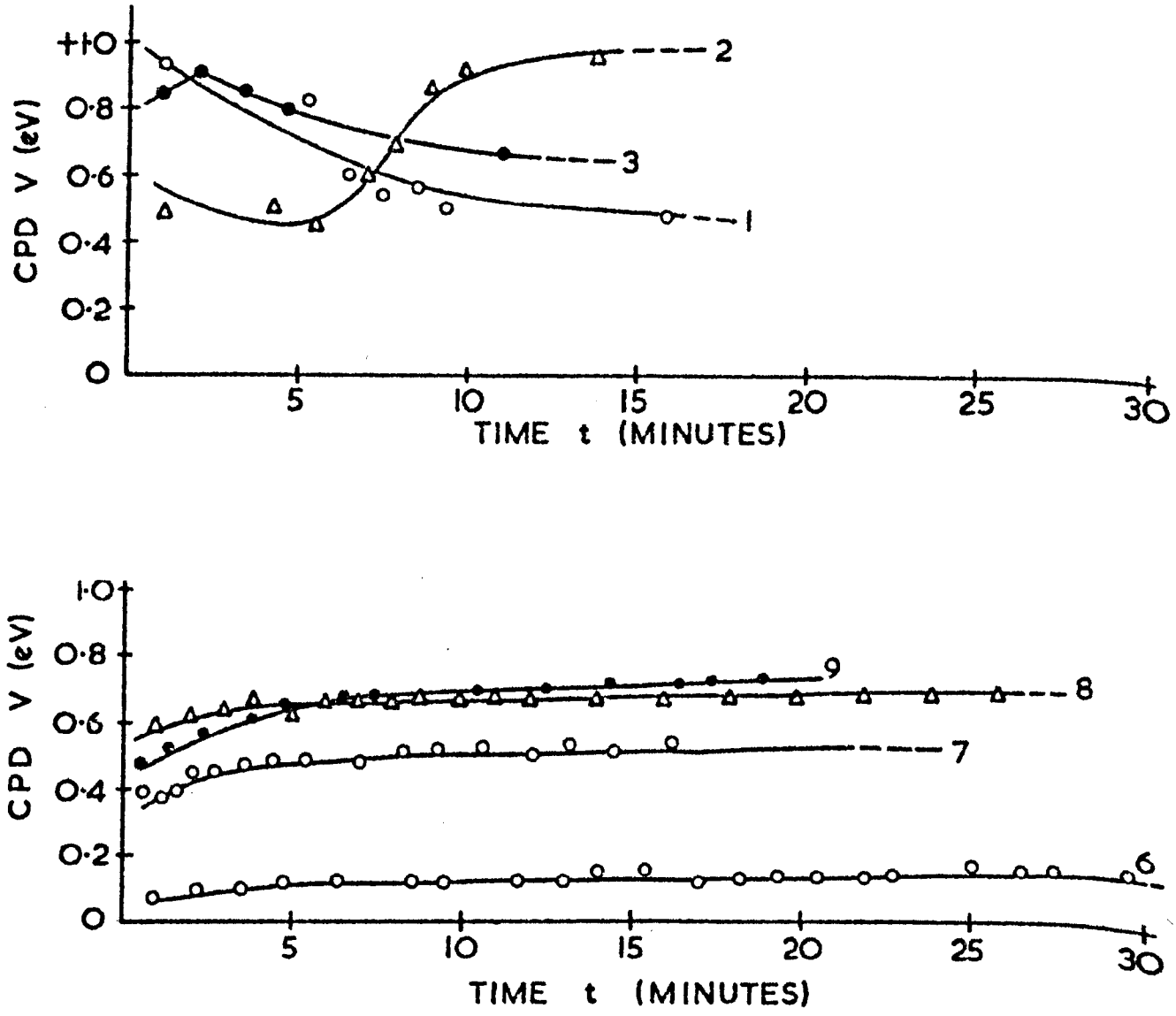

Figure 7.1 Variation of the cpd $V = \phi_{Au} - \phi_s$ between gold films deposited onto pyrex at 2.10^{-6} torr (experiment A) and stainless steel ($\phi_s = 4.64$eV at equilibrium). Films 1-5 were deposited onto the clean glass and afterwards coated with titanium (no results for films 4 and 5). Films 6-9 were deposited onto the titanium layer.

(cf. Chapters 3 and 5). Measurements were always made at the centre of the substrate unless otherwise stated. This precaution was taken because of the large changes in the apparent cpd across the substrate due to stray capacitive effects as described below.

7.2 Gold Films

Gold films were deposited onto pyrex sybstrates. Sensible cpd measurements were only obtained when the film was sufficiently thick to prevent electrical charging of the glass surface. In experiment A five transparent gold films were deposited at 2.10^{-6} torr but technical problems prevented accurate measurements on the last two films. The results are shown in Figure 7.1 which were obtained using the mode 1 method of contact potential measurement (cf. Chapter 3). The gold was later coated with Ti (section 7.4 below) and afterwards the system was let up to air with N_2 gas. The evaporation source was renewed and the system pumped out again. A second series of gold films numbers 6-9 were deposited (Figure 7.1). The cpd for each increased by 0.1 - 0.2 eV just after deposition and the stable values progressed to a reproducible contact potential between the steel and the films of + 0.65 $\bar{+}$ 0.05 eV in close agreement with the previous gold film number 3 before deposition of Ti.

In ultra high vacuum, experiment B, fourteen gold films were deposited onto a fresh glass substrate at a pressure of ~ 2.10^{-9} torr which did not increase during the evaporation. Anomalous contact potentials* as large as 6 eV resulted for the initial deposits but successive films thickened the deposit and sensible results

---

* using mode 1 measurement.

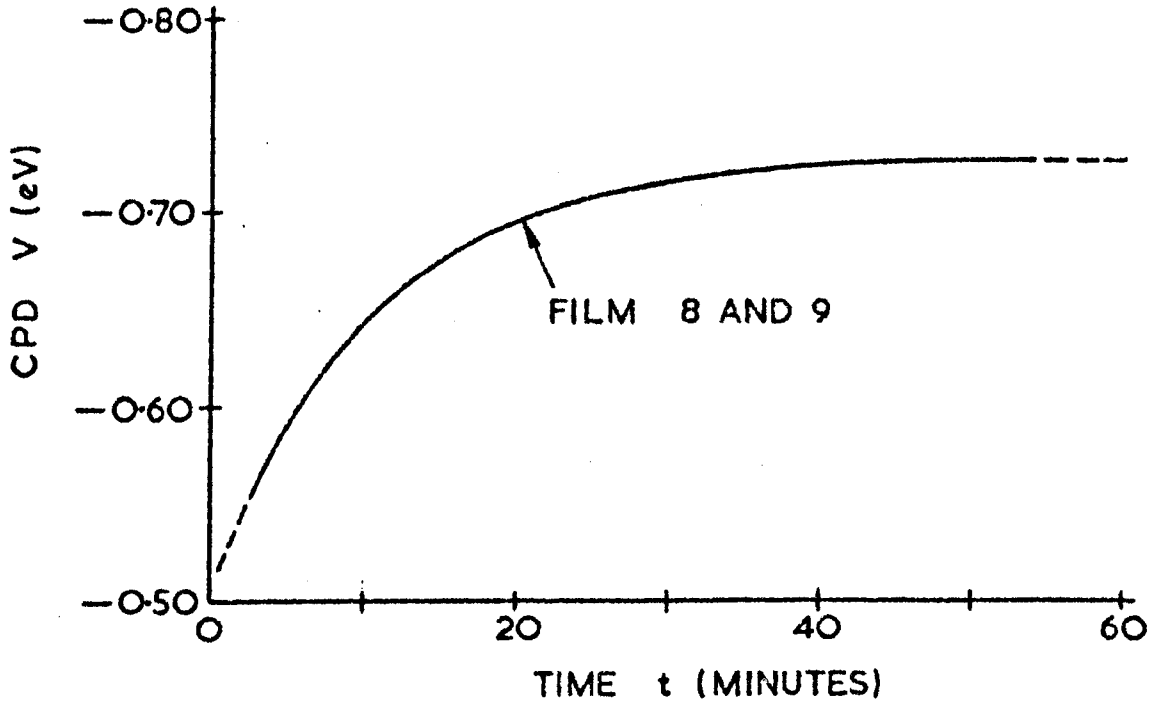

Figure 7.2 Typical variation of the cpd $V(V = \phi_{Au} - \phi_s)$ between freshly deposited gold films on the pyrex substrate and the steel probe (ϕ_s) at 2.10^{-9} torr (experiment B).

were obtained. The results for two of the later films are shown in Figure 7.2. The cpd increased by ≈ 0.17 eV after deposition and eventually became constant after thirty minutes or so. The final cpd between the last gold film and the steel probe was + 0.3 eV. In each case the equilibrium value of the cpd was constant in vacuum for several hours or more and was not affected by increasing the pressure of neutral hydrogen to ~ 10^{-6} torr (cf. Chapter 5.2).

The final values of the cpd in these two experiments yield the work function of the steel probes to be 4.65 eV and 5.60 $\mp$ 0.05 eV in experiments A and B respectively. The steel electrodes were not the same in these and in the latter experiment (cf. Chapter 5.2) it was known that the work function was sensitive to illumination and charged particles from the ion pump. Measurements of the spatial variation of the cpd across gold films are discussed later.

7.3 Silver Films

The steel probe was coated in-situ at 1.10^{-7} torr with Ag from the evaporator filament (experiment C). In order to do this the substrate was rotated as far as possible out of sight of the evaporator. The substrate in this experiment was an erbium coating on a Mo base and one half of it was covered with a gold film. A film resistance monitor was used near the evaporator and the resistivity of the film deposited on the probe was ~ 20 Ω per square. In previous experiments (cf. Chapter 5) the probe work function was affected by optical irradiation during evaporation. Tests were made to establish that the Ag surface was stable. In

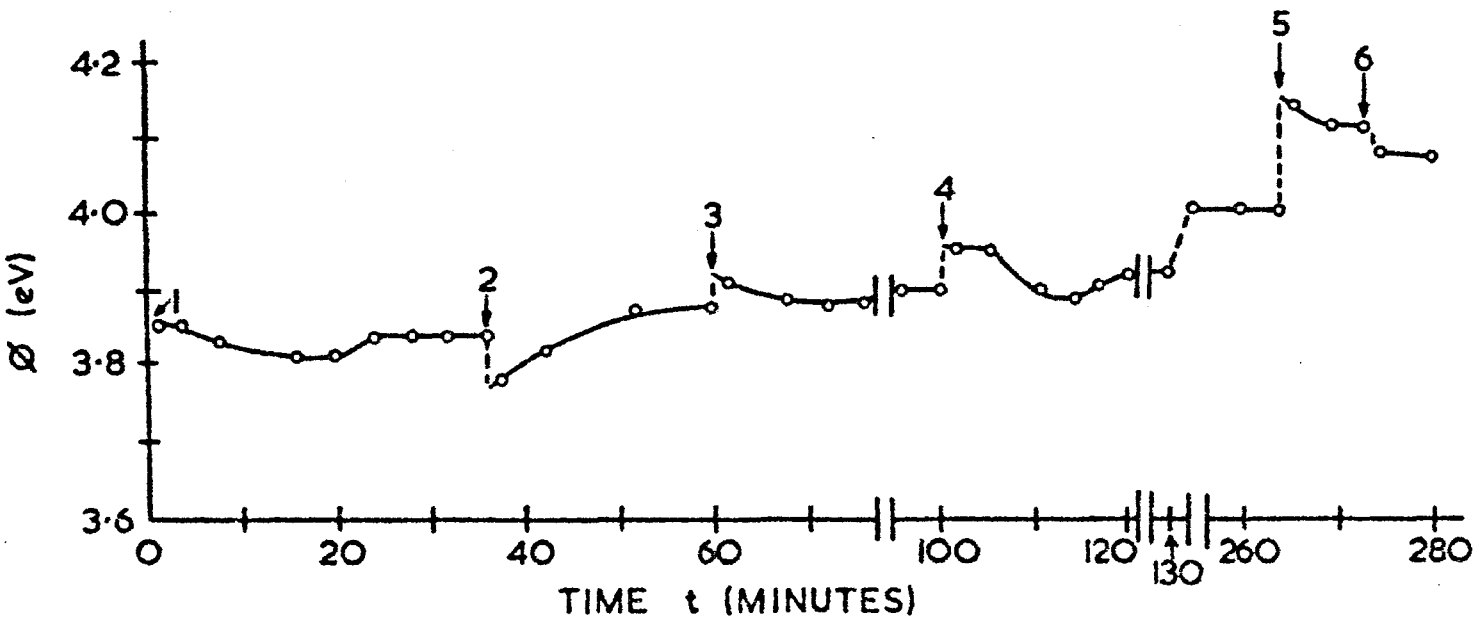

Figure 7.3 Change in the work function ϕ of the erbium substrate (ϕ = 3.5eV before depositing A_g) with successive films (1-6) of A_g at 1.10^{-7} torr (experiment C). The data for films 7 and 8 (on titanium) is shown in Figure 7.6. Reference surface - silver ϕ = 4.3eV.

one of these the substrate was positioned so that its surface and also that of the probe were screened from the Ag evaporator by the substrate support. The temperature of the evaporator was gradually increased until Ag was evaporated and then it was decreased. During this period the cpd between the probe and the substrate was continuously monitored. It decreased when the filament became white hot but quickly regained its former value when the temperature was reduced. The changed corresponded to a reduction in the probe work function of approximately 0.15 eV. The cpd did not change in the following 30 minutes with $\bar{+}$ 30 mV. In other similar tests the cpd did not change at all.

Silver films were successively deposited onto the substrate at 1.10^{-7} torr and there was no increase of the gas pressure during the evaporation. The cpd between the Ag probe and the substrate progressively decreased from one evaporation to the next as the film thickness increased. With the assumption that the work function of the probe was 4.3 eV (cf. Chapter 6.4) the substrate work function ϕ increased from 3.83 to about 4.1 eV as shown in Figure 7.3 ϕ generally decreased to a steady value by as much as 60 mV in about ten minutes after deposition. Two evaporation filaments were used and the films numbers 5 and 6 were deposited with the second filament. Titanium was deposited onto the substrate (as discussed in the section below). Two more silver films were deposited onto the Ti layer to check the contact potential between the Ag coated probe and fresh Ag films on the substrate. The initial values after deposition of the work function of these two films were 4.08 and 4.38 eV respectively (assuming ϕ = 4.3 eV for the probe). The first film increased to 4.28eV and then decreased to 4.08eV (Figure 7.6a), the second decreased to

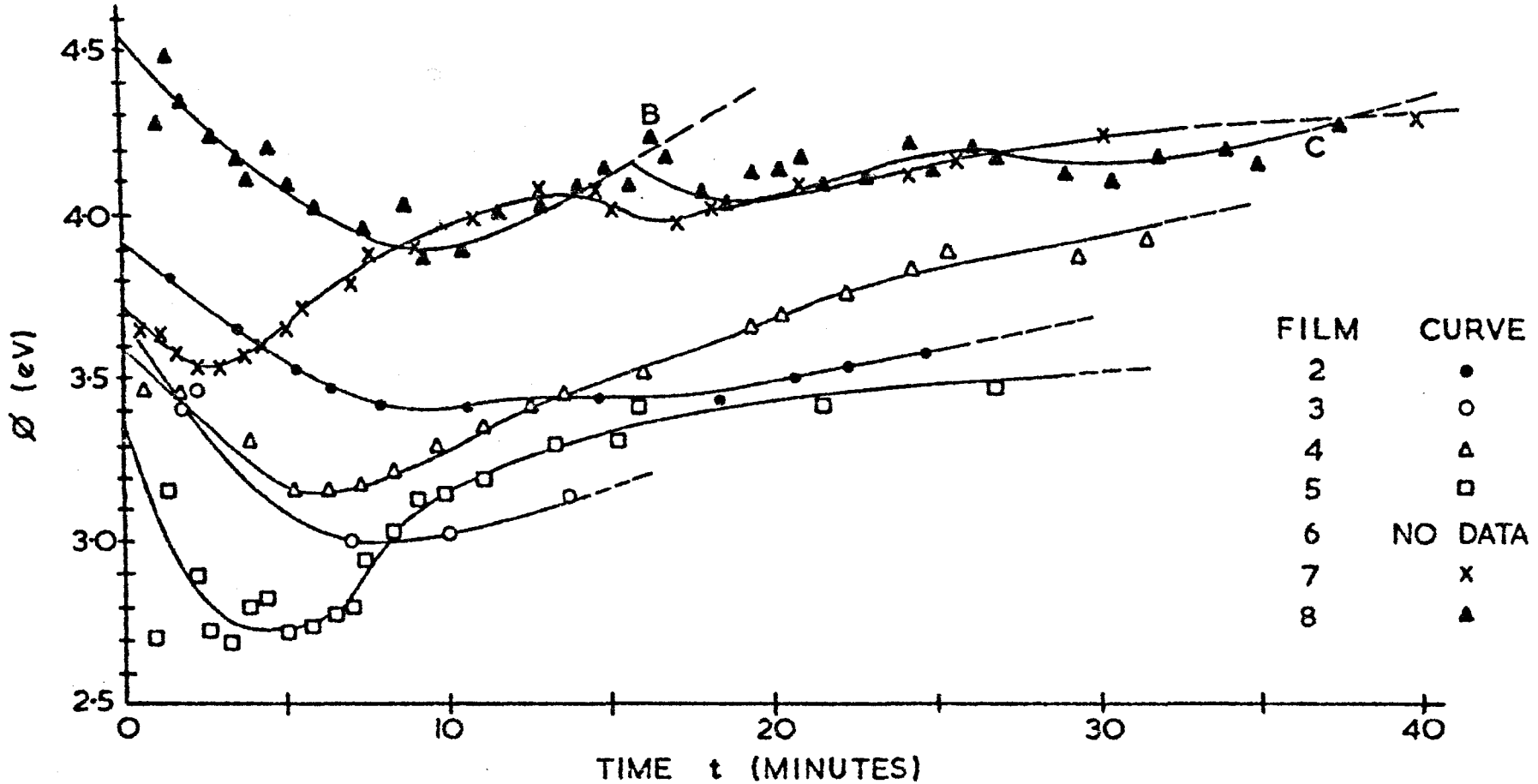

Figure 7.4 Variation of the work function ϕ of Ti films deposited at 5.10^{-7} - 2.10^{-6} torr onto gold (experiment A). The backing voltage was switched off between cpd measurements after point B (film 8). Reference surface - steel ϕ = 4.65eV.

approximately 4.20 eV in the twenty minutes or so after evaporation after which they became constant.

7.4 Titanium Films

Eight films were deposited in experiment A in high vacuum onto the gold film substrate on glass. During deposition the pressure rapidly decreased from 2.10^{-6} torr to 5.10^{-7} torr and evaporation was continued for 30 seconds after the minimum pressure was reached. Often several hours elapsed before the pressure rose to its former value. With the assumption that the work functions of the gold film and the steel probe were 5.30 and 4.65 eV respectively (cf. section 7.2) the results are shown in Figure 7.4 The initial values ϕ_o varied from about 4.55 to 3.35 eV and in each case ϕ decreased by an amount between 0.2 and 0.6 eV within about ten minutes and subsequently apparently increased to an equilibrium value of $\approx 4.6 \pm 0.1$ eV after several hours. The results for two films are omitted because of technical difficulties. In the case of film number 8 the backing voltage V_b was switched off between measurements of the cpd after the point B was reached. Before this, A-B in the diagram, and also for all the other films V_b was continuously applied. The application of V_b was apparently disturbing the measurements causing the apparent ϕ to increase with time.

In the ultra high vacuum, experiment B, eleven films were deposited onto the gold film substrate on glass at 2.10^{-9} torr. There was no increase in the pressure during deposition. The seventh film was deposited at $\sim 7.10^{-7}$ torr (H_2) and during the period following

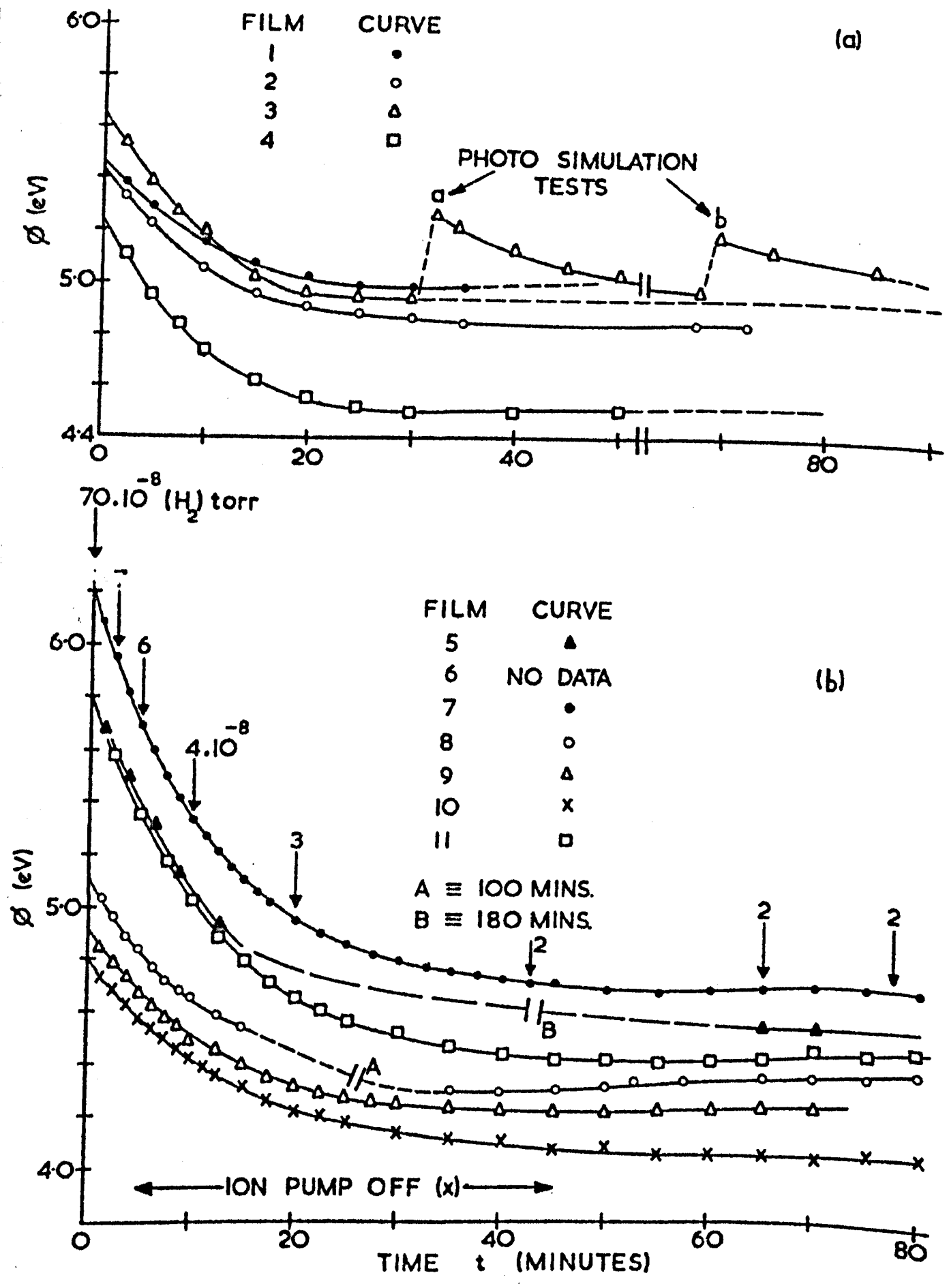

Figure 7.5 Variation of the work function ϕ of titanium films deposited onto a gold film substrate at 2.10^{-9} torr (experiment B): (a) films 1-4 (b) films 5-11. The work function of the reference steel probe (ϕ = 5.60eV) was assumed stable. The results corrected for photo-instability are summarised in Table 7.1.

evaporation the pressure fell to 2.10^{-8} torr. The cpd between the steel probe and the films was measured with the pen recorder in mode 2 since the application of V_b in the mode 1 method disturbed the probe work function (cf. Chapter 5). In ultra high vacuum the equilibrium work function of the steel probe was 5.6 eV (cf. section 7.2 above) and assuming it was constant the results for titanium are shown in Figure 7.5. The work function ϕ_s of the probe reversibly decreased during evaporation, however, due to the illumination from the filament. In order to estimate the effect on the measured cpd two photo-simulation tests were made in the same way as for the silver films described in section 7.3. The evaporation filament was heated in exactly the same way as for the real depositions. The results are shown for film number 3. The filament was heated at points a and b in Figure 7.5. The reduction in ϕ_s is shown as an apparent change in ϕ_{Ti}. The results for the initial work function ϕ_o and the surface potential $\phi_o - \phi_f$ for the films are too large by 0.30 ∓ 0.06 eV. The final values ϕ_f of the films are not affected by the probe instability. Similarly the initial rate of change $d\phi/dt_{t\to o}$ is too large by 17 ∓ 3 mV min^{-1}. These correction factors are the mean values derived from the two simulation tests. The corrected values are given in Table 7.1. ϕ_o varied widely from about 4.8 to 5.9 eV and ϕ decreased to a final value ϕ_f between about 4.0 and 5.0 eV. The time t_f taken to attain ϕ_f varied from about 30 to 60 minutes. In the case of three films (numbers 1, 4 and 5) the cpd was measured for a period after ϕ_f had been attained and in each case ϕ increased by about 0.1, 0.75 and 0.2 eV after about 1, 17 and 2 hours respectively.

Film	ϕ_o eV	ϕ_f eV	V_f eV	t_f mins	$d\phi/dt_{t\to o}$ mV min^{-1}
1	5.25	4.99	+ 0.26	35	- 53
2	5.15	4.83	+ 0.33	35	- 33
3	5.46	4.94	+ 0.52	30	- 63
4	5.01	4.50	+ 0.51	40	- 63
5	5.61	$\leq$4.55	$\geq$ 1.06	$\leq$65	- 88
6	-	$\leq$4.29	$\geq$ 0.46	-	-
7*	5.97	4.67	+ 1.30	55	-103
8	4.86	$\leq$4.30	$\geq$ 0.56	$\leq$35	- 53
9	4.62	4.24	+ 0.38	45	- 38
10	4.51	4.04	+ 0.47	55	- 38
11	5.55	4.42	+ 1.13	55	- 88
Error $\simeq$	$\mp$0.10	$\mp$0.06	$\mp$ 0.10	$\mp$5	$\mp$ 10

Table 7.1 Summary of the corrected measurements on titanium deposited on gold at 2.10^{-9} torr in experiment B shown in Figure 7.5 of the initial value ϕ_o, the final value ϕ_f, the surface potential $V_f = \phi_o - \phi_f$, the initial rate of change of ϕ and the time t_f taken to achieve the final value.

* deposited at 7.10^{-7} - 2.10^{-3} torr (H_2)

In this experiment a stray electrical current was known to be incident on the electrodes (cf. Chapter 5.2) although it had been shown previously to be too small in ultra high vacuum to affect the measurements. In order to firmly establish this fact the ion pump was switched off from t=5 to t=40 minutes after depositing the tenth film. There was no apparent effect on the magnitude or rate of change of the cpd.

In experiment C nineteen films were deposited onto the silver film substrate at 1.10^{-7} torr. The reference surface was a silver film on the steel probe and the results are not affected by the photo-instability which occurred in experiment B (cf. section 7.3 above). The cpd between the reference surface and the films was measured in mode 1. The evaporator temperature was initially set low, but since it became apparent that little Ti was being evaporated the filament temperature was gradually increased from one deposition to the next. The resistance R of the film resistivity monitor was measured during each deposition. It was initially covered with a Ag film R $\simeq$ 20 Ω per square onto which Ti was deposited (cf section 7.3). The variation of the work function of each film is shown in Figure 7.6 and a summary of the initial and final values, the maximum surface potentials and the direction of change of R is given in Table 7.2. The substrate work function progressively decreased from one deposition to the next although there was no change in R or little in ϕ from the initial value. ϕ_o continued to decrease and reached a minimum value of about 2.5 eV but in the case of the later films, numbers 6 - 12, R increased and also ϕ after deposition by as much as 0.9 eV. Two fresh silver films were

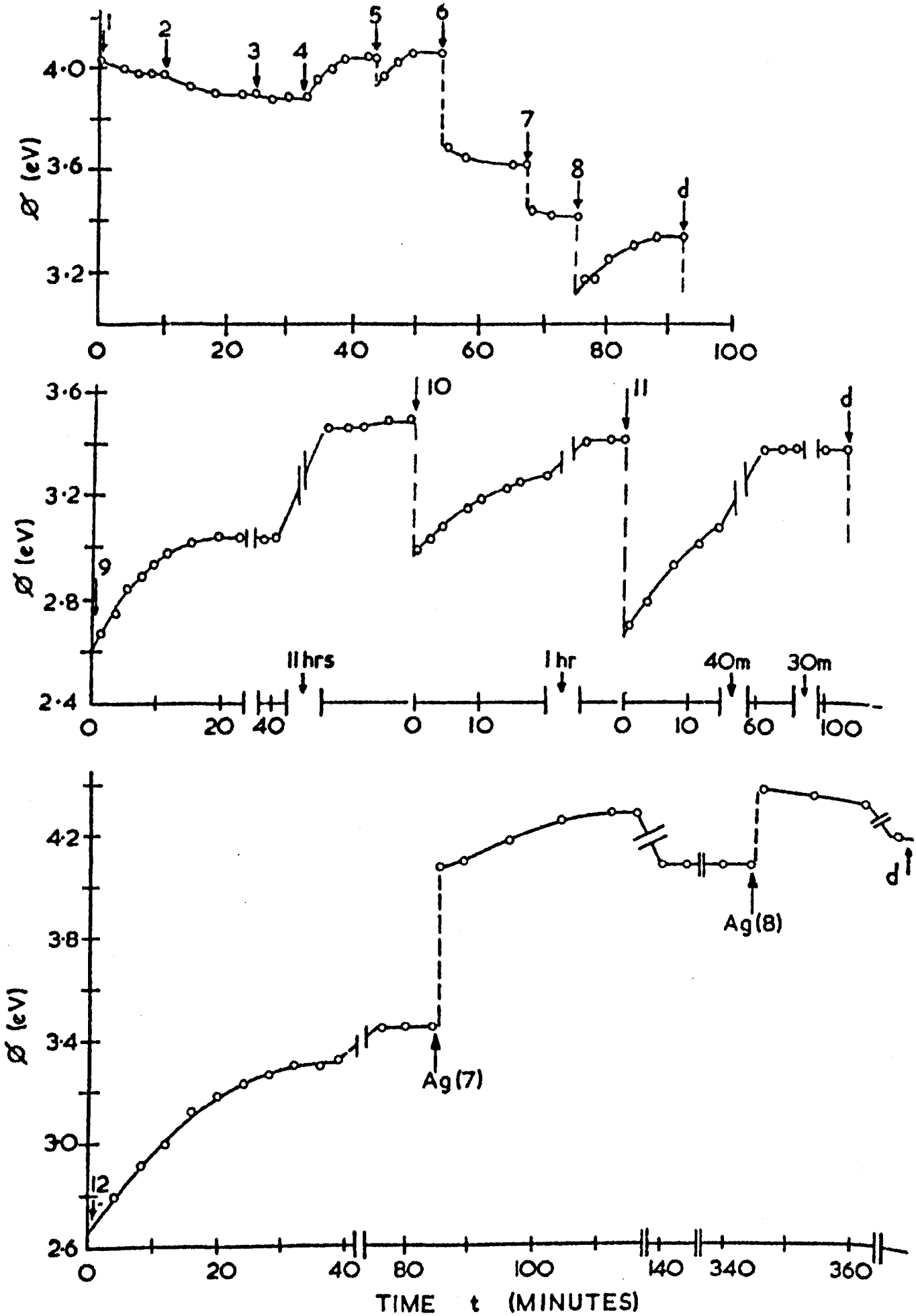

Figure 7.6(a) Variation of the work function ϕ of titanium films (1-16) deposited onto a silver film substrate at 1.10^{-7} torr (experiment C). At points d the succeeding films were deposited. Results are summarised in Table 7.2. Reference surface - silver $\phi = 4.3$eV

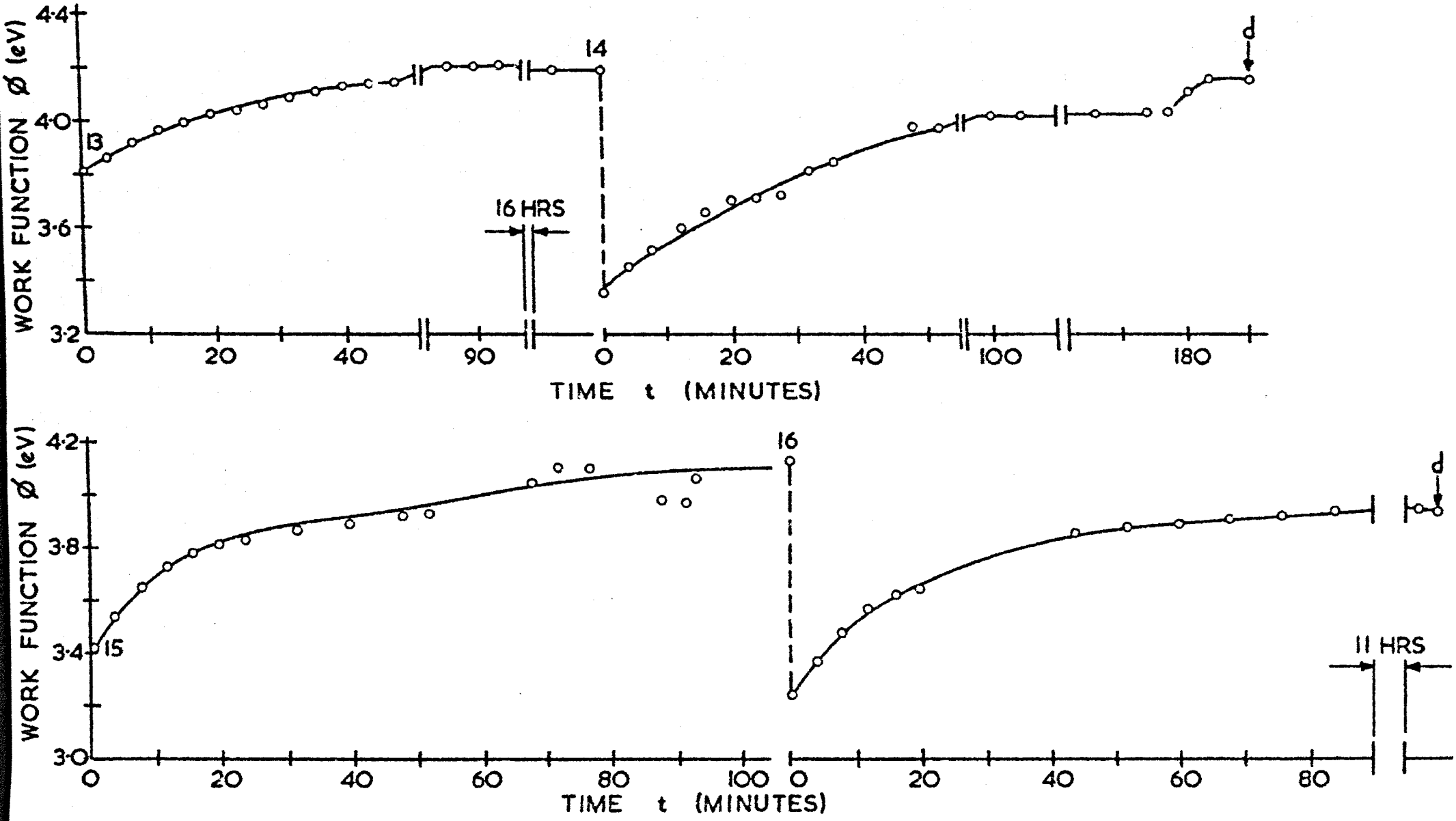

Figure 7.6(a) (continued) The succeeding films were deposited at point d.

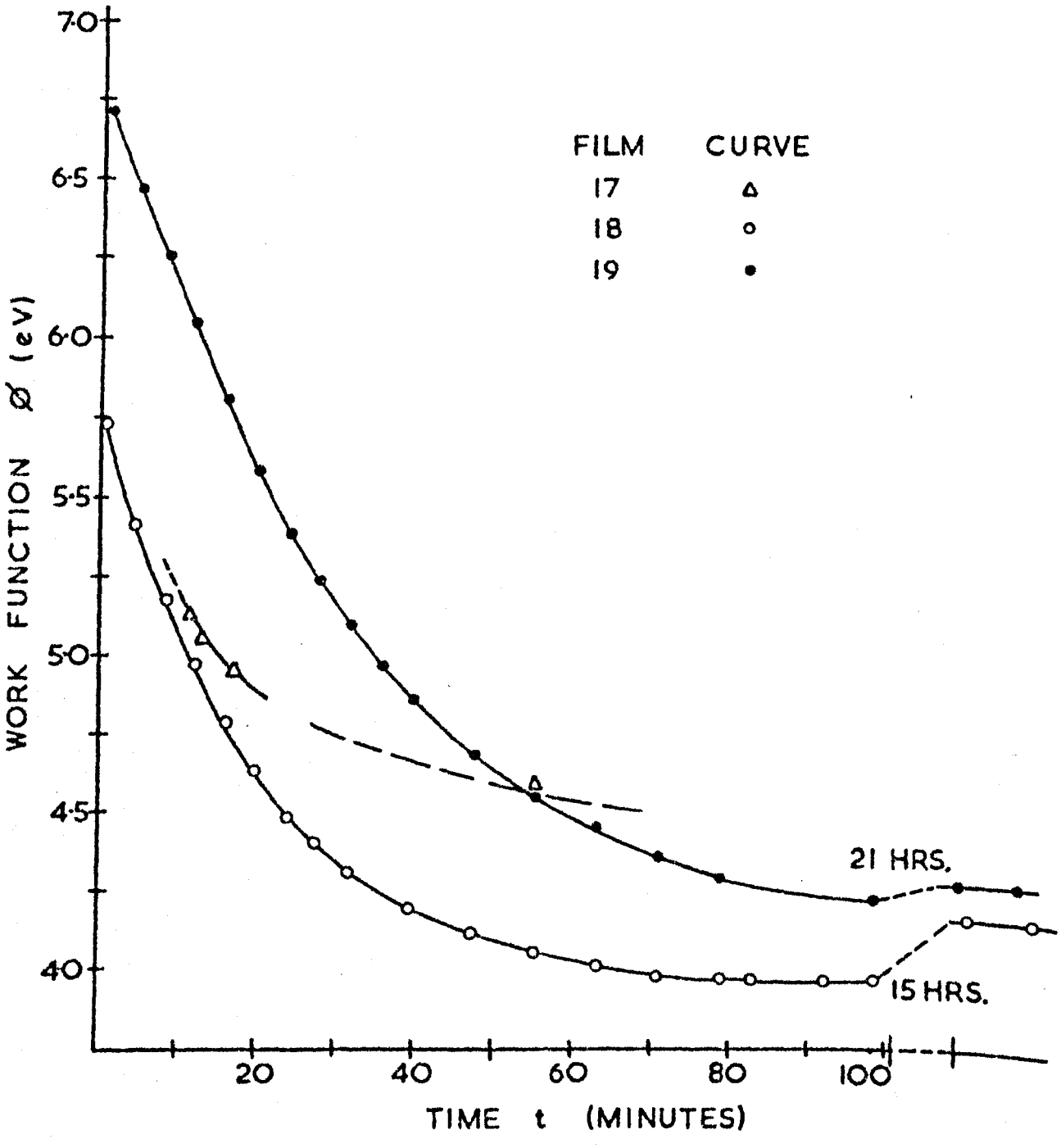

Figure 7.6(b) Variation of the work function ϕ of titanium films (numbers 17 - 19) rapidly deposited onto silver at 1.10^{-7} torr (experiment C); cf. Table 7.2. Reference surface - silver ϕ = 4.3eV.

deposited onto the substrate to check the stability and value of the reference work function (cf. section 7.3).

A second series of films were deposited onto the fresh silver substrate surface, numbers 13-19. For the first the evaporation temperature was not changed from that for number 12 but afterwards the temperature was gradually increased further for each deposition. The films 13-16 showed a similar behaviour to the previous (and thinner) ones except that the initial value of ϕ_o lay between 3.3 and 3.8 eV and their final value of ϕ_f lay between 4.0 and 4.2 eV. R increased during each deposition for all the films which possessed a negative SP, numbers 6-16. The evaporator heater current was increased by ≈ 30% before depositing film number 17 but it was not changed for the remaining films. All of these films 17-19 reduced R. Technical difficulties limited the measurements on one film. The results are shown in Figure 7.6b. In the case of these thicker films ϕ_o lay between 5.6 and 7.0 eV, ϕ decreased after deposition by as much as 2.6 eV, and ϕ_f lay between 3.95 and 4.3 eV after about 90 minutes. ϕ generally slowly increased by a small amount after ϕ_f was reached.

The results for films 18 and 19 are free from stray capacitance errors since in these instances it was possible to connect the vibrating probe to the "earthy" side of the head amplifier (cf. Chapter 4). Two tests were made to check the photo-stability of the reference surface (as described above) for films number 9 and 14. The reference surface was stable to within $\pm$ 50 mV.

Film	ϕ_o eV	ϕ_f eV	V_f eV	t_f mins	$\delta R\Omega$	$d\phi/dt$ mV min^{-1} $t\to o$
1	4.04	3.98	+ 0.06	6	0	- 4
2	3.98	3.90	+ 0.08	9	0	- 10
3	3.91	3.92	- 0.01	6	0	0
4	3.94	4.04	- 0.10	6	0	+ 19
5	3.94	4.06	- 0.12	5	0	+ 27
6	3.68	3.62	+ 0.06	6	+	- 14
7	3.48	3.44	- 0.04	5	+	- 14
8	3.15	3.32	- 0.17	12	+	+ 30
9	2.56	3.04	- 0.48	22	+	+ 56
10	2.95	3.42	- 0.47	44	+	+ 31
11	2.72	3.42	- 0.70	50	+	+ 54
12	2.64	3.44	- 0.80	~60	+	+ 44
	Two fresh Ag films deposited on substrate					
13	3.81	4.18	- 0.37	≤50	+	+ 15
14	3.34	4.06	- 0.72	≤80	+	+ 24
15	3.42	4.10	- 0.68	~80	+	+ 33
16	3.24	3.95	- 0.71	~90	+	+ 38
	Higher Evaporation Temperature					
17	5.84*	≤4.59	≥+ 1.25*	≥50	-	≤- 43
18	5.80	4.05	+ 1.75	80	-	- 80
19	6.74	4.22	+ 2.52	≥80	-	- 64

Table 7.2 Summary of the measurements on titanium films deposited on silver at 1.10^{-7} torr in experiment B from Figure 7.6. δR is the direction of change of the resistance of the thin film resistance monitor during the deposition and $|\delta R| \simeq 0.5\%$ R where R ≃ 20 Ω sq^{-1}. Reference surface was silver ϕ = 4.30 eV.

* $\overline{+}$ 0.3eV

7.5 Patch Effects

The spatial variation of the work function was measured by rotating the substrate to bring a different portion of the film opposite the reference probe. The substrates were not perfectly circular (cf. Figure 7.7) and the interelectrode distance d varied with their position. All the spatial measurements are affected by a non-linear capacitive error except for those for film s numbers 17 and 13 for experiment C. Some typical results for gold, silver and titanium films are shown in Figures 7.8 and 7.9. The measurements were made when the work function was no longer varying in time. The values of ϕ_{Au} and ϕ_{Ag} at the centre positions of the substrate are assumed to be 5.3 and 4.3 eV respectively. The effect of the capacitive error is shown for one of the Ti films by repeating the measurements in the presence of the stray capacitance (by reversing the electrical connections between the Kelvin electrodes and the head amplifier).

7.6 Residual Gas Composition

The gas composition was measured with an MS10 magnetic mass spectrometer (A.E.I) and thirteen minutes were needed to make a complete spectral scan. There were negligible quantities of gas with a m/e > 48 in comparison with the other gases present. The sensitivity factors for the instrument were taken to be the arithmetic averages of the values published (A.E.I. 1969, Craig and Harden 1965 and Bailey 1963). The range of values given in these sources is shown as an error width in table 7.3 which also shows the typical composition of the system before and after baking. There

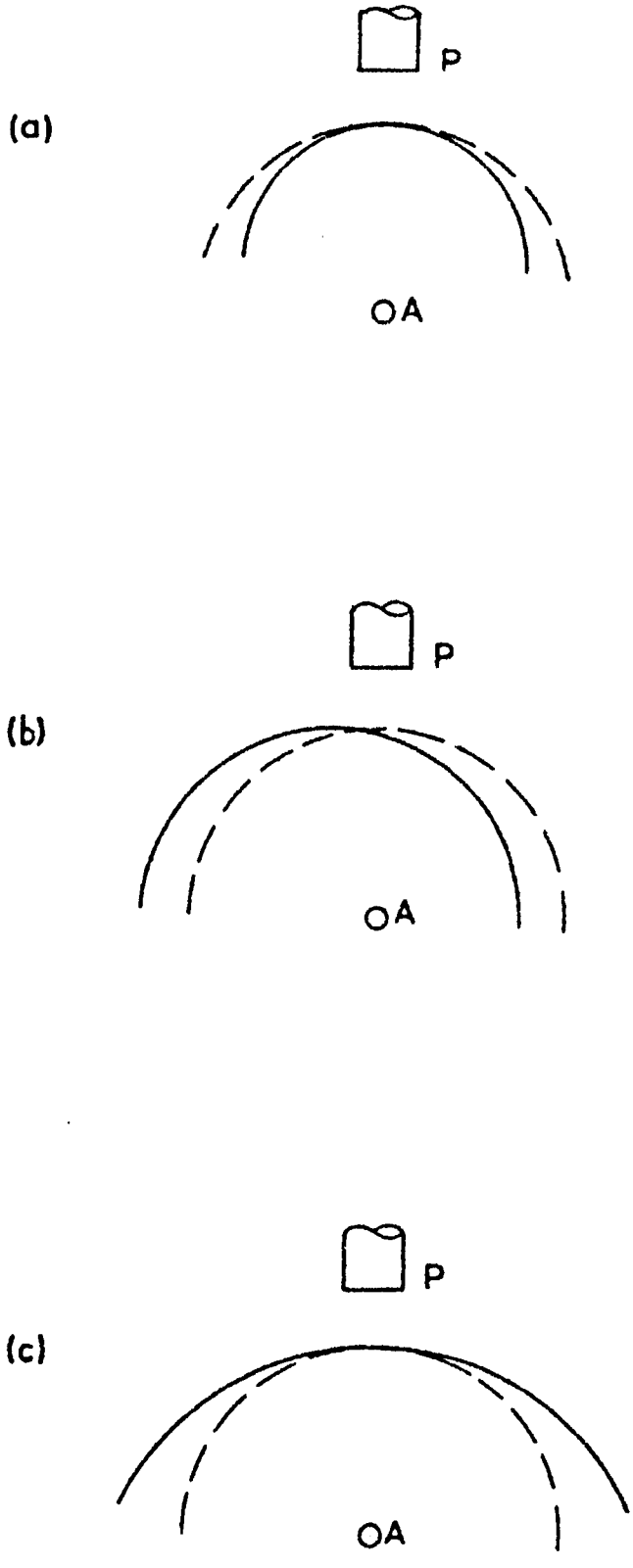

Figure 7.7 Schematic illustration of the cross-sections of the substrates used in experiments (a)A, (b)B and (c)C where P is the reference vibrating probe, A is the axis of rotation and the dotted line (---) is that of an ideal circular substrate. The inter-electrode distance d varies in a different way for each case as the substrate is rotated in front of P about A.

was no appreciable change in the partial pressures of the other gases when hydrogen was introduced from the base pressure to ~ 3.10^{-8} torr (H_2) except for H_2O and A which increased by + 20% and + 100% respectively. The original spectrum was recovered on pumping the H_2 away.

7.7 Discussion: Gold and Steel Results

The large and variable cpds between the reference steel probe and gold in experiments A and B when the films were very thin may be caused by electrical charge on the pyrex substrate. This may arise from (a) photo-excitation of electrons in the glass to the surface, (b) electron bombardment from the evaporation filament or by (c) charge transfer between the insulator surface and metal islands in the film. The latter possibility has been suggested to account for electrical conduction in thin discontinuous films and Hill 1969 has made a theoretical study of this. The transfer of charge apparently establishes a Schottl barrier V_s at the insulator surface (similar to the case of semi-conductors cf. Chapter 5) and he gives experimental evidence that for gold and silver on various glasses V_s varied from about 0.5 to 1.4 eV. In some cases the magnitude of V_s was disturbed by an impressed electric field perpendicular to the substrate. Previous work has shown that sensible cpd measurements only result for sufficiently thick films on insulators (~ 500 A^o) by Maddison 1964 and by Hampson 1966. The large and variable cpds in the present experiments did not occur when the deposit was thickened sufficiently and they were also sensitive to the applied backing potential V_b. These effects therefore may be related to the charge transfer hypotheses discussed above.

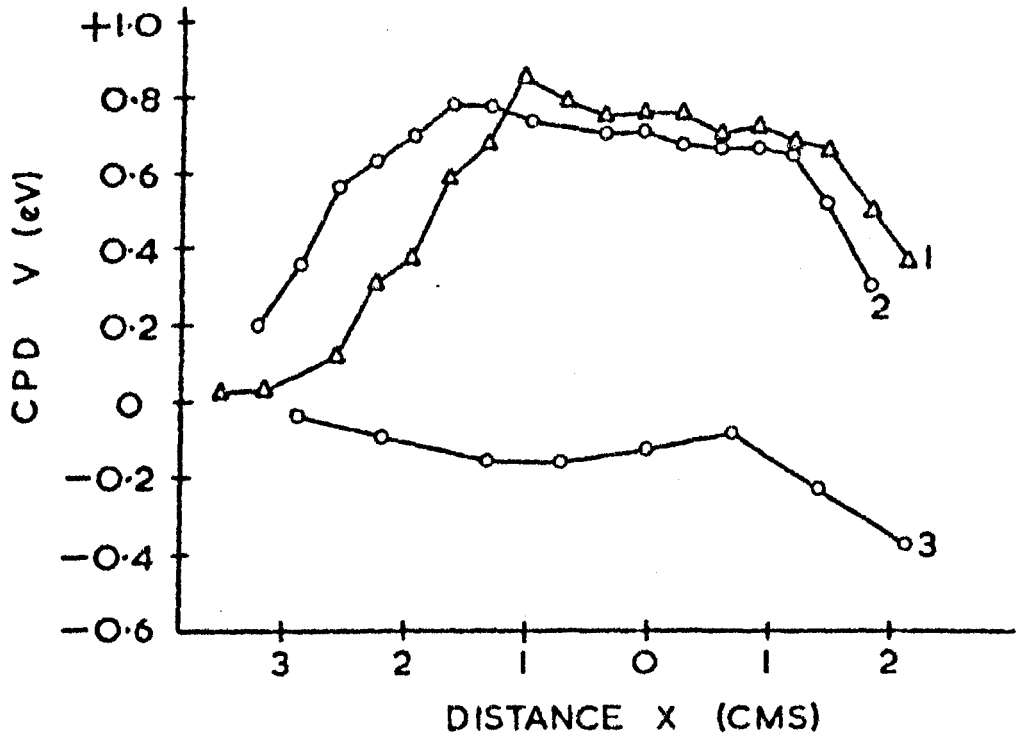

Figure 7.8 Typical apparent spatial variation of the cpd V due to stray capacitance across gold films numbers 8(1) and 9(2) in experiment A at 2.10^{-6} torr and across film number 14(3) in experiment B at 2.10^{-9} torr. Substrate centre: x = o.

Sensible cpds were measured with thicker gold films (i.e. film number 3 in Figure 7.1) and the final value for the third film was the same as that of the later films numbers 8 and 9 which were deposited onto a titanium layer. The gradual increase in the equilibrium value for films numbers 6-9 may be caused by a change in the coverage of the substrate by the gold film. If this was the case the underlayer was completely covered eventually and the value of ϕ_f was reproducible for the last two films. There is an apparent increase in time of ϕ from ϕ_o to the final value ϕ_f by as much as 0.15 eV. ϕ_{Au} is stable under these conditions (cf. Chapter 6) and this change may be related to either adsorption or desorption of gas from exposed Ti patches if the substrate was not completely covered or to a photo-instability of the reference steel probe (cf. Chapter 5). The direction and magnitude of the change of ϕ is consistent with this possibility and the apparent change is due to the return to equilibrium of the probe surface. A similar effect occurred for the gold films in experiment B in ultra high vacuum (Figure 7.2) which is also attributed to the photo-instability of the reference steel surface. The equilibrium cpd decreased from one film to the next and finally reached a value of + 0.3V which is probably due to a change of coverage of the substrate with an increasing thickness of the deposit. In ultra high vacuum the cpd between the steel probe and the Au film was constant (within $\mp$ 20 mV) for at least several hours and did not change when the pressure of H_2 was increased to ~ 2.10^{-6} torr for a few minutes. This is consistent with the previous reports of the stability of clean gold in hydrogen (cf. Chapter 6) unless ϕ_{Au} and ϕ_{Steel} fortuitously changed by an equal and opposite amount.

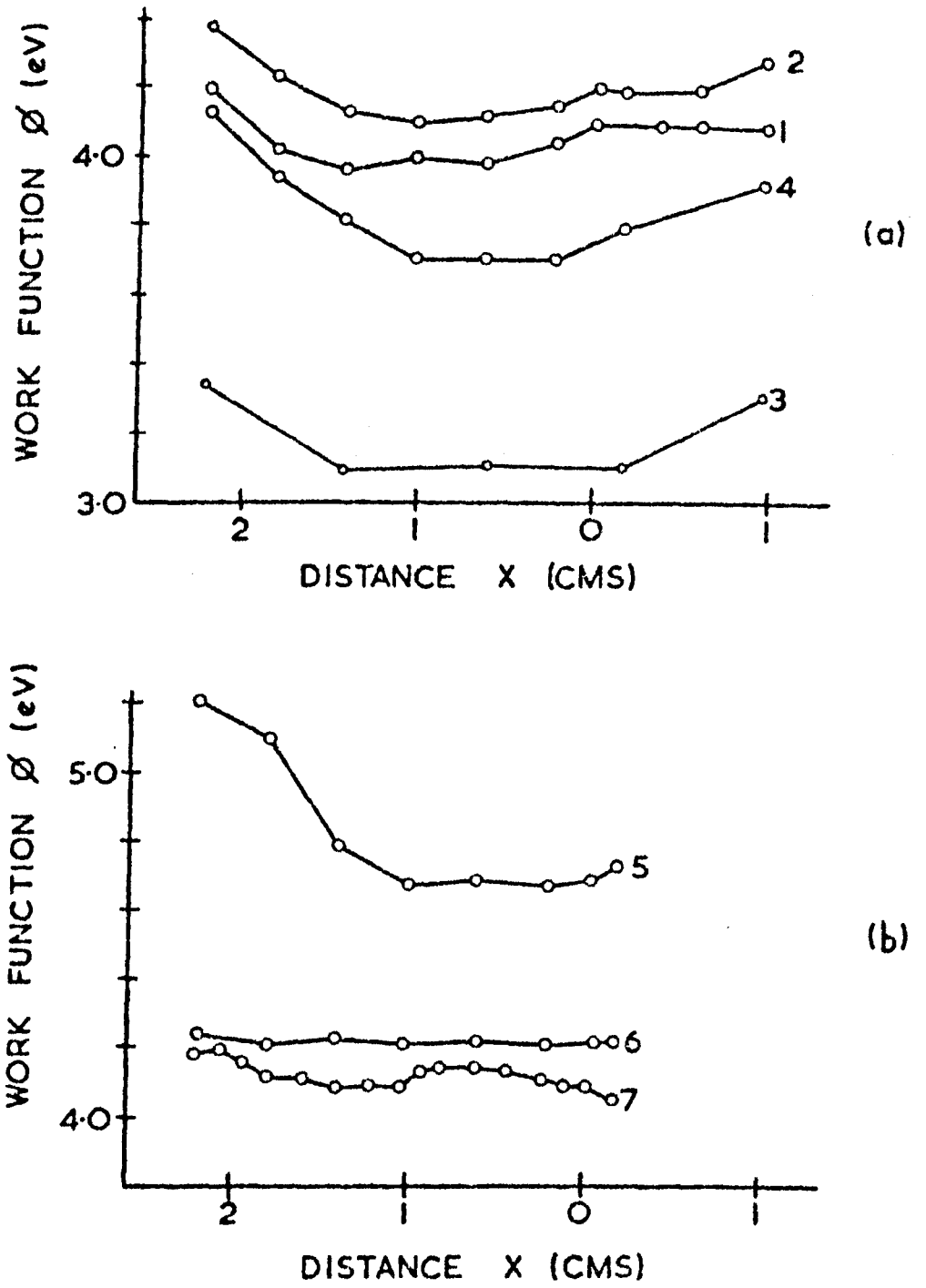

Figure 7.9 Typical apparent spatial variation of the work function ϕ with distance x across: silver films 7 and 8 (curves 1 and 2 respectively); titanium films 9 and 12 (curves 3 and 4 respectively), for titanium film 17 (curve 5 was obtained due to stray capacitive effects and curve 6 in their absence is the real variation) and the real variation for film number 18 (curve 7). Reference surface - silver ϕ = 4.3eV. Substrate centre: x = o.

The results from experiments A and B enable the work function ϕ_s of steel to be found assuming a value of 5.30 eV for ϕ_{Au} (cf. Chapter 6). The values of ϕ_s are 4.65 eV (experiment A) and 5.60 eV $\mp$ 0.1 eV (experiment B). Although there is a large difference between these it was shown in Chapter 5 that ϕ_s was decreased by large exposures to H_2 at ~ 10^{-6} torr. Consequently a lower value might be expected in experiment A apart from any differences in their preparation and thermal history which may have occurred. The values of ϕ_s are the equilibrium ones. During evaporation illumination decreased ϕ_s by ~0.1 to ~0.3 eV and afterwards ϕ_s relaxed to its pre-illumination value thus causing an apparent change in ϕ_{Au} after deposition (Figures 7.1 and 7.2).

7.8 Discussion: Silver Results

Visual examination confirmed after experiment C was completed that the probe reference surface was coated with a thick film of silver. The reference work function is assumed to be 4.3 eV (cf. Chapter 6). The surface was stable during evaporation to within 50 mV and the photo-instability experienced with the steel surface alone was absent. There was, however, a small and reversible change of cpd between the silver reference and the erbium substrate during the first photo-test which did not occur in other later tests between the reference and the substrate covered with titanium. Assuming the probe reference work function was that above the value for the erbium substrate was 3.5 eV. The first silverfilm increased the work function to ≈ 3.8 eV and further depositions increased it by an additional 250 mV. After deposition

Gas	Pressure 10^{-8} torr A	B	Error $\mp$ %
H_2	2.0	0.9	40
H_2O	10.0	0.1	-
CO,N_2	20.0	0.16	15
O_2	<1.0	0.01	20
A	0.8	0.05	20
CO_2	4.0	0.02	5
CH_4	4.0	-	35
He,Ne	<0.03	<0.03	25
MS/10	4.10^{-7}	1.10^{-8}	~50
Boostivac	2.10^{-7}	2.10^{-9}	

Table 7.3 Typical residual gas composition in the unbaked (A) and baked (B) system and the total pressures measured by the MS/10 spectrometer and the ion pump (N_2 equivalent).

is each case (except one) ϕ decreased in time by 30 - 60 mV. The initial and final values are plotted in Figure 7.10 as a function of N the film number. The temperature and time of the evaporation was similar for each film for $1 \leq N \leq 4$. The linear change in ϕ with N may be caused by a change in coverage θ of the substrate by the silver overlay on the erbium substrate. This possibility would account for both the magnitude and direction of change of ϕ. For small film thicknesses θ may not vary linearly with N but when the film had become continuous to an island - pathwork structure the enclosed and exposed patches of the substrate may progressively shrink in size with the mass of the deposit. The first film was apparently sufficiently thick to establish the patch network and later films increased the average thickness and reduced the area of the substrate. In this model the substrate work function ϕ is given by:

$$\phi = \{\phi_{Ag} + (1-N\ \delta\theta)\phi_{Er}\}/2 \qquad (7.1)$$

for $N > 1$ where $\phi_{Ag} = 4.3$, $\delta\theta$ is the fractional change in θ for $\Delta N = 1$ and N is the film number. For $N = o$ $\phi = \phi_{Er} = 3.5$ eV and since the total change in ϕ was about 0.25 eV then the total change in coverage is predicted from (7.1) to be about 15%. This result implies the first film covered $\simeq$ 85% of the substrate which is consistent with the resistivity measurements on the silver film which indicated that they were probably continuous. ϕ eventually became apparently independent of N (Figure 7.10) which implies that the substrate was completely covered. If account is taken of the probable error due to stray capacitance 0.3 ± 0.1 eV then the final work function of the film was 4.4 ± 0.1 eV in reasonable agreement with previous measurements (cf. Chapter 6). The linear variation of ϕ

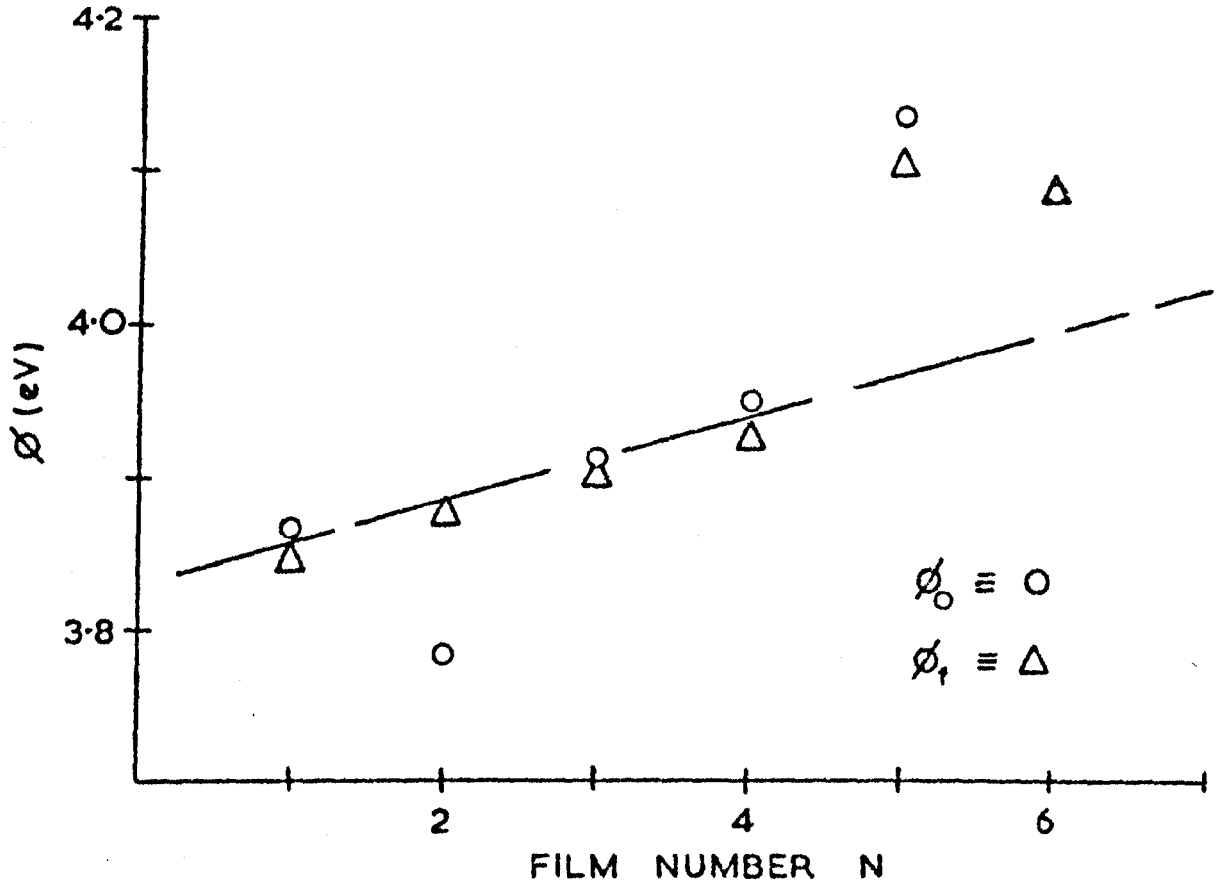

Figure 7.10 Variation of the work function ϕ of the erbium substrate with the number N of silver films deposited at 1.10^{-7} torr (experiment C) from Figure 7.3. Reference surface: silver film ϕ = 4.3eV.

with N may be circumstantial and other possible causes include stray capacitance effects, structural changes or impurities in the film but these do not so readily account for the results.

The small change in the cpd following each deposition may be caused by: (a) a residual photo-effect on the silver coated steel probe, (b) adsorption on the exposed erbium substrate patches in the film or (c) on the silver film. There is some evidence for (a) and also (c) for the case of oxygen and water vapour (cf. Chapter 6) but it is not possible to distinguish which is the cause, although the latter is more probable.

7.9 Discussion: Titanium Results

7.9.1 Introduction

The results from the preliminary experiment A shown in Figure 7.4 are not very accurate because of the technical problems which were encountered with the stability of the probe amplitude of vibration. As discussed in section 7.7 titanium was deposited in this experiment at 2.10^{-6} torr onto a gold surface which did not apparently completely cover the glass substrate. It is not known whether the Ti covered the substrate although the second series of Au films which were deposited later onto the Ti were apparently continuous. The initial and minimum values of the work function of Ti films varied widely. In each case ϕ decreased after deposition and the SP was positive. In the unbaked system the principal residual gases were H_2O and CO (and N_2). The maximum SP varied from + 0.2 to + 0.6 eV and this variation may reflect the effect of impurities, adsorption of different gases or some dependance on the

Experiment	Substrate	ϕ_o eV Type	ϕ_o eV Range	SP eV Sign	SP eV Range	ϕ_f eV	Film No.	Type
B	Au	High	4.5-5.9	Pos	0.26-1.13	4.0-5.0	1-11	1
C	Ag	Low	2.5-3.8	Neg	0.06-0.8	3.0-4.2	6-16	2
		High	5.8-6.7	Pos	1.2-2.5	4.0-4.6	17-19	3

Table 7.4 Summary and classification of the results and film type numbers for titanium from Tables 7.1 and 7.2.

film structure. It was shown, however that the backing voltage V_b was disturbing the measurements. It is possible therefore that (a) the maximum values of the SP include a contribution from this bias effect and that (b) the whole of the increase in ϕ after the maximum value had been reached was due to the bias effect which increased the apparent value of ϕ. The cause of this is unknown but it may be due to the effects observed for thin Au films on glass substrates discussed above or to the reference steel surface due to the electric field effect as described in Chapter 5. These results are not reliable and at most are indicative of the occurrence of positive surface potentials and of the large variations which may result for the initial and time dependent changes of the work function.

7.9.2 Work Function

The results from experiments B and C are shown in Figures 7.5 and 7.6 and are summarised in Tables 7.1 and 7.2. They incur an error due to stray capacitive effects (cf. Chapter 4) in the absolute values of ϕ_o and ϕ_f but their difference (the SP) is not affected to a first approximation. If account is taken of the probable error ϕ_o and ϕ_f should be reduced by 0.3 ∓ 0.1 eV. The results fall into three classes as shown in Table 7.4. Titanium films deposited (a) at 2.10^{-9} torr onto gold possessed a high value of ϕ_o between 4.51 and 5.97 eV; type 1 films, (b) at 1.10^{-7} torr onto silver possessed a low value of ϕ_o between 2.56 and 3.81 eV; type 2 films, (c) and thicker films at 1.10^{-7} torr in the same experiment possessed . high values of ϕ_o between 5.84 and 6.74 eV. The equilibrium value of ϕ_f lay between 4.04 and 4.99 eV for types 1 and 3 films and

between 3.04 and 4.18 eV for type 2 films. The SP of adsorbed gas was positive when ϕ_o was high and negative when ϕ_o was low. In this classification the initial films (numbers 1-5 in Table 7.2) in experiment C which produced no change in the film resistance ($\delta R = o$) monitor have been excluded. Type 2 films produced an anomalous positive increase of δR (Table 7.2). Lucas 1964 and Chopra and Randlett 1967 have observed that the resistivity of a thick metal film may be increased by depositing a thin film of another element onto it. These results suggest that type 2 films were thin and that the type 3 films which reduced the resistivity as expected were much thicker as concluded for other reasons previously.

The work functions of gold and silver are not affected by most of the residual gases at room temperature except in the latter metal which adsorbs oxygen and possibly water vapour. ϕ_{Ag} generally decreased by a small amount after deposition of the films at 1.10^{-7} torr and this is likely to be caused by the adsorption of these gases, although it may have been due to other causes. The real substrates were therefore (a) for type 1 films at 2.10^{-9} torr a gold surface free from adsorbed gases and (b) for types 2 and 3 films at 1.10^{-7} torr a silver surface probably covered with oxygen and water vapour. For the sake of clarity a substrate covered with gases or impurities which are reactive to titanium is referred to as active. An active substrate may lead to contamination of a slowly growing or thin film of titanium.

In the high vacuum experiment C the evaporation time was the same for each film but the evaporation temperature T_e of the sublimation filament was gradually increased during the sequence

of depositions from a low to a high value and consequently also the rate of deposition. The residual gas contamination rate of the films during their growth was therefore initially high and fell to a lower value as T_e was increased. Thus type 2 films which possessed low values of ϕ_o were (i) thin (ii) deposited onto an active substrate and (iii) had a high residual gas contamination rate. The later (type 3) films in this sequence which had a high value of ϕ_o were (i) thicker (ii) deposited onto a Ti - gas sandwich type layer substrate on silver and (iii) had a lower residual gas contamination rate. It may be concluded that (a) thin films of titanium deposited slowly onto an active substrate in high vacuum have low values of ϕ_o and that (b) thicker films of titanium which are deposited more quickly onto active substrates have high values of ϕ_o. It follows that (c) type 2 films which had low value of ϕ_o are less representative and that type 3 films having high values are more representative of clean surfaces of titanium.

If the above conclusion were true then films of titanium which (i) were thick or thin, (ii) had a low residual contamination rate and (iii) were deposited onto an inactive substrate would have high values of ϕ_o representative of clean titanium. The films deposited at 2.10^{-9} torr in experiment B onto the gold film substrate of unknown thickness satisfy these three criteria and they also possessed a high value of ϕ_o as predicted (Table 7.4).

The conclusion is drawn therefore that high values of ϕ_o are characteristic of clean titanium films (types 1 and 3) and that low values of ϕ_o result from impurities. The source of these appears

to be (1) adsorbed gas on the substrate or on the surface of the previously deposited film and (2) residual gas adsorbed on the growing film. The SP results are discussed in detail below. The previous measurements for films of titanium were discussed in Chapter 6 and were summarised in Table 6.2. The values of ϕ_o vary from 3.5 to 4.17 eV (Rentschler and Henry 1945, Jain and Krischnan 1952, Suhrmann et al. 1962 and Magee 1967). These are close agreement with the low values measured in the present experiments for type 2 films. As described previously the measurements of Rentschler and Henry and also Jain and Krischnan were made in poor vacuum, Magee did not state the base pressure in his system. Suhrmann et al. deposited their films in ultra high vacuum but at a very slow rate (~ $1A^{o}hr^{-1}$) for about an hour. Their films may also therefore have been contaminated from the residual gas during their growth. In all four measurements active substrates made of nickel, graphite or glass were used which were probably covered with reactive adsorbed gases. These films were (i) of unknown or very small (~ 70 A^{o}) thickness, (ii) deposited onto active substrates and (iii) deposited in poor vacuum or exposed to the residual gas for an unknown time before the measurements were made. These satisfy the criteria for type 2 films having a low value of ϕ_o in the present experiments due to contamination. In support of this conclusion the low values for type 2 films and also the previous results above are within the range of values of ϕ for the oxide and carbide of titanium 2.7 - 4.7 eV (cf. Chapter 6.3). Rentschler and Henry 1945 reported that when thin titanium films were deposited onto oxygenated metal substrates a value of ϕ was measured which was lower than that of thicker films. Anderson and Thompson 1971 have also found that bulk impurities in Ti reduce ϕ by a volt or more (cf. Chapter 6.3.1). These facts circum-

stantially support the conclusion that impurities on active substrates may have led to low values of ϕ_o for thin films.

It has been assumed in the above interpretation that (i) the films of Ti (and Au and Ag) were continuous, the films of Ti (ii) were sufficiently thick for them to be a film and not a dilute layer on a substrate of another element and (iii) that they had the same atomic structure irrespective of thickness, evaporation rate or base pressure, (iv) the structure was of the normal room temperature hexagonal close packed α phase of Ti (v) there was no alloying or interdiffusion of the substrate material with the Ti film and that (vi) there were no impurities evaporated from the sublimator filament. The first two assumptions may not have been the case for the initial films in experiment C which had an anomalous resistivity. The first five of these however were discarded and were not included in the analysis. There is no evidence in the present work to believe the assumptions (iii) and (iv) were not true although it is known that in the initial stages of the growth of some metal films that atomic structural changes may occur* cf. Chopra et al. 1967. There is evidence for Ni and Cu films that inter-diffusion may rapidly occur at room temperature (cf. Chapter 2). Even if assumption (v) was not true it would be difficult to account for the high values of ϕ_o observed for films on both Au ($\phi \simeq 5.3$eV) and on Ag ($\phi \simeq 4.3$eV) substrates. The last assumption was optimistic. In both experiments B and C the sublimation filament was extensively outgassed. However, impurities may only have been desorbed at the sublimation temperature. If this were true it is likely that the initial films in either experiments were more contaminated than the latter ones. This may have been an additional cause of the low ϕ_o values for type 2 films in high vacuum (and also for those in experiment A). Evaporated impurities may also be a contributing cause of the variation of ϕ_o in each experiment.

---

* Epitaxed bcc modifications at 293°K of thin ($\theta \leq 2$) Ti films on W(bcc) have been reported for which $\phi < \phi(\alpha)$ which converted at greater thicknesses to α-Ti(hcp) cf. (Chapter 6.3.1). A similar effect may be responsible for the reduction in ϕ_o (cf. Table 6.2) with successive depositions since the substrate was Ag (fcc).

The initial values of ϕ_o for types 1 and 3 films were concluded to be representative of clean surfaces but vary widely from 4.8 to 6.7 eV (Table 7.4). The values for the contaminated type 2 films also vary widely but this may be simply due to differing degrees of contamination. If the above six assumptions are true then the results for the clean films imply a variation in ϕ of about 2.0 eV between the single crystal faces of titanium. The maximum difference for tungsten, however, is much less than this amount (cf. Chapter 2). This suggests that some of the divergence may have been caused by impurities from the residual gas, substrate or evaporation filament as well as a natural variation of ϕ with the surface structure.

7.9.3 Surface Potential

In ultra high vacuum the predominant residual gas was hydrogen with traces of water vapour, carbon monoxide (and nitrogen) as shown in Table 7.3. The partial pressure of hydrogen was increased to about 8.10^{-7} torr before depositing one film. The SP for each was positive and the conclusion is drawn that the adsorbate was hydrogen. This disagrees with the sign of the SP for hydrogen reported by Suhrmann et al. (Table 6.3) but as discussed previously their results may not refer to clean surfaces. Magee 1967 observed a positive SP of hydrogen also but the purity of this surface is also in doubt. The values in both of these experiments refer to large concentration of hydrogen in the film which probably exceeded the solubility limit. Consequently the interpretation of the results may be complicated by the precipitation of hydridic phases in the films

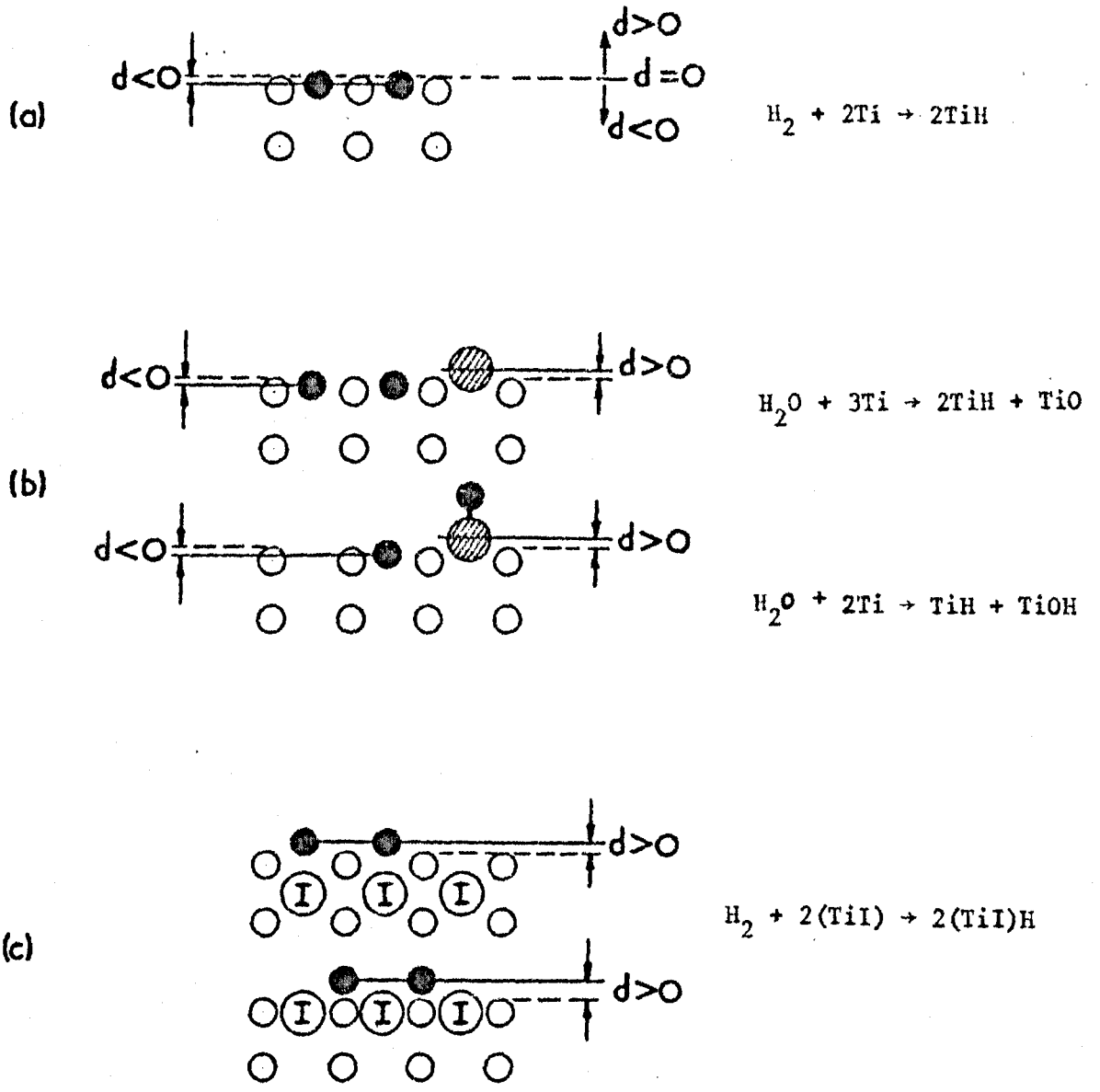

Figure 7.11 Schematic illustration of dissociative adsorption of hydrogen and water vapour on titanium surfaces where d is the distance of the effective centre of charge of the adatom from the surface electronic plane (---). The vacuum is above and the metal below d = o: (a) electronegative hydrogen in deep sites for which d < o and the SP is positive, (b) water vapour, (c) electronegative hydrogen on impure surfaces where presence of the impurity (I) results in d > o and negative SP.

(cf. Chapter 6.3). These measurements therefore do not substantiate or dispute the present conclusion on the positive SP for pure titanium surfaces.

Positive surface potentials at low coverage (cf. Chapter 2.5) have been interpreted as the result of penetration of the adsorbed electronegative adatoms below the surface electronic plane. A positive SP may also result from an electropositive adatom located above the electronic plane. Studies of the bulk properties of titanium hydride have not distinguished whether the predominant bonding is of the form $Ti^- - H^+$ or $Ti^+ - H^-$ (cf. Chapter 6.3). The present SP results cannot distinguish the direction of charge transfer between the adsorbed hydrogen atom and the titanium film since its position with respect to the electronic surface plane is unknown. However, it is known that hydrogen is rapidly absorbed by Ti at 300°K with a small activation for solution, that in dilute concentrations absorbed hydrogen atoms are located in interstitial holes in the lattice (cf. Chapter 6) and that transition metal M to hydrogen bonds are normally viewed as having a partial negative ionicity of the form $M - H^{-x}$, $o \leq x \leq 1$. It is probable therefore that the positive SP arises from the dissociative adsorption of hydrogen and the formation of a negative atomic layer* located in interstitial surface sites below the surface electronic plane. The situation is shown in Figure 7.11a.

It is known for titanium from Chapter 6 that (i) the activation energy for solution of hydrogen is small (ii) the diffusion rate is high at room temperature (iii) the sticking coefficient (or getter

---

* recent theoretical work (Chapter 2.6.2) predicts that H_s adatoms on Ti acquire partial negative charge.

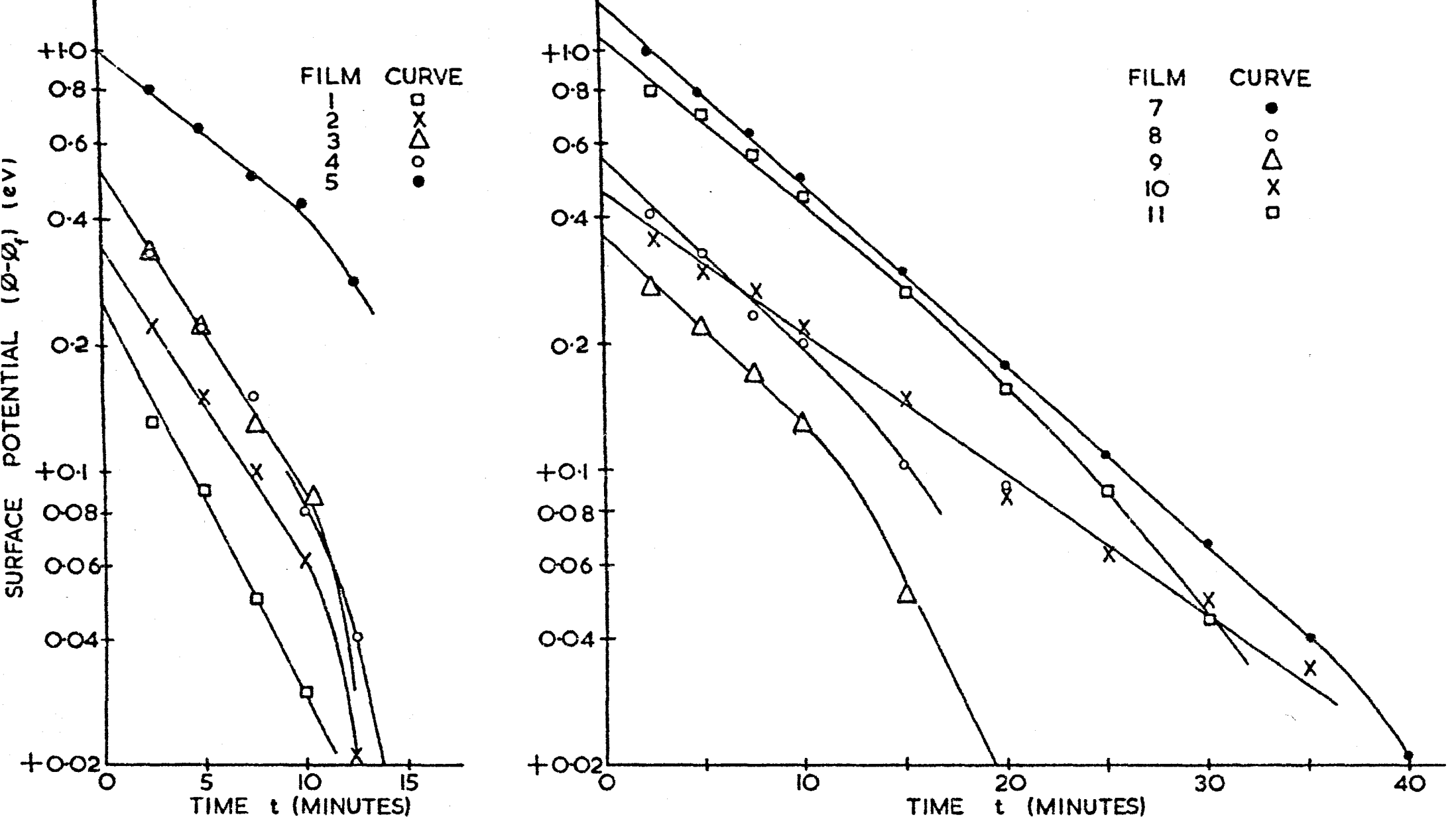

Figure 7.12 Variation of the surface potential (ϕ-ϕ_f) with time for titanium films (numbers 1-11) deposited onto a gold substrate at 2.10^{-9} torr (experiment B), ϕ_f is the final and minimum value of the work function; from Figure 7.5. Film number 7 was deposited at 7.10^{-7} torr (H_2).

rate) for hydrogen can be constant for long periods at 10^{-9} - 10^{-7} torr (H_2) and for longer than expected for a monolayer to be formed (iv) large concentrations may be dissolved at 300°K even ~ 10^{-10} torr. The time dependent change in the SP may be derived from a model which takes account of dissociative adsorption of molecular hydrogen and solution of adatoms into the film. Suppose there is only one state in which adatoms penetrate below the surface plane so the SP $V > 0$ then V is related to the number N of adatoms by:

$$V = \phi_o - \phi = 4\pi e M_o N, \; M_o > o \qquad (7.2)$$

where the dipole moment $M_o = q\,d$ and q is the magnitude of the negative adatom charge. The rate of change of N is

$$dN/dt = 2s\,Ng - N \exp(-eQ/kT) - 2N_d \qquad (7.3)$$

where s is the sticking coefficient, Ng is the rate of incidence of molecular hydrogen on the film surface, $2N_d$ is the rate of desorption of molecular hydrogen, N exp - eQ/kT and Q are the rate and activation energy for solution of atomic hydrogen respectively. The solution of (7.3) is given in Appendix F for the assumptions that (a) N_d is negligible, (b) s is independent of coverage, (c) there is only one state and that dissolved hydrogen diffuses rapidly away from the sub-surface so that $V = f(N)$ only. Then:

$$\phi - \phi_f = (\phi_o - \phi_f)\exp - t/\tau \qquad (7.4)$$

where $\phi_o - \phi_f = 4\pi s M_o e Ng \exp eQ/kT$

and $\tau = \exp eQ/kT$

The model also predicts that

$$- d\phi/dt_{t\to o} = (\phi_o - \phi_f)/\tau = 8\pi s M_o e Ng \qquad (7.5)$$

The experimental results shown in Figure 7.5 are replotted on a logarithmic scale in Figure 7.12 and the initial rate of change of ϕ

against the final surface potential in Figure 7.14 (curve B). The experimental results are in reasonable agreement with the prediction of the model given in equations (7.4) and (7.5). The plots of log ϕ against t or log(t) and log $(\phi - \phi_f)$ against log(t) were non-linear. The time constants τ of the curves shown in Figure 7.12 lie within the range $4.3 \leq \tau \leq 13.0$ mins. The model therefore predicts from (7.4) that:

$$4.3 \leq \exp eQ/kT \leq 13.0 \text{ mins}$$

and since 1 eV $\equiv$ 20 Kcal mole^{-1} then the activation energy for solution Q is:

$$0.73 \leq Q \leq 1.3 \text{ Kcal gr-atom}^{-1} \qquad (7.6)$$

The results for experiment B (Curve B in Figure 7.14) are described by:

$$d\phi/dt_{t\,o} = - a - b\,(\phi_o - \phi_f) \text{ mV min}^{-1} \qquad (7.7)$$

where $a = 17 \pm 17$ mV min^{-1} and $b = 0.066 \pm 14$ min^{-1}. The model predicts from (7.5) that:

$$0.052 \leq 1/\tau \leq 0.080 \text{ min}^{-1}$$

and from (7.4) the activation energy Q is:

$$1.26 \leq Q \leq 1.48 \text{ Kcal gr-atom}^{-1} \qquad (7.8)$$

The two values of Q predicted by the model and given in (7.6) and (7.8) are in reasonable agreement with each other and are plausible values for the rapid solution of hydrogen which is known to occur at room temperature. The values are much smaller than those derived from high temperature and high pressure studies of the hydrogen-titanium system which yield values 5 - 10 Kcal gr-atom^{-1} (cf. Chapter 6.3.6). However, impurities are known to increase Q and it

does not seem unreasonable to suppose that the surfaces of the films were much purer than the bulk samples used in the other studies. Consequently, the values of Q for the former would be expected to be lower than those for the latter as in fact observed. The scatter in the values of τ (and Q) in the figures may be partly due to stray capacitive errors, impurities or effects of surface structure in the film since the value of Q may be dependent on the crystallographic orientation. The model also predicted from (7.4) that the maximum surface potential $\phi_o - \phi_s$ was proportional to M_o,s,Ng and exp Q. Although it may be circumstantial the maximum surface potential was in fact observed for largest partial pressure of hydrogen (film number 7, table 7.1).

Three major assumptions were made in the model. Firstly the SP was assumed linearly dependent on the number of adsorbed hydrogen atoms. There is evidence in other gas-metal systems that this may be so for hydrogen adsorption where mutual depolarisation effects are apparently small over a fractional range of coverage (cf. Chapter 2). Qualitatively this may also be favoured if the adion sinks below the surface electronic plane as in the present case (or if the coverage is small). Secondly, the sticking coefficient was assumed independent of coverage. There is evidence from independent sources that this may be so for H_2 on Ti as described in Chapter 6.33. Thirdly, the pressure p of H_2 was assumed constant. For film number 7 (Figure 7.5b) p varied by more than a factor of 10 but the linearity of the logarithmic plot was unaffected (Figure 7.12) suggesting that variations of p were not of first order importance. The departure from linearity in the logarithmic plots may indicate a breakdown of the former two assumptions.

In the high vacuum experiment C both positive and negative values of the SP were observed. The former occurred in type 3

	Partial Pressure (10^{-8} Torr)				
GAS	A	B	C	D	E
H_2	4.4	4.9	6.3	5.0	4.6
CH_4	8.2	6.2	4.6	4.1	3.7
H_2O	34.4	26.8	22.0	19.6	17.5
N_2+CO	67.0	65.0	61.8	61.0	61.0
O_2	4.0	2.0	2.7	3.3	4.0
A	2.9	2.5	2.9	2.9	2.9
CO_2	16.1	9.5	7.1	5.7	4.8

(a)

	Relative Incidence Rate		
GAS	C	D	E
H_2	0.39	0.31	0.28
CH_4	0.09	0.08	0.08
H_2O	0.45	0.39	0.35
N_2+CO	1.0	0.98	0.98
O_2	0.04	0.05	0.06
CO_2	0.09	0.07	0.06

(b)

Table 7.5 Variation of (a) the partial pressures and (b) the incident rates (relative to $\{N_2 + CO\}$) in experiment C at 1.10^{-7} torr just before (A,B) and after evaporation of T_i film number 19 t ≈ 15 (C), t ≈ 30 (D) and t ≈ 45 minutes (E).

films and the latter on type 2 films, Table 7.4. It was concluded above that the low values of ϕ_o (type 2 films) were due to contamination and that the type 3 films were much purer. In these experiments the precise gas composition was unknown although typically the major species were H_2O, CO(and N_2) as shown in Table 7.3 The mass spectrometer was functioning at the end of experiment C, however, and the gas composition before depositing Ti film number 19 and its change afterwards is given in Table 7.5. The differences between the figures in columns B and C suggest the residual composition was apparently changed by heating the sublimation filament to its evaporation temperature, H_2 and O_2 appear to have been evolved and the pressures of the other major gases were reduced. The increase in the argon peak is probably due to the Boostivac ion pump. However, H_2, H_2O and CO_2 are apparently being adsorbed and O_2 evolved in time after depositing the film but it is uncertain whether this is due predominantly to the ion pump or the film. The rates of incidence of the component gases on the film relative to nitrogen (calculated from the partial pressures) are given in Table 7.5b and the predominant gases incident on the film are $(N_2 + CO)$, H_2O and H_2. The latter two gases are dissociatively adsorbed on clean titanium and the relative incidence rates of atomic hydrogen and oxygen are 1.68 and 0.45 respectively for column C assuming dissociated $H_2O \rightarrow 2H + O$. The incidence rate of atomic hydrogen therefore is much larger than that for (N_2+CO). Since (1) the partial pressure of $(N_2 +CO)$ varies little in comparison to that of H_2 and H_2O and (2) the relative incidence rates of atomic hydrogen, atomic oxygen and molecular (N_2+CO) are

1.68, 0.45 and 1.0 respectively (assuming $H_2O \rightarrow 2H + O$), then it appears that the predominant adsorbate is atomic hydrogen providing the sticking coefficient of oxygen is not greater than that of hydrogen by a factor of about four. This latter assumption does not seem unreasonable. If dissociation proceeded via $H_2O \rightarrow H + OH$ then the incidence rates become 1.23, 0.45 and 1.0 for atomic H_2, OH and $(N_2 + CO)$ respectively. If dissociation of H_2O did not occur (although this is unlikel,) then the incidence rates become 0.78, 0.45 and 1.0 for atomic H_2, H_2O and $(N_2 + CO)$ respectively. Consequently it is reasonable to suppose that the positive SP arises from a predominant adsorbate of hydrogen adatoms due to dissociative adsorption of molecular H_2 and H_2O since the SP of oxygen and nitrogen on Ti is negative and probably also the OH radical (cf. Chapter 6.32 and Table 6.3).

Suppose dissociative adsorption of H_2O proceeds as $H_2O \rightarrow 2H + O$ and that N(X) and Ng(X) denote the number of adatoms X and their rate of incidence on the surface, then the rate of change of the number of N of adatoms for dissociative adsorption of H_2 and H_2O is:

$$dN/dt = dN(H)/dt + dN(O)/dt \qquad (7.9)$$

where $dN(H)/dt = 2s_1\, Ng(H_2) + 2s_2 Ng(H_2O) - N(H)\exp -eQ/kT$

and $dN(O)/dT = s_2\, Ng(H_2O)$. Similar equations are obtained if dissociation proceeded via $H_2O \rightarrow H + OH$. At low coverage $N \sim N(H)$ and since from above $Ng(H) \sim 4Ng(O)$ then (7.9) becomes:

$$dN/dt \simeq dN(H)/dt \simeq 2s_1 Ng(H_2) + 2s_2 Ng(H_2O) - N(H)\exp -eQ/kT \qquad (7.10)$$

i.e. $$dN/dt \simeq dN(H)/dt \simeq a - bN(H) \qquad (7.11)$$

which is of the same form as the continuity equation in the hydrogen surface potential model (equation (7.3)). This model predicted that

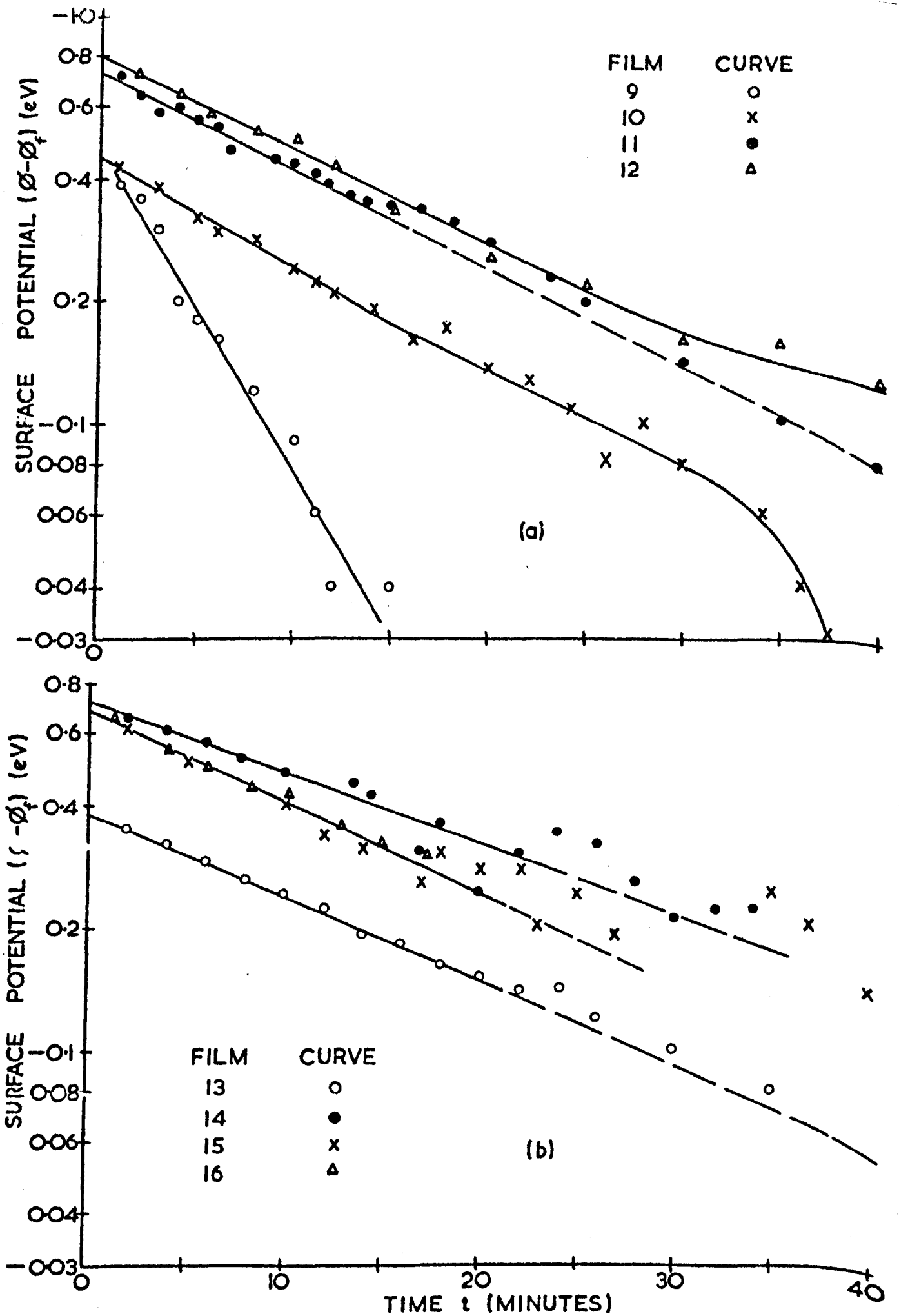

Figure 7.13 Variation of the surface potential ($\phi - \phi_f$) with time for titanium films numbers 9-12(a) and 13-16(b) deposited on a silver substrate at 1.10^{-7} torr (experiment C); from Figure 7.6.

log $(\phi - \phi_f) \alpha t$. The results for type 3 films which had a positive SP are reported in Figure 7.13c. The logarithmic curves are bilinear suggesting a two component adsorption process. The model suggests that the initial linear portion is due to hydrogen. After about ten minutes the measured SP is smaller than expected from the model. This may be caused by: (a) oxygen adatoms (or OH) which arise from dissociated water vapour or similarly N_2 or CO which have a negative SP (cf. Chapter 6 and Table 6.3). An increasing concentration of these electronegative adspecies would tend to progressively reduce the magnitude of the positive SP due to hydrogen with increasing coverage; (b) the sticking coefficient s_2 of water vapour may not be independent of coverage; (c) the sticking coefficient s_1 of hydrogen may no longer be independent of coverage in the presence of other adspecies. Both (b) and (c) would invalidate the assumption in the model that the sticking coefficient is independent of coverage. The SP of adsorbed gas on the low initial work function films was negative (type 2 in Table 7.4). The gas composition above these was unknown. Adsorption of O_2 and N_2 on Ti are known to result in a negative SP (Table 6.3). The low values of ϕ_o were concluded above to be caused by impurities. A negative SP may also result from H_2O and it may be speculated also for hydrogen if the impurities prevent the negative hydrogen adion from entering the interstitial surface sites so that it rests above the surface electronic plane. The situation is shown in Figure 7.11c for the two cases of an occluded and a surface impurity for hydrogen adsorption. The negative SP for each of the type 2 films is also described by the empirical equation $\log (\phi - \phi_f) = - t/\tau$ for values of τ in the range $5.6 \leq \tau \leq 24$ minutes as shown in Figure 7.13 (a and b). The model developed for the adsorption of hydrogen is not applicable for oxygen or nitrogen since for these gases the sticking coefficient is known

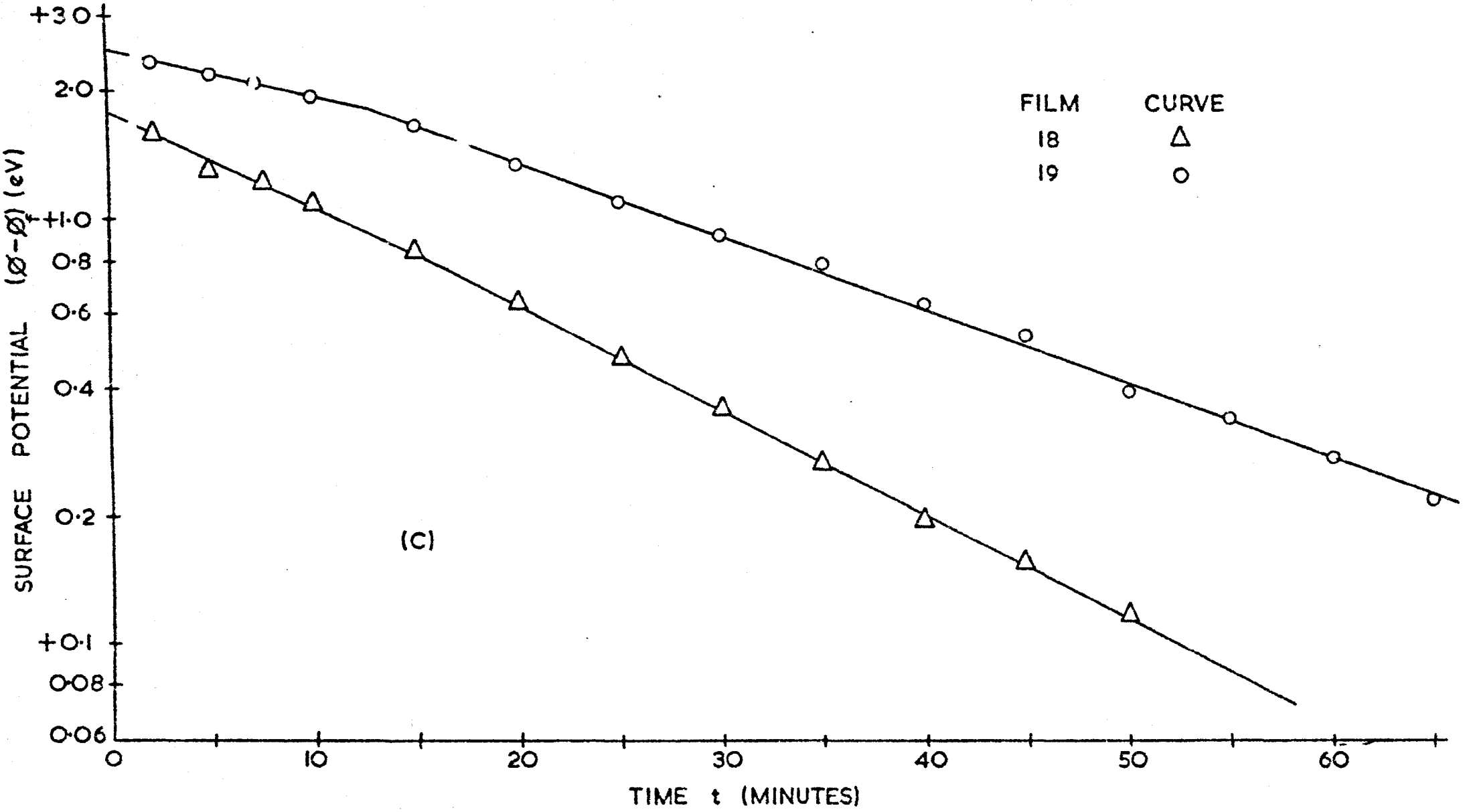

Figure 7.13(c) Variation of the surface potential ($\phi - \phi_f$) with time for titanium films 18 and 19 at 1.10^{-7} torr (experiment C) from Figure 7.6.

to be linearly and exponentially dependent on coverage respectively (cf. Chapter 6). The time dependent change for each may be estimated if it assumed that the surface potential V is related to the number N of adsorbed atoms by:

$$V = \phi_o - \phi = 4\pi e M_o N, \; M_o < o \tag{7.12}$$

If for oxygen $s = s_o (1 - kN)$ where k is a constant then the continuity equation becomes:

$$dN/dt = 2s_o (1 - kN)Ng - N_d$$

where N_d is a term accounding for desorption. This equation is of the form:

$$dN/dt = a - bN$$

which after integration and using the boundary conditions: $t = o$ $N = o$, $t \to \infty$ $N = N_f$ leads to

$$\phi - \phi_f = (\phi_o - \phi_f)\exp - bt \tag{7.13}$$

where $\phi_f > \phi_o$ and $b = 8\pi M_o s_o kNge$. This predicts that $\log (\phi - \phi_f) \alpha -t$ which is consistent with the experiment results shown in Figures 7.13 (a and b). Although this result was obtained for oxygen, a similar result would be found for any electronegative adspecies for which s linearly decreased with N. In the case of nitrogen $s = s_o \exp(-N/N_o)$ where N_o is a constant and the continuity equation becomes:

$$dN/dt = 2s_o Ng\exp(-N/N_o) - N_d \tag{7.14}$$

but this leads to a dependence of the SP (or $\phi - \phi_f$) on log(t) which is not consistent with the experimental results. In the case of hydrogen, it is known that hydrogen may be dissolved by titanium even though the surface may be contaminated (cf. Chapter 6)

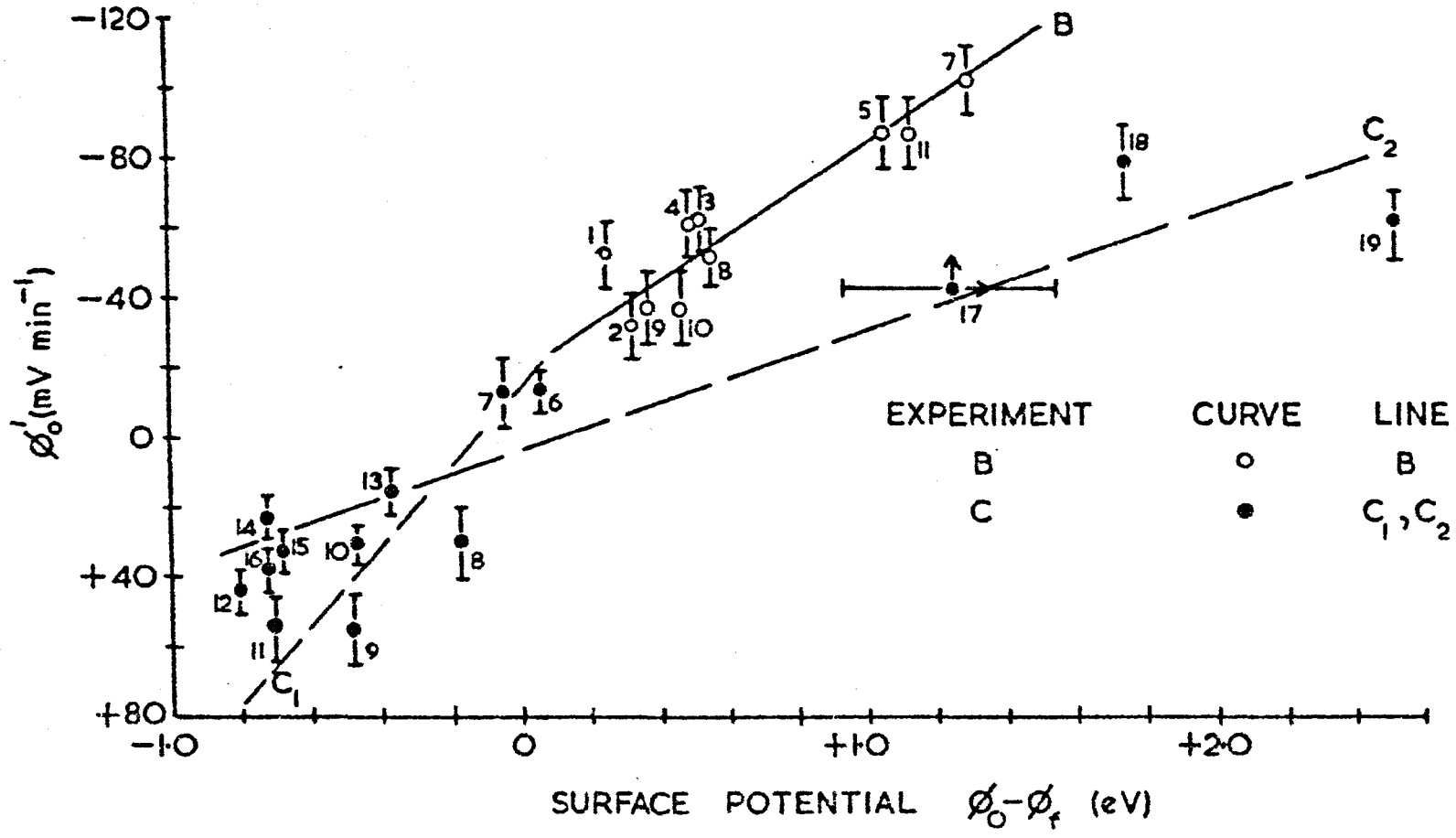

Figure 7.14 Variation of the initial rate of change of the work function $\phi_o' - d\phi/dt_{t\to o}$ with the maximum surface potential $(\phi_o - \phi_f)$ for the titanium films in experiments B (2.10^{-9}torr) and C (1.10^{-7}torr). The numbers indicate the film numbers and the points for films 1-5 in C are omitted. The points are taken from Tables 7.1 and 7.2.

which implies that molecular hydrogen may still be dissociatively absorbed. If this is so, the model developed previously above for the SP of H_2 on clean surfaces may be applied to the results for contaminated films by reversing the sign of the dipole moment (i.e. SP) in equation (7.2). This results in a solution of the continuity equation identical to that in the model (equations (7.4 and (7.5)) except that $\phi_f > \phi_o$ and $d\phi/dt_{t\to o} > o$. This model then predicts a result in close agreement with the SP changes shown in Figure 7.13 for the contaminated type 2 films. The agreement may be fortuitous since the assumptions in the model may not be valid for a contaminated surface. However, it is expected in such a case that the activation energy Q would be much larger than for pure surfaces as in fact seen in the logarithmic figures since the time constants are much longer. The model for dissociative adsorption of hydrogen on a contaminated surface which gives rise to a negative SP is shown in Figure 7.11c for the two types of impurities in the films. This proposal is consistent with the results of Suhrman et al. (cf. Chapter 6) who measured a negative SP of hydrogen on films which were concluded previously to be possibly contaminated.

The initial rate of change of ϕ for the type 2 films is plotted against the maximum SP in Figure 7.14 for comparison with the other results. The points as expected do not lie on the curve B for hydrogen (experiment B at 2.10^{-9} torr). The first series of films numbers 6-12 lie apparently on C_1 after which a fresh silver substrate had been deposited. The later films lie on another curve apparently C_2. The scatter in the points may be due to several causes but it is probably associated with impurities in the film, their effects on

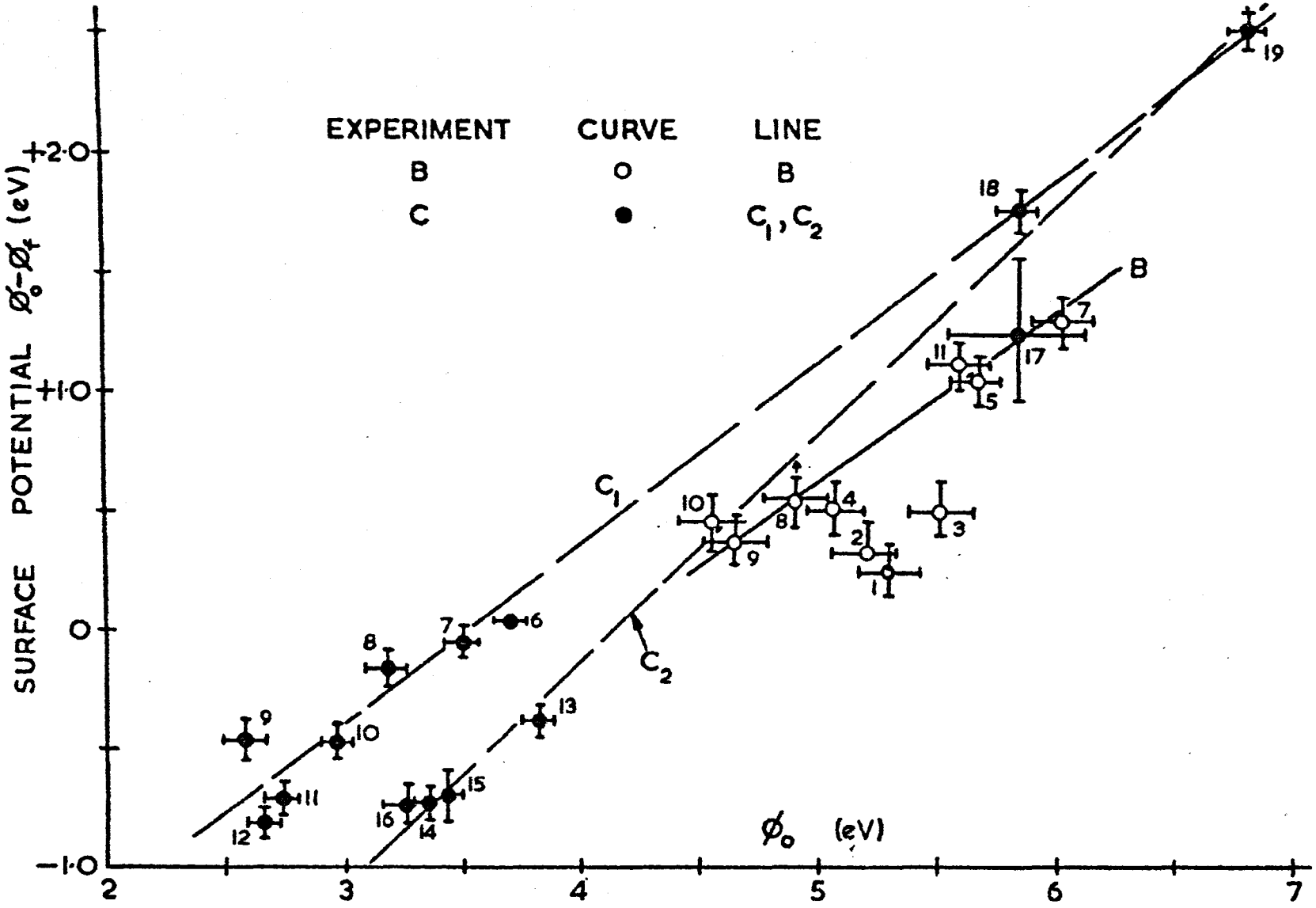

Figure 7.15 Variation of the maximum surface potentials $\phi_o - \phi_f$ with the initial work functions ϕ_o of the clean surfaces of titanium films at 2.10^{-9} torr (experiment B) and at 1.10^{-7} torr (experiment C). In C the results for films 1-5 are omitted. c.f. Tables 7.1 and 7.2. Line B is drawn omitting the initial films 1-3. Fresh A_g was deposited onto the substrate following film 12 in experiment C. Lines C_1 and C_2 are drawn through the points for the films deposited before (6-12) and after (13-19) the fresh silver substrate was formed.

the SP of hydrogen and the multi-component nature of the adsorbate.

The maximum surface potential $\phi_o - \phi_f$ is shown as a function of the initial work function ϕ_o for each film in experiments B and C in figure 7.15. The surface potential increases (i.e. becomes more positive) as ϕ_o increases. The scatter in the data points about the line maybe caused by stray capacitance effects. The results are described by:

$$\phi_o - \phi_f = a(\phi_o - b) \qquad (7.15)$$

where for:

Experiment B $\quad a \simeq 0.75 \quad b = 4.1eV$

and Experiment C $\quad a \simeq 0.82 \quad b \simeq 3.5eV$ (Curve C_1)

$\quad a \simeq 0.95 \quad b \simeq 4.1eV$ (Curve C_2)

The results for the high vacuum experiment fall apparently on two curves: C_1 for films 6-12 and C_2 for the later films 13-19 which were deposited onto a fresh Ag substrate. It is difficult to comment significantly on the results for experiment C since these films were probably contaminated resulting in low ϕ_o values. For the ultra high vacuum experiment B however the adsorbate was hydrogen as concluded above. The hydrogen surface potential model predicted that $\phi_o - \phi_f = 8\pi seM_o Ng \exp Q/kT$ where $M_o = qd$. The values of s and M_o for oxygen and hydrogen and other gases are known to vary with the structure of the adsorbent (cf. Chapter 2.5.2 and 2.6.2). Thus the linear variation may be a fortuitous consequence of the particular values that s, M_o and Q take for the films. Alternatively, however, the results may be due to a variation of the dipole moment M_o with the work function ϕ_o if s, Ng and Q are not the dominent variables. With this assumption the present results may be compared with those for

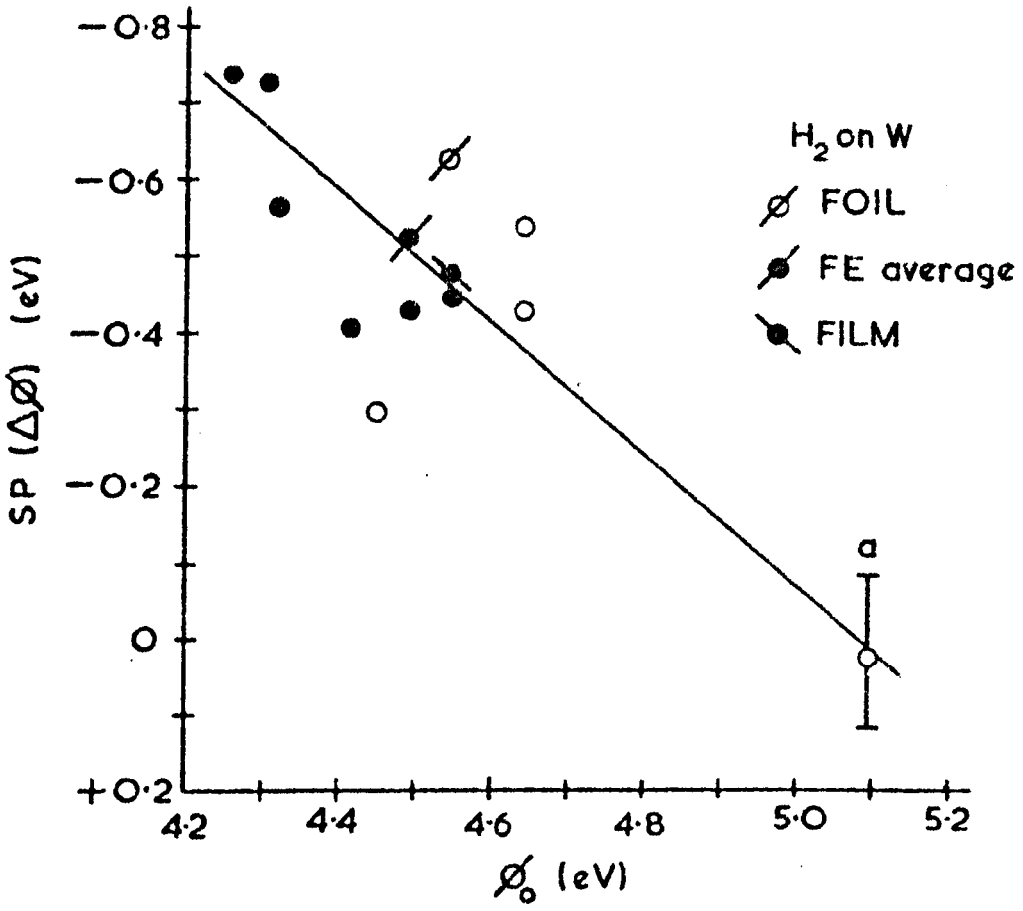

Figure 7.16 The maximum surface potential ($\Delta\phi$) of hydrogen on the single crystal planes of tungsten as a function of the clean surface work function (ϕ_0) from Hopkins and Pender 1966 (o) and their cited works (●). The SP for point a was initially negative at low coverage but turned positive, the error bar includes the maximum positive and negative excursion and the average value is plotted.

hydrogen on the single crystal planes of tungsten (figure 7.16). The largely negative SP in this system becomes increasingly positive as ϕ_o increases in agreement with the present results (figure 7.15) for Ti. The results for W are also empirically described by equation (7.15), where a = 0.88 $\pm$ 0.25 b = 5.09 $\mp$ 0.12eV. The values of the empirical constant a for Ti and W substrates are in reasonable agreement. For oxygen on tungsten, Engel and Gomer 1970(a) have also found the negative SP to become increasingly positive as the work function ϕ_o of the adsorbing plane increased.

It is of interest to compare the results for H_2 on W and Ti with the recent model of metal-adsorbate interaction suggested by Engel and Gomer 1970(a). This was an extension of their previous model for low ionisation potential I adatoms to those having a high electron affinity A and ionisation potential such as H and O . The energy level diagram for the former is shown in figure 2.6 (discussed in Chapter 2.6.2) and for the latter case the diagram is shown in figure 7.17(a). The affinity level A is depressed and broadened near the metal where it is shown schematically as a resonance level filled to the height of the metal Fermi level. The resonance adatom band will be qualitatively maximally filled on the lowest work function surface. Thus the excess negative charge on the adatom increases as ϕ_o reduces. Consequently the dipole moment and the SP become more positive as ϕ_o increases. Engel and Gomer state this is satisfactory only if $\phi \approx$ A. For oxygen and hydrogen the level A is too high but these may have a resonance affinity level R in between the A and I levels and for a free hydrogen atom R = - 6.5eV (they cite). For the R level Engel and Gomer show that there is no excess charge q_e on the adatom when the R band is

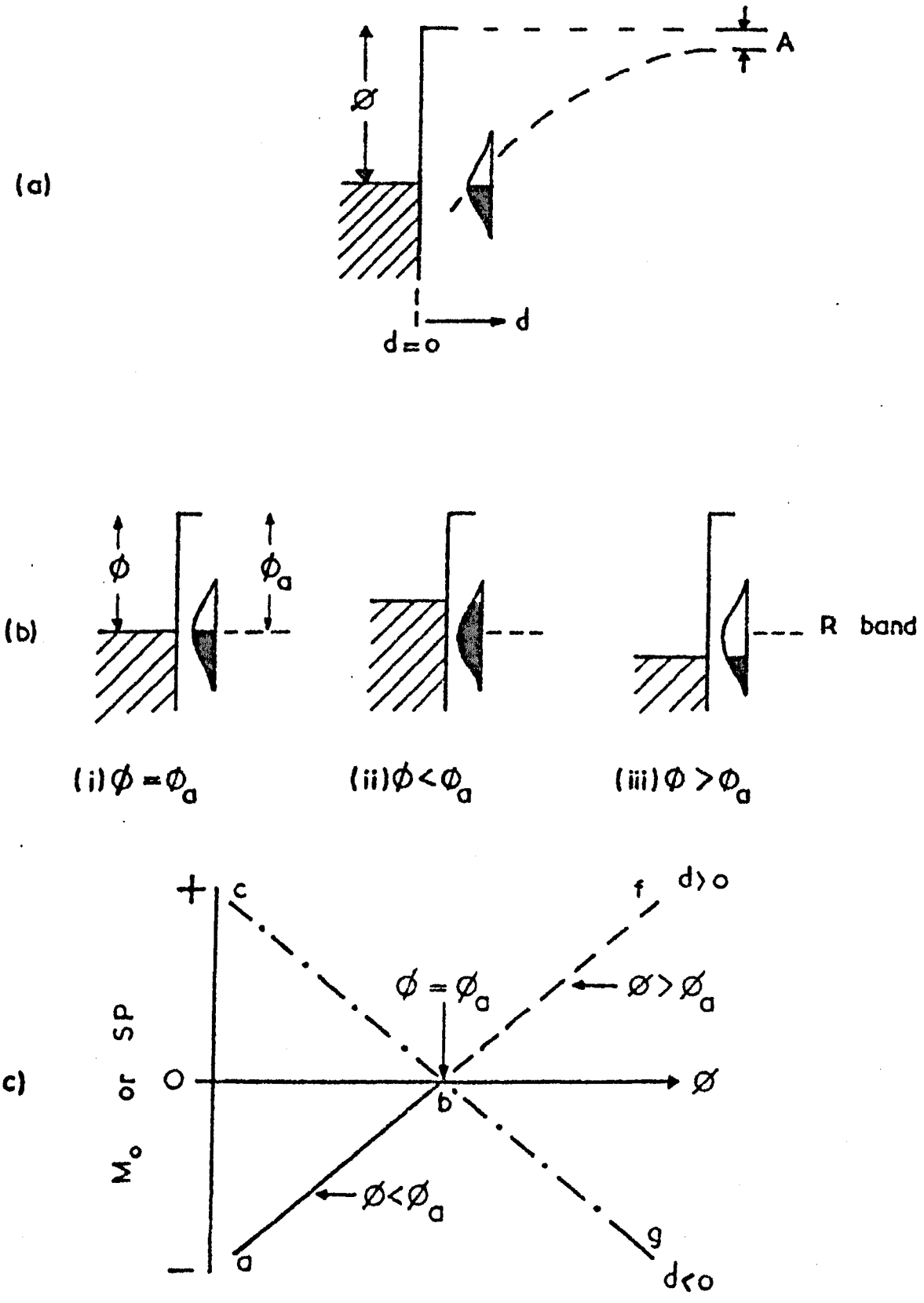

Figure 7.17 Schematic energy level diagram for metal-adsorbate interaction for an adatom with a high electron affinity A and large ionisation potential: (a) broadening and depression of the A level with distance d (Engel and Gomer 1970(a)); (b) change in the occupancy of the resonance affinity (R) level with ϕ resulting in (i) zero, (ii) a negative and (iii) positive adatom charge; (c) variation of the adatom dipole moment $M_o = qd$ or surface potential (SP) with ϕ for an adatom outside of the metal surface (a-f) and penetrating below the surface

half full and this corresponds to figure 7.17(a). If the occupancy is greater than one half the adatom acquires an excess negative charge and the SP is negative. The variation of q_e with ϕ is illustrated in diagram (b) (for a constant spacing) where the position of the R level at a distance d is ϕ_a say. For $\phi = \phi_a$ $q_e = o$ and there is no charge transfer; q_e becomes negative for $\phi < \phi_a$ and $|q_e|$ increases as ϕ reduces. The variation of the dipole moment and the SP with ϕ is shown in diagram (c) ($M_o = qd$). The region of the negative q_e corresponds to the curve ab (for simplicity a linear variation is assumed) for an adatom outside of the metal surface (i.e. $d > o$). The form of the curve ab is consistent with the experimental results for O_2 on W (Engel and Gomer) and also for H_2 (cf. figure 7.16). The resonance model seems to imply that the adsorbate band occupancy may become less than a half if ϕ is sufficiently large resulting in an effective positive charge on the adatom (diagram (b)) and consequently a positive dipole moment and SP denoted by curve bf (for $d > o$). A mirror image is obtained for penetrating adatoms ($d < o$), curve cbg.

The results for the H_2-Ti system are qualitatively of the same form as the curve bf in diagram (c). That is, they are consistent with the predictions of the resonant affinity model for effectively positively charged H adatoms in sites outside of the surface plane (i.e. the bond is of the form $Ti^- - H^+$). In the previous discussion, the positive SP was accounted for by penetration of negatively charged hydrogen adatoms below the surface plane (i.e. the bond was of the form $Ti^+ - H^-$). This direction of charge transfer was assumed because of the lack of evidence for $M^- - H^+$ metal bonds among other factors. The experimental results however are not in accord

with the resonance model which predicts the curve cb for negative adatoms penetrating below the surface plane. The penetration model may however still be plausible if other factors cause the negative adatom charge q or the penetration depth d to increase with ϕ_o. Since the atomic packing density increases with ϕ_o then d would vary inversely with ϕ_o which predicts an inverse variation of the SP with ϕ_o, contrary to the experimental results. The resonance model did not account for: (1) polarisation which is probably a small factor in the present case (2) negatively charged hydrogen adatoms in interstitial sites which would probably reduce the degree of smoothing of the electron distribution due to the Smolochowski effect. This would constitute a negative contribution to the positive dipole moment the magnitude of which would decrease with the atomic packing density (3) the ionicity of a $Ti^+ - H^-$ bond would tend to be maximised by an increase in the atomic packing density. If the latter two factors had a greater influence on the effective dipole moment of the penetrating adatom than the reduction in the effective negative charge predicted by the resonance model with increasing ϕ_o, then the SP would increase with ϕ_o for penetrating electronegative adatoms as observed.

The positive surface potentials of hydrogen on titanium and the empirical relationship SP $\alpha(\phi_o - b)$ are consistent with:

(a) hypothetical predictions of the resonance model for a $Ti^- - H^+$ bond with the effectively positively charged adatoms situated outside of the surface plane

(b) penetration of effectively negatively charged adatoms below the surface plane for a $Ti^+ - H^-$ bond providing there are

various factors which effectively increase the magnitude of the negative adatom charge with the density of atomic packing in the surface plane (or with ϕ_o) over and above the reduction in the charge predicted by the resonance model.

The empirical relationship above however is not consistent with:

(c) hypothetical predictions of the resonance model for penetrating and effectively negatively charged adatoms below the surface with a bond type $Ti^+ - H^-$ since this model predicts the positive SP to decrease with ϕ_o.

It is unfortunate that the position of the adatom with respect to the surface plane is unknown since otherwise it may have been possible to examine the validity of the models more exactly.

7.10 Discussion: Patch Effects

The spatial variation of ϕ across the gold, silver and titanium films shown in figures 7.8 and 7.9 are primarily due to the effects of stray capacitance. The cross-sections fo the substrates used in the experiments are shown in figure 7.7. As the substrate was rotated opposite the reference probe P the interelectrode distance d charged. The variation of ϕ reflects the effects of stray capacitive errors and their dependence on d (as discussed in Chapter 5). The results in figure 7.9 for two titanium films are free from these errors. The average value of ϕ measured over an area of the order of the probe area (~ 0.1 cm^2) varied by less than the error of measurement $\pm$ 20 mV. The apparent reduction

across the surface of film number 18 is due to a change in ϕ during the period (~ 10 minutes) taken to scan the film surface. The work function of the previous film however was stable in time. These results are consistent with the expectation that the measured spatial variation would be small owing to the micro-crystalline structure of the film and the macroscopic dimensions of the probe electrode.

CHAPTER 8

CONCLUSIONS

8.1 Contact potential differences between various metal surfaces have been measured at room temperature and at low pressure with a scanning probe version of the Kelvin-Zisman dynamic capacitor. The rigid mechanical coupling between the vibrating bar carrying the probe and the vacuum system was unsatisfactory since it introduced a difficult problem of instability of the vibration amplitude. On occassions it limited the accuracy of measurements to $\pm$ 0.1 eV. Under favourable conditions an accuracy of a few millivolts was possible using phase sensitive detection and narrow band amplifiers.

The Boostivac getter-ion pump was the source of a stray current of charged particles which entered the experimental chamber. Metal surfaces within the chamber collected a current whose magnitude and charge was dependent on the potential of the metal and the gas pressure. The current was too small (typically $\leq 10^{-11}$ A cm^{-2}) to affect the measurements on metallic surfaces but it had a significant effect at pressures above ~ 10^{-8} torr on the potential of insulating surfaces. The stray current was finally avoided by placing a metal baffle in between the pump and the chamber.

Technical problems and the use of a differential input head amplifier caused the measurements of the contact potential to be sensitive to stray capacitive coupling between the vibrating

electrode and other ancillary metal surfaces within the experimental chamber. The coupling was experimentally shown to be a major source of error if suitable precautionary measures were not taken. Previous experimental and theoretical work on their effects was reviewed. An expression was derived for the apparent contact potential due to these effects. A method was developed which enabled their effects to be experimentally investigated. Experimentally the magnitude of the error increased linearly with the amplitude of vibration, the interelectrode distance and the sum of the cpd and any dc potential between the vibrating electrode and the other surface forming the stray capacitance. The predictions of the model were only in partial agreement with these results since the error was predicted to be proportional to the distance squared. This disagreement was probably the result of some of the simplifying assumptions in the model. The results showed Simon's analysis to be correct and they were consistent with the qualitative conclusions of Anderson and Mignolet. They dispute, however, the earlier results arrived at by Potter.

8.2 Stainless steel was chosen as the reference material for the vibrating probe in order to reduce (hopefully) the errors due to capactive coupling between the probe and the stainless steel vacuum chamber walls. This was an unfortunate choice due to charge effects on an oxide layer on the probe surface which disturbed its work function as described below. There is apparently only one value reported for the work function of steel. The values for the probes were derived from the cpd between them and reference surfaces of gold films deposited in-situ onto pyrex substrates for which the work function is

reasonably established to be 5.3 $\pm$ 0.1 eV. The reference gold films also served as a conducting and pure metallic substrate for titanium films which were deposited onto them. In a later experiment silver was used for the same purpose and also to provide an alternative reference work function surface.

The work function of the stainless steel probes was constant at 2.10^{-9} torr. It reversibly decreased by as much as 0.5 eV when the surface was indirectly illuminated with white light from a mercury discharge lamp, by less than a few tens of millivolts on short exposure to hydrogen at pressures upto 10^{-6} torr and by as much as 0.25 eV on prolonged exposure to hydrogen, and as much as 1.6 eV by applied electrostatic fields. It was reversibly increased by as much as ~ 0.2 eV by an incident low energy electron current ($\leq 10^{-11}$ A cm^{-2}). It was qualitatively shown that the the probes had probably become oxidised during their preparation. Three models were considered of an n-type semiconducting oxide on the surface. The first took accounted for changes in the density of electrons in the conduction band, the second for changes in the density of surface states at the oxide-vacuum surface and similarly at the metal-oxide interface for the third model. The first two models predicted a reversible and exponential increase of the work function due to the electron current which was in agreement with the experimental results although the latter might fit equally well other time-dependent laws. The predictions of the first model were also in agreement with the experimental results of Petit-Clerc and Carette but neither predicted those published recently by Dobrozemsky and Haltau. The latter two models predicted a reversible and exponential reduction in time of

the work function on illumination which was in agreement with the experimental results. Unfortunately the results could not distinguish whether the photo-potential was caused by a photo-hole current to the oxide-vacuum surface (second model) or by a photo-electron current to the metal-oxide surface (third model). The variation of the photo-potential with the intensity of illumination was consistent with the predictions of the second model, but the third predicted a more complex relationship. The stability of the work function for short exposures to hydrogen was consistent with previous studies of the adsorption of H_2 on iron oxides. The reduction of ϕ on prolonged exposure was consistent with the predictions of a simple model of adsorption of hydrogen donors on semiconductor surfaces in which physically adsorbed hydrogen was converted to a partially and positively charged form. The electrostatic field effect was unidirectional and no simple explanation could be found for it.

3.3 Contact potentials as large as 6 eV were measured between thin metal (gold) films on glass and the steel probe at 2.10^{-9} and at 1.10^{-7} torr. The cpd varied in time and also with a bias potential to the film. The films were probably discontinuous since the effects no longer occurred when the deposit became sufficiently thick. They were qualitatively discussed in terms of a localisation of electrical charge on exposed portions of the substrate due to charge transfer processes between the insulator surface and metal islands in the film among other possibilities.

The cpd between the steel probe and a series of gold films deposited on glass was measured at ~ 2.10^{-6} torr (experiment A) and at 2.10^{-9} torr (experiment B). The cpd increased after depositing

the films and assymptoted to an equilibrium value. This change was due to the photo-instability and charge effects on the probe. The work function of the gold films deduced from the equilibrium values of the cpd increased with the thickness of the deposit until a reproducible value was obtained. In the case of experiment A this was probably due to a progressive increase of coverage of the lower work function (titanium) metal substrate. The final values of the work function for the films was assumed to be 5.3 eV. The work function did not change within $\mp$ 10 mV when the partial pressure of hydrogen was increased from the base pressure of 2.10^{-9} torr to about 10^{-6} torr in agreement with previous measurements by others. The equilibrium work functions for the two reference steel surfaces were 4.65 $\mp$ 0.10 and 5.60 $\mp$ 0.10 eV in experiments A and B respectively. The difference between these is probably due to the effects of baking the second probe and prolonged exposure to the residual gas in the case of the former.

Silver was used instead of gold in the final experiment C at 1.10^{-7} torr for the reasons given above. A thick silver film was deposited in-situ onto the steel probe which eliminated the charge effects experienced before. The reference work function of the probe was assumed to 4.3 eV. The glass substrate was replaced by an erbium one (supplied by the U.K.A.E.A.). Its work function was deduced to be 3.5 eV from the cpd. Silver was deposited onto the substrate to provide a relatively pure substrate surface for titanium. The work function of the substrate increased approximately by the same amount with each fresh deposition of silver from 3.8 to about 4.1 eV after the initial deposition. These results were

consistent with the predictions of a simple model in which the film deposit progressively covered the lower work function substrate with increasing average thickness. The model implied that the initial film covered approximately 85% of the substrate. The work function of each fresh film changed generally by as much as 60 mV after deposition apparently due to adsorption of residual gas on the exposed patches of the substrate or of oxygen or water vapour on the silver film itself. The work function generally decreased but on some occassions it increased.

8.4.1 Films of titanium were deposited onto gold or silver film substrates in each of the three experiments A, B and C. In each experiment the values of the work function for the clean films varied widely and this is probably due to impurities and structural differences in their surfaces. The films were deposited at 2.10^{-6} torr in experiment A onto a probably discontinuous gold film substrate. The work functions varied between 3.3 and 4.6 eV. The residual gas composition was unknown but the major constituents were probably water vapour and a mixture of carbon monoxide, nitrogen and hydrogen. The work function decreased after deposition by as much as 0.6 eV. This was probably due to the adsorption of water vapour and hydrogen since the surface potential of nitrogen is known to be negative and other experiments had shown that the combined partial pressures of carbon monoxide and nitrogen did not change appreicably relative to the others above fresh titanium films. After the minimum value was reached the work function increased over a period as long as several hours to ~ 4.6 eV for all the films. The application of the backing voltage in the measurements was shown to disturb the apparent value of the contact potential. Consequently the maximum values of the

surface potential and also the later increase of the work function (and its cause) are uncertain. This may have been caused by the charging phenomena observed for discontinuous metals if the titanium was not continuous or to the electric field instability of the steel reference probe. These preliminary results are perhaps only indicative of the large variations which may be measured in the work functions of titanium films and in the surface potentials of adsorbed gases and also of the occurence of large positive values of the surface potential at low coverage.

8.4.2 The work functions of the clean surfaces of titanium films deposited onto a gold film substrate at 2.10^{-9} torr in experiment B lay within the range from 4.5 to 6.0 eV. These values are much higher than those previously reported for pure films but are significantly close to the extrapolated thermionic values of Wilson at room temperature (4.9 to 5.6 eV) in ultra high vacuum. After deposition the work functions decreased in time to minimum values between 4.0 and 5.0 eV. Analysis of the residual gas composition and other experimental evidence showed that the positive surface potential arose from the adsorption of hydrogen. A qualitative discussion was given of the properties of the hydrogen-titanium system. The positive surface potential could be explained by dissociative adsorption of molecular hydrogen and the penetration of the hydrogen adatoms with a partial negative ionicity into surface interstitial sites in the lattice where the adsorbate was below the surface electronic plane. The dipole moment of the adsorbed hydrogen atom in this situation would be positive resulting in a positive surface potential and a reduction of the work function of the

titanium films. A simple model was proposed of the surface potential of hydrogen (the HSP model) which accounted for dissociative adsorption of molecular hydrogen and solution of the adsorbed atoms into the film. The predictions of the model were consistent with the experimental results for the time dependant changes of the surface potential and a value between 0.7 and 1.5 Kcal gr-atom^{-1} was derived for the activation energy for solution of atomic hydrogen in titanium. Previous measurements of the activation energy with bulk titanium at high temperatures and pressures have resulted in larger values (5 - 10 Kcal . gr-atom^{-1}) but this may be expected since these were probably not so pure as the thin films. The variation in the values derived from the present experiments is probably caused by capacitive errors, impurities and structural differences in the film surfaces.

8.4.3 The values of the work function of the clean surfaces of thin titanium films slowly deposited onto silver film substrates were much lower than those above and lay between 2.5 and 3.8 eV. It was concluded from a qualitative analysis of the relative conditions of the growth of the films that the low values resulted from impurities. These apparently arose from the evaporation source or from gettering of the residual gas or adsorbed reactive gases on the substrate during the growth of the film. Previous measurements of the work function of titanium films lie within the range from 3.5 to 3.8 eV for recent determinations and between 3.9 and 4.2 eV from early investigations. It was concluded in the review and discussion of these previous results that the latter were unlikely to refer to clean surfaces and similarly for the former because of the conditions

in which the films were grown. In support of the conclusion and also that the low values measured in the present experiments are due to impurities are the results of Rentschler and Henry who reported that the work functions of thin films of titanium deposited on to oxygenated surfaces are lower than those of thicker (and apparently purer films. The previous results and also the present ones for slowly deposited films are significantly within the range of values reported for the oxides and carbides of titanium. Impurities provide a logical explanation for the variation of the work functions of the clean surfaces of the films. The work function of these impure films increased after deposition and the final values lay between 3.0 and 4.2 eV. The residual gas composition was not exactly known, however, although previous experiments had shown that the major gases were typically water vapour, hydrogen and a mixture of carbon monoxide and nitrogen. A simple model of the time dependent change of the work function gave predictions for oxygen in agreement with the results; but not for nitrogen although the surface of both of these is known to be negative on titanium films. The change in surface potential was of a similar form to that of hydrogen alone and this was in agreement with the predictions of the HSP model if the sign of the surface potential in the latter was negative. Evidence for dissociative adsorption of molecular hydrogen and water vapour on contaminated titanium was discussed and a negative moment might arise if the impurities prevented the hydrogen adatom from penetrating below the surface electronic plane. If this was assumed to be the case the modified HSP model resulted in values of the activation energy for solution larger than those for the pure surfaces as expected.

Thicker and more rapidly deposited titanium films in the last experiment possessed a high value of the work function for the clean surface between 5.8 and 6.7 eV. The surface potential of the adsorbed gas was positive and experimental evidence was given for the adsorption of hydrogen and/or water vapour. The time dependent changes of the surface potential were similar to those of hydrogen alone on pure surfaces in experiment B and were largely consistent with the predictions of the HSP model. The differences between them could be qualitatively explained by a breakdown of one of the assumptions in the model due to the presence of atomic oxygen from the dissociative adsorption of water vapour (or from OH or another impurity gas) or due to changes in the sticking coefficient of hydrogen or water vapour. Non-dissociative adsorption of water vapour was considered unlikely but might also account for the results if its SP were positive but this is probably unlikely.

8.4.4 The maximum surface potential of hydrogen increased with the work function of clean titanium surfaces. The HSP model predicted that the surface potential should increase with the sticking coefficient; the activation energy for solution, the hydrogen adatom dipole moment and the adsorbate pressure. The linear variation of the SP with ϕ_o may have been fortuitous. If the change was due to a variation of the dipole moment then the results were consistent with the hypothetical predictions of the Engel and Gomer Resonance affinity model for metal-adsorbate interaction for (effectively) positively charged hydrogen adatoms on the outer surface of the metal. The results were also consistent with penetration of electronegatively charged adatoms below the surface providing the (effective) negative adatom charge

increased with the atomic packing density. Various factors which might lead to this dependence were discussed. The experimental results could not determine the position of the adatom or clearly distinguish the direction of charge transfer. The positive surface potential of hydrogen measured in this work is in disagreement with the results of Suhrmann and colleagues. However, in the latter case their films were possibly impure and atomic structural changes may have also occurred since the concentrations of hydrogen were high. The negative surface potentials they observed are consistent with those measured for impure films in the present results which are also possibly due to hydrogen.

8.5 The spatial variation of the work function of metal films was shown to be distorted due to the effects of stray capacitive coupling. In the few instances where their effects were avoided the average value (over an area of the order of 0.1 cm^2) varied by less than 20 mV (for titanium films). This result is in agreement with previous measurements for films of other elements as intuitively expected if the average crystal size in the film surface was much less than the area of the probe electrode when the measurements are made with the Kelvin-Zisman technique.

8.6 It has been concluded from this work that the work function of clean titanium films is decreased when hydrogen is dissociatively adsorbed onto the surface at room temperature. Positive surface potentials on other metals have been observed previously by others for physisorbed hydrogen or weak molecular chemisorption of hydrogen on top of primary electronegative adlayers. A similar case has not

apparently been observed previously for a positive surface potential of a primary hydrogen adatom layer on a clean metal surface. This may be partly due to the fact that experimental studies have been more concerned with metals which have a low solubility for hydrogen at normal temperatures. The present results and conclusions are partly based on the validity of the arguments pertaining to the cleanliness of the films deposited in ultra high vacuum which possessed work functions significantly higher than those measured by others previously. If the former are not valid the conclusions regarding the surface potential of hydrogen may require revision.

BOOKS AND REVIEW REFERENCES

Bardeen, J., Morrison, S.R., 1954, Surface Barriers and Surface Conductance, Physica, 20, 873.

Becker, J.A., 1935, Thermionic Electron Emission and Adsorption, Revs. Mod. Phys., 7, 95.

1955, Adsorption on Metal Surfaces and Its Bearing on Catalysis, Adv. Catalysis, /, 135.

Blyholder, G., 1968, Spectra of Adsorbed Species, In Experimental Methods in Catalytic Research, ed. R.B. Anderson, Academic Press, p.323.

Bowkett, K.M., Smith, D.A., 1970, Field-Ion Microscopy, North Holland Publ. Co., Amsterdam.

Compton, K.T., Langmuir, I., 1930, Electrical Discharges in Gases, Pt.1, Survey of Fundamental Processes, Rev. Mod. Phys., 2, 123.

Culver, R.V., Tompkins, F.C., 1959, Surface Potentials and Adsorption Processes on Metals, Adv. Catalysis, 11, 67.

DeBoer, J.H., 1935, Electron Emission and Adsorption Phenomena, Cambridge University Press.

Dushman, S., 1930, Rev. Mod. Phys., 2, 381.

1962, Scientific Foundation of Vacuum Technique, J. Wiley and Sons, New York; Second Edition.

Eberhagen, A., 1960, Die Anderung der Austrittsarbeit von Metallen durch eine Gasadsorption, Fort. Physik, 8, 245.

Ehrlich, G., 1963, Modern Methods in Surface Kinetics: Flash Desorption, Field Emission Microscopy and Ultrahigh Vacuum Techniques, Adv. Catalysis, 14, 255.

1966, Chemisorption on Single Crystal Planes Disc.Far. Soc. 41, 7.

Farnsworth, H.E., 1968, Low Energy Electron Diffraction, in Experimental Methods in Catalytic Research, ed. R.B. Anderson, Academic Press, London, p.323.

Frankl, D.R., 1967, Electrical Properties of Semiconductor Surfaces, Pergammon Press, Oxford.

Frumkin, A.N., 1964, editor, Surface Properties of Semiconductors, Consultants Bureau, New York.

Gomer, R., 1955, Field Emission Microscopy and Some Applications to Catalysis and Chemisorption, Adv. Catalysis, 7, 93.

1961, Field Emission and Field Ionisation, Oxford University Press.

Good, R.H., Muller, E.W., 1956, Field Emission, Encycl. Phys. 21, 176-235, Springer-Verlag, Berlin.

Gundry, P.M., Tompkins, F.C., 1968, Surface Potentials, in Experimental Methods in Catalytic Research, ed. R.B. Anderson, Academic Press, London, p.101.

Hair, M.L., 1967, Infra red Spectroscopy in Surface Chemistry, Arnold Press, London.

Hansen, R.S., Gardner, N.C., 1968, Field Electron and Field Ion Emission Microscopy, in Experimental Methods in Catalytic Research, ed. R.B. Anderson, Academic Press, London, p.169.

Hansen, R.S., Mimeault, V.J., 1968, Chemisorption in Ultra High Vacuum Systems, in Experimental Methods in Catalytic Research, ed. R.B. Anderson, Academic Press, London, p.217.

Hayward, D.O., Trapnell, B.M.W., 1964, Chemisorption, 2nd ed., Butterworths, London.

Herring, C., Nichols, M., 1949, Thermionic Emission, Revs. Mod. Phys. 21, 185.

Herrmann, G., Wagener, S., 1951, The Oxide Coated Cathode, Volume 2, Chapman and Hall , London.

Hofer, L.J.E., 1968, Conventional Magnetic Methods in Catalysis, in Experimental Methods in Catalytic Research, ed. R.B. Anderson, Academic Press, London, p.402.

Hopkins. B.J., 1968, Ultra High Vacuu, Contemporary Phys., 9, 115.

Hren, J.J. 1970 ed., Field-Ion, Field Emission Microscopy and Related Topics, Surface Sci., 23, (1).

Hughes, A.L., DuBridge, L.A., 1932, Photoelectric Phenomena, McGraw-Hill, New York.

Jenkins, R.O., Trodden, W.G., 1965, Electron and Ion Emission from Solids, Routledge and Kegan Paul Ltd., London.

Kaminsky, M., 1965, Atomic and Ionic Impact Phenomena on Metal Surfaces, Springer-Verlag, New York.

Many, A.J., Goldstein, Y., Grover, N.G., 1965, Semiconductor Surfaces, North Holland Publ. Co., Amsterdam.

Menzel, E., 1963, Studies in the Preparation and Behaviour of Nearly Perfect Metal Surfaces, Rep. Prog. Phys. 26, 47.

Michaelson, H.B., 1950, Work Function of the Elements, J. Appl. Phys., 21, 52.

Muller, E.W., 1960, Field Ionisation and Field Ion Microscopy, Adv. Elec. Electron Phys., 13, 83.

Nottingham, W.B., 1956, Thermionic Emission, Encyclopaedia of Physics, 21, p1-175, Springer,Verlag, Berlin.

Plummer, A.R., 1962, The Semiconductor Gas and Semiconductor-Metal Systems, in The Electrochemistry of Semiconductors, ed. P.J. Holmes, Academic Press, p61.

Reiman, A.L., 1935, Thermionic Emission, Chapman and Hall, London.

Riviere, J.C., 1970, Work Function: Measurements and Results, Solid State Surf. Sci., 1, 180.

Roberts, M.W., 1970, The Incorporation of Chemisorbed Species, Recent Prog. Surf. Sci., 3, 1.

Roberts, R.W., 1963, Generation of Clean Surfaces in High Vacuum, Brit, J. Appl. Phys., 14, 537.

Roberts, R., Vanderslice, T., 1964, Ultrahigh Vacuum and its Applications, Prentice Hall.

Robertson, A.J.B., 1970, Catalysis of Gas Reactions, Logas Press, London.

Suhrmann, R., 1955, Electronic Interaction between Metallic Catalysts and Chemisorbed Molecules, Adv. Catalysis, 7, 303.

Thomson, S.J., Webb, G., 1968, Heteorogeneous Catalysis, Oliver & Webb Publ., London.

Volkenstein, F.F., 1963, The Electronic Theory of Catalysis on Semiconductors, Pergammon Press, Oxford.

Weissler, G.L., 1956, Photoionization in Gases, Handbook der Physik, 21,304.

Wright, D.A., 1953, Survey of Present Knowledge of Thermionic Emitters, Proc. I.E.E.E., 51, 733.

1966, Semiconductors, Methuen and Co. Ltd., London.

Young, D.M., Crowell, A.D., 1962, Physical Adsorption of Gases, Butterworth, London.

CITED REFERENCES

Abey, A.E., 1968, J. Appl. Phys., 39, 120.

Abon, M., Teichner, S.J., 1967, Suppl. Nuovo Cim., 5, 521.

Adams, D.L., Germer, L.H., May, J.W., 1970, Surf. Sci., 22, 45.

Adams, D.L., Germer, L.H., 1971, Surf. Sci., 27, 21.

A.E.I., 1969, M.S. 10 Manual, Publ. 2032-69 and Tech. Info. Suppl. 1.

Anderson, J.R., Alexander, A.E., 1952, Aust. J. Appl. Sci., 3, 201.

Anderson, J.R., Gani, M.S., 1962, J. Phys. Chem. Sols., 23, 1087.

Anderson, J.R., Thompson, N., 1971, Surf. Sci., 26, 397.

Anderson, J.S., Klemperer, D.F., 1960, Proc.Roy.Soc., A258, 350.

Anderson, P.A., 1936, Phys. Rev., 49, 320.
1938, Phys. Rev., 54, 753.
1941, Phys. Rev., 59, 1034.
1952, Phys. Rev., 88, 655.

Antypas, G.A., Tinder, R.F., 1968, J. Appl. Phys., 39, 1967.

Avoird, A Van Der, 1969, Surf. Sci., 18, 159.

Bachmann, L., Shin, J.J., 1966, Surf. Sci., 37, 242.

Bailey, J.R., 1963, Suppl. Nuovo Cim., 1, 494.

Bassett, D.W., 1968, Trans. Far. Soc., 64, 489.

Bell, A.E., Swanson, L.W., Crouser, L.C., 1968, Surf. Sci., 10, 254.

Bennett, A.J., 1968, J. Chem. Phys., 49, 1340.

Bishop, H.E., Riviere, J.C., Cood, J.P., 1970, A.E.R.E. Rept. No. R6485 (Also in 1971, Surf. Sci., 23, 259).

Blackmer, L.L., Farnsworth, H.E., 1950, Phys. Rev., 77, 826.

Blott, B.H., Hopkins, B.J., Lee, T.J., 1965, Surf. Sci. 4, 493.

Bond, G.C., 1969, Surf. Sci., 18, 11.

Boudart, M., 1952, J. Amer. Chem. Soc., 74, 3556.

Brennan, D., Hayward, D.O., Trapnell, B.M.W., 1960, Proc.Roy.Soc.(London), A256, 81.

Bryla, S.M., Feldman, C., 1962, J. Appl. Phys., 33, 774.

Burshtein, R.C., Shurmovskaya, N.A., 1964, Surf. Sci., 2, 210.

Calder, R., Lewin, G., 1967, Brit. J. Appl. Phys., 18, 1459.

Camp, M., Lecchini, S.M.A., 1965, Proc. Phys. Soc., 81, 815.

Cardwell, A.B., 1949, Phys. Rev., 76, 125.

Chalmers, T.A., 1942, Phil. Mag., 33, 399 and 417.

Chen, J.M., Papageorgopoulos, C.A., 1970, Surf. Sci., 21, 377.

Chopra, K.L., Randlett, M.R., 1967, J. Appl. Phys., 38, 3144.

Chung, F.Y., Farnsworth, H.E., 1952, Phys. Rev., 85, 485.

Clarke, E.N., Farnsworth, H.E., 1952, Phys. Rev., 85, 484.

Clausing, R.E., 1961, Trans. 8th. Nat. Amer. Vac. Symp., Pergammon Press, p.345

Clavenna, L.R., Schmidt, L.D., 1970, Surf. Sci., 22, 365.

Coburn, J.W., 1968, Surf. Sci., 11, 61.

Coggins, J.L., Stickney, R.E., 1968, Surf. Sci., 11, 355.

Collins, R.A., Blott, B.H., 1968, Surf. Sci., 9, 1.

Craig, R.D., Harden, E.M., 1965, Vacuum, 15, 22.

Craig, P.P., 1969, Phys. Rev. Lett., 27, 700.

Crossland, W.A., Pritchard, J., 1964, Surf. Sci., 2, 217.

Culver, R.V., Pritchard, J., Tompkins, F.C., 1957, Proc. 2nd Int. Cong. Surf. Activity, London; Butterworth, London 1957, Vol. 2, p.243.

Cutler, P.H., Nagy, D., 1964, Surf. Sci., 3, 71.

Czarycki, W., 1967, LeVide, Nov-Dec, No. 132, 351.

Davies, D.E., Dawson, G.A., Gozna, C.F., 1961, Proc. 5th. Int. Conf. Ion. Phen. Gases, Munich 1961, North Holl. Publ. Co., Amsterdam, p.671.

Davies, R.W., 1968, Surf. Sci., 11, 419.

Dawson, P.T., Hansen, R.S., 1968, J. Chem. Phys. 48, 623.

Dayton, B.B., 1960, Trans.Natl.Amer.Vac.Symp., Pergammon Press, 1962, p.42.

Degeilh, R., 1969, LeVide, Jan-Feb, No. 139, p.29.

Delchar, T.A., Eberhagen, A., Tompkins, F.C., 1963, J. Sci.Inst., 40, 105.

Delchar, T.A., English, G., 1965, J. Chem. Phys., 42, 2686.

Delchar, T.A., Tompkins, F.C., 1967, Proc. Roy. Soc., A300, 141.

Delchar, T.A., Tompkins, F.C., 1968, Trans. Far. Soc., 64, 1915.

Delchar, T.A., 1971, Surf. Sci., 27, 11.

Dillon, J.A., Farnsworth, H.E., 1957, J. Appl. Phys., 28, 174.

Dillon, J.A., Oman, R.M., 1963, Trans. Natl.Amer.Vac.Symp., Pergammon Press, p.471.

Dobrozemsky, R., Haltau, E., 1970, Nederlands Tijdschrift Voor Vacuum Techniek, 8, 133 (in English).

Domenicali, C.A., 1954, Rev. Mod. Phys., 26, 237.

Duell, M.J., Ross, R.L., 1964, Brit. J. Appl. Phys., 15, 157.

Duell, M.J., Davis, B.J., Ross, R.L., 1966, Disc. Far., Soc., 41, 43.

Ehrlich, G., Kirk, C.F., 1968, J. Chem. Phys., 48, 1465.

Ehrhardt, J.J., Cassuto, A., 1969, LeVide, Jan-Feb, No. 139, p.68.

Engel, T., Gomer, R., 1970(a) J. Phys. Chem., 52, 1832.
1970(b) J. Phys. Chem., 52, 5572.

Enikeev, E.K., Isaev, O.V., Margolis, L.Y., 1960, Kin. Catalysis (U.S.A.), 1, 402.

Elsworth, L., Holland, L., Laurenson, L., 1965, Vacuum 15, 337.

Estrup, P.J., Anderson, J., 1966, J. Chem. Phys. 45, 2254.

Estrup, P.J., McRae, E.G., 1971, Surf. Sci., 25, 1.

Farnsworth, H.E., 1958, Proc. Phys. Soc., 17, 703.

Farnsworth, H.E., Winch, R.P., 1940, Phys. Rev., 58, 812.

Farnsworth, H.E., Tuul, J., 1958, Phys. Chem. Sols., 9, 48.

Farnsworth, H.E., Hayek, K., 1967, Suppl. Nuovo Cim. 5, 451.

Fedorus, A.G., Naumovets, A.G., 1970, Surf. Sci., 21, 426.

Fehlner, F.P., 1966, Trans. 3rd Int. Vac. Congr., p.691.

Fehrs, D.L., Stickney, R.E., 1967, Surf. Sci., 8, 267.
1969, Surf. Sci., 17, 298.
1971, Surf. Sci., 24, 309.

Fehlner, F.P., 1966, Trans. 3rd. Int. Vac. Congr., p.691.

Frances,.A.B., Jepsen, R.L., 1963 2nd. Int. Conf. Residual Gases in El. Tubes, Milan, 1963.

Frank, C.W., Schmidt, L.D., 1968, Surf. Sci., 10, 275.

Fry, R.K., Cardwell, A.B., 1962, Phys. Rev., 125, 471.

Gadzuk, J.W., 1967(a), Surf. Sci., 6, 133 and 159.
1967(b), Phys. Rev., 154, 662.
1968, Surf. Sci., II, 465.
1969(a), J. Phys. Chem. Sols., 30, 2307.
1969(b), Surf. Sci., 18, 193.
1970, Surf. Sci., 23, 58.

Garron, R., 1962, CR.Acad. Sci. (Paris), 254, 243.

Gerlach, R.L., Rhodin, T.N., 1969, Surf. Sci., 17, 32.
1970, Surf. Sci., 19, 403.

Germer, L.H., 1966, Surf. Sci., 5, 147.

Gibb, T.R., 1962, Prog. Inorganic Chem., 3, 315.

Giorgi, T.A., Ricca, F., 1967, Suppl. Nuovo Cim., 5, 472.

Glasoe, G.N., 1931, Phys. Rev., 38, 1490.

Goldwater, D.L., Haddard, R.E., 1951, J. Appl. Phys., 22, 70.

Gordy, W., Thomas, W.T., 1956, J. Chem. Phys., 24, 439.

Gulbransen, E.A., Andrews, K.F., 1949, Trans. Amer. Inst. Min. Met. Engrs., J. Metals, 185, 741.

Gundry, P.M., Tompkins, F.C., 1960, Quart. Rev. (London), 14, 257.

Gyftopoulos, E.P., Levine, J.D., 1962, J. Appl. Phys., 33, 67.

Haas, T.W., 1968, J. Appl. Phys., 39, 5854.

Haas, G.A., Thomas, R.E., 1966, Surf. Sci., 4, 64.
1969, J. Appl. Phys., 40, 3919.

Hackerman, N., Lee, E.H., 1955, J. Phys. Chem., 59, 900.

Hampson, D., 1966, Ph.D. Thesis, Univ. Keele, Staffs.

Harra, D.J., 1967, Trans. 14th. Amer.Vac.Symp., Pergammon Press, 1967, p.129.

Harra, D.J., Hayward, W.H., 1967, Suppl. Nuovo Cim., 5, 56.

Harris, L.A., 1968, J. Appl. Phys., 39, 1428.

Hapase, M.G., Gharpurey, M.K., Biswas, A.B., 1968, Surf. Sci., 9, 87.

Hayek, K., Farnsworth, H.E., Park, R.L., 1968, Surf. Sci., 10, 429.

Hensley, E.B., 1961, J. Appl. Phys. 32, 301.

Herring, C., 1952, in Metal Interfaces, Am.Soc. Metals, 1952, p.1.

Hickmott, T.W., Ehrlich, G., 1958, J. Phys. Chem. Sols, 5, 47.

Hill, R.M., 1969, Proc. Roy. Soc. (London), A309, 377-417.

Holden, S.J., Rossington, D.R., 1964, J. Phys. Chem., 68, 1061.

Holland, L., Laurenson, L., Allen, P.G.W., 1961, Trans. 8th. Nat.Amer.Vac.Symp. Pergammon Press, p.208.

Holscher, A.A., 1964, J. Chem. Phys., 41, 579.
1966, Surf. Sci., 4, 89.

Hopkins, B.J., Vick, F.A., 1960, Brit. J. Appl. Phys. 11, 223.

Hopkins, B.J., Riviere, J.C., 1963, Proc. Phys. Soc., 81, 590.
1964, Brit. J. Appl. Phys., 15, 941.

Hopkins, B.J., Ross, K.J., 1964, Brit. J. Appl. Phys., 15, 89.

Hopkins, B.J., Mee, C.H.B., Parker, D., 1964, Brit. J. Appl. Phys. 15, 865.

Hopkins, B.J., Pender, K.R., 1966, Surf. Sci., 5, 316.

Hopkins, B.J., Pender, K.R., Usami, S., 1967, in Fundamentals of Gas Surface Interactions, ed. H. Saltzburg, J.N. Smith (Jr.), M. Rogers, Academic Press, p.284.

Hopkins, B.J., Smith, B.J., 1968, Brit. J. Appl. Phys., 39, 213.

Hopkins, B.J., Lee, T.J., Williams, C.B., 1969, J. Appl. Phys. 40, 1728.

Hopkins, B.J., Usami, S., 1970, Surf. Sci., 23, 423.

Hopkins, B.J., Williams, C.B., Wilmer, P.C., 1971, Surf. Sci., 25, 633.

Horgan, A.M., King, D.A., 1970, Surf. Sci., 23, 259.

Horiuti, J., Toya, T., 1969, Sol. State Surf. Sci., 1, 1.

Huber, E.E., 1966, Appl. Phys. Lett., 8, 169.

Huber, E.E. (Jr.), Kirk, C.T.(Jr.), 1967, Surf. Sci., 8, 458.

Ingold, J.H., 1967, J. Appl. Phys., 34, 2033.

Iwanoski, G.F., Schirjaev, A.T., 1965, Trans. 3rd. Int. Vac. Long. 1965, ed. H. Adam, Pergammon Press, 2, 451.

Jaeger, H., Mercer, P.D., Sherwood, R.G., 1969, Surf. Sci., 13, 349 and 502.

Jain, S.C., Krischnan, K.S., 1952, Proc. Roy. Soc., A215, 431.
1953, Proc. Roy. Soc., A217, 451.
1954, Proc. Roy. Soc., A225, 159.

Johnson, R.P., Shockly, W., 1936, Phys. Rev., 49, 436.

Jowett, C.W., Dobson, P.J., Hopkins, B.J., 1969, Surf. Sci., 17, 474.

Jowett, C.W., Hopkins, B.J., 1970, Surf. Sci., 22, 392.

Juretschke, H.J., 1953, Phys. Rev., 92, 1140.

Kelvin, Lord, 1898, Phil. Mag., 46, 82.

Kellner, K., 1952, Research, 5, 341.

King, D.A., Tompkins, F.C., 1968, Trans. Far. Soc., 64, 496.

Kisluik, P., 1961, Phys. Rev., 122, 405.

Kisselev, W.F., 1967, Z.f.Chemie, 7, 369.
Klein, O., Lange, E., 1938, Z. Electrochem., 44, 542.
Klein, R., 1970, Surf. Sci., 20, 1.

Klemperer, D.F., 1962, J. Appl. Phys., 33, 1532.

Kobayashi, H., Kato, S., 1969, Surf. Sci., 18, 341.

Kolachev, B.A., 1968, Hydrogen Embrittlement of Non-Ferrous Metals, Maxwell and Co., Jerusalem.

Kowasaki, K., Hayashi, N., Ebisawa, S., Sugita, T., 1970, Surf. Sci., 20, 209.

Kruger, J., Yolken, H.T., 1964, Corrosion, 20, 296.

Lander, J.J., 1964, Surf. Sci., 1, 125.

Langmuir, I., 1916, Trans. Electrochem. Soc., 29, 125.

Lawson, R.P.W., Carter, G., 1968, Vacuum, 18, 205.

Lea, C., Mee, C.H.B., 1968, J. Appl. Phys., 39, 5890.

Lee, T.J., Blott, B.H., Hopkins, B.J., 1967, Appl. Phys. Lett., 11, 361.

Levine, L., Lichtman, D., 1960, Rev. Sci. Inst., 37, 731.

Lewis, T.J., 1954, Proc. Phys. Soc., B67, 187.

Lewis, R., Gomer, R., 1969, Surf. Sci., 17, 333.

Libowitz, G.G., 1960, J. Nucl. Mat., 2, 1.

Lichtman, D., Simon, F.N., Kirst, T.R., 1968, Surf. Sci., 9, 325.

Linder, E.G., 1927, Phys. Rev., 30, 649.

Lindholm, E., 1960, Rev. Sci., Inst., 31, 210.

Loucks, T.L., Cutler, P.H., 1964, J. Phys. Chem. Sols., 25, 105.

Lucas, M.S., 1964, Appl. Phys. Lett., 4, 73.

MacDonald, J.R., Edmondson, D.E., 1961, Proc. Inst. Radio Engrs., 49, 453.

MacDonald, J.R., Barlow, C.A.(Jr.) 1963, J. Chem. Phys., 39, 412.
1966, J. Chem. Phys., 44, 202.

Macfadyen, K.A., Holbeche, T.A., 1957, J. Sci., 34, 101.

Mackay, K.M., 1966, Hydride Compounds of the Metalic Elements, Spon.

Macrae, A.U., Muller, K., Lander, J.J., Morrison, J., 1969, Surf. Sci., 15, 483.

Maddison, R., 1964, Ph.D. Thesis, Univ. Keele, Staffordshire.

Madey, T.E., Yates, J.T.,(Jr.), 1967, Suppl. Nuovo Cim., 5, 483.

Magee, C.B., 1967, April, Quarterly Rept. No. 7 (DRI-2395), Denver Res. Inst., Univ. Denver, Colorado.

Malamud, H., Krumbein, A.D., 1954, J. Appl. Phys., 25, 591.

Mark, P., 1965, J. Phys. Chem. Sols., 26, 1767.

Marmet, P., Morrison, J.D., 1962, J. Chem. Phys., 36, 1238.

Martin, S.T., 1939, Phys. Rev., 56, 947.

Mathews, L.D., 1970, Surf. Sci., 23, 423.

May, J.W., 1965, Ind. Eng. Chem., 57, (7), 19.

May, J.W., Linnett, J.W., 1967, J. Catalysis, 7, 324.

May, J.W., Germer, L.H., 1968, Surf. Sci., 11, 443.

Mendenhall, C.E., de Voe, C.F., 1937, Phys. Rev., 51, 346.

Mignolet, J.C.P., 1950, Disc. Far. Soc., 8, 105 and 326.
1952, J. Chem. Phys., 20, 341.
1953, J. Chem. Phys., 21, 1298.
1957, in Chemisorption, Proc. Symp. Keele, Butterworth, London 1956, p.118.

Mikheeva, V.I., 1960, Hydrides of the Transition Metals, Publ. House of Acad. Sci. (Moscow), 1960, (translated from the Russian), U.S.A. En. Comm. AEC-tr-5224.

Minc, S., Siejka, J., 1968, Nukleonika (Poland), 13, 1137 (in English).

Mitchell, E.W.J., Mitchell, J.W., 1952, Proc. Roy. Soc. (London), A210, 70.

Modinos, A., 1967, Brit. J. Appl. Phys., 18, 531.

Morant, M.J., House, H., 1956, Proc. Phys. Soc., B69, 14.

Morozova, D., Popovskii, V.V., 1962, Kin, i Kataliz, 3, 39.

Morris, L.W., 1931, Phys. Rev., 37, 1263.

Muller, E.W., 1937, Z.f. Physik, 106, 541.
1955, J. Appl. Phys., 26, 732.

Muller, J., 1968, Private communication (1971).

Muller, K., 1966, Z.f. Physik, 195, 105.

Mulliken, R.S., 1952, J. Amer. Chem. Soc., 74, 811.

Myers, H.P., 1953, Proc. Phys. Soc., B66, 493.

McCracken, G.M., Barton, R.S., Dillon, W., 1967, Suppl. Nuovo Cim., Ser. 1., 5, 146.

McCracken, G.M., Jefferies, D.J., Goldsmith, P., 1968, Proc. 4th. Int. Vac. Cong., Manchester, p.149.

McQuillan, A.D., 1951, J. Inst. Metals, 79, 371.
1950, Proc. Roy. Soc., A204, 309.

Nelson, R.C., 1963, J. App. Phys., 34, 629.

Newnes, D.M., 1969, Phys. Rev., 178, 1123.

Ovchinnikov, A.P., 1967, Sov. Phys. Sol. St. (U.S.A.), 9, 483.
1968, Sov. Phys. Sol. St., 9, 1508.

Ovchinnikov, A.P., Tsarev, B.M., 1968, Sov. Phys. Sol. St., 9, 1519.

Paddock, A.D., Magee, C.B., 1966, Internal Report (Unnumbered), Denver Res. Inst., Univ. Denver, Colarado; August.

Palmberg, P.W., 1971, Surf. Sci., 25, 598.

Parker, J.H., Warren, R.W., 1962, Rev. Sci. Inst., 33, 948.

Patai, I.F., Pomerantz, M.A., 1951, J. Franklin Inst., 252, 239.

Pearce, D.R., Richardson, P.C., Dudham, R., 1969, Proc. Roy. Soc. (London), A310, 121.

Petit-Clerc, Y., Carette, J.D., 1968(a), Vacuum, 18, 7.
1968(b), Appl. Phys. Lett., 12, 227.

Potter, J.G., 1940, Phys. Rev., 58, 623.

Prevot, F., Sledziewski, Z., 1968, LeVide, Jan., No.133, p1.

Pritchard, J., Tompkins, F.C., 1960, Trans. Far. Soc., 56, 541.

Pritchard, J., 1962, Nature, 194, 38.

Quinn, C.M., Roberts, R.W., 1964, Trans. Far. Soc., 60, 899 and 61, 1775.

Rasor, N.S., Warner, C., 1964, J. Appl. Phys., 35, 2589.

Rauh,E.G., Thorn, R.J., 1959, J. Chem. Phys., 31, 1481.

Rentschler, H.C., Henry, D.E., 1945, Trans. Electrochem. Soc., 87, 289.

Riviere, J.C., 1957, Proc. Phys. Soc., B70, 676.
1964, Brit. J. Appl. Phys., 15, 1341.
1965, Brit. J. Appl. Phys., 16, 1507.
1966, Appl. Phys. Lett., 8, 172.
1967, Suppl. Nuovo Cim., 5, 466.
1969, Physics. Bulletin, 20, 85.

Roberts, R.W., 1963, Brit. J. Appl. Phys., 14, 485.

Roberts, M.W., Wells, B.R., 1966, Disc. Far. Soc., 41, 162.
1967, Surf. Sci., 8, 453.
1969, Surf. Sci., 15, 325.

Rohatgi, V.K., 1957, J. Appl. Phys., 28, 951.

Rootsaert, W.J.M., Van Reijen, L.L., Sachtler, W.M.H., 1962, J. Catalysis, 1, 416.

Rork, G.D., Consoliver, R.E., 1968, Surf. Sci., 10, 291.

Rose, B.A., 1943, Phys. Rev., 44, 585.

Rossington, D.R., Runk, R.B., 1967, J. Catalysis, 7, 365.

Rutherford, S.L., Mercer, S.J., Jepsen, R.L., 1961, Trans.Nat.Amer.Vac.Symp., Pergammon Press, p.380.

Sachs, R.G., Dexter, D., 1950, J. Appl. Phys., 21, 1304.

Sachtler, W.H., Dorgelo, G.J.H., 1965, J. Catalysis, 4, 654.

Sachtler, W.H., Dorgelo, G.J.H., Holscher, A.A., 1966, Surf., Sci., 5, 221.

Sargood, A.J., Jowett, C.W., Hopkins, B.J., 1970, Surf. Sci. 22 343.

Schmidt, L.D., Gomer, R., 1965, J. Chem. Phys., 42, 3573.
1966, J. Chem. Phys., 45, 1605.

Schulze, R., 1934, Z.f. Physik, 92, 212.

Shand, E.B., 1958, Glass Engineering Handbook, 2nd ed., McGraw-Hill Book Co., New York, p.65.

Simon, R.E., 1959, Phys. Rev., 116, 613.

Simon, F.N., Lichtman, D., Kirst, T.R., 1968, Surf. Sci., 12, 299.

Singleton, J.H., 1966, J.Chem. Phys., 45, 2819.
1967, J. Chem. Phys., 47, 73.
1968, J. Vac. Sci. Tech., 5, 109.

Smith, J.R., 1969, Phys. Rev., 181, 522.

Smolochowski, R., 1941, Phys. Rev., 60, 661.

Steiger, R.F., Morabito, J.M.(Jr.), Somorjai, G.A., Muller, R.H., 1969, Surf. Sci., 14, 279.

Stewart, R.L., 1934, Phys. Rev., 45, 488.

Stout, V.L., Gibbon, M.D., 1955, J. Appl. Phys., 26, 1488.

Stow, R.L., 1959, Nature, 184, 542.

Suhrmann, R., Hermann, A., Wedler, G., 1962, Z.f. Phys. Chem., 35, 155.

Surplice, N.A., Singh, B., 1971, private communication.

Tamm, P.W., Schmidt, L.D., 1970, J. Chem. Phys., 52, 1150.

Taylor, N.J., 1964, Surf. Sci., 2, 544.
1966, Surf. Sci., 4, 161.

Tinder, R.F., 1968, J. Appl. Phys., 39, 355.

Trapnell, B.M.W., 1953, Proc. Roy. Soc. (London), A218, 566.
1956, Trans. Far. Soc., 52, 1618.

Uhlig, H.H., 1951, J. Appl. Phys. 22, 1399.

Vaidya, W.M., Daudawate, V.B., 1966, J. Opt. Soc. Amer., 56, 1[illegible]3.

Van Oostrom, A., 1963, Phys. Lett., 4, 34.

Varley, J.H.O., 1960, Phil. Mag., 5, 64.

Vladimirov, G.G., 1968, Sov. Phys. Sol. St., 10, 957.

Volkenstein, F.F., 1967, Sov. Phys. Uspekni (U.S.A.), 9, 743.

Voronin, V.B., 1968, Sov. Phys. Sol. St. (U.S.A.), 9, 1758.

Waclawski, B.J., Hughey, L.R., 1970, Surf. Sci., 19, 464.

Wagner, S., 1957, J. Phys. Chem., 61, 267.

Wallis, G., Farnsworth, H.E., 1956, J. Appl. Phys., 27, 594.

Weissler, G.L., Wilson, T.N., 1953, J. Appl. Phys., 24, 472.

Weissmann, E., Petrescu, Ch., Tarina, D., 1968, J. Sci. Inst. (J. Phys. E) Ser. 2, 1, 426.

Wesolowski, J., Rosenfield, B., Szuszkiewiez, M., 1963, Acta. Phys. Polon. (Poland), 24, 729.

Wilson, R.G., 1966, J. Appl. Phys., 37, 2261 and 3170.

Wolff, M., Guile, A.E., Bell, D.J., 1969, J. Phys. E., Sci. Inst., 2, 921.

Ying, C.F., Farnsworth, H.E., 1952, Phys. Rev., 85, 485.

Yonehara, K., Schmidt, L.D., 1971, Surf. Sci., 25, 238.

Zdanuk, E.J., Wolsky, S.P., 1961, Trans. 8th Natl. Amer.Vac.Symp., Pergammon Press, p. 188.

Zingerman, Ya.P., Ischuk, V.A., 1967, Sov. Phys. Sol. St. (U.S.A.), 9, 623.

Zisman, W.A., 1932, Rev. Sci. Inst., 3, 367.

APPENDIX A

The continuity equation in model A is given by:

$$dn/dt = f\ I_1 + P - A \exp - eV/kT + I_m \qquad (5.2)$$

If the change in the electron density n in the oxide conduction band is linearly related by the constant C to the change in potential V then

$$C\ dV/dt = -\ dn/dt \qquad (A.1)$$

The constant C is related to the capacitance of the oxide. If constants a and b are defined by $a = -A \exp - eV/kT$ and $b = f\ I_1 + P + I_m$ then from (5.2) and (A.1):

$$C\ dV/dt = -\ (a + b) \qquad (A.2)$$

and since $da = -\ (e/kT)a\ dV$ then (A.2) becomes:

$$\int\{a(a + b)\}^{-1}\ da = (e/CkT)\ \int dt$$

$$\log\ \{(a + b)/a\} = b\ et/CkT$$

and substituting for a and b gives

$$\exp\ eV/kT = c_1\ \exp\ \{-\ e(f\ I_1 + P)t/CkT\} + c_2 \qquad (A.3)$$

since I_m is constant and where c is a constant. If the change in V is small then $\exp x \approx 1 + x$ and using the boundary conditions: $t = o\ \ V = V_o$, $t = \infty\ \ V = V_\infty$ then (A.3) reduces to:

$$V_\infty - V = (V_\infty - V_o) \exp - dt$$

where $d = e(f\ I_1 + P)/CkT$. The work function ϕ and V are related by equation (5.1) and therefore it follows that:

$$\phi_\infty - \phi = (\phi_\infty - \phi_o)\ \exp - e(f\ I_1 + P)\ t/CkT \quad (A.4)$$

which describes the time dependant change of ϕ at a constant incident electron current I_1 or illumination intensity P.

The equilibrium change $\phi_\infty - \phi_o$ may be derived using the boundary conditions: $t < o$ and $t = \infty$, $dn_s/dt = o$, then from Equation (5.2)

$$I_m = A\ \exp - eV_o/kT$$

and $f\ I_1 + P + I_m = A\ \exp - eV_\infty/kT$

and if these equations are divided then

$$e\ (V_o - V_\infty)/kT = \log\ (f\ I_1 + P + I_m)/I_m$$

and since $\delta\phi = -\delta V$ then assuming the current I_m is negligible in comparison to the incident electron and photo-generation rate terms then

$$\phi_\infty - \phi_o = (kT/e)\ \log(f\ I_1 + P) \quad (A.5)$$

This equation predicts that the equilibrium change increases with $\log I_1$ and $\log P$ in the absence of illumination ($P = o$) and charged incident particles ($I_1 = o$) respectively.

APPENDIX B

The continuity equation in model B describing the surface state density at the vacuum-oxide surface is:

$$dN_s/dt = G + (I_1 + P + Aexp - eV_s/kT)(N_s^o - N_s)\gamma - N_s(J+P)\eta \quad (5.4)$$

For low pressures the gas term G may be neglected and after rearrangement (5.4) is of the form:

$$dN_s/dt = - aN_s + b \quad (B.1)$$

where $a = (I_1 + P + Aexp - eV_s/kT)\gamma + (J+P)\eta$

$$b = N_s^o (I_1 + P)\gamma$$

If the terms I_1 and P are dominant over the thermal current Aexp - eV/kT then Equation (B.1) becomes:

$$\int (b - aN_s)\, dN_s = \int dt$$

$$N_s = c_1 \exp(- at) + c_2$$

where the constants c_1 and c_2 are found from the boundary conditions: $t = o \quad N_s = N_{s_o}$, $t = \infty \; N_o = N_{s_\infty}$, giving:

$$N_{s_\infty} - N_s = (N_{s_\infty} - N_{s_o}) \exp - a\, t \quad (B.2)$$

The barrier height V_s is described by the Schottky formula:

$$V_s = \omega N_s^2 \quad (5.5)$$

and for small changes in V_s and N_s then

$$N_{s_\infty}^2 - N_s^2 = 2\,\omega\, N_{s_\infty} (N_{s_\infty} - N_s) = V_{s_\infty} - V_s$$

Since ϕ and V_s are directly related by $\delta\phi = \delta V_s$ from equation (5.1) then (B.2) becomes after substituting for a:

$$\phi_\infty - \phi = (\phi_\infty - \phi_o)\exp -\{(I_1 + P)\gamma + (J+P)\eta t\} \qquad (B.3)$$

which describes the time dependant change of the work function for a constant incident electron current and photo-electron generation rate.

The equilibrium change $\phi_\infty - \phi_o$ is derived from the continuity equation using the conditions:

$t < o \quad N_s = N_{s_o} \quad dN_s/dt = o, \; t = \infty \quad N_s = N_{s_\infty} \quad dN_s/dt = o,$

which gives:

$$A\exp - eV_{s_o}/kT = N_{s_o}\eta J/(N_s^o - N_{s_o})\gamma$$

and $I_1 + P + A\exp - eV_{s_\infty}/kT = N_{s_\infty}\eta(J+P)/(N_s^o - N_{s_\infty})\gamma$

If the last equation is rearranged and the equations are divided then:

$$\exp - e(V_{s_o} - V_{s_\infty})/kT = \{(N_s^o - N_{s_\infty})N_{s_o}\eta J\}/\{(N_s^o - N_{s_o})(N_{s_\infty}\eta(J+P) - (I_1+P)(N_s^o - N_{s_\infty})\gamma)\}$$

Since from above $\delta\phi = \delta V$ then this equation reduces to:

$$\phi_\infty - \phi_o = (kT/e)\{\log a - \log(N_{s_\infty}\eta(J+P) - (I_1+P)(N_s^o - N_{s_\infty})\gamma)\} \qquad (B.4)$$

where $a = (N_s^o - N_{s_\infty})\, N_{s_o}\eta J/(N_s^o - N_{s_o})$

This equation predicts: (a) $\phi_\infty - \phi_o$ increases with the incident electron current I_1 in a log fashion and (b) if the photo-hole current is the dominant term in the absence of an incident electron current ($I_1 = o$) then $\phi_\infty < \phi_o$ since $\log N_{s_\infty}\eta(J+P) > \log a$ and $\phi_o - \phi_\infty$

increases with log P. In the absence of charged particles or illumination $N_{s_o} = N_{s_\infty}$ and $\phi_\infty - \phi_o = 0$ as intuitively expected.

APPENDIX C

The continuity equation for model C which describes the surface state density of the metal-oxide interface is:

$$dN/dt = I_4(N^o-N)\gamma \quad - N(P+J)\eta \tag{5.7}$$

which may be written in the form:

$$dN/dt = - a N + b \tag{C.1}$$

where $a = I_4 \gamma + (P+J)\eta$

$b = I_4 N^o \eta$

Equation (C.1) is similar to Equation (b.1) in Appendix B if I_4 is independent of N where the solution was shown to be:

$$N = c_1 \exp - a t + c_2$$

where the constants c_1 and c_2 are found from the boundary conditions: $t = o$, $N = N_o$, $t = \infty$ $N = N_\infty$, giving:

$$N_\infty - N = (N_\infty - N_o) \exp - a\,t \qquad (C.2)$$

The barrier height V is described by the Schottky formula given by:

$$V = \omega N^2 \qquad (5.5)$$

and for small changes in V and N then

$$N_\infty^2 - N^2 = 2\omega N(N_\infty - N) = V_\infty - V$$

and since ϕ and V are related by $\delta\phi = -\delta V$ from Equation (5.1) then Equation (C.2) becomes after substituting for a:

$$\phi - \phi_\infty = (\phi_o - \phi_\infty) \exp - (I_4\gamma + (P+J)\eta)t \qquad (C.3)$$

This equation describes the time dependent change of ϕ for a constant intensity of illumination. The electron current I_4 from the oxide CB to the surface states for non-thermal photo-electrons is

$$I_4 = P + A\exp - eV/kT \qquad (5.8)$$

and for thermalised photo-electrons

$$I_4 = (P + A) \exp - eV/kT \qquad (5.9)$$

The solution given in (C.3) is valid only for non-thermalised electrons since in the derivation it was implicitly assumed that $I_4 \neq f(V)$ and this condition is satisfied when the photo-electron term in (5.8) is dominant. A solution of the continuity equation thermalised current given in (5.9) is complex and is not derived.

The equilibrium change $\phi_o - \phi_\infty$ is derived from the continuity equation using the boundary conditions:

$t < o \quad N = N_o, \; dN/dt = o; \; t = \infty \quad N = N_\infty, \; dN/dt = o$

and for I_4 as defined in Equation (5.8), then from the continuity equation:

$$A\exp(-eV_o/kT)\ (N^o - N_o)\gamma = N_o J\eta$$

and

$$A\exp(-eV_\infty/kT)\ (N^o - N_\infty)\gamma = N_\infty(P+J)\eta - P(N^o - N_\infty)\gamma$$

When these equations are divided and rearranged they give:

$$V_\infty - V_o = (kT/e)\{\log(N_o J\eta) - \log\ (P(N_\infty\eta - (N^o - N_\infty)\gamma) + JN_\infty\eta) - \log\ (\ (N^o - N_o)/(N^o - N_\infty)\ )\}$$

Since from above $\delta\phi = -\delta V$, this equation reduces to:

$$\phi_o - \phi_\infty = (kT/e)\ \{\log a - \log\ (P(N_\infty\eta - (N^o - N_\infty)\gamma) + JN_\infty\eta)\} \qquad (C.4)$$

where $a = N_o J\eta\ (N^o - N_\infty)/(N^o - N_o)$.

If the photo-electron current term $P(N^o - N_\infty)\gamma > PN_\infty\eta$ the hole current term this equation predicts that $\phi_o - \phi_\infty$ will increase with the photo-generation rate P and also that $\phi_\infty < \phi_o$ since in this case the first term log a on the right handside of the equation is greater than the second term. In the absence of illumination (P=0) the model predicts that $\phi_o - \phi_\infty = o$ since then $N_o = N_\infty$ as intuitively expected. If the above condition is not true and the photo-hole current is greater than the photo-electron current then $\phi_\infty > \phi_o$ and $\phi_\infty - \phi_o$ increases with P.

APPENDIX D

The continuity equation from model B describing the surface state density in the presence of an electronically active adsorbing gas is:

$$dN_s/dt = G + A\exp(-eV_s/kT)(N_s^o - N_s)\gamma - N_s J\eta \qquad (5.13)$$

The rate of change of the density n of adsorbed $\alpha - H_2$ is related to the pressure and the sticking coefficient s at low coverage by

$$dn(\alpha)/dt = a\ s$$

where a is a function of pressure. If the density of $\beta - H_2$ is directly related to $n(\alpha)$ by

$$n(\beta) = b\ n(\alpha)$$

then the rate of change of $\beta - H_2$ is:

$$dn(\beta)/dt = b\ a\ s \qquad (D.1)$$

The density of occupied surface states N_s is related to $n(\beta)$

$$N_s = N_{s_o} - n(\beta) \qquad (D.2)$$

assuming $\beta - H_2$ is a donor molecule and that $\alpha(H_2)$ is only physically bound and does not disturb N_s, η or γ. The barrier height V_s is related to N_s by the Schottky formula

$$V_s = \omega N_s^2 \qquad (5.5)$$

and

$$dV_s/dt = 2\omega N_s\ dN_s/dt \qquad (D.3)$$

The term dN_s/dt is given in the continuity equation. If the assumption is made that the rate of adsorption of electronically active gas molecules is dominant and that $\alpha(H_2)$ does not disturb N_s, γ or η then equation (5.13) reduces to:

$$dN_s/dt = G = - dn(\beta)/dt$$

and therefore substituting for dN_s/dt, N_s and $dn(\beta)/dt$ from Equations (D.1) and (D.2) into (D.3) gives:

$$dV_s = - 2\ abs\omega\ (N_{s_o} - n(\beta))dt$$

which is of the form

$$\int dV_s = c \int (N_{s_o} - f\ t)dt$$

where $c = - 2\ abs\omega$ and $f = abs$

$$V_s = c\ (N_{s_o} - (ft/2))t + k$$

The constant k is found with the boundary condition: $t = o\ V_s = V_{s_o}$ $n(\beta) = o$, the equation gives:

$$V_s - V_{s_o} = c\ (2N_{s_o} - ft)t/2 \qquad (D.4)$$

If $n(\beta) << N_{s_o}$ and since from Equation (5.1) $\delta\phi = \delta V_s$ then (D.4) becomes after substituting for c and f

$$\phi_\infty - \phi \simeq 2\ abs\omega N_{s_o} t \qquad (D.5)$$

for small t. This equation predicts a linear reduction in ϕ at a constant pressure of H_2 with time which is dependant on the pressure, sticking coefficient and proportionality factor between the α and β states.

APPENDIX E

The photo-generation rate P is related to the optical intensity T and the quantum efficiency σ for electron-hole pair production by the equation

$$P = q\,T \tag{E.1}$$

where $q = \sigma/h\nu$ and h is Planck's constant and it is assumed for simplicity that the reflection coefficient is zero and that σ and T are independant of frequency ν. The optical intensity T is related to the source intensity T_o and the number N_b of optical absorbers in the optical path by:

$$T = T_o \exp - a_b N_b$$

where a_b is the absorption coefficient and therefore P is given by:

$$P = q\,T_o \exp - a_b N_b \tag{E.2}$$

APPENDIX F

The continuity equation describing the rate of change in the number N of adsorbed hydrogen atoms in the surface layer is:

$$dN/dt = 2sNg - N\exp(-eQ/kT) - 2N_d \tag{7.3}$$

where s is the sticking coefficient, Ng is the rate of incidence of hydrogen molecules on the surface, Nexp - eQ/kT and Q are the rate and activation energy for solution of hydrogen atoms and $2N_d$ is the desorption

rate of molecular hydrogen. If the surface potential V is linearly related to N by

$$V = \phi_o - \phi = 4\pi e M_o N, \; M_o > o \tag{7.2}$$

and if s is independent of N then:

$$dV/dt = a - b\,V \tag{F.1}$$

where $a = 8\pi esNg$ and $b = \exp -eQ/kT$, assuming the desorption rate N_d may be neglected. Integration of (F.1) leads to:

$$V = g_1 \exp - bt + q_2$$

where the constant g is found by the conditions: $t = o \; N = o \; V = o$, $t \to \infty \; N = N_f \; V = V_f$ giving after substituting for V from (7.2):

$$\phi - \phi_f = (\phi_o - \phi_f) \exp - t/\tau \tag{F.2}$$

where $\tau = \exp eQ/kT$. The rate $dN/dt = o$ when $t \to \infty \; N \to N_f$ giving from (7.3);

$$N_f = 2sNg \exp eQ/kT$$

and it follows from (7.2) that:

$$\phi_o - \phi_f = 8\pi e M_o sNg \exp eQ/kT \tag{7.4}$$

It has been implicitly assumed that the dissolved hydrogen atoms do not contribute to V (i.e. that their dipole moment is very small or that they diffuse rapidly away from the subsurface region), that the activation energy for dissociation of H_2 is small so that dissociation is not rate limiting in the continuity equation and also that adatoms are adsorbed into only one (electropositive) site on the metal surface.

APPENDIX G

PUBLISHED WORK

(a) D'Arcy, R.J., Surplice, N.A., 1970, J.Phys.D: Appl. Phys., 3, 482; The Effects of Stray Capacitance on the Kelvin Method for Measuring Contact Potential Difference.

(b) Surplice, N.A., D'Arcy, R.J., 1970, J. Phys.E: Scientific Inst., 3, 477; A Critique of the Kelvin Method of Measuring Work Functions.